



Programa de doctorado en Neurociencias

**Characterization of progenitor cell types and lineages in  
ferret cerebral cortex and its conservation in  
mammalian phylogeny**

Lucía Jimena del Valle Antón

Thesis Director

Dr. Víctor Borrell Franco

Universidad Miguel Hernández de Elche

2023











This Doctoral Thesis, entitled “*Characterization of progenitor cell types and lineages in ferret cerebral cortex and its conservation in mammalian phylogeny*”, is presented under the modality of conventional with the following quality indicator:

L. Del-Valle-Anton, V. Borrell, Folding Brains: From Development To Disease Modeling. *Physiol. Rev.* **102**, 511–550 (2022). DOI: [10.1152/physrev.00016.2021](https://doi.org/10.1152/physrev.00016.2021)





Sant Joan d'Alacant, 1st September 2023

Dr. Víctor Borrell Franco, director of the Doctoral Thesis entitled "*Characterization of progenitor cell types and lineages in ferret cerebral cortex and its conservation in mammalian phylogeny*"

**INFORMS:**

That Lucía Jimena del Valle Antón has carried out under my supervision the work entitled

*"Characterization of progenitor cell types and lineages in ferret cerebral cortex and its conservation in mammalian phylogeny"*

in accordance with the terms and conditions defined in her Research Plan and according to the Code of Good Practices from the Miguel Hernández University, satisfactorily fulfilling the set objectives for its public defense as a Doctoral Thesis.

In witness whereof, I hereby sign, in Sant Joan d'Alacant on 1st of September of 2023.

Thesis Director  
Dr. Víctor Borrell Franco  
SIGNATURE





Sant Joan d'Alacant, 1st September 2023

Dr. Elvira de la Peña García, Coordinator of the PhD Program in Neurosciences from the Instituto de Neurociencias, a joint center participated by the Miguel Hernández University (UMH) and the Spanish Council for Scientific Research (CSIC),

**INFORMS:**

That Lucía Jimena del Valle Antón has carried out under the supervision from our PhD Program the work entitled

*“Characterization of progenitor cell types and lineages in ferret cerebral cortex and its conservation in mammalian phylogeny”*

in accordance with the terms and conditions defined in her Research Plan and according to the Code of Good Practices from the Miguel Hernández University, satisfactorily fulfilling the set objectives for its public defense as a Doctoral Thesis.

In witness whereof, I hereby sign, in Sant Joan d'Alacant on 1st of September of 2023.

Dr. Elvira de la Peña García  
Coordinator of the PhD Program in Neurosciences  
SIGNATURE





This Doctoral Thesis, entitled “*Characterization of progenitor cell types and lineages in ferret cerebral cortex and its conservation in mammalian phylogeny*”, has been carried out in the Instituto de Neurociencias, a joint center participated by the Miguel Hernández University (UMH) and the Spanish Council for Scientific Research (CSIC), with funding from the Spanish Ministry of Science, Innovation and Universities: BES-2016-077737.





**AGRADECIMIENTOS/ACKNOWLEDGEMENTS**

Quiero agradecer a mi supervisor Prof. Víctor Borrell por la oportunidad y el apoyo esencial que me ha brindado para realizar esta Tesis, en la que he podido descubrir el inmenso mundo de las ómicas. Ha sido un reto monumental que me ha permitido formarme como científica y como persona. Igualmente, debo agradecer a mis compañeros de laboratorio por aunar esfuerzos día a día, muy especialmente a Salma y Anna, que han estado siempre ahí en lo personal y dándome valiosas ideas para enriquecer este proyecto. Salma, has sido un pilar fundamental en esta historia.

También quiero agradecer la meticulosidad con la que nuestros colaboradores de otras Instituciones han llevado a cabo su trabajo. Ha sido un verdadero placer trabajar con Daniela (Götz lab) y Florian (Mayer lab). Del mismo modo, debo agradecer al laboratorio Huttner en general por acogerme durante mi estancia en Dresde, y muy especialmente a Michaela. No conseguimos encontrar nuestras ansiadas sinápsis, pero gracias por tu dedicación, incansable esfuerzo e inmenso apoyo. He aprendido mucho de tí.

Hay muchas otras personas sin las cuales esta tesis no podría haberse llevado a cabo: Eva y los compañeros del animalario han proporcionado un apoyo fundamental con los hurones; Ángel me guió en mis primeros pasos con la bioinformática y ha sido imprescindible para elegir las piezas del ordenador; Caler ha supuesto un apoyo básico en la sala de ómicas, siempre con Radio 3 de telón de fondo; Trini siempre ha facilitado nuestro trabajo y se ha interesado en lo personal por cada uno de nosotros. Del mismo modo, hay personas de mi pasado como estudiante que despertaron mi interés por investigar el sistema neviioso, tales como Carmen Rúa, profesora de neuroanatomía comparada de la Universidad Complutense de Madrid, los laboratorios de Sabine Lévi del Intitut de Fer à Moulin, Manuel Guzmán de la Universidad Complutense de Madrid y Helmut Kettenmann del Max-Delbrück-Centrum. Gracias por descubrirme el mundo de la investigación.

## AGRADECIMIENTOS/ACKNOWLEDGEMENTS

También hay gente desconocida que ha sido clave en la materialización de la tesis. Sin Justine, Aydan y Zuleyma, del equipo de 10x Genomics, hubiera sido imposible obtener nuestras muestras de alta calidad. Del mismo modo, el apoyo de la comunidad de Github, Biostars y Stack Overflow ha sido crucial para resolver problemas que parecían no tener solución. Finalmente Alexandra por darme a mí y a tantos otros la llave al conocimiento.

En lo personal quiero agradecer a mis padres, Marta y Andrés, y mi hermano, Arturo, su apoyo incondicional. Habéis estado a mi lado a lo largo de este duro trabajo dándome sabios consejos, y sé que lo habríais estado en cualquier otro proyecto que me hubiera propuesto. Sin vosotros, yo no estaría aquí. Igualmente, debo agradecer a mis tíos, Margarita y Ricardo, por ser mis padres adoptivos alicantinos y alimentarme durante estos largos años.

Del mismo modo, debo agradecer a mi otra familia, la familia escogida: A los compañeros de la aventura alicantina Ana, Aída, Álvaro, Ingrid y Michael por compartir esos días de cine, excursiones y siempre buena comida. Boris, me has ayudado a ver el mundo de otra manera y a encarar las situaciones siempre como oportunidades. A mis teatreros Celia, Javi, Clara, Sandra y José, y a mis incondicionales Carlota, María, Ceci, Ire e Ichi. Gracias por aguantar estoicamente mis lamentos y darme el cariño que necesitaba. Todos sois una parte fundamental en mi vida y este trabajo también lleva vuestro nombre.

## AGRADECIMIENTOS/ACKNOWLEDGEMENTS

I would like to thank my supervisor Prof. Víctor Borrell for the opportunity and the essential support he has given me to conduct this Thesis, in which I have been able to discover the immense world of omics. It has been a monumental challenge that has allowed me to develop as a scientist and as a person. Likewise, I must thank my fellow labmates for pulling together our efforts everyday, especially Salma and Anna, who have always been there personally and have given me valuable ideas to enrich this project. Salma, you have been a cornerstone in this story.

I would also like to acknowledge the thoroughness with which our collaborators from other Institutions have carried out their work. It has been a real pleasure working with Daniela (Götz lab) and Florian (Mayer lab). In the same way, I must thank the Huttner lab in general for hosting me during my stay in Dresden, and particularly Michaela. We could not find our long-awaited synapses, but thank you for your commitment, tireless effort and immense support. I have learned a lot from you.

There are many other people without whom this thesis could not have been carried out: Eva and colleagues from the animal facility have provided a fundamental support with the ferrets; Ángel guided me in my first steps with bioinformatics and has been essential for choosing the parts of the computer; Caler has been a core support in the omics room, always with Radio 3 in the background; Trini has always facilitated our work and taken a personal interest in each one of us. Likewise, there are people from my past as a student who awakened my interest in investigating the nervous system, such as Carmen Rua, professor of comparative neuroanatomy at the Complutense University of Madrid, the laboratories of Sabine Lévi from the Institut de Fer à Moulin, Manuel Guzmán from the Complutense University of Madrid and Helmut Kettenmann from the Max-Delbrück-Centrum. Thank you for introducing me to the world of research.

There are also unknown people who have been key in the completion of the thesis. Without Justine, Aydan and Zuleyma, from the 10x Genomics team, it would have been impossible to obtain our high quality samples. Similarly, the support of the Github community, Biostars and Stack Overflow has been crucial in solving

## AGRADECIMIENTOS/ACKNOWLEDGEMENTS

problems that seemed to have no solution. Finally Alexandra for giving me and so many others the key to knowledge.

Personally, I want to thank my parents, Marta and Andrés, and my brother, Arturo, for their unconditional support. You have been by my side throughout this hard work giving me wise advices, and I know that you would have been there in any other project that I had set myself. Without you, I would not be here. Likewise, I must thank my uncles, Margarita and Ricardo, for being my adoptive parents from Alicante and feeding me during these long years.

In the same way, I must thank my other family, the chosen one: My companions on the Alicante adventure Ana, Aída, Álvaro, Ingrid and Michael for sharing those days of movies, hiking and always good food. Boris, you have helped me to see the world in a different way and to always face situations as opportunities. To my “teatrerros” Celia, Javi, Clara, Sandra and José, and to my stalwarts Carlota, María, Ceci, Ire and Ichi. Thank you for stoically enduring my complaints and giving me the love I needed. You are all a fundamental part of my life and this work also bears your name.



<b>I. ABBREVIATIONS.....</b>	<b>19</b>
<b>II. ABSTRACT/RESUMEN.....</b>	<b>23</b>
<b>III. INTRODUCTION</b>	
1. Neocortical histogenesis in mammals.....	25
2. Archetypal progenitor cells in mammals.....	28
3. Cellular mechanisms for cortex folding.....	29
4. Genetic protomap of cortex folding.....	35
5. Ferret for cortical modeling.....	37
6. Technological race to describe single-cell diversity.....	39
<b>IV. OBJECTIVES.....</b>	<b>45</b>
<b>V. MATERIALS AND METHODS</b>	
1. Animals.....	47
2. Brain extraction and microdissection.....	47
3. Single-cell suspension, cell concentration and sample viability.....	48
4. Single-cell isolation and cDNA library preparation.....	48
5. Library sequencing.....	49
6. Genome alignment.....	49
7. Cell barcode filtering.....	50
8. Cell quality assessment.....	50
9. Normalization, regression and sample integration.....	50
10. Clustering and resolution.....	51
11. Cluster quality assessment.....	51
12. Cell type identity identification.....	52
13. DEG analyses and cluster enrichment.....	53
14. Subset analyses.....	53
15. Cell-cycle regression analyses.....	55
16. Functional enrichment analyses.....	55
17. Trajectory analyses.....	56
18. Electroporation.....	57
19. Analysis of barcoded cell lineages.....	58
20. Species dataset integration and DEG analyses.....	61
21. Pseudobulk expression analyses.....	63
22. Cell downsampling.....	63

## TABLE OF CONTENTS

23. Analysis of MCD genes.....	64
24. Tissue processing for ICC, conventional ISH and FISH.....	64
25. Constructs.....	65
26. ISH.....	66
27. FISH.....	67
28. Imaging.....	69
29. FISH counting.....	69
30. HOPX sequence identification.....	69
31. Statistics.....	70
32. Single-cell data plotting.....	70

## VI. RESULTS

1. Transcriptomic atlas of ferret cortical germinal layers at single-cell resolution.....	71
2. RGC clusters are repeated in VZ and OSVZ, while they remain distinct between SG and LS.....	73
3. Three parallel transcriptomic trajectories arise from RGCs in VZ and in OSVZ.....	79
4. Parallel lineages originate from RGCs in the ferret cortex.....	81
5. Multiple RGC classes are conserved in ferret and human.....	84
6. Parallel transcriptomic trajectories from RGCs are conserved in ferret and human but not in mouse cortex.....	88
7. Distinct maturation of newborn ENs in gyrus and sulcus linked to human malformations of cortical development.....	91
8. Supplementary figures	
i. Fig. S1. Cell barcode filtering and high-quality cell parameters for each scRNAseq library.....	95
ii. Fig. S2. Cluster resolution and evaluation after sample integration.....	97
iii. Fig. S3. Ferret cell cluster characterization.....	98
iv. Fig. S4. Cluster composition across experimental conditions and IPC cluster enrichment.....	99
v. Fig. S5. Differential gene expression between conditions in main cell types.....	100

## TABLE OF CONTENTS

vi. Fig. S6. Patterns of gene expression across experimental conditions.....	101
vii. Fig. S7. High similarity in cell clustering and transcriptional trajectories between partial and complete cell-cycle regression of the ferret dataset.....	102
viii. Fig. S8. RGC markers and morphologies in the neonatal ferret cerebral cortex.....	104
ix. Fig. S9. Characterization of P1 RGC classes 8 and 16.....	106
x. Fig. S10. Differential gene expression between germinal layers in P1 RGC clusters 8 and 16.....	107
xi. Fig. S11. Differential gene expression between cortical areas in P1 RGC clusters 8 and 16.....	108
xii. Fig. S12. RNAscope analysis of marker gene expression for RGC classes at P1.....	109
xiii. Fig. S13. RNAscope analysis of marker gene expression for microdissected layers at P1.....	111
xiv. Fig. S14. Transcriptional profile of progenitor cell trajectories.....	113
xv. Fig. S15. Cell trajectories in the developing ferret cortex.....	114
xvi. Fig. S16. Identification of cell lineages with barcode lineage tracing.....	116
xvii. Fig. S17. Integration of ferret, human and mouse scRNAseq datasets, and analysis of similarities.....	118
xviii. Fig. S18. Expression in ferret cells of canonical marker genes for human RGC types.....	119
xix. Fig. S19. Cell clustering and transcriptional trajectories of integrated multispecies datasets after equalizing cell abundance.....	120
xx. Fig. S20. Immature neuron markers.....	121
xxi. Fig. S21. Gene score of MCD.....	122

## VII. DISCUSSION

1. Increasing progenitor cell diversity in folds and fissures.....	123
--	-----

## TABLE OF CONTENTS

2. Identical cell lineages emerge from distinct germinal layers.....	126
3. Similar cell types and conserved trajectories between gyrencephalic species.....	127
<b>VIII. CONCLUSIONS/CONCLUSIONES.....</b>	<b>131</b>
<b>IX. REFERENCES.....</b>	<b>135</b>
<b>X. APPENDIX: author's published scientific contribution.....</b>	<b>163</b>

**ABBREVIATIONS**

<b>AQP4</b>	Aquaporin 4	<b>ERBB2</b>	Erb-B2 receptor tyrosine kinase 2
<b>aRGC</b>	Apical RGC (=vRG)	<b>FABP7</b>	Fatty acid binding protein 7; BLBP
<b>ASPM</b>	Abnormal spindle-like microcephaly-associated	<b>FACS</b>	Fluorescence-activated cell sorting
<b>ATP5I</b>	ATP synthase membrane subunit E; ATP5ME	<b>FC</b>	Fold change
<b>bp</b>	Base pair	<b>fCl.</b>	Primary ferret cluster
<b>bRGC</b>	Basal RGC (=oRG)	<b>FDR</b>	False discovery rate
<b>bRGC 2-basal-P</b>	bRGC with bifurcated basal process	<b>FGF</b>	Fibroblast growth factor
<b>bRGC apical-2-basal-P</b>	bRGC with apical and bifurcated basal processes	<b>FGFR2/3</b>	FGF receptors 2 and 3
<b>bRGC apical-P</b>	bRGC with apical process	<b>FLRT1/3</b>	Fibronectin leucine rich transmembrane proteins 1 and 3
<b>bRGC both-P</b>	bRGC with basal and apical processes	<b>fw</b>	Forward
<b>BSA</b>	Bovine serum albumin	<b>G1</b>	Gap I cell-cycle phase
<b>CABLES2</b>	CDK5 and ABL enzyme substrate 2	<b>G2</b>	Gap II cell-cycle phase
<b>Cas9</b>	CRISPR-associated 9	<b>G3BP1</b>	Ras-GTPase-activating protein SH3-domain-binding protein
<b>CDK5</b>	Cell division protein kinase 5	<b>GAD65</b>	Glutamate decarboxylase 2; GAD2
<b>cDNA</b>	Complementary DNA	<b>GADD45B</b>	Growth arrest and DNA damage inducible beta
<b>cds</b>	CellDataSet class	<b>GDPD2</b>	Glycerophosphodiester phosphodiesterase domain
<b>COX7A1</b>	Cytochrome C oxidase subunit 7A1	<b>GEM</b>	Gel bead-in Emulsion
<b>CP</b>	Cortical plate	<b>GFAP</b>	Glial fibrillary acidic protein
<b>CRISPR</b>	Clustered regularly interspaced short palindromic repeat	<b>GFP</b>	Green fluorescent protein
<b>cRNA</b>	Complementary RNA	<b>GTF</b>	Gene transfer format
<b>CRYAB</b>	Crystallin alpha B	<b>GW</b>	Gestational week
<b>CSF</b>	Cerebrospinal fluid	<b>GZ</b>	Germinal zone
<b>DAPI</b>	4',6-diamidino-2-phenylindole	<b>HES1</b>	Hes family BHLH transcription factor 1
<b>DEG</b>	Differentially expressed gene	<b>HMGN1</b>	High mobility group nucleosome binding domain 1
<b>DEPC</b>	Diethyl pyrocarbonate	<b>HOPX</b>	Homeodomain-only protein
<b>DIG</b>	Digoxigenin	<b>iCl.</b>	Species integrated cluster
<b>DNA</b>	Deoxyribonucleic acid	<b>ID1</b>	Inhibitor of DNA binding 1
<b>DNMT1</b>	DNA methyltransferase 1	<b>ILKAP</b>	Integrin linked kinase associated Serine/Threonine phosphatase
<b>Drop-seq</b>	Droplet sequencing	<b>IN</b>	Inhibitory interneuron
<b>E</b>	Embryonic day	<b>INM</b>	Intekinetic nuclear migration
<b>EC</b>	Endothelial cell	<b>IPC</b>	Intermediate progenitor cell
<b>ECM</b>	Extracellular matrix	<b>ISH</b>	<i>In situ</i> hybridization
<b>EGFP</b>	Enhanced GFP	<b>ISVZ</b>	Inner SVZ
<b>EN</b>	Excitatory neuron		
<b>EOMES</b>	Eomesodermin; TBR2		

## ABBREVIATIONS

<b>IUE</b>	In utero electroporation	<b>PTTG1</b>	Pituitary tumor-transforming gene 1
<b>IZ</b>	Intermediate zone	<b>QC</b>	Quality check
<b>KO</b>	Knockout	<b>RARRES2</b>	Retinoic acid receptor responder 2
<b>LGALS1</b>	Galectin 1	<b>RGC</b>	Radial glia cell
<b>LIS</b>	Lissencephaly	<b>RNA</b>	Ribonucleic acid
<b>LS</b>	Lateral sulcus	<b>ROBO</b>	Roundabout guidance receptor
<b>M</b>	Mitosis	<b>RPS15</b>	Ribosomal protein S15
<b>MAB-T</b>	Maleic acid buffer containing Tween20	<b>RT</b>	Retrotranscribed
<b>MCD</b>	Malformations of cortical development	<b>at RT</b>	At room temperature
<b>MICU2</b>	Mitochondrial calcium uptake 2	<b>rv</b>	Reverse
<b>mRNA</b>	Messenger RNA	<b>S</b>	DNA synthesis
<b>MST</b>	Mitotic somal translocation		cell-cycle phase
<b>MZ</b>	Marginal zone	<b>S100B</b>	S100 calcium binding protein B
<b>NDFIP1</b>	Nedd4 family interacting protein 1	<b>SAP</b>	Subapical progenitor
<b>NE</b>	Neuroepithelium	<b>scRNAseq</b>	Single-cell RNA sequencing
<b>NEC</b>	Neuroepithelial cell	<b>SD</b>	Standard deviation
<b>NES</b>	Nestin	<b>SEM</b>	Standard error of the mean
<b>NFIA</b>	Nuclear factor I/A	<b>SERPINE2</b>	Serpin family E member 2
<b>NFIX</b>	Nuclear factor I/X	<b>SG</b>	Splenic gyrus
<b>NGS</b>	Next-generation sequencing	<b>SLC1A3</b>	Solute carrier family 1 member 3; GLAST
<b>NSL1</b>	Component of MIS12 kinetochore complex	<b>SNP</b>	Short neural precursor
<b>o.n.</b>	Overnight	<b>SNRPA1</b>	Small nuclear ribonucleoprotein polypeptide A'
<b>OPC</b>	Oligodendrocyte progenitor cell	<b>SOX2</b>	Sex-determining region Y-box transcription factor 2
<b>oRG</b>	Outer radial glia (=bRGC)	<b>SP</b>	Subplate
<b>OSVZ</b>	Outer SVZ	<b>SPARC</b>	Secreted protein acidic and cysteine rich
<b>P</b>	Postnatal day	<b>SPC25</b>	Component of NDC80 kinetochore complex
<b>PAX6</b>	Paired box 6	<b>SSC</b>	Saline sodium citrate
<b>PB</b>	Phosphate buffer	<b>STMN1</b>	Stathmin 1
<b>PBS</b>	Phosphate buffered saline	<b>SUMO</b>	Small ubiquitin like modifier
<b>PBS-T</b>	Phosphate buffered saline containing tween20	<b>SVZ</b>	Subventricular zone
<b>PC</b>	Principal component	<b>tbRGC</b>	bRGC with transient phases between having basal and/or apical process and without any process
<b>PCA</b>	Principal component analysis	<b>TCF12</b>	Transcription factor 12
<b>PCR</b>	Polymerase chain reaction	<b>TMEM196</b>	Transmembrane protein 196
<b>PFA</b>	Paraformaldehyde	<b>TOP2A</b>	DNA topoisomerase II alpha
<b>PKIA</b>	cAMP-dependent protein kinase inhibitor alpha		
<b>PMG</b>	Polymicrogyria		
<b>PP</b>	Preplate (=PPL)		
<b>PPL</b>	Primordial plexiform layer (=PP)		
<b>PSMB1</b>	Proteasome 20S subunit beta 1		

## ABBREVIATIONS

<b>TOX3</b>	Thymocyte selection associated high mobility group box family member 3
<b>tRGC</b>	Truncated RGC
<b>t-SNE</b>	t-distributed stochastic neighbor embedding
<b>TUBA1</b>	Tubulin alpha I
<b>TUBB4B</b>	Tubulin beta 4B class IVb
<b>UMAP</b>	Uniform manifold approximation and projection
<b>UMI</b>	Unique molecular identifier
<b>VGLUT2</b>	Solute carrier family 17 member 6; SLC17A6
<b>VIM</b>	Vimentin
<b>vRG</b>	Ventricular radial glia (=aRGC)
<b>VZ</b>	Ventricular zone
<b>YPEL3</b>	Yippee like 3
<b>ZEB1</b>	Zinc finger E-box binding homeobox 1
<b>ZFP36L1</b>	ZFP36 ring finger protein Like 1





**ABSTRACT/RESUMEN**

Development of the mammalian cerebral cortex, the cell types involved in this process and their lineage relationships have been studied for years. Cortical neurogenesis is viewed as a linear process where apical radial glial cells (aRGCs) give rise to intermediate progenitors (IPCs), and these in turn give rise to excitatory neurons (ENs). Thanks to advances in animal models and the technology for their study, discoveries in recent years show that this *a priori* simple process actually involves a greater diversity of neural progenitors and more complex relationships than previously thought. But how this process is articulated in gyrencephalic mammals (including humans), where the cerebral cortex undergoes very significant expansion and folding, is unclear. In this PhD Thesis, I have characterized the process of cortical neurogenesis in the gyrencephalic ferret using single-cell RNA sequencing (scRNAseq) and cell lineage tracing technology on isolated germinal layers. We have identified different transcriptomic classes of radial glial cells (RGCs) that populate both the ventricular zone (VZ) and the outer subventricular zone (OSVZ), plus an additional type of RGC thought to exist only in the human cortex. We have found that this progenitor cell diversity establishes parallel lineages that converge onto a single type of immature EN. We have also found that the most immature clusters of ENs are prone to express genes related to human malformations of cortical development, especially in the prospective gyrus. Intriguingly, progenitor cell diversity is more similar between gyrencephalic species (i.e. human, ferret) than with lissencephalic species (i.e. mouse). Finally, we have found that the parallel lineages are conserved in human and ferret, while they seem to have been simplified in mouse. My results contribute significantly to our understanding of the evolution of cerebral cortex folding.

## ABSTRACT/RESUMEN

El desarrollo de la corteza cerebral en mamíferos, los tipos celulares involucrados en este proceso y sus relaciones de linaje han sido objeto de estudio durante años. La neurogénesis cortical se considera un proceso lineal por el cual células de glía radial apical (aRGCs, en inglés) dan lugar a progenitores intermedios (IPCs), y estos a su vez a neuronas excitatorias (ENs). Gracias a los avances en modelos animales y tecnología para su estudio, los descubrimientos en los últimos años muestran que este proceso *a priori* simple en realidad implica una mayor diversidad de progenitores neuronales y relaciones más complejas de lo que se pensaba. Pero cómo se articula este proceso en mamíferos girencefálicos (incluidos los seres humanos), en los que la corteza cerebral experimenta una importante expansión y plegamiento, no está claro. En esta tesis doctoral, he caracterizado el proceso de neurogénesis cortical en el hurón, mamífero girencefálico, utilizando la secuenciación de RNA en células únicas (scRNAseq) y tecnología de trazado de linaje celular en capas germinativas aisladas. Hemos identificado diferentes clases transcriptómicas de células de glía radial (RGC) que pueblan al mismo tiempo la zona ventricular (VZ) y la zona subventricular externa (OSVZ), más un tipo de RGC adicional que se pensaba que existía únicamente en la corteza del ser humano. Hemos encontrado que esta diversidad de células progenitoras establece linajes paralelos que convergen en un solo tipo de EN inmadura. También hemos encontrado que los grupos de ENs más inmaduras son proclives a expresar genes relacionados con malformaciones del desarrollo cortical en humanos, especialmente en la región del futuro giro. Sorprendentemente, la diversidad de células progenitoras es más similar entre especies girencefálicas (i.e. humano, hurón) que con especies lisencefálicas (i.e. ratón). Finalmente, hemos encontrado que los linajes paralelos están conservados en humano y hurón, mientras parecen haber sido simplificados en ratón. Mis resultados contribuyen significativamente a la comprensión de la evolución del plegamiento de la corteza cerebral.

## **INTRODUCTION**

### **1. Neocortical histogenesis in mammals**

The nervous system is a complex structure responsible for the reception, integration and generation of responses of our body. It comprises two major components: peripheral (spinal and cranial nerves, and ganglia) and central (tracts and nuclei), that are located outside or inside the brain and spinal cord respectively (Purves et al., 2004). In early development of the central nervous system (CNS), the anterior region of the neural tube expands dramatically and begins to be defined and specialized in the primary, and latter on the secondary, vesicles (Puelles et al., 2013). The most anterior secondary vesicle is known as telencephalon, which undergoes an exponential growth along embryonic development and gives rise to the brain hemispheres (Shiraishi et al., 2015). The internal cavities of the brain hemispheres, derived from the neural tube's inner space, are the lateral ventricles, where cerebrospinal fluid (CSF) flows (Purves et al., 2004). The dorsal mantle of the brain hemispheres gives rise to the neocortex, which is responsible for the integration of motor, perceptual and elaborated cognitive functions (Kandel et al., 2000).

The neocortex emerges from the cortical neuroepithelium (NE), a monolayer of founding neural stem cells, or neuroepithelial cells (NECs), that are in contact with the lateral ventricle (Bayer and Altman, 1991). Sauer in 1935 described a to-and-fro movement of NECs nuclei throughout the thickness of this cortical primordium in the course of the cell cycle (Sauer, 1935). During the Gap I (G1) cell-cycle phase, the nucleus moves from the internal, apico-ventricular surface to the external, basal face. Next, a DNA Synthesis (S) step occurs in the basal side, before the nucleus descends again to the apical side during the Gap II (G2) phase, and finally Mitosis (M) occurs at the ventricular surface. This process is called interkinetic nuclear migration (INM) (Fig. 1A) and is asynchronous between neighboring NECs, producing the illusory appearance of a stratified layer (Sauer, 1935; Sidman et al., 1959).

## INTRODUCTION

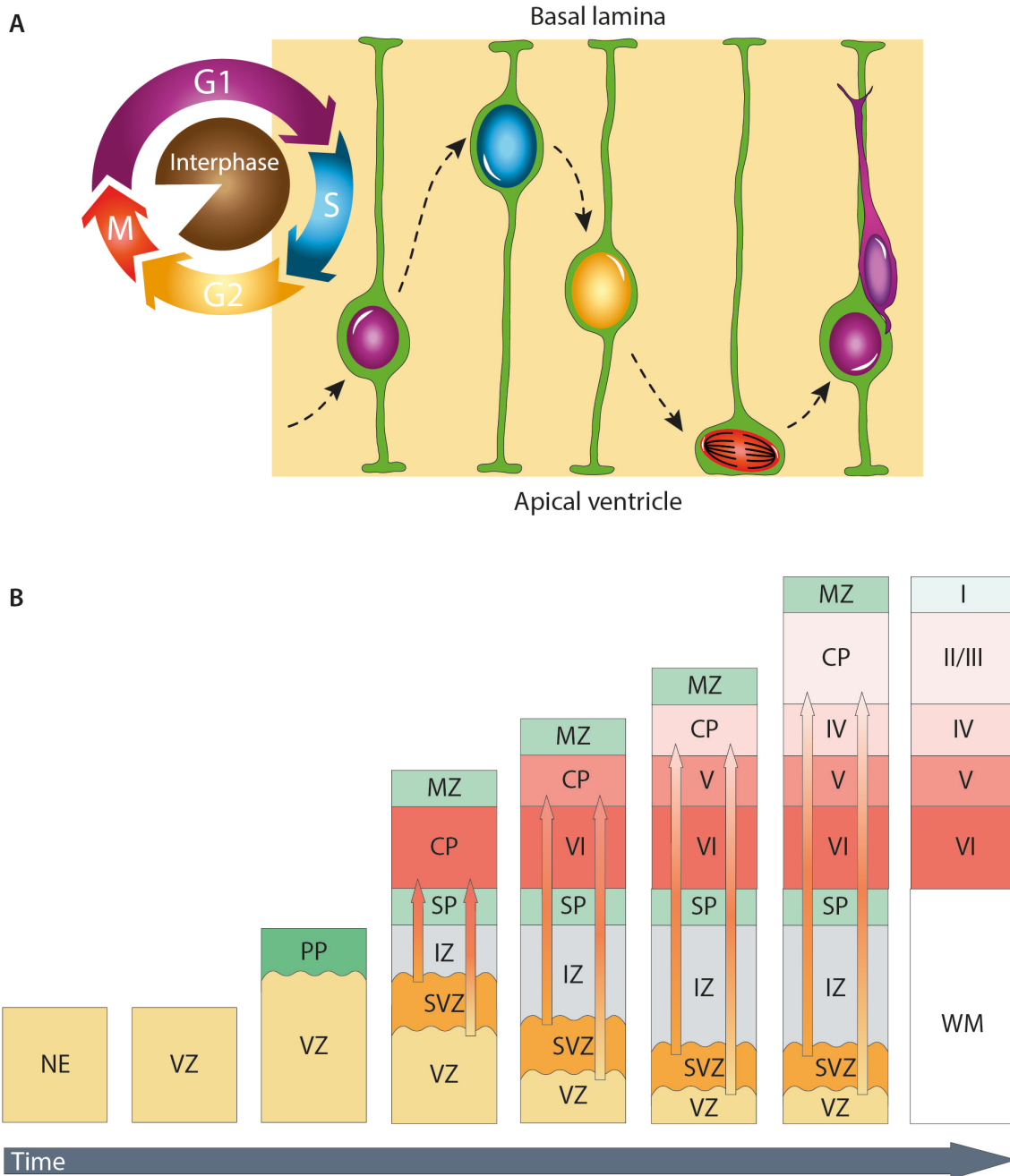


**FIGURE 1. Cortical development.** (A) Movement described by the nucleus of progenitor cells populating the NE and the VZ along cell cycle, known as interkinetic nuclear migration. NEC/aRGC depicted in green, newborn excitatory migrating neuron in purple. (B) Layering in the course of cortical development that includes the CP formation following an inside-out pattern. G1, gap I; S, DNA synthesis; G2, gap II; M, mitosis; NE, neuroepithelium; VZ, ventricular zone; PP, preplate; SVZ, subventricular zone; IZ, intermediate zone; SP, subplate; CP, cortical plate; MZ, marginal zone; WM, white matter. Adapted from [Del-Valle-Anton and Borrell, 2022](#).

At the onset of neurogenesis, the NE is gradually replaced by a new pseudostratified layer, known as ventricular zone (VZ) (Fig. 1B), populated by

radial glia cells (RGCs) (Noctor et al., 2002). The firstly born neurons accumulate above the VZ and assemble into the primordial plexiform layer (PPL), also called preplate (PP) (Marin-Padilla, 1971; Bystron et al., 2008). As neurogenesis progresses, RGCs in the VZ produce a second type of progenitor cells that do not carry out INM and accumulate in a second germinal layer, separated from the lateral ventricle, named subventricular zone (SVZ) (Kershman, 1938; Angevine Jr. et al., 1970; Bystron et al., 2008). As newborn excitatory neurons (ENs) emerge from the VZ and the SVZ, they migrate radially and then accumulate in the cortical plate (CP), a densely packed layer that splits the PP into the subplate (SP, below) and the marginal zone (MZ, above) (Marin-Padilla, 1971; 1978; 1983). The MZ is a layer with low cell density containing mostly Cajal-Retzius cells (Ramón y Cajal, 1890; Retzius, 1893; Kölliker, 1896), which sets an outer boundary for migratory cortical neurons (Chai et al., 2009). On the other hand, the SP is a transient layer that facilitates the connection of the CP with other cortical and subcortical areas (Bystron et al., 2008; Fleiss et al., 2018). The onset of the CP also brings forth a heterogeneous layer above the SVZ called the intermediate zone (IZ) (Kershman, 1938; Stensaas 1967). It includes migrating ENs and inhibitory interneurons (INs), as well as extrinsic axons (Bystron et al., 2008). Further on in development, the newborn ENs that populated the CP mature while successive waves of newly produced neurons migrate from the germinal layers towards the CP (Bayer and Altman, 1991). Neurons build layers on top of each other in an inside-out pattern, starting from the older layer VI to the youngest layer II (Angevine and Sidman, 1961; Rakic, 1974; Jackson et al., 1989). At the end of neurogenesis, the MZ transforms into layer I by a progressive invasion of interneurons, dendritic arbors and axons (Marin-Padilla and Marin-Padilla, 1982). Simultaneously, the IZ becomes the white matter (WM) containing myelinated axons, and SP cells become white matter interstitial neurons (WMINs) (Bystron et al., 2008; Sedmak and Judaš, 2021). This process finally results in a six-layered neocortex structure (Fig. 1B).

## INTRODUCTION

### **2. Archetypal progenitor cells in mammals**

As mentioned in the previous section, the early NE from the mammalian telencephalon is composed by NECs (Bayer and Altman, 1991). These initial progenitors are characterized by a bipolar morphology, with an apical process in close connection with the lateral ventricle through adherens and tight junctions, and a basal process in contact with the basal lamina (Bentivoglio and Mazzarello, 1999; Götz and Huttner, 2005). The strong binding with the ventricle gives NE the starting consistence to generate the cortex, and it adjusts any exchange with CSF carried out through the primary cilia (Bentivoglio and Mazzarello, 1999; Lehtinen and Walsh, 2011). NECs are also characterized by a high capacity of self-amplification and are classically identified by the expression of SRY-box transcription factor 2 (SOX2) and nestin (NES) proteins (Shimozaki, 2014).

At the beginning of neurogenesis, the NECs give rise to apical radial glia cells (aRGCs), which maintain the bipolar structure with an apico-basal contact, but whose basal process elongates as the cortex thickens, it develops lamellate expansions and serves as the migratory substrate for newborn ENs (Rakic, 1972). Similarly, aRGCs conserve adherens junctions between them at the apical site, carry out INM (within the VZ) and express the gene *NES* at early stages (Götz and Huttner, 2005). However, aRGCs start expressing proteins related to their glial nature such as glial fibrillary acidic protein (GFAP), vimentin (VIM), astrocyte-specific glutamate transporter (SLC1A3, also known as GLAST), astrocytic calcium-binding protein (S100B) and fatty acid binding protein (FABP7, also called BLBP), and new proteins like paired box 6 (PAX6) (Hartfuss et al., 2001; Götz and Huttner, 2005). Another glial feature that can be observed is the storage of glycogen in granules at the tip of the basal process (Rakic, 1972). Their characteristic high self-amplification capacity enables aRGCs to symmetrically divide, that is to produce two daughter cells with the same cell fate, thus maintaining the pool of progenitors. In addition, they can also asymmetrically self-renew and generate ENs or other type of progenitor cells, known as basal progenitors. Finally aRGCs can also carry out symmetric neurogenic divisions (Huttner and Kosodo, 2005; Götz and Huttner, 2005).

Basal progenitors arise at late stages of neurogenesis and move their cell body to the SVZ via a process called delamination (Sokpor et al., 2022). There are two types of basal progenitor cells: basal radial glia cells (bRGCs) and intermediate progenitor cells (IPCs). bRGCs have a unipolar morphology, by which they only maintain the connection with the basal lamina and lose the adherens junction apical connection (Fietz et al., 2010; Hansen et al., 2010; Reillo et al., 2011; Shitamukai et al., 2011; Wang et al., 2011). This basal fiber is also used by newborn ENs to migrate radially to the CP (Reillo et al., 2011; Lui et al., 2011). bRGCs express the same proteins as aRGCs, as well as some specific signatures in certain species at a particular developmental time, such as the homeodomain-only protein (HOPX) in human from gestational week (GW) 18.2 (Pollen et al., 2015). They do not carry out INM, however they effectuate a short movement towards the CP before cytokinesis, known as mitotic somal translocation (MST), possibly enabling the accumulation of bRGCs (Hansen et al., 2010; LaMonica et al., 2013; Gertz et al., 2014). bRGCs have an unequal distribution across mammals that is directly related to their amplifying capacity. In rodents, there are low numbers of bRGCs, which symmetrically divide into two neurons, quickly exhausting their pool, while primates and carnivores present a greater number of these cells that mostly self-amplify and, to a lesser extent, generate IPCs (Gertz et al., 2014; De Juan Romero and Borrell, 2015). Later on in development, this expanded pool of bRGCs will be the major source of ENs in the primate and carnivore cortex (Fietz and Huttner, 2011). On the other hand, IPCs display a multipolar morphology with no apico-basal contact, and therefore no adherens junction connection either (Haubensak et al., 2004; Miyata et al., 2004; Noctor et al., 2004). IPCs do not exhibit INM nor MST (LaMonica et al., 2013), and express eomesodermin (EOMES) but no glial markers (Englund et al., 2005). IPCs are highly neurogenic in all mammals, sometimes preceded by a few rounds of self-renewing mitoses (De Juan Romero and Borrell, 2015).

### **3. Cellular mechanisms for cortex folding**

An additional level of complexity in the developing mammalian cortex is its folding. Cortex folding results in the formation of gyri (peaks) and sulci (valleys) along the

## INTRODUCTION

cerebral surface, and it is a mammalian trait typically associated to large brains (Lewitus et al., 2014). This characteristic has been secondarily lost in some species during mammalian evolution, distinguishing between mammals with a folded cortex (gyrencephalic) and with a smooth cortex (lissencephalic) (Kelava et al., 2012; O'Leary et al., 2013; Lewitus et al., 2014; Heuer et al., 2019). Among gyrencephalic mammals, we will specifically focus on the order of carnivores and primates, with ferret and macaque/human as representatives. These will be compared to mouse, a lissencephalic species in the order of rodents.

The specialization of ferret, macaque and human to build large folded brains stems from the beginning of cortex development. The abundance of the NE founder cells prior to neurogenesis is larger in species with a folded cortex (Rakic, 1995). Their period of self-amplification is longer, allowing a greater amplification and larger starting pool of aRGCs (Rakic, 1995). Likewise, the proliferative period of aRGCs is also extended throughout neurogenesis in ferret compared to rodents, ultimately conferring them a higher capacity to generate neurons (Martínez-Cerdeño et al., 2006).

The relative thickness of the SVZ is greater in ferret, macaque and human compared to mouse, containing the larger amount of basal progenitors produced by aRGCs. This enlargement also leads to its specialization in two sublayers: the inner subventricular zone (ISVZ) closer to the ventricle, and outer subventricular zone (OSVZ) further away (Smart et al., 2002; Zecevic et al., 2005; Reillo et al., 2011). These layers contain IPCs and, more importantly, abundant self-amplifying bRGCs (Gertz et al., 2014), specifically accumulated in areas of prospective gyri (Reillo et al., 2011). In addition, the self-renewing potential of IPCs and bRGCs is higher in gyrencephalic than lissencephalic species (Hansen et al., 2010; Betizeau et al., 2013). Some studies have established a direct relationship between the relative abundance of bRGCs in the OSVZ and the degree of cortex folding (Reillo et al., 2011; Lui et al., 2011; Nowakowski et al., 2016). Despite this correlation, bRGCs are also present in the OSVZ of marmoset, a near lissencephalic primate (García-Moreno et al., 2012; Hevner and Haydar, 2012; Kelava et al., 2012), likely due to a process of evolutionary reversal (Kelava et al., 2012; Kelava et al., 2013). This



means that a large number of bRGCs is key for cortex folding, but their mere presence is not sufficient (Kelava et al., 2012; Kelava et al., 2013).

Gyrencephaly is additionally related to a large diversity of progenitor cell types. Betizeau and colleagues described in 2013 that, in addition to the archetypal progenitor cells (Fig. 2A), macaque embryos display three additional types of bRGCs (Betizeau et al., 2013). The soma of these cells is located in the OSVZ and they have different proliferative and neurogenic potentialities. Based on the direction and number of their processes, bRGCs may have a basal process and an apically directed process (bRGCs both-P), only one apically directed process (bRGCs apical-P), or alternate phases having a basal and/or an apical process and stages without any process (tbRGCs) (Fig. 2B). The direction in which these bRGC morphotypes perform MST varies according to the position of their process: the soma of bRGCs with an apical-P goes downward (towards the ventricle), while the somas from bRGCs with both-P and tbRGCs goes as many times up as down. The set of five types of basal progenitors populating macaque OSVZ (including archetypal IPCs and bRGCs) can shift between them in a specific manner according to developmental time (Betizeau et al., 2013). In the same year, Pilz and colleagues demonstrated the presence of bRGCs with both-P and with apical-P in the ISVZ and OSVZ of the ferret cortex (Pilz et al., 2013) (Fig. 2B). At late neurogenesis, these bRGCs comprise 20% and 15% of the total mitotic cells in the ISVZ and OSVZ, respectively (Pilz et al., 2013). In 2019, Kalebic and colleagues identified the bRGC morphotypes containing both-P and apical-P in ferret cortex, and then also in mouse and human (Fig. 2B), representing 30%, 8% and 36% of bRGCs respectively (Kalebic et al., 2019). This team also observed two new bRGC types associated to an increased proliferative capacity at mid-neurogenesis (human GW 11-16): bRGCs with a bifurcated basal process (bRGCs 2-basal-P, following Betizeau's nomenclature), and with an apical process and a bifurcated basal process (bRGCs apical-2-basal-P) (Fig. 2B). These morphotypes were absent in the mouse cortex, but they account for 5% of bRGCs in ferret and 19% of bRGCs in human (Kalebic et al., 2019).

## INTRODUCTION

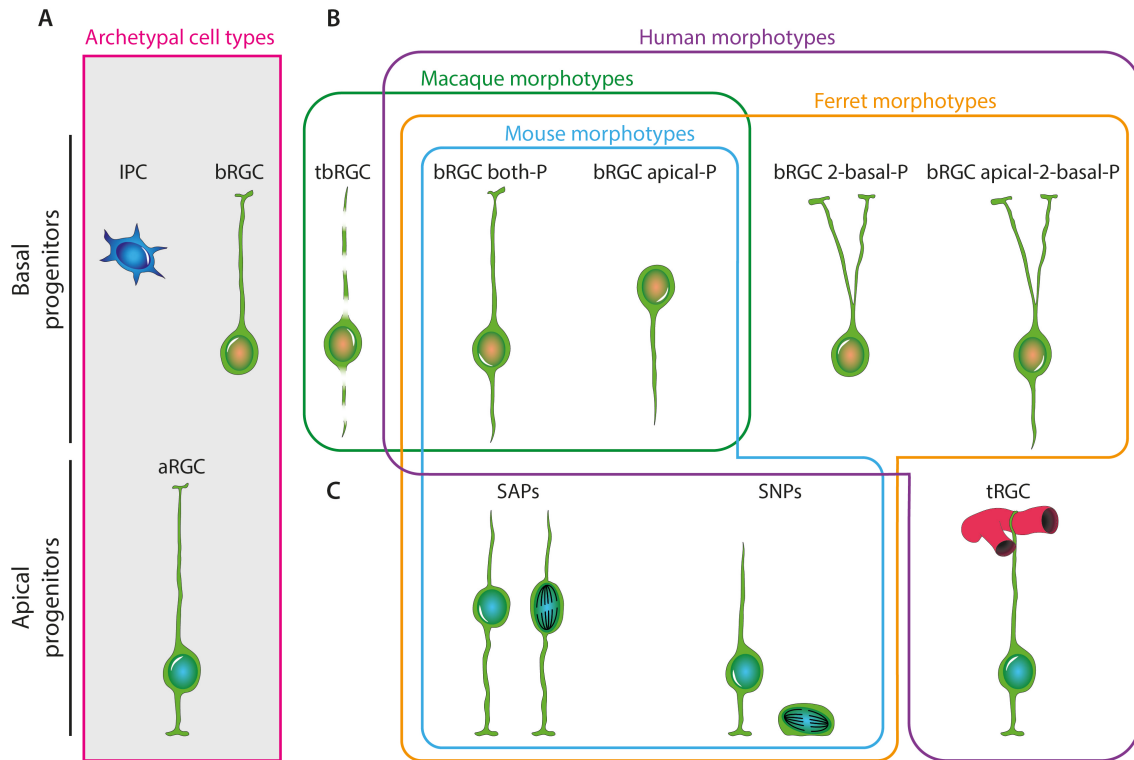


**FIGURE 2. Cortical progenitor cell types.** (A) Archetypal progenitor cells found in different proportions in mammals. (B) Specialized morphotypes of bRGCs identified in human (purple), macaque (green), ferret (orange) and/or mouse (blue). (C) Specialized morphotypes of apical progenitors found in human (purple), ferret (orange) and/or mouse (blue). IPC, intermediate progenitor cell; bRGC, basal radial glia cell; tbRGC, transient basal radial glia cell; bRGC both-P, basal radial glia cell with basal and apical processes; bRGC apical-P, basal radial glia cell with apical process; bRGC 2-basal-P, basal radial glia cell with bifurcated basal process; bRGC apical-2-basal-P, basal radial glia cell with apical and bifurcated basal processes; aRGC, apical radial glia cell; SAPs; subapical progenitors; SNPs; short neural precursors; tRGC, truncated radial glia cell. Adapted from [Del-Valle-Anton and Borrell, 2022](#).

On the other side, Pilz et al. in 2013, also characterized a new type of apical progenitors that carry out mitosis at a short distance from the ventricular surface but within the VZ parenchyma, named subapical progenitors (SAPs) ([Pilz et al., 2013](#)) (Fig. 2C). These are anchored to the ventricle but do not undergo INM, and exhibit diverse morphologies including bipolar. SAPs constitute a minority of the total number mitosis in mouse cortex at mid-neurogenesis, reaching 6%, however they represent 30% of ferret mitosis at the VZ by late neurogenesis ([Pilz et al., 2013](#)). Finally, Nowakowski and colleagues detected a new human aRGC morphotype that was named truncated RGC (tRGC) ([Nowakowski et al., 2016](#)) (Fig. 2C). These cells are in contact with the ventricular surface, as the archetypal aRGC,

but their basal process ends abruptly at the OSVZ or onto blood vessels running through the ISVZ. The basal fiber is sometimes horizontal to the ventricular surface. These cells express crystallin alpha B (CRYAB) and replace aRGCs by mid-neurogenesis (GW 17-18), when cortical layers II/III start their expansion (Sidman and Rakic, 1973). The RGC fiber discontinuity between the VZ and the CP may be behind the cortical folding in human (Nowakowski et al., 2016).

There are other progenitor morphotypes that have not been related to cortex folding, but that further enrich the developmental relationships between cortical cells. Among apical progenitors, whose soma is within the VZ and are in contact with the ventricular surface, we find short neural precursors (SNPs) (Fig. 2C). These progenitors have been described in mouse and ferret cortex, where they have a short basal process limited to the VZ (Gal et al., 2006; Stancik et al., 2010; Reillo et al., 2017), or, in the case of ferret, they completely lack a basal process (Reillo et al., 2017). The Haydar laboratory posits that these progenitors express tubulin alpha I (TUBA1) (Gal et al., 2006; Stancik et al., 2010). Unlike SAPs, SNPs retract their basal process during mitosis, which takes place at the apical surface, and mainly produce ENs by direct neurogenesis, becoming quickly depleted (Gal et al., 2006; Stancik et al., 2010). Human tRGCs and mouse and ferret SNPs have been suggested to be evolutionary related (Arai and Taverna, 2017).

Neuronal migration also has an impact on cortex folding. Newborn ENs use the basal process of RGCs as physical substrate to move radially through the cortical thickness (from the germinal zones (GZs) to the corresponding layer at the CP), a process called radial migration (Rakic, 1972). The arrangement of bRGCs in the ISVZ and OSVZ, without the adherens junctions that tightly hold aRGCs to the ventricular surface, allows these cells to have their cell bodies relatively nearby, while their basal processes contact the pial surface at very distant locations (Lui et al., 2011; Borrell and Reillo, 2012) (Fig. 3A). Hence, newborn ENs radially migrating on a bRGC process follow divergent trajectories, spreading tangentially along the CP (Reillo et al., 2011). This fan-shaped dispersion favors the local expansion of the cortical surface area and, thus, it facilitates the formation of folds (Reillo et al., 2011) (Fig. 3A). The emergence of tRGCs in the embryonic human

## INTRODUCTION

cortex by mid-neurogenesis leads to the formation of a gap between the VZ and CP, enhancing the divergent arrangement of radial glia fibers (Nowakowski et al., 2016). Additionally, the leading process of newborn neurons displays collateral branches, which are greater in number in ferret compared to mouse (Martínez-Martínez et al., 2019) (Fig. 3A, B). This allows the lateral displacement of migrating neurons from the basal process of the mother RGC to a neighboring one, mediating an even greater tangential dispersion of the migrating neuron (Lui et al., 2011; Gertz and Kriegstein, 2015; Martínez-Martínez et al., 2019) (Fig. 3A). In light of the recent characterization of bRGCs with a bifurcated basal process (Kalebic et al., 2019), this may represent a potential improvement to further promote neuronal dispersion.

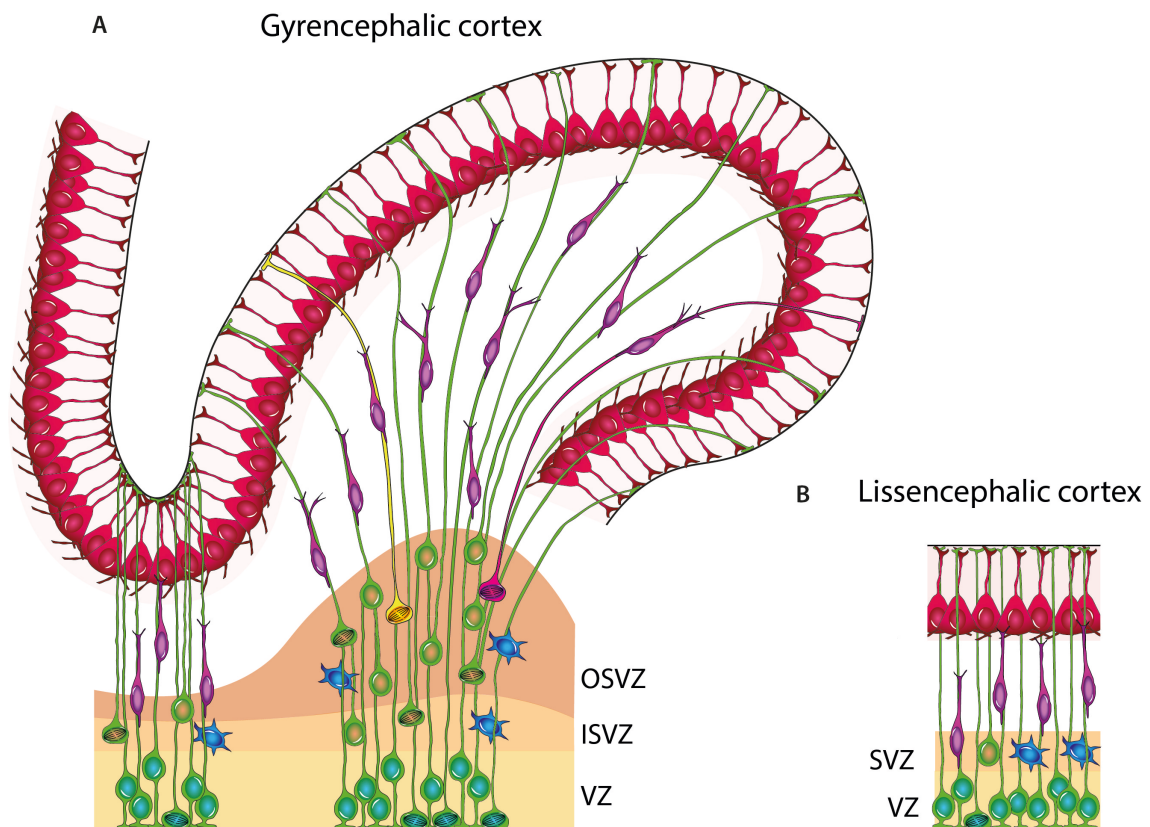


**FIGURE 3. Neuronal migration influence on cortical folding.** (A) Gyrencephalic mammalian cortex has a high proportion of bRGCs, whose close cell bodies (depicted in yellow and magenta) can project to distant pial surfaces, thereby forming the fan-shaped neuronal dispersion characteristic of gyri. Migrating newborn neurons at the gyri have a branched leading process that enables their lateral displacement between neighboring RGC processes. (B) Lissencephalic mammalian cortex comprises a low proportion of bRGCs and a high number of bipolar-shaped newborn neurons, thus promoting straight migratory trajectories. OSVZ, outer subventricular zone; ISVZ, inner subventricular zone; VZ, ventricular zone; SVZ, subventricular zone. Adapted from Del-Valle-Anton and Borrell, 2022.

The gestational period correlates with the length of cortical neurogenesis (Lewitus et al., 2014; Glatzle et al., 2017; Stepien et al., 2020). Longer gestational and neurogenic periods are observed in species that develop large-sized, folded brains (Kriegstein et al., 2006; Stepien et al., 2021). Moreover, the extended neurogenic period enables a disproportionate generation of ENs populating layers II/III/IV (called upper layers) with respect to layers V/VI (lower layers) (Sousa et al., 2017; Stepien et al., 2020; 2021). The expansion of upper layer neurons is especially remarkable in the primate cortex, followed by carnivores compared to rodents (Marin-Padilla, 1978; Hutsler et al., 2005; Molnár et al., 2006). The specific impairment of upper layer neuronal migration by cell division protein kinase 5 (CDK5) inhibition results in a decrease of cortical folding in ferret, while the same manipulation in lower layers does not have an effect on gyrification (Shinmyo et al., 2017).

All cellular mechanisms mentioned within this section are framed by the physical forces that rule brain expansion. The higher growth rate of the superficial neuronal layers with regard to the deep germinal layers triggers the tangential expansion of the former (Kroenke and Bayly, 2018; Garcia et al., 2018). These two regions display different viscoelasticity properties, related to their cellular and extracellular matrix (ECM) composition (Karlinski and Reiner, 2018; Amin and Borrell, 2020; Long and Huttner, 2022). The compression of this non-uniform cortical structure by intracortical mechanical forces facilitates its folding (Richman et al., 1975; Garcia et al., 2018).

#### **4. Genetic protomap of cortex folding**

Within the complexity entailing cortex folding, thousands of genes are expressed in a particular pattern along the cerebral cortex that is key for this process (Toro et al., 2017; Matsumoto et al., 2017b; Juan Romero et al., 2015). The presence of these genes along the germinal layers delineate the regions where future gyri or sulci will emerge, having opposite levels of expression in these areas (Toro et al., 2017; Matsumoto et al., 2017b; Juan Romero et al., 2015). Accordingly, this gene expression pattern was named *protomap of cortical folding*, emulating the

## INTRODUCTION

terminology from the protomap hypothesis that posited the representation of prospective cytoarchitectonic areas of the cortex at the early germinal layers (Rakic, 1988).

An example of differentially expressed genes (DEGs) between prospective gyrus and sulcus are fibronectin leucine rich transmembrane proteins 1 and 3 (*FLRT1/3*), two members of a family of cell adhesion molecules (Jackson et al., 2016; Toro et al., 2017). In the developing ferret cortex, *FLRT1/3* are more highly expressed in the most caudal fold where primary visual cortex is located, known as splenial gyrus (SG), compared to the neighboring lateral sulcus (LS) (Toro et al., 2017). A very significant distinction among these areas is at P0 in the OSVZ, prior to the onset of folding, which is even increased by P6, when folding is already visible in ferret cortex (Smart and McSherry, 1986; Toro et al., 2017). The disruption of *FLRT1/3* in mutant mice produces the ectopic development of sulci in their otherwise smooth cortex, by imbalancing cell-cell adhesion and speeding the migration of neurons to the CP (Toro et al., 2017).

Another group of genes that endorses the existence of a protomap of cortical folding is the fibroblast growth factor receptor (*FGFR*) family (Matsumoto et al., 2017b). *FGFR2/3* have a regional arrangement in the OSVZ at E40 in ferret cortex that coincides with the emerging gyri by P6 (Matsumoto et al., 2017b). The OSVZ cells containing *FGFR2/3* are predominantly bRGCs and *FGFR3* ablation in ferret cortex reduces their proliferation, leads to a decrease in upper layers thickness and, ultimately, a reduction in cortical folding (Matsumoto et al., 2017b).

Lastly, a gene with proven importance for cortical progenitors, *EOMES* (also known as *TBR2*), displays an expression pattern in accordance with the protomap of cortical folding (Englund et al., 2005; Toda et al., 2016; de Juan Romero et al., 2015). In ferret OSVZ dorsal and caudal cortices at P2, *EOMES* shows pre-folding modules of high expression (de Juan Romero et al., 2015) (Fig. 4A). When folding becomes discernible at P6, these modules overlay with the dorsal and caudal pattern of circumvolutions (Fig. 4B), with the highest levels corresponding again to the SG in the adult (de Juan Romero et al., 2015) (Fig. 4C). Similarly, the human

frontal lobe at GW 16 and ventral temporal lobe at GW 21, prior to the process of folding (Kinoshita et al., 2001), display significant variations in *EOMES* expression at neighboring germinal layers (de Juan Romero et al., 2015). On the contrary, *Eomes* is expressed in a continuous gradient in the lissencephalic mouse cortex (de Juan Romero et al., 2015) (Fig. 4D).

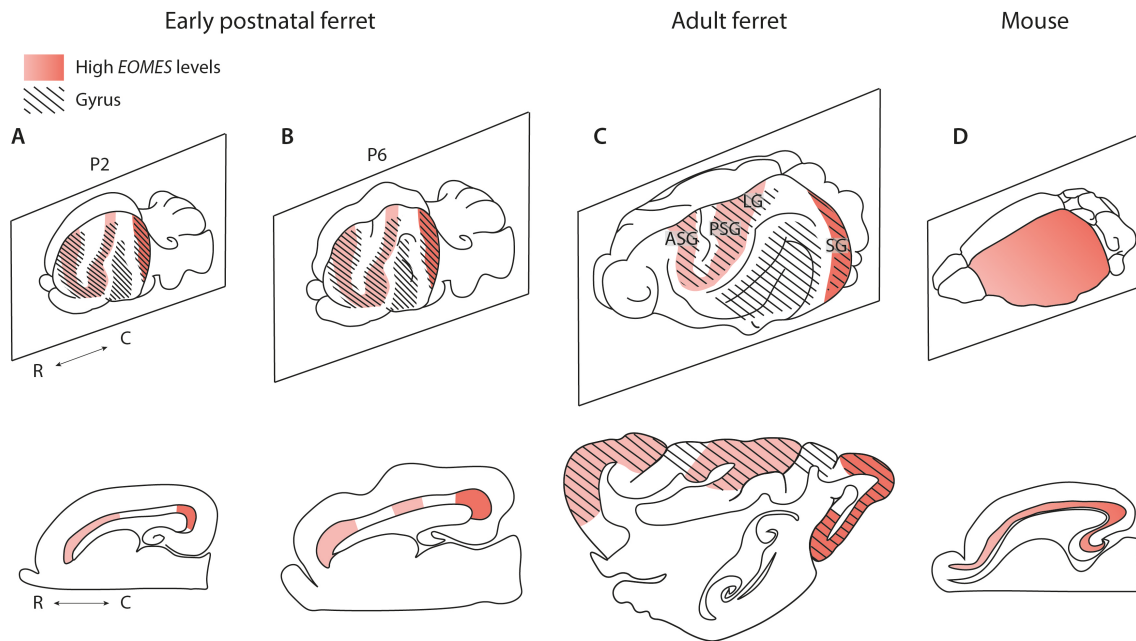


**FIGURE 4. *EOMES* protomap of cortical folding along ferret development.** (A) Schema from P2 ferret cortical surface and sagittal section showing the spatial correlation between *EOMES* expression (pink gradient) and the prospective cortical gyri (dashed lines). (B) Schema from P6 ferret cortical surface and sagittal section with emerging gyri overlapping *EOMES* expression. (C) Schema from adult ferret cortical surface and sagittal section showing the overlapping localization of *EOMES* expression with the ASG, PSG, LG and SG, with its highest expression within the most caudal gyrus. (D) Schema from mouse cortical surface and sagittal section exhibiting a continuous rostro-caudal gradient of *Eomes* expression. P, postnatal day; R, rostral; C, caudal; ASG, anterior sigmoid gyrus; PSG, posterior sigmoid gyrus; LG, lateral gyrus; SG, splenial gyrus. Adapted from Del-Valle-Anton and Borrell, 2022.

## 5. Ferret for cortical modeling

So far, we have described the cellular and genetic processes enabling cortex folding. On multiple occasions along the previous sections, we have found that human cortex development and folding is closer to ferrets than rodents (Smart and McSherry, 1986; Hutsler et al., 2005; Martínez-Cerdeño et al., 2006; Reillo et al.,

## INTRODUCTION

2011; Kelava et al., 2012; Pilz et al., 2013; Gertz et al., 2014; Gertz and Kriegstein, 2015; Juan Romero et al., 2015; Toda et al., 2016; Matsumoto et al., 2017b; Reillo et al., 2017; Shinmyo et al., 2017; Toro et al., 2017; Kroenke and Bayly, 2018; Kalebic et al., 2019; Martínez-Martínez et al., 2019). Although mice and rats are essential for scientific research, ferret is emerging as an invaluable model to understand processes of brain development seemingly unique to human or primates, absent in lissencephalic rodents.

Folding patterns across mammal phylogeny vary widely (Welker, 1990; Zilles et al., 2013). Primary folds are the first to form, are deep, simple and conserved across individuals from the same order, while secondary and tertiary folds are more superficial and whimsical (Welker, 1990; Budday et al., 2015; Garcia et al., 2018). The ferret is particularly valuable as a model for cortical folding because it only develops stereotyped primary folds, so that prospective folding regions can be identified before the process starts (Smart and McSherry, 1986; Welker, 1990). In addition, cortex folding occurs postnatally in ferrets, starting circa P5, so the physiological course of events and the researcher's capacity to influence them can be studied outside of the maternal womb (Smart and McSherry, 1986; Barnette et al., 2009; Sawada and Watanabe, 2012; Gilardi and Kalebic, 2021).

The well-conserved patterns of primary folds by mammalian orders, especially within monozygotic twins, lead to the notion that there is an important genetic control of cortex folding (Welker, 1990; Lohmann et al., 1999; Lohmann et al., 2008; Pizzagalli et al., 2020). The ferret genome has been sequenced and is publicly available for omics research, proving to be genetically closer to human than the mouse (Peng et al., 2014). This has driven my host laboratory (the Borrell lab) to take advantage of the stereotypic formation of the ferret SG and LS, and to deeply characterize the genetic and cellular mechanisms that lead to their formation (Reillo et al., 2011; Nonaka-Kinoshita et al., 2013; de Juan Romero et al., 2015; Reillo et al., 2017; Toro et al., 2017; Martínez-Martínez et al., 2019).

The genetic mechanisms of cortex folding can be studied in ferret thanks to the implementation of electroporation and viral vector delivery of DNA constructs,



first postnatally and then in utero (Borrell et al., 2010; Kawasaki et al., 2012a; Kawasaki et al., 2012b; Nonaka-Kinoshita et al., 2013; Martínez-Martínez et al., 2016). Transgenic ferrets have also been generated by somatic cell nuclear transfer (SCNT), but this technique can be inaccessible in terms of cost-effectiveness (Li et al., 2006; Sun et al., 2008). Recently, mutant ferrets have been generated by genome editing technologies such as transcription activator-like effector nuclease (TALEN) and clustered regularly interspaced short palindromic repeat (CRISPR)/CRISPR-associated 9 (Cas9) system (Johnson et al., 2018; Kou et al., 2015; Shinmyo et al., 2017; Yu et al., 2019; Güven et al., 2020).

The above-mentioned strategies open the door to carry out *in vivo* developmental studies of human malformations of cortical development (MCD) in ferrets. The emergence of multiple small folds (polymicrogyria), a simplified gyral pattern (lissencephaly) or smaller brain size with or without impact on gyral patterning (microcephaly) are some examples of disorders that have been successfully modeled in ferret (Bizzotto and Francis, 2015; Masuda et al., 2015; Matsumoto et al., 2017a; Matsumoto et al., 2018; Kou et al., 2015; Poluch and Juliano, 2015; Shinmyo et al., 2017; Matsumoto et al., 2017b; Johnson et al., 2018). Hence, these studies promote the use of animal models with naturally folded cortex to understand the etiology behind human brain development pathologies.

Other convenient characteristics for ferret housing such as their small size (average body weight 800g for females and 1,500g for males), their relatively short gestational period (39-42 days), and the abundant kits per litter (average of 8 kits, from late March to early August), end up making the ferret a very suitable research model for cortical folding (Lindeberg, 2008; Risi, 2014).

## **6. Technological race to describe single-cell diversity**

Since the first characterization of a cell by Hooke as a result of his improvement in compound microscopes (Hooke, 1665), scientists have always sought to develop new procedures to scrutinize cells. Histochemical stainings such as the silver impregnation from Golgi and Ramón y Cajal to describe cells from the nervous

## INTRODUCTION

system (Golgi, 1898; Ramón y Cajal, 1890), the invention of the electron microscope by Ruska and Knoll to access cell organelles (Knoll and Ruska, 1932), or the Sanger sequencing to determine cell genomic sequence (Sanger et al., 1977), are a few examples of the interwoven progress of cell biology and technology along history. Single-cell sequencing represents one of the last qualitative leaps forward in the study of cell diversity. It makes use of fast and affordable next-generation sequencing (NGS) technology for genetic profiling, and applies it to up to tens of thousands of individual cells per sample (Dai et al., 2022).

Single-cell sequencing methods start in 2009 with Tang and colleagues (Svensson et al., 2018; Zhang et al., 2022; Jia et al., 2022) (Fig. 5). Tang's method lies in the manual collection of a cell under the microscope, lyse it to obtain its messenger RNAs (mRNAs), retrotranscribe (RT) them into complementary DNAs (cDNAs), amplify them by polymerase chain reaction (PCR), construct a library and sequencing it (Tang et al., 2009). Since then, there has been an outbreak of procedures towards isolating and characterizing cell types in an automated and efficient manner, where the transcriptome has been the common currency (Svensson et al., 2018; Dai et al., 2022).

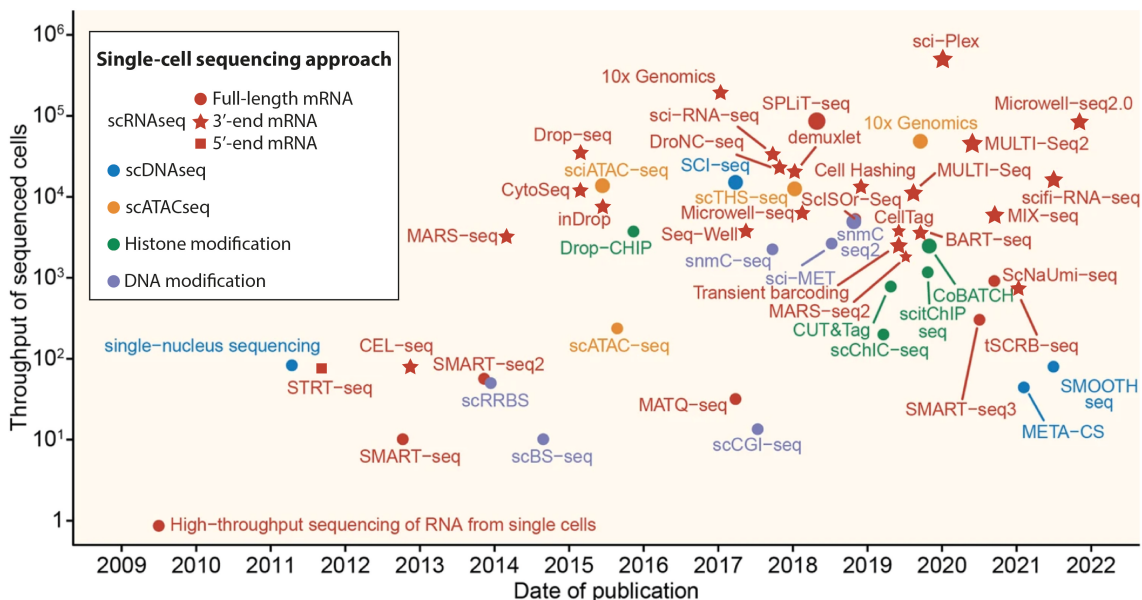


**FIGURE 5. Single-cell sequencing chronology.** Number of individual cells sequenced from 2009 to 2022 by single-cell transcriptome (red), genome (blue) and epigenome (orange, green and purple) state-of-art technologies. Key single-cell approaches are ordered by publication date. Adapted from Jia et al., 2022.

The single-cell RNA sequencing (scRNAseq) technologies can target full-length mRNAs or their 3' or 5' ends (Zhang et al., 2022; Jia et al., 2022) (Fig. 5). The two main approaches of cell isolation are split into: 1) Plate capture, normally by the use of fluorescence-activated cell sorting (FACS) or microfluidics [like the widely used technologies Smart-Seq (Switch Mechanism at the 5' End of RNA Templates sequencing; Ramsköld et al., 2012) or CEL-Seq (Cell Expression by Linear amplification and Sequencing; Hashimshony et al., 2012)] (Fig. 5). 2) Cell encapsulation in droplets [like Drop-seq (Droplet sequencing; Macosko et al., 2015) or 10x Genomics scRNAseq; Zheng et al., 2017)] (Fig. 5). The droplet-based technology is able to retain a larger number of cells with lower sequencing depth (Jia et al., 2022), but there is no prior knowledge of any feature required to select the cells. To do so, 10x Genomics scRNAseq conducts the individual cell lysis and polyadenylated (poly(A)) mRNA RT steps inside an oily emulsion where there is a gel bead (Zheng et al., 2017). This Gel bead-in-EMulsion (GEM) is shaped by a standard Illumina forward read coupled to a specific DNA barcode, a unique molecular identifier (UMI) and an oligomer deoxythymidine (oligo(dt)) tail (Zheng et al., 2017). The so-called 10x barcode is associated to all the cDNAs from the individual cell during the RT, while the UMI is exclusive to each of its mRNA molecules, helping latter to reduce PCR amplification noise (Zheng et al., 2017).

More recently, techniques directed to study genome, epigenome, proteome or metabolome have been implemented, and even spatially resolved, for single cells (Jia et al., 2022; Dai et al., 2022) (Fig. 5). As you are reading this, probably a new technique to study single cells from a different perspective is stemming from a scientist's head. Moreover, there is a clear trend to integrate multiple omics information to fully characterize a cell type in all its complexity (Dai et al., 2022). Undoubtedly, this will refine our definition of what is a cell type.

Developmental biologists want to unravel not only cell diversity but also the relationships between cells. Developmental trajectories towards a specific cell fate can be reconstructed from single-cell mRNA dynamics using prediction algorithms, such as Monocle or RNA velocity (Kester and van Oudenaarden, 2018; Trapnell et al., 2014; La Manno et al., 2018). Furthermore, Trapnell and colleagues introduced

## INTRODUCTION

the concept of “pseudotime” which gives each cell a value of the transcriptional change that it had underwent regarding its position towards the final cell fate in the trajectory (Trapnell et al., 2014). On the other side, lineage-tracing techniques are able to tag progenitor cells and connect them with their descendants (Kester and van Oudenaarden, 2018; Wagner and Klein, 2020). Live imaging of transgenic fluorescent reporters has long been the methodology to track progenitor cell divisions and their progeny behavior (Wagner and Klein, 2020). In recent years, there have arisen successful procedures that use limitless DNA barcodes to provide each progenitor with an exclusive heritable label for its clones that is compatible with NGS (Kester and van Oudenaarden, 2018). These new lineage approaches require genome editing to generate transgenic animals through retroviral/transposon integration, Cre-*loxP* recombination or CRISPR/Cas9 editing (Kester and van Oudenaarden, 2018; Wagner and Klein, 2020). TrackerSeq by means of the piggyBac transposon system electroporation has made this technique accessible for tagging mitotic progenitors in restricted brain areas (Bandler et al., 2022).

scRNAseq, developmental trajectories and lineage tracing technology has brought a significant progress for cortical development and evolution (Pollen et al., 2015; Nowakowski et al., 2017; Johnson et al., 2018; Polioudakis et al., 2019; Li et al., 2020). The heterogeneity of cortical cells is growing as new transcriptional features are being discovered (Johnson et al., 2015; Pollen et al., 2015; Nowakowski et al., 2016; Nowakowski et al., 2017). In mouse, different types of apical and basal progenitors have been sorted along a transcriptional continuum that occurs during neurogenesis (Telley et al., 2016; Yuzwa et al., 2017; Telley et al., 2019; Li et al., 2020). The accumulation of mRNAs in their cytoplasm further repressed before their translation into proteins, process known as transcriptional priming, has being proposed as the cause behind the overlapping (Yuzwa et al., 2017; Zahr et al., 2018; Li et al., 2020). Within the subtle differences between mouse progenitors, there is a key group of genes that leads newborn neuronal diversity through sequential transcriptional programs (Telley et al., 2016; Telley et al., 2019). For example, *Eomes* is behind the shift between apical to basal progenitors and the potential acquisition of a specific neuronal lineage identity (Li

et al., 2020). Final neuronal fate is also the result of their response to extracellular signals (Telley et al., 2019).

As in mouse, human developmental trajectories also show a continuous track towards neuronal differentiation (Polioudakis et al., 2019). Human progenitors have a window of time at the end of G1 cell-cycle phase from which they take a cell fate decision (e.g. aRGC  $\rightarrow$  aRGC + basal progenitor; or aRGC  $\rightarrow$  aRGC + neuron; or basal progenitor  $\rightarrow$  basal progenitor + neuron; etc) that they carry with them by displaying overlapping transcriptomes of the two different cell types until nearly the end of mitosis (Polioudakis et al., 2019). Human scRNAseq also showed crucial differences between progenitors that define their behavior (Pollen et al., 2015; Liu et al., 2016). In contrast to aRGC, bRGC contain high abundance of transcripts for growth factor production and membrane proteins that interact with ECM components and trigger intracellular cascades that ultimately reinforce their proliferative capacity (Pollen et al., 2015). RGC proliferation is also regulated by particular long non-coding RNAs (lncRNAs) (Liu et al., 2016). Moreover, human scRNAseq analyses uncovered the presence of *CRYAB* in apical progenitors for the first time, which definitely aided in the discovery of the new aRGC morphotype known as tRGC (Pollen et al., 2015; Nowakowski et al., 2016). The high proliferative capacity and this specialized progenitor morphotype are direct causes of human cortical expansion and folding (Pollen et al., 2015; Nowakowski et al., 2016).

So far, ferret scRNAseq data has only been published as a model of human respiratory and cortical disease (Lee et al., 2021; Johnson et al., 2018), due to the greater similarity between human and ferret cells compared to rodents in these two systems (Johnson-Delaney and Orosz, 2011; Johnson et al., 2015). Ferret modeling of microcephaly by knocking out (KO) abnormal spindle-like microcephaly-associated (*ASPM*) gene has been proved very valuable in the characterization of the developmental course of the disease (Johnson et al., 2018). KO ferrets showed an increase in IPCs and oligodendrocyte progenitor cells (OPCs), while the total number of RGCs was preserved (Johnson et al., 2018). Transcriptomically RGC types were indistinguishable; however, there was an early

## INTRODUCTION

delamination of aRGCs to the OSVZ, increasing bRGC proportion prematurely ([Johnson et al., 2018](#)). Misregulation of basal progenitor generation resulted in a smaller brain size ([Johnson et al., 2018](#)).

Despite the proven usefulness of ferret as a model for the study of cerebral cortex physiological development and its folding, there are no scRNAseq analyses or high throughput lineage studies addressing this topic.

**OBJECTIVES**

The main aim of this PhD project was to fully characterize the diversity of cells populating two germinal layers essential for cortical development: VZ and OSVZ. We also pursued the detailed description of the relationships between the main players within cortical expansion: RGCs and ENs. Finally, our intent was to study the conservation of the above features along mammalian phylogeny. To this end, we focused on the following specific objectives:

1. To build a single-cell transcriptomic atlas of ferret germinal layers at key developmental stages for cortical expansion and folding.
2. To identify markers for the main RGC types and validate them.
3. To reconstruct RGC transcriptomic trajectories towards generating cortical ENs, and validate their existence as lineages.
4. To conduct a comparative study of ferret cortical progenitor cell types with mouse and human using public single-cell datasets at equivalent developmental stages.
5. To investigate the conservation of ferret transcriptomic trajectories in mouse and human scRNAseq data.
6. To characterize the diversity of excitatory neurons in the developing ferret cortex and their relationship to human malformations of cortical development.





## **MATERIALS AND METHODS**

### **1. Animals**

Pregnant pigmented ferrets (*Mustela putorius furo*) were obtained from Euroferrets (Denmark) and kept on a 12:12-h light:dark cycle at the Animal Research Facility (SEA) of the Miguel Hernández University (UMH). All animals were treated according to Spanish and European regulations. Experimental protocols were approved by the Institutional Animal Care and Use Committee (IACUC) from the Spanish Council for Scientific Research (CSIC).

### **2. Brain extraction and microdissection**

For single-cell experiments, embryonic day (E) 34 ferret embryos were obtained by cesarean section of timed-pregnant females under deep anesthesia with sodium pentobarbital (Dolethal, Vetoquinol). E34 ferret embryos and postnatal day (P) 1 kits were anesthetized and decapitated. The brains were extracted; meninges, choroid plexus, cervical spinal cord and cerebellum were removed in cold Leibovitz's (1X) L-15 medium with L-Glutamine, without pH indicator (Gibco). Telencephalic hemispheres were split by the midline and embedded in 4% low melting agarose (SeaPlaque, Lonza) diluted in autoclaved phosphate buffered saline (PBS) (1X) within histology square molds (Peel-A-Way, Polysciences). Agarose blocks containing each brain hemisphere were vibratome-cut (Leica VT1000S) in ice-cold L-15 medium obtaining 300 $\mu$ m-thick sagittal slices. Living cortical slices were further microdissected under a dissecting scope equipped with transmitted illumination (Leica MS5) using microsurgical knives (MSP) in ice-cold L-15 medium. The VZ of E34 embryos and P1 kits, and the OSVZ of P1 kits, were isolated from the prospective SG and LS. The prospective SG was recognized as the region where the caudal end of the cortex curves back forming a 45<sup>o</sup> angle over the hippocampal region; LS was identified as the cortical region overlying the hippocampus immediately caudal to the dentate gyrus. The use of these landmarks as faithful indicators of LS and SG has been demonstrated previously by means of cell lineage tracing (Reillo et al., 2011; Borrell et al., 2010), dye tracing and tracking of the radial fiber scaffold in the developing ferret cortex (Reillo et al., 2011). We identified the VZ as the most cell-dense, opaque layer, extending from

## MATERIALS AND METHODS

the apical side of the cortex; the OSVZ was determined as the bottom half of a translucent zone located between two cell-dense layers: the apically located ISVZ and the basal CP (Fig. 1B). The microdissected tissue pieces were transferred to 2ml DNA LoBind tubes (Eppendorf) using a P20 pipette (Gilson) with RNase-free filter pipette tips (JETbiofil). Each E34 sample comprises the microdissected regions of 2 to 4 embryos from the same litter (n = 4 litters). P1 samples are composed of 1 animal per litter (n = 5 litters).

### **3. Single-cell suspension, cell concentration and sample viability**

Tissue pieces were enzymatically dissociated for 20-30min at 37°C using MACS Neural Tissue Dissociation Kit P (Miltenyi Biotec) according to the manufacturer's instructions. Cells were mechanically suspended using a wide-tipped, fire-polished Pasteur pipette (Fisher Scientific) followed by a P1000 pipette (Gilson). Cell suspensions were filtered to new 2ml DNA LoBind tubes (Eppendorf) through 40µm PluriStrainer Mini (PluriSelect), pre-wet with Hank's Balanced Salt Solution (1X) without CaCl<sub>2</sub>/MgCl<sub>2</sub>/pH indicator (HBSS, Gibco). Cells were centrifuged (Spectrafuge 24D, Labnet) 2 times for 5min at 1000rpm, and cell pellets were resuspended in 40µl of PBS pH7.4 (1X) without CaCl<sub>2</sub>/MgCl<sub>2</sub> (Gibco) containing 0.04% Bovine Serum Albumin (BSA, Sigma-Aldrich). Cell concentration from homogeneous suspensions was measured and cell death was estimated twice using trypan blue 0.4% stain (Thermo Fisher Scientific): first on an automatic cell counter (Countess II FL, Thermo Fisher Scientific) and second using a hemocytometer (BLAUBRAND Neubauer, BRAND) on an inverted microscope (Leica DM IL). Debris-free suspensions with cell viability over 90% used immediately for single-cell isolation.

### **4. Single-cell isolation and cDNA library preparation**

Cell suspensions from 400 to 1200 cells/µl were loaded into the Chromium Single Cell Controller (10x Genomics) to target a recovery from 7k to 10k cells/sample. Single-cell GEMs were generated, cells were lysed and the released RNAs were RT and barcoded inside the GEMs according to Single Cell 3' Reagent Kits v2 and v3 (10x Genomics) protocols. After GEMs break, barcoded cDNAs were pooled and cleaned from leftover RT reagents using DynaBeads MyOne Silane Beads

(Invitrogen), and amplified (8 to 14 cycles) according to Single Cell 3' Reagent Kits v2 and v3 (10x Genomics) protocols. Enzymatic fragmentation, size selection and cleanup with SPRIselect Reagent kit (Beckman Coulter) were followed by library construction compatible with standard Illumina sequencing constructs (12 to 16 total sample index cycles). All steps were performed according to Single Cell 3' Reagent Kits v2 and v3 (10x Genomics) protocols.

During the process, cDNA and library concentration and quality check (QC) were assessed using Bioanalyzer High Sensitivity DNA Kit (Agilent) and 2100 Expert Software (Agilent).

Libraries for a total of 18 samples (E34VZSG n = 3, E34VZLS n = 3, P1VZSG n = 3, P1VZLS n = 3, P1OSVZSG n = 3, P1OSVZLS n = 3) were generated.

## 5. Library sequencing

Libraries were sequenced in the Centre of Genomic Regulation (CRG; Barcelona, Spain) on an Illumina HiSeq2500 system with 1 sample/lane, paired-end (125bp R1 and R2 or 50bp R1 100bp R2) reads. QC on the raw sequence data was performed by FastQC-0.11.8.

## 6. Genome alignment

Ferret gene annotation from [Johnson et al., 2018](#), comprising Ensembl *Mustela putorius furo* annotation expanded with bulk RNAseq data, was further enriched with NCBI's RefSeq mitochondrial genes from *Mustela putorius furo* annotation release 101 and transformed from general feature format (GFF3) into gene transfer format (GTF) using Cufflinks-2.2.1 ([Trapnell et al., 2010](#)). Johnson's GenBank accessions were matched to RefSeq accessions through cthreepo-0.1.1 and gene\_name and transcript\_name attributes were added to GTF rows where they were missing by appending gene\_id and transcript\_id entries using Dylan Kotliar's code.

Cell barcodes were corrected, scRNAseq reads were mapped to NCBI ferret reference genome (MusPutFur1.0/GCF\_000215625.1) and UMIs were collapsed and corrected by STAR-2.7.3a ([Dobin et al., 2013](#)) adapting the parameters to v2 or v3 10x Genomics chemistry, depending on the sample.

### **7. Cell barcode filtering**

Count matrices from each sample were loaded and cell-containing droplets were identified and distinguished from empty droplets retaining ambient RNA by DropletUtils-1.6.1 (Lun et al., 2019). To achieve this, barcode ranks from the total UMI count were calculated and knee and inflexion points from the curve were established (Fig. S1A). Increased niters argument to 100,000, and decreased false discovery rate (FDR) to 0.1% were applied to all samples. A lower bound of 80 was implemented for replicates P1VZLS\_1 and E34VZSG\_1. Mitochondrial genes were removed before cell calling for replicates E34VZLS\_2, P1VZSG\_2, P1VZLS\_3, P1OSVZSG\_1 and P1OSVZLS\_1 to promote potential unhealthy cell removal using Aaron Lun proposal implemented by Alex Pickering's code. This reduced the differences between droplets containing broken cells and ambient RNA, and sharpened the distinction from healthy cell-containing droplets. The automatic retention of droplets with large total UMI counts (determined by the knee point) was disabled for replicate P1VZLS\_3. The distribution of p-values for the categorized empty droplets was computed for each sample (Fig. S1A).

### **8. Cell quality assessment**

Seurat-3.1.5 software (Stuart et al., 2019) was used to merge samples, add sample's metadata and further select high quality cells from the filtered cell barcodes. All cells included in this study had > 500 UMIs (Fig. S1C, E) and > 250 genes (Fig. S1D, E) per cell, and < 15% of reads mapping to mitochondrial genes (Fig. S1G). Genes were included if they were expressed in a minimum of 10 cells. An adaptive threshold was applied for the maximum number of genes, which consisted on keeping cells with < 3 standard deviations (SD) above the mean number of genes detected for each sample (Fig. S1B). This cell selection resulted in a total of 16,227 genes from 111,291 high quality cells retained for downstream scRNAseq analyses.

### **9. Normalization, regression and sample integration**

Samples were preliminarily evaluated for the effects of biological (litter, age, dissecting area, layer) and technical covariates (10x Genomics chemistry, sequencing batch, sequencing depth). Cell-cycle phase for differentiating cells was

assessed by assigning S and G2/M scores to normalized cell counts using an imported list of ferret cell-cycle stage markers and Seurat-3.1.5 (Stuart et al., 2019) 'CellCycleScoring' function.

The merged object was split into a list divided by batch with each litter as an element and normalization was performed along with regressing out cell-cycle difference between S and G2/M scores and mitochondrial mapping percentage variables by Seurat's 'SCTransform' (Hafemeister and Satija, 2019). 5,000 variable genes and scaled data output matrices containing variable and non-variable genes (return.only.var.genes = FALSE) were selected for downstream analyses. Sample integration was performed using 5,000 genes for anchoring (Stuart et al., 2019).

## 10. Clustering and resolution

Seurat-3.1.5 software (Stuart et al., 2019) was used to perform Principal component analysis (PCA) of the integrated dataset. An elbow plot of the SD from the first 100 Principal Components (PCs) was traced. The threshold identifying the majority of the sample's variation was established at 32PCs +/- 5PCs. K-nearest neighbors (KNN) graph construction for cell clustering was tested for 27, 32 and 37PCs, together with different resolutions (0.5, 0.8, 1.1, 1.4, 1.7, 2.1) using Seurat's 'FindNeighbors' and 'FindClusters' functions. Clustree-0.4.2 (Zappia and Oshlack, 2018) enabled the visualization of the relationships between clusters by the increasing resolution. Resolutions were ruled out when cells comprising one cluster were coming from > 2 clusters from the previous resolution or did not constitute an independent cluster in the following resolution. 37PC and 1.1 resolution values were selected for cell clustering (Fig. S2A). Results were visualized using t-distributed stochastic neighbor embedding (t-SNE) and uniform manifold approximation and projection (UMAP) dimensional reductions.

## 11. Cluster quality assessment

t-SNE plots were colored by metadata to check cell distribution using Seurat-3.1.5 software (Stuart et al., 2019). Although the great majority of cells were shuffled, and therefore free from confounding sources of unwanted variation, clusters 5, 12, 21 and 27 stood out for 10x Genomics chemistry (Fig. S2B), sequencing batch (Fig. S2C) and/or litter (Fig. S2D) variables. Further examination of these clusters

## MATERIALS AND METHODS

showed that indeed clusters 5, 12 and 27 did not include cells from all biological replicates from the same condition, but mostly cells from a single litter (Fig. S2E). These three cell clusters were considered litter-specific and were not included in downstream analyses (in grey in Fig. 1C, Fig. S3A).

PCA confirmed the removal of S/G2/M cell-cycle phase differences (performed as explained above: Normalization, regression and sample integration), while maintaining the distinction between cycling (S/G2/M) and non-cycling (G1) cells (Fig. S2F).

### 12. Cell type identity identification

Cluster composition was homogeneous across conditions, without clusters being specific to a certain age, layer or region; therefore cluster markers were computed by 'FindConservedMarkers' function in Seurat-3.1.5 (Stuart et al., 2019). In brief, this function firstly segregated cells by condition and then carried out differential gene expression analyses for each cluster against all others on the normalized data matrix from the object's RNA assay. Wilcoxon Rank Sum test was used together with the following parameters: only positive genes were reported (only.pos = TRUE), genes detected in  $\geq 10\%$  of the cells in either of the two compared cell groups were tested (min.pct = 0.1), and genes with a log<sub>2</sub> fold change (FC)  $\geq 0.25$  of average expression between the two compared cell groups were checked (logfc.threshold = 0.25). Gene-level p-values were calculated for each condition as well as a combined p-value across them. Top 20 markers by average FC with the largest p-value  $\leq 0.05$  across conditions were extracted for each cluster and evaluated to identify cell types. Canonical markers for known cell identities during cortical development were explored (Wonders et al., 2006; Martínez-Cerdeño et al., 2012; Cauli et al., 2014; Johnson et al., 2015; Pollen et al., 2015; Telley et al., 2016; Nowakowski et al., 2017; Yuzwa et al., 2017; Florio et al., 2018; Johnson et al., 2018; Lim et al., 2018; Mi et al., 2018; Mizrak et al., 2019; Polioudakis et al., 2019; Telley et al., 2019; Vaid and Huttner, 2020; Eze et al., 2021; Safran et al., 2022; Irvin et al., 2001; Attardo et al., 2008; Li and Zhang, 2009; Graczyk and Leśniak, 2014; Yamada et al., 2014; Azzarelli et al., 2015; Nowakowski et al., 2016; Aiken et al., 2017; Nemes et al., 2017; Rasmussen et al., 2017; Willems et al., 2018; Camargo Ortega et al., 2019; Kalebic et al., 2019; Bertacchi et al., 2020; Matsumoto

et al., 2020; Kyrousi et al., 2021). Identified cell types were assigned to the different clusters (Fig. S3B) and clusters 5, 12 and 27 were removed (as explained above: Cluster quality assessment), remaining a total of 101,811 cells.

### 13. DEG analyses and cluster enrichment

DEGs between two cell groups were obtained by Seurat's function 'FindMarkers' (Stuart et al., 2019) on the normalized data matrix from the object's RNA assay. This function constructed a logistic regression model out of the expression from each gene to predict cell membership and used a likelihood ratio to compare the built model to a null one where the cell membership does not depend on gene expression. Cell phase S and G2/M scores, mitochondrial mapping percentage, sequencing depth, 10x Genomics chemistry, sequencing batch and litter were selected as latent variables. Additionally, the following parameters were applied: positive and negative genes were reported (only.pos = FALSE), genes detected in  $\geq 10\%$  of the cells in either of the two compared cell groups were tested (min.pct = 0.1), and genes with a  $\log_2$  FC  $\geq 0.25$  of average expression between the two compared cell groups were checked (logfc.threshold = 0.25). The obtained DEG list was subsequently filtered (Fig. 1G, Fig. 6E, Fig. S5) by the following criteria: gene detected in  $\geq 44.5\%$  of cells from the first group (pct.1  $\geq 0.445$ ), gene difference  $\geq 14.5\%$  between the two groups (pct.1-pct.2  $\geq 0.145$ ),  $\log_2$ FC  $\geq 0.445$  of the average expression between the two groups (avg\_logFC  $\geq 0.445$ ) and p-value adjusted  $\leq 0.05$  based on Bonferroni correction using the total number of genes in the dataset (p\_val\_adj  $\leq 0.05$ ).

To identify cluster enrichment, the percentage of RGCs (Fig. 2A) or IPCs (Fig. S4C) per cluster for each replicate was normalized and  $\log_2$ FC from the mean between replicates for each cluster was calculated.

### 14. Subset analyses

Distinct subsets of the dataset were selected from the RGC or IPC-newborn EN clusters. The RNA assay was kept by the 'DietSeurat' function (Stuart et al., 2019) to be re-analyzed as detailed above (Normalization, regression and sample integration; Clustering and resolution; Cluster quality assessment; Cell type

## MATERIALS AND METHODS

identity identification; DEG analyses and cluster enrichment) with the following adjusted parameters:

P1 RGC clusters 8 and 16 (Fig. 2B-J, P-Q; Fig. S8A; Fig. S9-S13) – Integration nfeatures = 4000, Clustering dims = 1:26, resolution = 1.4, Cluster marker identification by 'FindAllMarkers', DEG filtering criteria 1) for cluster 8 or 16 VZ-OSVZ analyses and 2) for cluster 8 or 16 SG-LS enriched subcluster analyses (SG subclusters 1, 2, 9; LS subclusters 3, 4, 6): pct.1 >= 0.2, pct.1/pct.2 >= 1.45, p\_val\_adj <= 0.05, pct.2 <= 0.05 (for cluster 16 VZ-OSVZ comparison) and <= 0.1 (for cluster 8 LS-SG comparison), p\_val <= 0.05 (for cluster 16 OSVZ-VZ comparison), log2FC from the number of cells of each cluster per condition for each replicate.

IPC-newborn EN (Fig. 7, Fig. S20) – Normalization vars.to.regress = c("S.Score", "G2M.Score", "percent.mt"), Integration nfeatures = 4000, Clustering dims = 1:33, resolution = 1.4, Cluster marker identification by 'FindAllMarkers', QC cluster 21 removed, log2FC from the number of cells of each cluster per condition for each replicate, Canonical markers from [Krishna et al., 2009](#); [Molyneaux et al., 2009](#); [Rowell et al., 2010](#); [Zeng et al., 2012](#); [Toma and Hanashima, 2015](#); [Lake et al., 2016](#); [Nomura et al., 2018](#); [Di Bella et al., 2021](#); [Tutukova et al., 2021](#); [Safran et al., 2022](#); [Castellani et al., 1998](#); [Tarabykin et al., 2000](#); [Krajewska et al., 2002](#); [Uittenbogaard and Chiamello, 2002](#); [Demyanenko et al., 2004](#); [Oldham et al., 2008](#); [Dahlin et al., 2009](#); [de Olmos et al., 2009](#); [Jeong et al., 2009](#); [Brusés, 2010](#); [Hoeck et al., 2010](#); [McNair et al., 2010](#); [de Cárcer et al., 2011](#); [Hertel and Redies, 2011](#); [Huang et al., 2011](#); [Vallès et al., 2011](#); [Balamotis et al., 2012](#); [O'Dell et al., 2012](#); [Sato et al., 2012](#); [Tanaka et al., 2012](#); [DeBoer et al., 2013](#); [Gory-Fauré et al., 2014](#); [Matsumoto et al., 2014](#); [Azzarelli et al., 2015](#); [Johnson et al., 2015](#); [Pollen et al., 2015](#); [Fiorentino et al., 2016](#); [Lin and Lee, 2016](#); [Lin-Hendel et al., 2016](#); [Aiken et al., 2017](#); [Nowakowski et al., 2017](#); [Rasmussen et al., 2017](#); [van den Berg et al., 2017](#); [Baizabal et al., 2018](#); [Hasenpusch-Theil et al., 2018](#); [Johnson et al., 2018](#); [Mi et al., 2018](#); [Wang et al., 2018](#); [Cadwell et al., 2019](#); [Kalebic et al., 2019](#); [Khan et al., 2019](#); [Klingler et al., 2019](#); [Polioudakis et al., 2019](#); [Telley et al., 2019](#); [Han et al., 2020](#); [Popovitchenko et al., 2020](#); [Bedogni and Hevner, 2021](#); [Choi and An, 2021](#); [Kita et al., 2021](#); [Manganas et al., 2021](#); [Moon and Zhao, 2021](#); [Moreau et al., 2021](#); [Zhang et al., 2021](#); [Zhang et al., 2021](#); [Clark et al., 2022](#).



RGC with partial cell-cycle regression (Fig. S7A) – Integration nfeatures = 4000.

RGC with total cell-cycle regression (Fig. S7A) – Normalization vars.to.regress = c("S.Score", "G2M.Score", "percent.mt"), Integration nfeatures = 4000.

### 15. Cell-cycle regression analyses

Complete cell-cycle regression was performed on the full dataset during the normalization step [vars.to.regress = c("S.Score", "G2M.Score", "percent.mt")] in order to compare it with partial cell-cycle regression output (see Fig. S7B). Downstream analyses were carried out as detailed above (Normalization, regression and sample integration; Clustering and resolution; Cluster quality assessment) with the following adjusted parameters: Clustering dims = 1:42; resolution = 1.4; QC clusters 7, 17 and 30 removed.

Likewise, complete cell-cycle regression was performed on the RGC subset (Fig. S7A; for specific parameters see Subset analyses section).

### 16. Functional enrichment analyses

Pathway enrichment analyses were performed for the identified hub cell types using ReactomeGSA-1.8.0 (Griss et al., 2020), with Reactome database versions 79 and 80. For the subset of ferret P1 RGC clusters 8 and 16, (Fig. S9), ferret gene name nomenclature was standardized to capital letters. For the species integrated dataset (Fig. 5H, Fig. S17C), concurrent high-confidence orthologs in the three species were selected. Mean gene expression of the RNA-assay normalized data matrix for the compared cell groups was calculated and gene set variation analysis (GSVA) was performed. This analysis does not assign statistical significance for the enrichment of gene sets. Pathway-level expression values were sorted by the maximum difference between cell groups and the first 25 pathways were selected for heatmap plotting. PCA for the pathway-level expression values was run for the species dataset.

### 17. Trajectory analyses

Cells belonging to the glutamatergic neuronal lineage (from progenitor cells to EN; Fig. 1D) were selected. Clustering and partition metadata entries (monocle3\_clusters, monocle3\_partitions = 1) were assigned to the Seurat object for subsequent analyses with the Monocle package, and UMAP dimensional reduction for downstream 3D rendering was carried out. Seurat-Wrappers-0.3.0 was used to convert the RNA assay from the Seurat object into a CellDataSet (cde) class. Trajectories were constructed by 'learn\_graph' function from Monocle3-0.2.2.0 (Trapnell et al., 2014; Qiu et al., 2017; Cao et al., 2019) (Fig. 3A, B). Cells of origin for the trajectories were identified as the center of RGC clusters with the highest G2/M score using a graphical user interface (GUI). Monocle's pseudotime analyses ordered cells along the trajectories according to their progress through the neurogenic developmental program. For pseudotime analyses per condition (Fig. 3C, S15A), the Seurat object was split into conditions prior to cde construction.

To further characterize the pseudotime trajectories for each condition individually, the three replicates that constitute each condition were integrated as explained above (Cell quality assessment; Normalization, regression and sample integration: by replicate ("orig.ident")); Clustering and resolution: E34VZSG dims = 1:25 resolution = 1.4, E34VZLS dims = 1:37 resolution = 1.4, P1VZSG dims = 1:32 resolution = 1.1, P1VZLS dims = 1:40 resolution = 1.1, P1OSVZSG dims = 1:24 resolution = 1.1, P1OSVZLS dims = 1:24 resolution = 2.1; Cluster quality assessment) and pseudotime analyses were carried out (Fig. S15B-E).

To study DEGs dynamics over pseudotime trajectories, the common neuronal clusters that form part of the three trajectories identified in Fig. 3B were cut out from the analyses and clusters specific to trajectory 1, 2 or 3 were selected (Fig. S14). For this, DEGs were previously calculated in Seurat [filtering parameters: pct.1 >= 0.5, pct.2 <= 0.5, pct.1-pct.2 >= 0.345, avg\_logFC >= 0.445, p\_val\_adj <= 0.05, pct.1-pct.2 >= 0.055 (for trajectory1-trajectory2+3 comparison), avg\_logFC >= 0.345 (for trajectory1-trajectory2+3 comparison)], size factors were computed and gene names were added to cde.

Pseudotime examination was also performed for the IPC-newborn EN subset (Fig. 7C). Clusters 14 and 20 were excluded as they were found in different

partitions. Cells found at the center of clusters 9 and 10 (previous cluster 3 in the full ferret dataset; see Fig. 7A) were designated as the origin from the trajectory.

To build pseudotime trajectories for different species at comparable developmental stages (Fig. 6D-G; Fig. S19D, H), the integrated Seurat object with cells from ferret P1, human GW17-18 and mouse E15.5 (see Species dataset integration and DEG analyses; Cell downsampling) was analyzed as a whole or split into species metadata before cds construction.

### 18. Electroporation

E34 ferret embryos and P1 kits were electroporated following standard protocols as previously described ([Kawasaki et al., 2012b](#); [Borrell et al., 2010](#)). Briefly, for in utero electroporation (IUE) timed-pregnant females were deeply anesthetized with Isoflurane (IsoFlo, Eucuphar), the abdominal cavity was open, and the uterine horns were exposed. DNA solution (2.5 $\mu$ l) was injected into the lateral ventricle using pulled borosilicate glass capillaries (World Precision Instruments, 1B120F-4), and square electric pulses (75V; 50ms on, 950ms off, five pulses) were applied with an electric stimulator (Cuy21EDIT, Bex C. Ltd.) using round electrodes (CUY650P7, Nepa Gene). Uterine horns were placed back into the abdominal cavity, suture was closed, and the pregnant female was allowed to fully recover on a heating pad before returning to the home cage. For postnatal electroporation, kits were deeply anesthetized with Isoflurane, DNA solution (2.5 $\mu$ l) was injected into the lateral telencephalic ventricle with a glass micropipette through the skull, and square electric pulses were passed through the head (75V; 50ms on, 950ms off, five pulses) using the same electrodes.

For RGC labeling, plasmid concentrations were as follows: pCAG-FloxP-farnesylated-EGFP (1 $\mu$ g/ $\mu$ l), pCAG-Cre (10ng/ $\mu$ l).

For barcode lineage tracing, plasmid concentrations were as follows: pEF1a-pBase (1  $\mu$ g/ $\mu$ l; piggyBac-transposase; a gift from R. Platt), TrackerSeq library (2  $\mu$ g/ $\mu$ l) diluted in endo-free TE buffer and 0.002% Fast Green FCF (Sigma).

### 19. Analysis of barcoded cell lineages

TrackerSeq is a piggyBac transposon-based (Ding et al., 2005) library that was previously developed to be compatible with the 10x single-cell transcriptomic platform (Bandler et al., 2022). It records the *in vivo* lineage history of single cells through the integration of multiple oligonucleotide sequences into the genome. Each of these individual lineage barcodes is a 37bp long synthetic nucleotide that consists of short random nucleotides bridged by fixed nucleotides. This design results in a library with a theoretical complexity of approximately 4.3 million lineage barcodes ( $16^8$ ) with each barcode differing from another by at least 5bp. The barcode library was prepared as described in detail in (Bandler et al., 2022). We assessed the integrity of the TrackerSeq barcode library by sequencing to a depth of approximately 13 million reads to test whether any barcode was over-represented. A total of  $5 \times 10^6$  clusters of barcodes were identified, suggesting that the barcode library has a diversity that is at least in the  $10^6$  range.

E34 ferret embryos were electroporated with the piggyback-transposase and the TrackerSeq library. E37 embryos were obtained by cesarean section under deep anesthesia with sodium pentobarbital (Dolethal, Vetoquinol). Embryos were anesthetized and decapitated, the brains were extracted, telencephalic hemispheres separated in ice-cold Leibovitz's (1X) L-15 medium with L-Glutamine (Gibco), and blocks of caudal cerebral cortex containing EGFP+ cells including the prospective SG and LS were obtained with microsurgical knives (MSP) in ice-cold L-15 medium. Tissue pieces were enzymatically dissociated using papain (Worthington, LK003150) with DNase at 37°C for 20min. Earle's Balanced Salt Solution (EBSS, from the Worthington kit) was added to the digested tissue, and the mixture was triturated with a 10ml plastic pipette. Reconstituted Worthington inhibitor solution and DNase solution were added and gently mixed. Cells were pelleted by centrifugation at 300g for 5min at room temperature (at RT), resuspended in ice-cold L-15 medium containing 5% Fetal Bovine Serum (FBS), and were filtered to DNA LoBind tubes (Eppendorf) through 40µm PluriStrainer Mini (PluriSelect). Positive cells were isolated by flow cytometry using a BD FACSAria II Cell Sorter (BD, FACSDiva Software, version 6.1.3) with an 85µm nozzle. EGFP-positive cells were collected into BSA (Sigma-Aldrich)-precoated 2ml DNA LoBind tube for downstream processing on the 10x Genomics Chromium

platform. After sorting, 80,000 cells were divided into 4 samples and loaded onto 10x Genomics Chromium platform for GEMs and cDNA generation carrying cell- and transcript-specific barcode using the Chromium Next GEM Single Cell 3' Reagent Kit v3.1 with Feature Barcoding technology (PN-1000121) following the manufacturer's protocol (document number CG000205, 10x Genomics). Uniquely barcoded RNA transcripts were RT. 3' Gene Expression libraries were generated according to manufacturer's user guide with use of Chromium Library v3.1 kit (PN-1000121) and Dual Index Kit TT Set A (PN-1000215) (10x Genomics). Libraries were quantified with Agilent BioAnalyzer. The TrackerSeq lineage libraries were retrieved from cDNA. 10µl of cDNA were amplified with Q5 polymerase (NEB, M094S) in a 50µl reaction as described like in (Bandler et al., 2022). Libraries were purified with a dual-sided selection using SPRIselect (Beckman Coulter, B23318), and quantified with Agilent BioAnalyzer. Transcriptome and TrackerSeq barcode libraries were sequenced on an Illumina NovaSeq at the NGS Facility of the Max Planck Institute of Biochemistry (Munich, Germany).

FASTQ files for both transcriptome and barcoded sequences were obtained by bcl2fastq-2.20.0.422 (Illumina). For barcoded lineage preprocessing, TrackerSeq pipeline was used (<https://github.com/mayer-lab/TrackerSeq>). Raw barcoded sequence reads were trimmed by BBDuk-38.68 (Bushnell et al., 2017). Whitelist of cell barcodes and barcode extraction from sequence reads were obtained by UMI-tools-1.1.2 (Smith et al., 2017). After that, barcode-extracted FASTQ files were processed to generate sparse matrix with cell barcodes in rows and clone ids in columns. For further analysis, only Cell-UMI-Barcode triples with at least 10 reads and Cell-Barcode pairs with at least 9 UMIs were selected. Instead of the previously described clustering approach using Jaccard distance (Wagner et al., 2018; Bandler et al., 2022), we used a network-based approach to assign cells to their corresponding clones. Using the sparse matrix as input, an undirected network was built between cell barcodes (i.e. cells) as nodes, which are connected if at least one lineage barcode is present in both cells. After building the network we calculated connected components. Each connected component represents one clone. This approach requires fewer computational resources compared to the original method, and thus it can be applied to large datasets.

## MATERIALS AND METHODS

For lineage transcriptome preprocessing, 10x compatible expression matrices were generated by STARsolo in STAR aligner (Dobin et al., 2013) with specified parameters: `--soloType CB_UMI_Simple`, `--soloCBstart 1`, `--soloCBlen 16`, `--soloUMIstart 17`, `--soloUMIlen 12`, `--soloCBmatchWLtype 1MM_multi_Nbase_pseudocounts`, `--soloUMIfiltering MultiGeneUMI_CR`, `--soloUMIdedup 1MM_CR`, `--clipAdapterType CellRanger4`, `--outFilterScoreMin 30`, `--outSAMtype BAM SortedByCoordinate`, `--outSAMattributes CR UR CY UY CB UB`. These parameters are designed to ensure that STARsolo is as close as possible to the 10x compatible output of the Cell Ranger application. After obtaining the expression matrices, empty and pseudo drop cells were filtered by DropletUtils using 'emptyDrops' functions with 100,000 iterations and min UMI count < 500 (Lun et al., 2019). Finally, clone ids were matched with cell barcodes in transcriptome dataset and included into metadata of corresponding samples. Out of 51,006 EGFP-positive cells we filtered 15,326 cells with lineage barcodes. We have excluded from our analysis a clone that consisted of approximately 4,000 cells, as it was likely formed by low-quality cells present in our dataset. After these pre-processing and filtering steps, we obtain 11,933 single cell clones and 1,413 multi-cell clones.

Transcriptomic counts were pre-processed in a similar fashion as above. Briefly, cells were filtered for number of counts, number of features and percentage of mitochondrial reads (`nCount < 10,000`, `nFeature > 1,000`, `percent.mt < 5`), followed by log-normalization. We used DoubletFinder (McGinnis et al., 2019) to exclude putative doublets from the dataset. We used the Seurat workflow to identify highly variable features, scale log-normalized counts, and regress out read depth and the difference between S and G2/M scores (Stuart et al., 2019). We performed PCA and cells were embedded using UMAP algorithm as implemented in Seurat (Satija et al., 2015; Butler et al., 2018; Stuart et al., 2019; Hao et al., 2021). Expression of established marker genes was used to check for major cell types. Cells were annotated using correlation-based label transfer (Stuart et al., 2019) using the previous scRNAseq experiment as reference. Prior to label transfer we excluded all non-neuronal and inhibitory clusters from the reference set, to enable a more precise label transfer. Lineage coupling z-scores and correlations were

calculated as implemented in (Bandler et al., 2022). Lineage coupling correlation scores were visualized using Cytoscape (Shannon et al., 2003).

To infer heterogeneity of ENs originating from distinct RGC-populations (RGC-As or RGC-Bs), clones containing only cells in the more mature ENs (cluster 1 + 7) and cells in either RGC-As (clusters 23 + 11) or RGC-Bs (22 + 9) were identified. PCA was performed with scaled gene expression values from ENs and DE analysis was applied to ENs. DE analysis yielded 160 DEGs. To check if the number of DE-genes is significantly more than you would expect by chance, we performed a permutation test, by randomly sampling clone group labels.

## 20. Species dataset integration and DEG analyses

Raw counts and cell metadata from *Homo sapiens* (Polioudakis et al., 2019; GW17-18, GZ microdissected away from the CP, Drop-seq technology) and *Mus musculus* (Li et al., 2020; E15.5, whole cortex, ddSEQ technology) were downloaded.

High-confidence orthologous genes between human-ferret and human-mouse were selected for downstream analyses: 1) Dataframes containing gene names from ferret and downloaded human and mouse datasets were generated. 2) Ensembl datasets 'hsapiens\_gene\_ensembl', 'mpfuro\_gene\_ensembl' and 'mmusculus\_gene\_ensembl' were obtained from BioMart database thru 'useMart' function using biomaRt-2.42.1 (Durinck et al., 2005; Durinck et al., 2009). 3) Homologous genes between human-ferret and human-mouse, and their characteristics, were extracted from Ensembl datasets in accordance with different ferret and mouse attributes by biomaRt 'getLDS' and 'getBM' functions (Ensembl 104: 11,615 ferret entries and 13,779 mouse entries). 4) High-confidence orthologs were excerpted from the homolog lists of genes in line with the Ensembl criteria: 1:1 orthologs; last common ancestor/minimum gene order conservation (GOC) score/minimum whole genome alignment (WGA) coverage/minimum % target gene identical to query human gene/minimum % human query gene identical to target gene = *Bilateria*/\_/\_/25%/25%, *Chordata*/\_/\_/25%/25%, *Vertebrata*/\_/\_/25%/25%, *Gnathostomata*/\_/\_/25%/25%, *Euteleostomi*/50/50/25%/25%, *Sarcopterygii*/50/50/25%/25%, *Tetrapoda*/50/50/25%/25%, *Amniota*/50/50/25%/25%,

## MATERIALS AND METHODS

*Mammalia/75/75/50%/50%*, *Theria/75/75/50%/50%*,  
*Eutheria/75/75/50%/50%*, *Boreoeutheria/75/75/50%/50%*,  
*Euarchontoglires/75/75/50%/50%* (9,671 ferret genes and 3,366 mouse genes).  
5) Gene names from ferret and mouse datasets that were determined as high-confidence orthologs were replaced by human HGNC [HUGO (Human Genome Organization) Gene Nomenclature Committee] gene names or human Ensembl ids (in the lack of gene names), and ferret and mouse genes without a high-confidence ortholog were added a f- or a m- prefix respectively.

Ferret Seurat object was cleaned by 'DietSeurat' from the previously generated SCT and Integrated assays before genes from ferret and mouse Seurat objects were renamed using 'RenameGenesSeurat' function from Seurat.Utills. The CP from the human Seurat object was discarded for downstream analyses and the cell-cycle scores were assigned to the mouse dataset as explained above (Normalization, regression and sample integration). Lastly, metadata from the different species was labeled to match between datasets before merging them.

The merged object was split into a list divided by batch with each subject (i.e. human donor, mouse replicate or ferret litter) as an element. Normalization, regression and sample integration steps were performed as explained above. Clustering and resolution were established as 23PC and 1.1 (Fig. 5B) following the process explained previously (Clustering and resolution). The distribution of previous cluster labels given in [Polioudakis et al., 2019](#) and [Li et al., 2020](#) was explored on the integrated dataset as a control of integration (Fig. S17B).

DEG analyses of the concurrent high-confidence orthologs in the three species for integrated cluster (iCl.) 4 and iCl. 12 were performed as explained above (DEG analyses and cluster enrichment) with cell phase S and G2/M scores, mitochondrial mapping percentage and sequencing depth as latent variables. The following filtering criteria were applied: for upregulated genes  $pct.1 \geq 0.445$ ,  $pct.1 - pct.2 \geq 0.145$ ,  $avg\_logFC \geq 0.445$ ,  $p\_val\_adj \leq 0.05$ ; for downregulated genes  $pct.2 \geq 0.445$ ,  $pct.2 - pct.1 \geq 0.145$ ,  $avg\_logFC \leq -0.445$ ,  $p\_val\_adj \leq 0.05$ . Common upregulated genes between two of the species against the third one were obtained. Additionally, DEG analyses using 'FindConservedMarkers' function and "species" as grouping variable as explained before (Cell type identity identification) were carried out with Wilcoxon Rank Sum test and logistic



regression model to acquire common upregulated genes between the three species at the same time. An adjusted p-value  $\leq 0.05$  (mouse\_p\_adj\_val, human\_p\_adj\_val, ferret\_p\_adj\_val  $\leq 0.05$ ) was used as subsequent filtering criteria. Stacked violin plots from the top 10 genes from each comparison were produced from the scaled data using Ming Tang's code (Fig. S17D).

Dataset integration from the different species including only P1 ferret cells was also performed as explained in this section with the following specific parameters (Fig. 6A): Clustering dims = 1:24, resolution = 1.4, Cluster marker identification by 'FindAllMarkers', QC cluster 32 removed, log2FC from the number of cells of each RG cluster per species for each replicate.

## 21. Pseudobulk expression analyses

Clusters from progenitors in G1 cell-cycle phase and neurons were selected from the ferret dataset. A vector for canonical markers from human apical, basal or pan-RGCs from scRNAseq bibliography of cortical development was created (Pollen et al., 2015; Nowakowski et al., 2017; Polioudakis et al., 2019). Average gene expression of the normalized and scaled data matrix from the RNA assay for the selected clusters coming from different isolated germinal layers was calculated. Heatmap with expression level values was plotted for each gene using pheatmap-1.0.12.

## 22. Cell downsampling

Cells from our current P1 ferret (65,413 cells) and human available (Polioudakis et al., 2019; 17,136 cells) datasets were downsampled to match mouse dataset (Li et al., 2020) cell number (5,777 cells) before being merged. In order to achieve this, two methods were carried out using 'subset' function from base with different identity arguments and downsample cell numbers: 1) Random downsampling – To randomly select cells from the set of all cells in the dataset so the total number of cells is 5,777 cells. It produces a proportional decrease of all clusters. 2) Threshold downsampling – To randomly select cells from each identified cell cluster in the dataset so the maximum cells per cluster does not exceed 614 cells for human (that has 16 identified clusters in Polioudakis et al., 2019 dissected GZ) or 230 cells for

## MATERIALS AND METHODS

ferret (that has 26 identified clusters in this study). It results in a reduction of size from the most populous clusters.

Random downsampling resulted in a total of 17,331 cells (ferret 5,777 cells + human 5,777 cells + mouse 5,777 cells). Threshold downsampling resulted in a total of 17,319 (ferret 5,764 cells + human 5,778 cells + mouse 5,777 cells). Random or threshold downsampled cells were subsequently merged and analyzed as detailed above (Species dataset integration and DEG analyses) with the following adjusted parameters:

Random downsampling – Clustering dims = 1:16, resolution = 1.4, Cluster marker identification by 'FindAllMarkers', log2FC from the number of cells of each RG cluster per species for each replicate.

Threshold downsampling – Clustering dims = 1:19, resolution = 1.7, Cluster marker identification by 'FindAllMarkers', log2FC from the number of cells of each RG cluster per species for each replicate.

### **23. Analysis of MCD genes**

Databases from genes linked to MCD were explored ([Bizzotto and Francis, 2015](#); [Breuss et al., 2015](#); [Breuss et al., 2017](#); [Romero et al., 2018](#); [Ferent et al., 2020](#); [Oegema et al., 2020](#); OMIM database). Gene lists of cortical malformations markers for polymicrogyria (PMG; n = 53 genes), lissencephaly (LIS; n = 36 genes) and/or microcephaly (n = 10 genes) (total genes without repetitions = 96), were supplied to 'AddModuleScore' function from Seurat. This function calculated the enrichment of the provided gene set with regard to a randomly selected set of control genes and it assigned a gene score to each cell. Feature maps highlighting the clusters that might be susceptible to MCD were plotted by 'FeaturePlot\_scCustom' function using scCustomize-0.7.0.

### **24. Tissue processing for ICC, conventional ISH and FISH**

E34 ferret embryos were obtained by cesarean section of timed-pregnant females upon deep anesthesia with sodium pentobarbital (Dolethal, Vetoquinol). E34 embryos and P1-P6 kits were deeply anesthetized and perfused transcardially with ice-cold 4% paraformaldehyde (PFA, Sigma-Aldrich) in phosphate buffer (PB) pH7.4 with a peristaltic pump (Minipuls 3, Gilson).

P1 and P3 brains for immunocytochemistry (ICC) were extracted and postfixed in 4% PFA. Then, brains were cryoprotected in 30% sucrose (PanReac AppliChem) and sectioned. Brain sections were incubated with primary antibodies overnight (o.n.), followed by appropriate fluorescently conjugated secondary antibodies and counterstained with 4',6-diamidino-2-phenylindole (DAPI; Sigma-Aldrich, D9542). Primary antibodies used were against GFP (1:1000; Aves Lab, GFP-1020), anti-Cryab (1:500; Abcam, ab13496) and anti-Laminin (1:500; Merck Millipore, AB2034). Secondary antibodies were from Jackson ImmunoResearch [Alexa Fluor 488 anti-chicken IgY (1:250; 703-545-155)], and from Invitrogen [Alexa Fluor 555 anti-mouse IgG (1:250; A31570) and Alexa Fluor 488 anti-rabbit IgG (1:250; A21206)].

For clarification experiments, electroporated brains were immunostained and cleared using the iDisco+ protocol as described in (Renier et al., 2014). Briefly, individual brain hemispheres were incubated at 37°C for 7 days (P2) or 10 days (P6) with anti-GFP antibodies (1:1000, Aves Lab, GFP-1020), and 4 days (P2) or 7 days (P6) with appropriate Alexa Fluor 647-conjugated secondary antibodies (1:500, Jackson ImmunoResearch Labs, 703-605-155).

Brains for conventional *in situ* hybridization (ISH) were extracted in ice-cold PBS (1X), split by the midline and postfixed at 4°C for 72hr in 4% PFA (E34) or 4% PFA and 30% Sucrose (PanReac AppliChem) (P1). Brains for fluorescent ISH (FISH) by means of RNAscope, were dissected and postfixed at 4°C for 6 days in 4% PFA (E34 and P1). Brains were then sagittal-sectioned and handled as follows: E34 ISH brains were embedded in 4% low melting agarose (SeaPlaque, Lonza) diluted in PBS (1X) within histology square molds (Peel-A-Way, Polysciences) and vibratome-cut (Leica VT1000S) in PBS (1X) at 50µm thickness; P1 ISH brains were frozen and cryotome-sectioned (Leica SM2010R) at 50µm; E34 and P1 samples for FISH were frozen in embedding medium for frozen tissue (Neg-50, epreDia) by means of liquid nitrogen and iso-pentane (vwr), and cryostat-sectioned (Leica CM1860 UV) at 30µm on Superfrost Plus slides (epredia).

## 25. Constructs

For ISH, ferret RNA was extracted using RNeasy Mini Kit (Qiagen) and RT by Maxima First Strand cDNA Synthesis Kit (Thermo Fisher Scientific). Selected genes

## MATERIALS AND METHODS

were amplified by PCR using GoTaq G2 Flexi DNA Polymerase (Promega) with the following primers:

*CRYAB*-fw 5'-AGCTAGTGAAACAAGACCAGGA-3'

*CRYAB*-rv 5'-ACCATGTTTCATCCTGACGCT-3'

*EOMES*-fw 5'-ACTGGTTCCTACTGGATGAGAC-3'

*EOMES*-rv 5'-CTTCGCTCTGTTGGGGTGAAAGG-3'

*HOPX*-fw 5'-ACTCAGCTTCCAGATCCAGG-3'

*HOPX*-rv 5'-TTTTGACTCCCAGCCTGACT-3'

*NDFIP1*-fw 5'-ATTTCCAAAGCCGCCTTCCT-3'

*NDFIP1*-rv 5'-AAGACTGCCCCCTACTGACT-3'

*PAX6*-fw 5'-AGCATGCAGAACAGTCACAGC-3'

*PAX6*-rv 5'-GGCAAACACATCTGGATAATGG-3'

*PSMB1*-fw 5'-TCTCGCCCTACGCTTTCAAC-3'

*PSMB1*-rv 5'-CACACTGCTTACTTCAGCCTTT-3'

*SLC1A3*-fw 5'-CTTCCGCGCTACAAAACCAG-3'

*SLC1A3*-rv 5'-CAGAGGGGCGTACCACATTA-3'

The resulting amplicons were purified with illustra GFX PCR DNA and Gel Band Purification Kit (GE Healthcare) and cloned into pGEM-T Easy Vector System (Promega).

## 26. ISH

Plasmids containing ferret clones were linearized, purified, and sense or anti-sense complementary RNA (cRNA) probes were transcribed with T7 or SP6 RNA polymerases (Roche) and labeled with digoxigenin (DIG) RNA labeling Mix (Roche) according to the manufacturer's instructions. Correct probe size was verified by 1% agarose (Agarose D1 Low EEO, Condalab) electrophoresis gel.

Free-floating brain sections were mounted on Superfrost Plus slides (epredia) in RNase-free (Diethyl pyrocarbonate (DEPC), Sigma-Aldrich) PBS, and dried at 37°C for 4h. Sections were fixed with 4% PFA (Sigma-Aldrich) in PB pH7.4 for 10min and washed with RNase-free PBS, before being treated with proteinase K (10µg/ml) (Invitrogen) in RNase-free PBS-T (Tween20, Sigma-Aldrich) for 5min. After a new step of fixation and permeabilization with RNase-free PBS-T, brain sections were pre-hybridized in a humidified chamber for 1h at 62°C in tempered

hybridization buffer [50% Formamide (deionized) (Ambion); 10% Dextran sulfate sodium salt from *Leuconostoc* spp. (Sigma-Aldrich); salt solution (1X) containing 200mM NaCl, 10mM TrisHCl, 1mM Tris base, 50mM NaH<sub>2</sub>PO<sub>4</sub>·2H<sub>2</sub>O, 50mM Na<sub>2</sub>HPO<sub>4</sub>, pH 7.5; Denhardt's solution (1X from a 50X stock) (Sigma-Aldrich); 0.7mg/ml yeast transfer RNA (tRNA, Invitrogen)]. Then, brain slices were hybridized in a humidified chamber with denatured DIG-labeled cRNA probes diluted in hybridization buffer o.n. at 62°C. After sections were heavily washed [50% Formamide (Sigma-Aldrich); 0.5% Tween20; Saline sodium citrate (SSC) buffer (0.5X from a 20X stock) (Sigma-Aldrich)], they were incubated with blocking solution [Maleic acid buffer containing Tween20 (MAB-T) (1X); 10% sheep serum (Sigma-Aldrich); 10% Blocking Reagent (Roche)] in a humidified chamber for 1h at RT. Next, sections were incubated with anti-DIG alkaline phosphatase-coupled Fab fragments in blocking solution (1:3500, Roche) in a humidified chamber o.n. at 4°C. Slides were thoroughly washed with MAB-T (1X) and 2 times 10min washed with pre-staining NTMT buffer (1X) [100mM NaCl; 100mM TrisHCl pH 9.5; 50mM MgCl<sub>2</sub>; 0.5% Tween20], before revealed with developing solution [0.05mg/ml Nitrotetrazolium Blue chloride (NBT, Sigma-Aldrich); 0.18mg/ml 5-Bromo-4-chloro-3-indolyl phosphate p-toluidine salt (BCIP, Roche) in NTMT buffer (1X)]. Once the cRNAs were visible, brain sections were incubated in TE buffer [50mM TrisHCl pH 7.5; 1mM EDTA pH8.0], fixed for 5min with 4% PFA in PB pH7.4, washed again with TE buffer, dehydrated and coverslipped using Eukitt mounting medium (Fluka). Each probe was assayed on P1 (n = 2) and E34 (n = 1) animals.

## 27. FISH

Ferret probes were acquired from ACD biotechne catalog (<https://acdbio.com/species-common/domestic-ferret>): Mp-NFIA-C2 (#586521); Mp-NFIX (#586541); Mp-PAX6-C3 (#513391); and 3-plex Negative Control Probe (#320871); or designed upon request.

The RNAscope Multiplex Fluorescent Detection Kit v2 (ACD), Pretreatment Reagents (ACD), RNAscope Multiplex TSA Buffer (ACD) and RNAscope Wash Buffer Reagents (ACD) were used according to the manufacturer's instructions. Briefly, slides from frozen tissue were washed in PBS (1X) for 5min, dried at 60 °C for

## MATERIALS AND METHODS

50min, incubated in 4% PFA (Carl Roth) for 15min at 4 °C and dehydrated (50%, 70% and 2x100% ethanol (Fisher Scientific and Merck Millipore)) at RT. After drying, hydrogen peroxide solution was added for 10min and washed with RNase-free (DEPC, SERVA) water. For antigen accessibility, slides were incubated in 99°C antigen retrieval solution for 3min, washed with RNase-free water and dehydrated in 100% ethanol. Protease III was added for 13min at 40°C on dried slides and washed with RNase-free water. For hybridization, C2 and C3 probes were diluted in C1 probes at a 1:50 ratio and incubated on the slides for 2h at 40°C. Slides were then incubated in Wash Buffer (1X) (ACD) and stored in SSC buffer (5X) o.n. at RT. After washing in Wash Buffer (1X), target-probes signals were amplified by sequential incubation with the following amplifiers with 2 times 2min incubations in Wash Buffer (1X) at RT in between: 1) Multiplex FL v2 AMP 1 for 30min at 40°C, 2) Multiplex FL v2 AMP 2 for 30min at 40°C, 3) Multiplex FL v2 AMP 3 for 15min at 40°C. Probes were then developed one by one in a 3 steps incubation with 2 times 2min washes in Wash Buffer (1X) at RT in between: Probe C1 [1) Multiplex FL v2 HRP-C1 for 15min at 40°C, 2) TSA Plus fluorophore for 30min at 40°C, 3) Multiplex FL v2 HRP blocker for 15min at 40°C]; Probe C2 [1) Multiplex FL v2 HRP-C2 for 15min at 40°C, 2) TSA Plus fluorophore for 30min at 40°C, 3) Multiplex FL v2 HRP blocker for 15min at 40°C]; Probe C3 [1) Multiplex FL v2 HRP-C3 for 15min at 40°C, 2) TSA Plus fluorophore for 30min at 40°C, 3) Multiplex FL v2 HRP blocker for 15min at 40°C]. Before mounting with Aqua-Poly/Mount mounting medium (Polysciences), sections were counterstained with DAPI (1:1000, Sigma-Aldrich). Probes were developed with the following detection kits diluted in Multiplex TSA Buffer (ACD): TSA Plus Cyanine 3 [(1:1500, Akoya Biosciences) for Mp-NFIX, Mp-AQP4, Mp-ZEB1, Mp-PAX6 and Mp-ID1 and (1:750, Akoya Biosciences) for Mp-GADD45B probes], TSA Plus Cyanine 5 [(1:3000, Akoya Biosciences) for Mp-NFIA and (1:1500, Akoya Biosciences) for Mp-CRYAB, Mp-HOPX, Mp-ZEB1 and Mp-CABLES2 probes]. Each combination of probes was applied to the following number of animals: Mp-NFIX and Mp-NFIA to P1 (n = 3) and E34 (n = 3); Mp-ID1 and 2-plex assays to P1 (n = 3) and E34 (n = 1). Negative controls for each combination of probes were carried out on P1 (n = 1) and E34 (n = 1) animals.

## 28. Imaging

Images from immunolabeling were acquired with an Olympus FV10 confocal microscope using a 63x oil objective and FV10-ASW 4.2 Software. Stacks of single-plane images were acquired with a 1 $\mu$ m interval. To analyze clarified brains, three-dimensional imaging acquisition was performed using an ultramicroscope II using ImSpector Pro software (Miltenyi/LaVision BioTec) and images were generated using Imaris x64 software (Oxford Instruments). Images for ISH were acquired using transmitted light (Zeiss Imager.Z2 microscope) with a 10x lens coupled to a digital camera (AxioCam MRm). For FISH, images were acquired on a confocal laser-scanning microscope (Zeiss LSM710) with a 40x lens. Stack images of 5 steps with a 2.5 $\mu$ m interval were acquired.

## 29. FISH counting

Images for RGC probes were quantified through a generated macro using ImageJ-2.0.0-rc-65/1.51w ([Schindelin et al., 2012](#)) and MorphoLibJ ([Legland et al., 2016](#)) and 3D ImageJ Suite ([Ollion et al., 2013](#)) plugins. In brief, layers were delineated and measured their surface. The last slice from the stack of images was discarded to avoid uneven effect of probe penetrance into the tissue. Then images were gray-scaled and split into channels to create individual-channel binary masks using Gaussian Blur/Maximum filter difference and Default/Moments threshold for probes puncta. Particles of 1 pixel size were discarded. Puncta were identified in the 3D binary mask and counted using Connected Components Labelling and 3D Manager. For *PAX6*+ cell counting, cell binary masks were created using Unsharp Mask plus Gaussian Blur filters on the nuclei, followed by Find Maxima for each slice. Then, cells outline and puncta binary masks were merged for each slice and cells containing puncta from *PAX6* probe alone or together with the other probe for each slice were counted.

## 30. HOPX sequence identification

The sequence under ENSMPUG00000030542 Ensembl id in the ferret gene annotation from [Johnson et al., 2018](#) was identified as *HOPX*. In this GTF, ENSMPUG00000030542 was simultaneously associated with the positive (3 exons) and negative (2 exons) DNA strands. Our database has > 99% of alignment

## MATERIALS AND METHODS

to the positive strand and < 1% to the negative strand. It is the positive strand from the same location where NCBI's latest *Mustela putorius furo* annotation (ASM1176430v1.1/GCF\_011764305.1) using Gnomon predicted the presence of *HOPX* containing 3 exons with 100% identity with our transcript (Altschul et al., 1990). ENSMPUG00000030542 gene position (GL897112:1,462,992-1,492,582) (Peng et al., 2014) was searched in UCSC Genome Browser (Kent et al., 2002) where *HOPX* RNAs for numerous organisms (e.g. human, mouse, pig) were aligned to the positive strand with 82% - 86% identity (Kent, 2002; Pruitt et al., 2005; Pruitt et al., 2014). The protein sequences of human *HOPX* and the ferret positive-strand ENSMPUG00000030542 are 91,78% homologous (E value 6e-51) (Altschul et al., 1990).

### 31. Statistics

Wilcoxon Rank Sum test and Logistic regression model were used as described in previous sections (Cell type identity identification, DEG analyses and cluster enrichment, Species dataset integration and DEG analyses). Prism software was used for the statistical analyses of cluster enrichment and gene score. For this, ANOVA was followed by post-hoc Bonferroni test, and significance was set at adjusted p-value <0.05.

### 32. Single-cell data plotting

UMAPs and t-SNE plots from cells colored by different experimental features were randomly shuffled for plotting. UMAPs showing the expression level of marker genes and human MCD gene-score values were generated from the normalized data slot of Seurat's RNA assay. Cells were plotted in order of expression with a minimum cutoff value of 10%.



## **RESULTS**

### **1. Transcriptomic atlas of ferret cortical germinal layers at single-cell resolution**

To elucidate the complexity of cortical progenitor cells, we built a single-cell atlas of the ferret cortical germinal layers. Our sampling strategy was specifically designed to reveal features linked to cortex folding by analyzing separately two key germinal layers for this process (VZ and OSVZ), two prospective folding adjacent areas at the caudal cortex (SG and LS) and two developmental stages that are critical for bRGC genesis and the initial formation of the OSVZ (E34 and P1) ([Martínez-Martínez et al., 2016](#)) (Fig. 1A). Tissues were microdissected from living brain slices and processed for scRNAseq (Fig. 1B). We analyzed each type of sample from 3 independent biological replicas (Fig. S1), each replica profiled individually and containing cells from multiple embryos or one newborn ferret, thus gathering a solid single-cell transcriptomic atlas of cortical GZs (Fig. 1C). Optimum quality controls for cell barcode filtering (such as FDR = 0.1% and iterations for Monte Carlo p-value calculation = 100,000) and cell assessment (through the employment of fixed and adaptive thresholds) were used (Fig. S1). This was followed by analysis with R toolkit Seurat-3, with proven integration performance compared to other single-cell analytical methods ([Tran et al., 2020](#); [Chazarra-Gil et al., 2021](#)). Cluster resolution was carefully selected by the evaluation of 6 potential resolutions from 3 different groups of PCs (Fig. S2A). The use of this detailed appraisal process retained a total of 101,811 cells for further analyses.

## RESULTS

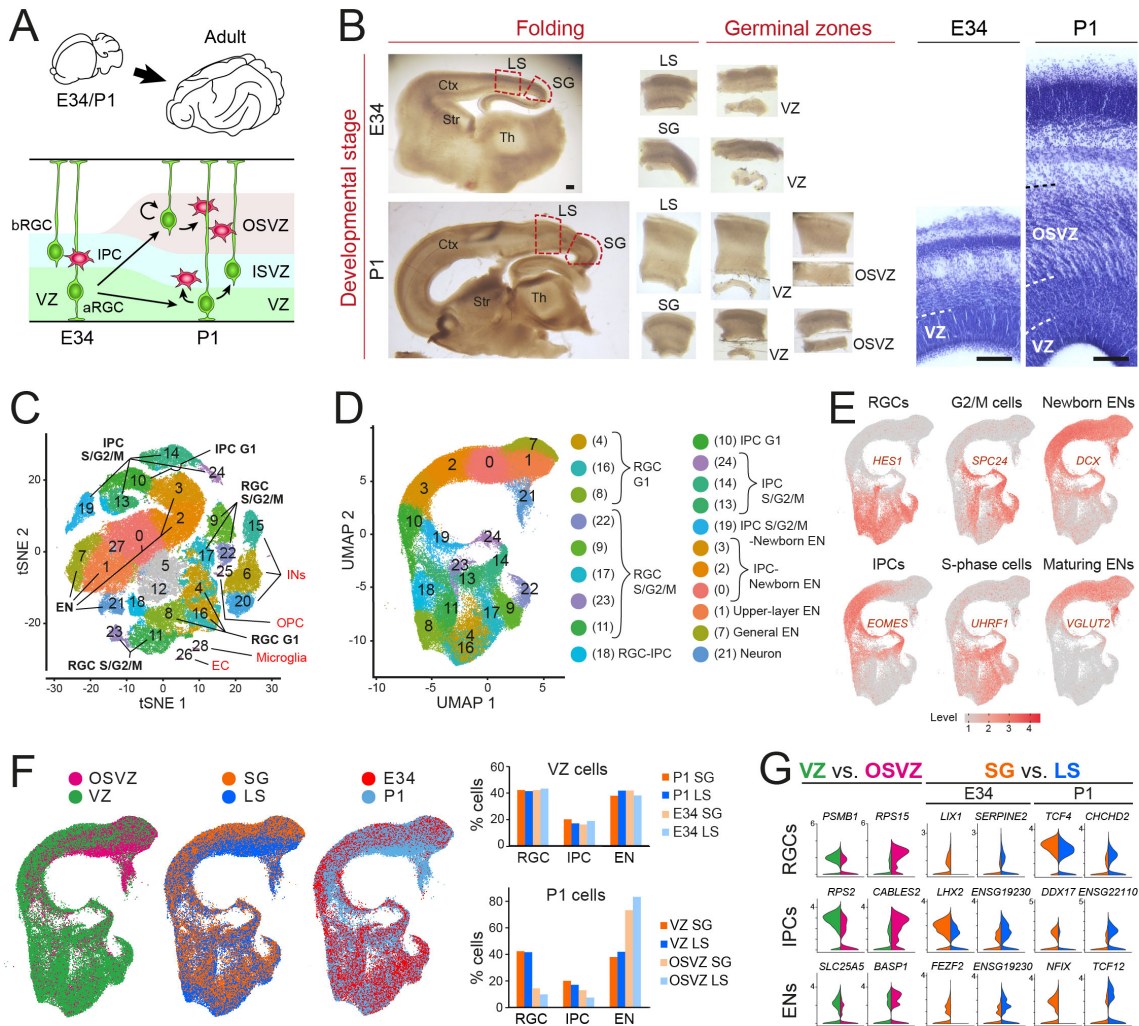


**FIGURE 1. Similar cellular composition of GZs across cortical areas and developmental stages.** (A) Germinal layers, and known major progenitor cell types and lineages in the developing ferret cortex. aRGC, apical radial glia cell; bRGC, basal radial glia cell; IPC, intermediate progenitor cell; VZ, ventricular zone; ISVZ, inner subventricular zone; OSVZ, outer subventricular zone; E, embryonic day; P, postnatal day. (B) Examples of live parasagittal tissue slice microdissections for scRNAseq analyses, and Nissl stains of the SG. Dashed lines indicate borders of germinal layers. Ctx, cortex; Th, thalamus; Str, striatum; LS, lateral sulcus; SG, splenic gyrus. Scale bars, 100  $\mu$ m. (C) t-SNE plot of the full dataset; clusters identified as in (D). EN, excitatory neurons; IN, inhibitory interneurons; EC, endothelial cells; OPC, oligodendrocyte progenitor cells. Clusters in grey were only found in some litters and excluded from further analyses. (D, E) UMAP and clustering of scRNAseq data from cells in the excitatory neuron lineage (D), and expression level of marker genes for the main cell classes (E). (F) UMAPs of cells from the indicated conditions, and frequency of main cell types across conditions. (G) Violin plots for DEGs between conditions in the three main cell types. Adjusted p-values range from 2.2E-308 to 0.02. Genes without name are shown as shorten Ensembl ids (ENSMYPUG000000XXXXX).

A number of transcriptomically distinct cell clusters were identified corresponding to cell types involved in the lineage of excitatory neurons: RGCs, IPCs and newborn ENs (Fig. 1C). Other less abundant cell clusters, such as immature INs from different origins, microglia, OPCs and endothelial cells (ECs) were not taken into account for further analyses (Fig. 1C, Fig. S3). The transcriptome of progenitor cells is highly dynamic and oscillatory as they progress through the cell cycle (Ohnuma and Harris, 2003; Shimojo et al., 2008). To minimize this effect on cell clustering and identify distinct progenitor cell classes, we partially regressed cell-cycle genes, meaning that we distinguished progenitors in G1 cell-cycle phase from those in S/G2/M phases (Fig. S2F). This segregation of cells together with the expression of canonical marker genes, allowed us to identify multiple clusters of RGCs, IPCs and ENs distributed along a transcriptional continuum (Fig. 1D, E). In spite of the partial regression of cell-cycle genes, their high expression still dominated the distinction of RGC and IPC clusters in S/G2/M phases (Fig. S3).

Cortical progenitor cells have different lineage behaviors between SG and LS (Reillo et al., 2011), between developmental stages (Martínez-Martínez et al., 2016), and have particular cell biology in the VZ (apical progenitors) and the OSVZ (basal progenitors) (Arai and Taverna, 2017) (Fig. 1A). However, all clusters of the main cortical cell types were found in both germinal layers, both cortical regions and at both developmental stages (Fig. 1F; Fig. S4A, B). Even the relative abundance of the major cell classes (RGC, IPC, EN) was similar between cortical regions and ages, with only RGCs exceeding in VZ compared to OSVZ, and OSVZ ENs outweighing VZ ENs (Fig. 1F). We found only a modest number of DEGs in RGCs, IPCs and ENs between VZ and OSVZ at P1, and between SG and LS in the VZ (Fig. 1G, Fig. S5, Fig. S6).

## **2. RGC clusters are repeated in VZ and OSVZ, while they remain distinct between SG and LS**

In spite of the known differences in the biology of major cortical progenitor cells between germinal layers, cortical regions and developmental stages (Reillo and Borrell, 2012; Arai and Taverna, 2017; Reillo et al., 2011; de Juan Romero et al., 2015; Martínez-Martínez et al., 2016), these were not identifiable at a global

## RESULTS

transcriptomic level, so we next focused on individual cell clusters. The composition and cell abundance of IPC clusters were similar across all conditions, suggesting a remarkable similarity in IPC composition (Fig. S4C). More strikingly, aRGCs and bRGCs were not identified as distinct cell clusters. Although we had microdissected VZ and OSVZ separately to faithfully isolate presumptive aRGCs (VZ) and bRGCs (OSVZ), all RGC clusters were present in both layers (Fig. 2A). Similarly, all RGC clusters were present in SG and LS, as well as at E34 and P1. At the quantitative level, we found enriched abundance of cells belonging fundamentally to clusters 8 and 16 (Fig. 2A). These corresponded to RGCs in G1 cell-cycle phase, so potentially constituting two different types of RGC. In contrast, the third cluster of RGC in G1 phase (cluster 4) was similarly abundant across conditions (Fig. 2A), thus probably representing a third type of ubiquitous RGC. Importantly, there was a 2-fold enrichment of cluster 8 cells in VZ and of cluster 16 cells in OSVZ (Fig. 2A), suggestive of these corresponding to aRGCs and bRGCs, respectively, although this was observed only in LS, and not in SG. The distinction between clusters 4, 8 and 16 did not depend on the phase of cell cycle, as complete cell-cycle regression analyses did not alter their separation nor the clustering pattern of our entire dataset (Fig. S7A-C). This reinforced the notion that these clusters were three distinct cell types, rather than distinct states of a single cell type.

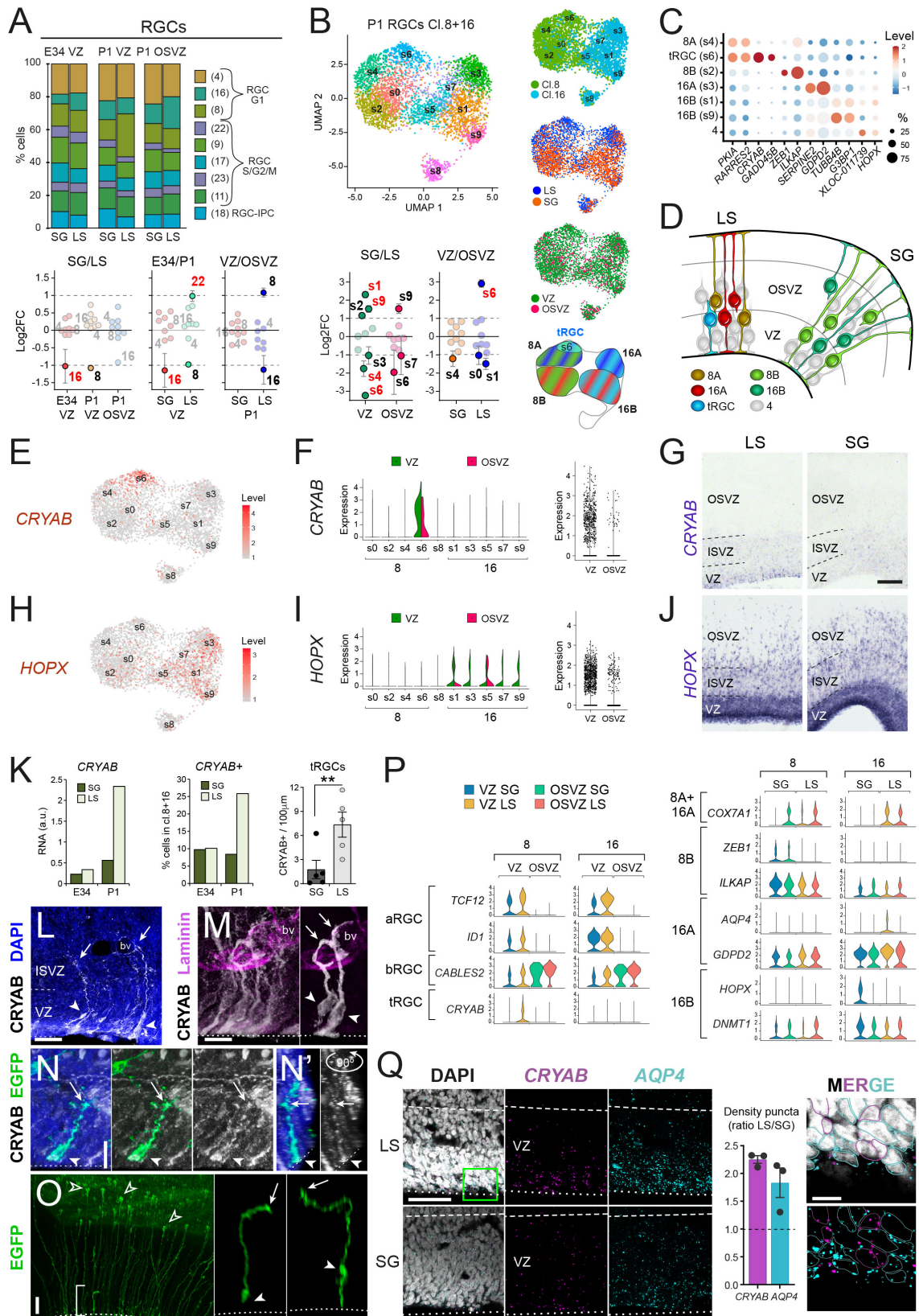


**FIGURE 2. Multiplicity of RGC types across GZs and cortical areas. (A)** Normalized frequency distribution of RGC clusters across conditions, and pairwise cluster enrichment between conditions. Clusters near or above  $\pm 1$  log<sub>2</sub>FC are highlighted (mean  $\pm$  SEM), with red numbers indicating statistical significance (p-value adj. < 0.05). **(B)** UMAP of P1 cells from primary clusters 8 and 16 after

## RESULTS

subclustering, UMAPs of the indicated features, pair-wise subcluster enrichment, and schema of RGC class distribution in UMAP space. tRGC, truncated radial glia cell. **(C)** Dot-plot of gene levels across cell classes at P1 (subclusters in parenthesis). **(D)** Schema of the six classes of ferret RGCs in G1 identified at P1, duplicated in VZ and OSVZ. **(E-J)** UMAPs (E, H), violin plots (F, I) and conventional ISH stains (G, J) of *CRYAB* and *HOPX* levels in RGC subclusters and germinal layers at P1. **(K)** Mean *CRYAB* RNA levels, abundance (RNA) and density (protein; P3) of *CRYAB*<sup>+</sup> cells, as indicated (mean  $\pm$  SEM; \*\* p-value < 0.01, t-test). **(L-N')** tRGCs in VZ of P1 (L, M) and P3 (N, N') ferrets identified with anti-*CRYAB* ICC. Full morphology confirmed by EGFP expression (N, N'). Laminin identifies blood vessels (bv). Arrows indicate the tip of the basal process and arrowheads the soma. (N') shows orthogonal view. **(O)** EGFP-labeled RGCs in clarified P2 ferret brains, with tRGCs shown in detail. Open arrowheads indicate basal endfoot arbors of aRGCs. **(P)** Violin plots for marker genes in RGC classes between conditions. p-values range from 2.2E-308 to 0.01. *ILKAP*, *GDPD2* and *DNMT1* are top markers for cl.8 and 16 ferret P1 subclusters (see Fig. S8A). *HOPX* does not appear as a DEG but has a specific distribution to define the cluster 16 VZ SG. **(Q)** RNAscope coexpression analysis at P1 for RGC marker genes between conditions. Green box indicates area shown at high magnification in a single plane confocal image. RGC cells containing *CRYAB* or *AQP4* puncta are indicated with colored contours. Scale bars 100 $\mu$ m (G, J), 30 $\mu$ m (L, O), 10 $\mu$ m (M, N, Q merge.), and 50 $\mu$ m (Q). Dashed lines indicate borders of germinal layers and dotted lines the apical VZ surface.

To characterize in greater depth the heterogeneity of RGCs, and in an attempt to distinguish aRGCs from bRGCs, we next subclustered RGCs from clusters 8 and 16 in our P1 samples (the only ones including both VZ and OSVZ) (Fig. 1A). Cells from the primary clusters 8 and 16 remained separate upon subclustering (Fig. 2B), confirming their distinct identity. Comparison between SG and LS showed that most subclusters were highly enriched in one or the other region, splitting in two groups each of the primary clusters 8 and 16 (Fig. 2B). Overall, this revealed the existence of four major subclasses of RGCs: two enriched in LS that we named A (8A and 16A) and two enriched in SG that we called B (8B and 16B) (Fig. 2B-D). These four transcriptomic subclasses still did not distinguish aRGCs from bRGCs, as most subclusters were similarly abundant in VZ and OSVZ, with only subcluster s6 being significantly enriched in this comparison (Fig. 2B). Subcluster s6 (part of RGC 8A) was highly enriched in VZ of LS ( $3.22 \pm 0.05$  log<sub>2</sub>FC compared to VZ of SG, p-value < 0.0001;  $2.91 \pm 0.20$  log<sub>2</sub>FC compared to OSVZ of LS, p-value = 0.011) (Fig. 2B). Interestingly, this subcluster had particular high levels of *CRYAB* (Fig. 2C, E, F), a marker of human tRGCs (Nowakowski et al., 2016). This was in agreement

with tRGCs being described as an exclusively apical cell type (Fig. 2F, G; Fig. S6), thus representing a sixth RGC type (Fig. 2C, D; Fig. S8A).

LS is located immediately rostral to SG, so the different abundance in tRGCs could simply reflect their slight difference in the anterior-posterior gradient of cortical maturation (so-called “longitudinal neurogenetic gradient” by [Bayer and Altman, 1991](#)). A detailed analysis of tRGCs revealed that *CRYAB* mRNA levels in individual cells were much higher at P1 than E34, paralleled with a 4-fold increase in the difference between LS and SG (Fig. 2K). The relative abundance of *CRYAB*<sup>+</sup> cells among RGCs in VZ from primary clusters 8 and 16 was similar between LS and SG at E34, but 3-fold higher in LS at P1 (Fig. 2K). Anti-*CRYAB* immunostains confirmed the truncated morphology of tRGCs, with a short basal process ending within the ISVZ, occasionally onto a blood vessel (Fig. 2L, M). *CRYAB*-immunoreactive cells were virtually absent at E34 but abundant in newborn ferrets (P1-P3), and highly enriched in LS compared to SG, in agreement with our transcriptomic results (Fig. 2K-M). To further characterize tRGC morphology in ferret, apical progenitors were labeled *in vivo* by EGFP electroporation at P1, and examined in both thick histological sections and clarified brains. Amid a majority of aRGCs spanning the full cortical thickness, tRGCs displayed a short basal process ending in the ISVZ, with its tip frequently in a horizontal disposition regarding the ventricular surface (Fig. 2N-O; Fig. S8B, C).

To specifically identify bRGCs, we examined the levels of *HOPX*, a canonical marker of this cell type ([Pollen et al., 2015](#); [Thomsen et al., 2016](#); [Nowakowski et al., 2016](#); [Nowakowski et al., 2017](#); [Johnson et al., 2018](#); [Vaid et al., 2018](#); [Polioudakis et al., 2019](#); [Matsumoto et al., 2020](#)). *HOPX* was present across all RGC subclusters derived from primary cluster 16, with a clear enrichment in VZ over OSVZ (Fig. 2H-J). This pattern was similar to the human embryo cortex before GW18.2 ([Pollen et al., 2015](#)), in line with prior studies questioning *HOPX* as a universal marker of bRGCs ([Thomsen et al., 2016](#); [Matsumoto et al., 2020](#)). Instead, *HOPX* expression labeled three RGC subclasses: 4, 16A and 16B, present in both layers (Fig. 2C, I, J; Fig. S6). Altogether, we identified six major types of RGCs (all in G1): two enriched in SG (8B, 16B), two enriched in LS (8A, 16A), one class enriched

## RESULTS

in VZ of LS (tRGC), and one class (4) common to all conditions (Fig. 2D). Importantly, these six cell populations were identified as transcriptomically different in both VZ and OSVZ (except for tRGCs), while the two known different cell types, aRGCs and bRGCs, remained transcriptomically indistinguishable, further supporting the identification of the former as different cell types.

To characterize the biological differences between SG- and LS-enriched RGC classes, we performed functional enrichment analyses (Fig. S9). Compared to RGC classes abundant in LS (8A, 16A), those in SG (8B, 16B) were enriched in functions related to cell-cycle progression, DNA replication and cell division (Fig. S9A), in agreement with the greater rates of cell proliferation previously observed in areas of prospective gyral formation compared to sulci (Kriegstein et al., 2006; Reillo et al., 2011). Within SG and LS, class 16 RGCs were enriched in mechanisms promoting cell-cycle progression and cell proliferation (what we can refer to as “amplifying RGCs”), whereas class 8 RGCs were enriched in genes related to cell differentiation (that can be termed “differentiating or neurogenic RGCs” (Fig. S9B, C).

Given that aRGCs and bRGCs were indistinguishable at the transcriptomic level, we finally focused on the analysis of specific genes. Differential expression analysis between microdissected germinal layers revealed that genes preferentially expressed in aRGCs (VZ) were related to enhancing progenitor cell amplification, via regulation of transcription (*TCF12*, *ID1*, *HMGN1*), mitochondrial function (*MICU2*) and cell proliferation (*YPEL3*) (Fig. 2P, Fig. S10). In contrast, genes preferentially expressed in bRGCs (OSVZ) were related to promotion of neurogenesis via oxidative phosphorylation (*ATP5I*), cell-cycle transition (*CABLES2*) and ribosomal activity (*RPS15*) (Fig. 2P, Fig. S10). Specific RGC types were characterized by enriched expression of certain genes, including *COX7A1*, *PKIA*, *RARRES2* (8A); *ZEB1*, *ILKAP* (8B); *COX7A1*, *AQP4*, *GDPD2*, *SERPINE2* (16A); *HOPX*, *DNMT1*, *SNRPA1*, *TUBB4B*, *G3BP1* (16B); and *CRYAB* (tRGCs) (Fig. 2C, P; Fig. S11). Of note, we also identified *GADD45B* and *TMEM196* as new tRGC markers (Fig. S11). The identity of cell classes as defined by these genes was confirmed by FISH analyses by means of RNAscope. In this way, *CRYAB* and *AQP4* distinguished



two populations of aRGCs coexisting in the VZ of LS (Fig. 2Q), the first of which coexpressed *GADD45B* (Fig. S12A, B). At the same time, *HOPX* and *ZEB1+PAX6+* RGCs identified two different groups of RGCs intermingled in the OSVZ of SG and more modestly in the VZ of SG (Fig. S12C-F). Microdissected VZ and OSVZ layer identity were also examined by RNAscope experiments, where *ID1* clearly defined VZ compared to OSVZ in the SG and LS (Fig. S13A), while *CABLES2+PAX6+* labeled OSVZ compared to VZ in the SG and more moderately in the LS (Fig. S13B, C).

Taken together, our results indicated the existence of six major types of RGCs in the germinal layers of the developing ferret cortex: three characteristic of LS, two of SG, plus one ubiquitous type. RGC classes were distinct in their amplifying (RGCs 16) versus differentiating/neurogenic (RGCs 8) profile, and populated VZ and OSVZ similarly (except for tRGCs), indicating that they existed in duplicate as aRGCs and bRGCs (Fig. 2D). *HOPX* marked three of the RGC classes common to VZ and OSVZ, not being, therefore, specific to bRGCs.

### **3. Three parallel transcriptomic trajectories arise from RGCs in VZ and in OSVZ**

After cell identity identification, we next used Monocle-3 to perform a transcriptomic trajectory analysis of our single-cell dataset (Fig. 3A). We identified three complementary trajectories running from mitotic RGCs to ENs. The roots of these trajectories were two distinct groups of dividing RGCs, each including two cell clusters: mitotic RGCs class A (clusters 23 + 11), and mitotic RGCs class B (clusters 22 + 9). Trajectory 1 stemmed from mitotic RGC-As, followed by class 8 RGCs, then IPCs that transited through mitosis (IPC class A, cluster 19) to produce ENs (Fig. 3B). Trajectory 2 stemmed from mitotic RGC-Bs, leading to class 4 and/or class 16 RGCs, followed by class 8 RGCs, and then IPCs that finally divided (IPC-A) producing ENs (Fig. 3B). Trajectory 3 stemmed again from RGC-Bs, but now giving rise to mitotic IPCs class B (clusters 24 + 14), then the common IPCs that finally divided (IPC-A) to generate ENs (Fig. 3B). The identification of these three trajectories did not depend on cell cycle, as analysis of the same dataset but subject to complete cell-cycle regression yielded the same result (Fig. S7D). Each of the three trajectories had a distinctive pseudotemporal transcriptomic signature at the

## RESULTS

level of progenitor cells. Trajectory 1 was characterized by expression of *PTTG1*, *TOX3* and *LGALS1*; trajectory 2 by expression of *SLC1A3* (canonical RGC marker), *ZFP36L1* and *SPARC*; and trajectory 3 was defined by expression of *TOP2A*, *NSL1* and *SPC25* (Fig. S14). Surprisingly, all three trajectories converged onto a single cluster of ENs (cluster 3) (Fig. 1D, Fig. 3A), suggesting that they are not specializations to produce distinct neuron types, but complementary lineages producing a single type of newborn neuron.

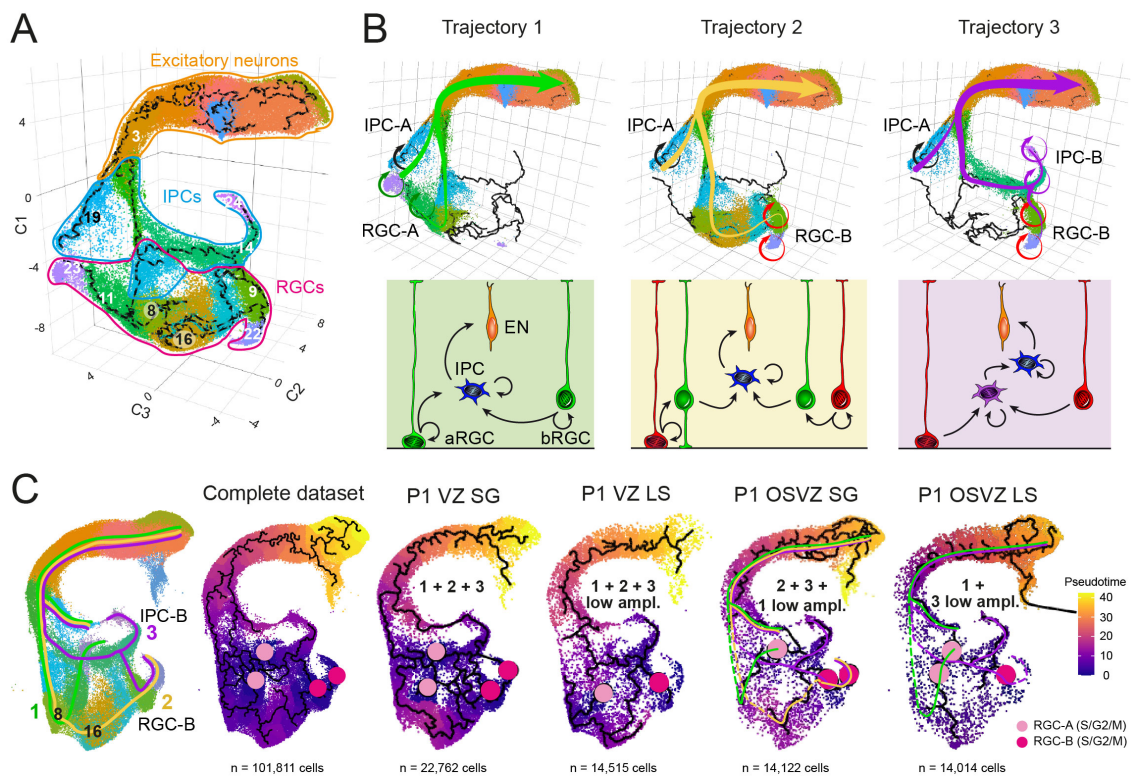


**FIGURE 3. Parallel cell trajectories converge into a single class of newborn EN.** (A) 3-D UMAP and cell trajectories of the clustered scRNAseq ferret dataset. Clustering is the same as in Fig. 1D and in (C). Numbers identify key clusters. (B) 3-D UMAPs showing the clusters involved in each of the three identified trajectories, each starting from a set of mitotic RGC clusters (RGC-As or RGC-Bs), and schematic drawings of summarized cell lineages. Circular arrows point out mitotic clusters of progenitor cells. (C) 2-D UMAP of cell clusters showing the three trajectories identified in the 3-D UMAP (color-coded as in B), and pseudotime and trajectory plots of the complete ferret dataset and individual P1 conditions, indicating the RGCs of origin (pink circles for RGC-As and red for RGC-Bs) and trajectories present in each case (illustrated with colored lines in OSVZ samples). Total number of cells in each condition is specified.

The three trajectories occurred in VZ, both at E34 and P1, and in SG and LS (Fig. 3C, Fig. S15A). However, the trajectory in P1 VZ LS involved fewer mitotic RGC

clusters, suggesting lower RGC amplification in agreement with previous histological studies (Reillo et al., 2011). The same three trajectories were also traced in the OSVZ of SG, whereas LS displayed only trajectories 1 and 3 (Fig. 3C). This was again consistent with previous analyses showing that OSVZ progenitors are more proliferative in SG than LS (Reillo et al., 2011). Taken together, our observations indicated that VZ and OSVZ of the developing ferret cortex contain three parallel transcriptional trajectories of apical and basal progenitor cells that converge onto a single cluster of newborn EN.

#### **4. Parallel lineages originate from RGCs in the ferret cortex**

To confirm the validity of the three observed transcriptomic trajectories as distinct cell lineages in ferret, we used TrackerSeq, a new technique that can simultaneously generate scRNAseq libraries and barcode lineage tracing (Bandler et al., 2022). This method involves integrating an EGFP reporter coupled to DNA barcodes randomly into the genome of electroporated RGCs, allowing us to track the clonal relationships with their progeny over time (Fig. 4A). We used IUE of E34 ferret embryos to deliver the TrackerSeq barcode library to apical progenitors in the VZ of the cerebral cortex (putative RGCs). We allowed the transduced cells to develop a cell lineage for three days *in vivo*, then collected them by FACS and created single-cell sequencing libraries, for both transcriptomes and lineage barcodes (Fig. 4A). We recovered a total of 1,038 multicell clones composed of both mitotic and postmitotic cells (Fig. 4B, Fig. S16A-E), as expected from the timing of our experiment. Furthermore, in agreement with previous findings in mice (Bandler et al., 2022), our results suggest that cortical RGCs in ferret only generate ENs, but not INs.

## RESULTS

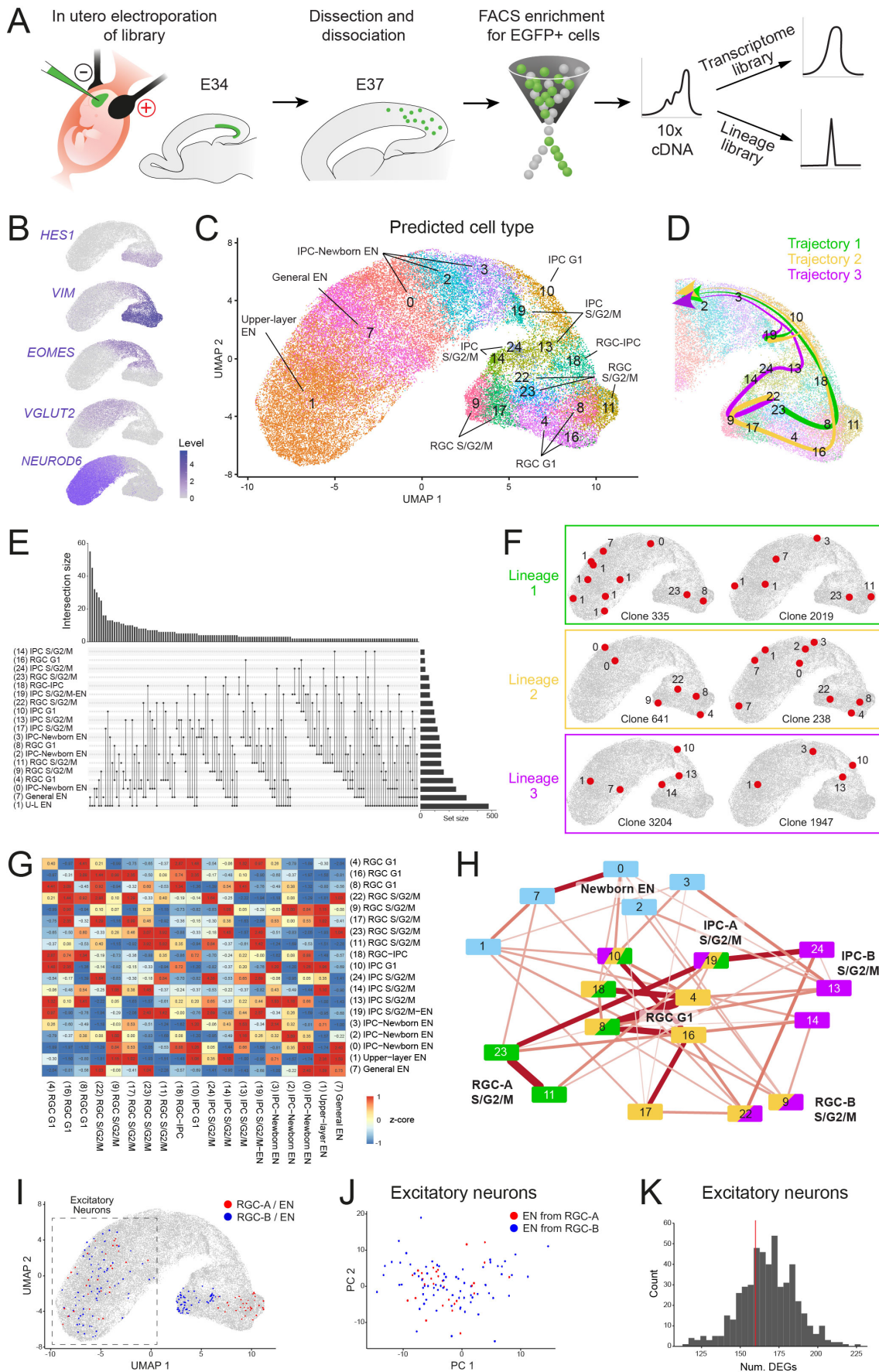


**FIGURE 4. Lineage relationships in the developing ferret cortex.** (A) Lineage barcodes were delivered by IUE at E34, EGFP-positive cells were extracted at E37,

and lineage barcode and transcriptome libraries were sequenced. **(B)** UMAP of generated database with levels for marker genes for the main cell types. **(C)** Cell class annotation after transferring previous labels using correlation-based label transfer. **(D)** Arrangement of cell trajectories identified in Fig. 3B on the UMAP of the new TrackerSeq library. **(E)** UpSet-plot showing observed combinations of clones in different cell clusters, size of the interaction (top), and absolute number of clones per cell cluster (right). **(F)** Position of cells in the UMAP-embedding of example clones for each of the three lineages. **(G)** Heatmap showing lineage coupling correlation scores between all cell clusters. **(H)** Cell cluster network visualization, with edges representing positive lineage coupling correlation scores. Position of nodes was set manually to facilitate reading. **(I)** UMAP highlighting cells from clones containing ENs coupled to RGC-As (clusters 23 + 11) or to RGC-Bs (clusters 22 + 9). **(J)** PCA of ENs from (I) color-coded according to their clone type of origin. **(K)** Number of DEGs between EN types as in (J) (red line), and frequency distribution of DEGs following a random distribution of clone cells (grey bars; 500 repetitions).

To examine cell lineage results in the context of our previous extensive characterization of cell clusters, we annotated clusters in the TrackerSeq dataset based on the scRNAseq data described above, employing correlation-based label transfer (Stuart et al., 2019) (Fig. 4C, D). A majority of clones contained cells assigned to the Upper layer-EN cluster (cluster 1: 472 clones, 636 cells), while much fewer contained class 16 RGC (19 clones, 19 cells) or mitotic IPCs (clusters 14 and 24: 38 clones, 39 cells) (Fig. 4E, Fig. S16 F-H). We then evaluated the probability of identifying shared clone ids among all pairs of cell clusters and quantified lineage coupling by calculating a z-score for clone counts relative to a random distribution (Wagner et al., 2018). These z-scores revealed groups of cell clusters with similar lineage coupling signatures (Fig. 4G). By visualizing lineage coupling scores as a network in which nodes represent cell clusters, we were able to validate clonal lineages for our three inferred trajectories (Fig. 4F, H; Fig. S16I, J). Specifically, mitotic RGC clusters 23 and 11 (RGC-As) were coupled with clusters 8 and 19, which largely recovered Trajectory 1. The second population of cell clusters that exhibited clonal coupling was composed of mitotic RGC clusters 22 and 9 (RGC-Bs) and 17, then RGC in G1 clusters 16, 8 and 4, followed by RGC-IPC cluster 18 and IPC cluster 10, and finally postmitotic IPCs-ENs (clusters 0, 1, 3), which nicely recovered Trajectory 2. We also observed clones containing RGC-Bs clusters 22 and 9, coupled to mitotic IPC clusters (24 and 14), then mitotic IPC cluster 19 and ENs, recovering Trajectory 3. Hence, the three transcriptomic

## RESULTS

trajectories were validated as cell lineages *in vivo* (Fig. 4F, H). Notably, we further observed robust coupling scores directly between mitotic RGCs and mature ENs, but without IPCs (Fig. 4H). This was observed in 4.3% of clones containing RGC-As (cluster 23) and 8.8% of clones containing RGC-Bs (clusters 9 and 22), and is consistent with the process of direct neurogenesis, in which RGCs undergo a cell division that directly produces newborn EN (De Juan Romero and Borrell, 2015). Thus, TrackerSeq represented yet additional parallel RGC lineages.

We then investigated whether the observed lineages starting from RGC-As and RGC-Bs gave rise to transcriptomically distinct ENs. We grouped individual ENs based on their coupling to either RGC-As or RGC-Bs (Fig. 4I), and performed a principal component and differential gene expression analysis to assess heterogeneity among these groups of ENs. We found no difference in PC-space between ENs originating from distinct RGC populations (Fig. 4J). Whereas we did identify some DEGs between these EN populations, their number was not significantly greater than expected by chance (Fig. 4K). Thus, our *in vivo* analyses of cell clones validated our above conclusions based on inferred cell trajectories: parallel cell lineages of RGCs coexist in the developing ferret cerebral cortex and converge onto a single cluster of early postmitotic EN.

### 5. Multiple RGC classes are conserved in ferret and human

The unprecedented diversity of cortical RGC classes and lineages observed in ferret led us to investigate their conservation in species with a larger and folded cortex (i.e., human), as well as smaller and smooth (i.e., mouse). We integrated our ferret datasets with public scRNAseq datasets from human and mouse cortex at equivalent stages of cortical development (Polioudakis et al., 2019; Li et al., 2020) (Fig. 5A). The integrated dataset cleanly clustered RGCs (*HES1+*), IPCs (*EOMES+*), ENs (*VGLUT2+*) and INs (*GAD65+*) from the three species (Fig. 5B, C). Previous single-cell studies of the embryonic human cortex identified aRGCs and bRGCs based on their presumed distinctive transcriptomic signatures. Therefore, we used our cross-species comparison to identify these cell types in ferret and mouse. Cells identified as ventricular radial glia (vRGs; in other words, aRGCs) in (Polioudakis et al., 2019) were mostly part of the species integrated cluster 4 (iCl.4), and were

largely segregated from those identified as outer radial glia (oRGs; i.e., bRGCs), found mostly in iCl.12 (Fig. 5D; Fig S17A, B). Ferret cells from each of these integrated clusters were identified in the initial UMAP containing only ferret cells, where they were found also segregated: iCl.4 cells mostly corresponded to the primary ferret cluster 8 (fCl. 8), and iCl.12 cells mainly correlated to fCl.4, fCl.16 (Fig. 5E). Even though cells in iCl.4 and iCl.12 were likely to correspond to aRGCs and bRGCs respectively, this was not the case in ferret, as both clusters were present and similarly abundant in VZ and OSVZ (Fig. 5E).

## RESULTS

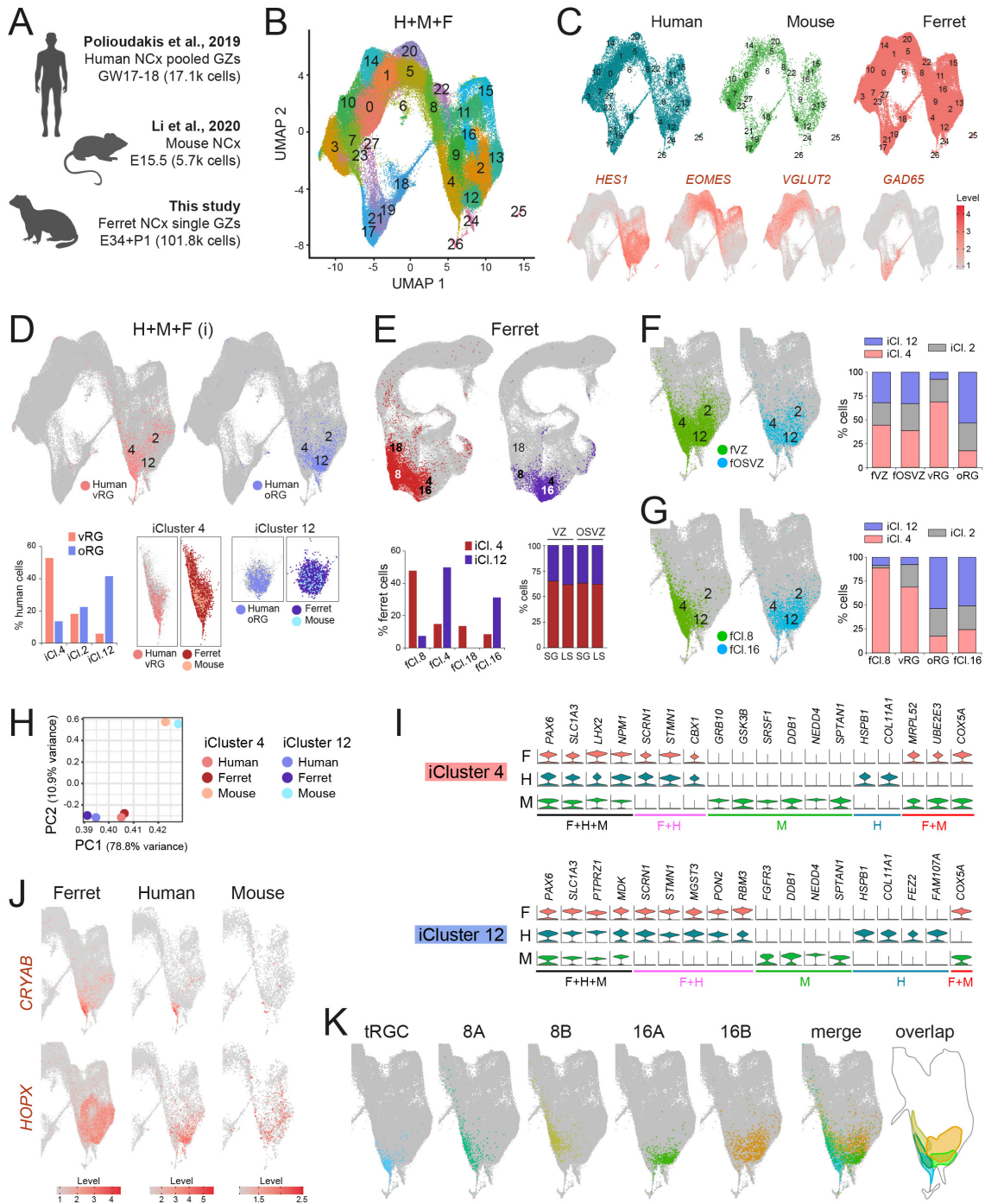


**FIGURE 5. Conserved RGC classes in ferret and human.** (A) Sources of species integrated scRNAseq datasets. NCx, neocortex; GZ, germinal zone; GW, gestational week. (B) UMAP and clustering of integrated human, mouse and ferret datasets. (C) Distribution of cells from each species within the integrated UMAP, and levels of genes identifying the main cell types. (D) Species integrated UMAP highlighting human cells identified as vRG (pink) and oRG (blue) in (Polioudakis et al., 2019), frequency distribution in the integrated clusters (iCl.), and ferret and mouse cells belonging to the same iCl. (E) UMAP of ferret dataset highlighting ferret cells from iCl. 4 (red) and 12 (purple), their frequency distributions among primary ferret clusters (fCl.) and in normalized P1 sample conditions. (F, G) Details from the species integrated UMAP highlighting P1 ferret RGCs in G1 collected from VZ or OSVZ (F), or belonging to fCl.8 or fCl.16 (G), and their normalized frequency



distributions in the indicated iCl. compared to human vRG and oRG. **(H)** Reactome-based PCA of iCl.4 and iCl.12 from each of the three species. **(I)** Violin plots for genes expressed in the indicated iCl. in each species. Adjusted p-values range from 2.2E-308 to 0.002. **(J)** Details from the species integrated UMAP for levels of *CRYAB* and *HOPX* in the indicated species. **(K)** Individual and merged distribution of RGC classes from Fig. 2D in species integrated UMAPs (detail), and schematic of their overlap.

In an attempt to finally identify the cell clusters corresponding to aRGCs and bRGCs, we located RGCs in G1 from P1 ferret VZ and OSVZ in the species integrated UMAP. Ferret RGCs from VZ and OSVZ had a very similar contribution to iCl.12, iCl.2 and iCl.4 (Fig. 5F), demonstrating that these species integrated RGC clusters do not separate aRGCs from bRGCs. This cell distribution across transcriptomic clusters was completely different from that of vRG and oRG cells as identified in the original human study (Polioudakis et al., 2019) (Fig. 5F), questioning the identity of the human clusters as genuine aRGCs and bRGCs. Because fCl.8 and fCl.16 distinguish two types of RGCs, we next studied their distribution within the species integrated dataset. We found that the distribution of fCl.8 and fCl.16 across clusters iCl.12, iCl.2 and iCl.4 was similar to that of human vRG and oRG cells, respectively (Fig. 5G). This led to the notion that human cells currently defined as vRGs and oRGs are in fact the two distinct classes of RGCs found in ferret, present both in VZ and OSVZ. This conception was later confirmed with the analysis of marker gene expression. In addition to *HOPX*, a number of genes have been used as canonical markers for human aRGC or bRGC (Pollen et al., 2015; Nowakowski et al., 2017; Polioudakis et al., 2019). In our ferret samples, expression of these genes correlated mostly with RGC clusters rather than with their layer of residence (Fig. S18).

Pathway enrichment analyses using Reactome database indicated that cells within iCl.4 and iCl.12 were functionally much more similar between human and ferret than with mouse (Fig. 5H, Fig. S17C). Interspecies differences involved signaling pathways regulating progenitors self-amplification and neurogenesis (*NOTCH*, *ROBO*, *FGF*), cell migration (*ERBB2*, *NETRIN*) and transcriptional regulation (*SUMO*) (Fig. S17C). In these integrated RGC clusters, canonical RGC genes were expressed similarly in the three species, but other genes were selectively

## RESULTS

expressed in human and ferret but not mouse, or vice versa, in addition to some human specific genes (Fig. 5I, Fig. S17D). For example, high expression of *STMN1* in human and ferret iCl.4 and iCl.12 compared to mouse might be correlated with the greater self-renewal of the former (Boekhoorn et al., 2014). The patterns of expression of *CRYAB* and *HOPX* further highlighted differences in progenitor cell populations between human and ferret versus mouse cortex (Fig. 5J). Finally, we searched the multiple ferret RGC populations that we previously identified (Fig. 2C, D), within the species integrated dataset. We observed distinct distributions with minimal overlap between these RGC classes (Fig. 5K). Taken together, our results strongly suggested that the embryonic human cerebral cortex contains a similar variety of RGC types as ferret, and that these may also be duplicated in VZ and OSVZ.

### **6. Parallel transcriptomic trajectories from RGCs are conserved in ferret and human but not in mouse cortex**

To analyze the conservation of cell lineages across ferret, human and mouse, we focused on cells from the glutamatergic lineage (Fig. 6A). All integrated RGC clusters were present in the three species, and some were highly enriched (2- to 4-fold) in ferret and human compared to mouse, or vice versa (Fig. 6B, C). Within the species integrated dataset, we identified the ferret mitotic RGCs and IPCs type A and B and reconstructed the three previously characterized trajectories (Fig. 6D-F). Trajectory analysis of ferret or human cells alone within the integrated UMAP, revealed a strong conservation between human and ferret, containing the same mitotic RGC clusters of origin and largely the same three main trajectories (Fig. 6G, H). In contrast, analysis of mouse cells alone within the integrated UMAP identified only one mitotic RGC-B cluster (corresponding to cluster 22) as origin of trajectory 2. Monocle did not identify the other two mitotic origins (cluster 17 / RGC-A; cluster 23 / RGC-B), which were at very low abundance in mouse (Fig. 6 C, G, H). To test whether differences between ferret and human with mouse were of technical origin due to their very different sample size, we repeated these analyses after equalizing the cell number for the three species. After downsampling the ferret and human datasets by two different approaches (see Materials and Methods), we still found a similar enrichment of specific RGC clusters in those

versus mouse (Fig. S19B, C, F, G). However, the complexity of the ferret and human transcriptomic trajectories across the species integrated dataset was lost, while in mouse it remained unchanged (Fig. S19D, H). Hence, downsampling to equalize cell numbers across species did not improve the characterization of cell populations, nor their trajectories. Taken together, our analyses indicated a marked conservation of RGC classes between human and ferret, but less in mouse. Concomitantly, three main trajectories of progenitor cells were found in human and ferret, but only one in mouse. Importantly, our analyses confirmed that the transcriptomic profile of aRGCs and bRGCs is remarkably similar, such that cell populations previously identified as aRGCs and bRGCs in human datasets may rather be distinct populations of RGCs that coexist in both VZ and OSVZ.

## RESULTS

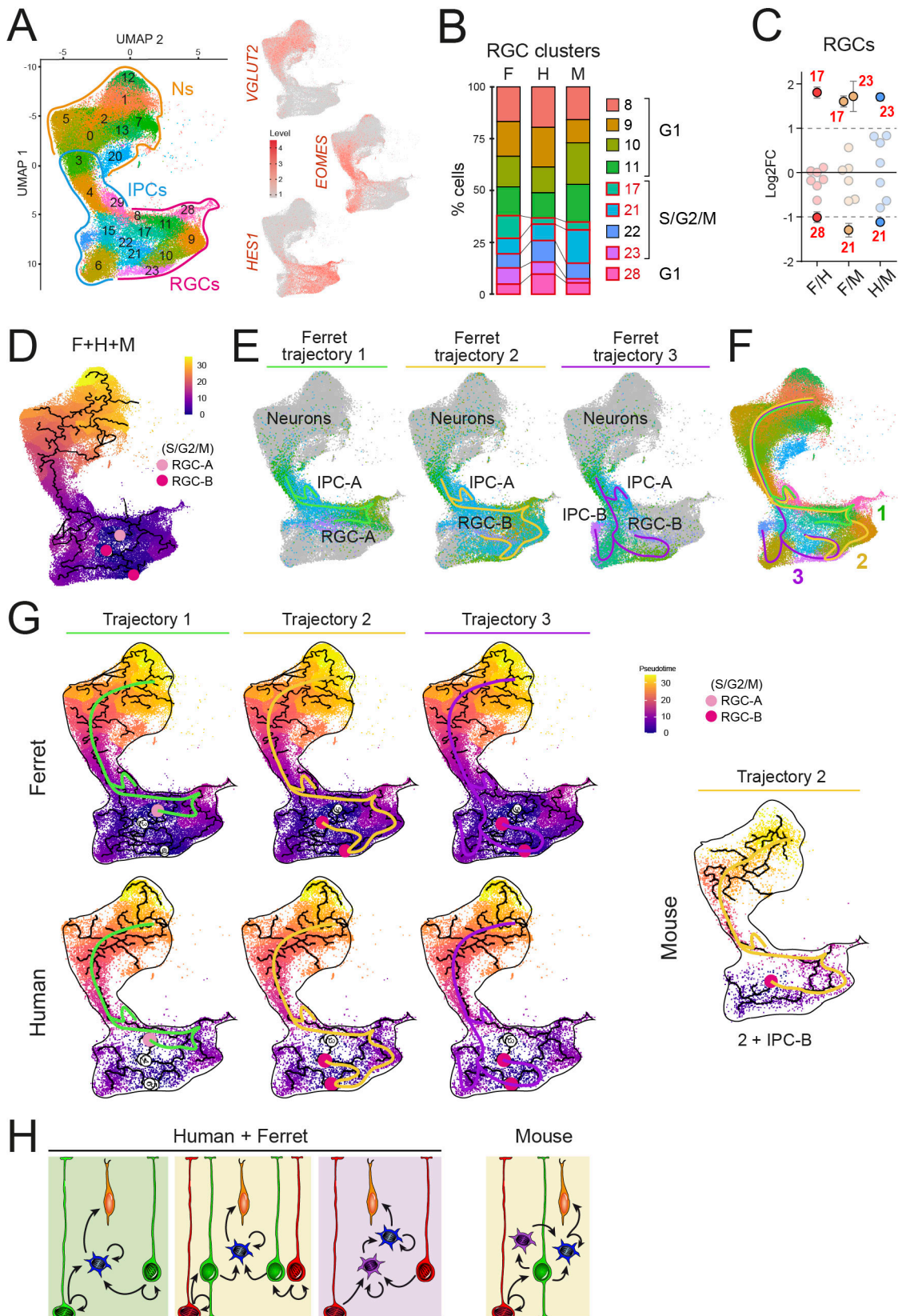


**FIGURE 6. Conserved and divergent RGC classes in ferret, human and mouse.** (A) UMAP and clustering of integrated human, mouse and ferret (P1) datasets (showing only cells in the excitatory neuron lineage) and levels of marker genes for main cell types. (B, C) Normalized frequency distribution of integrated RGC clusters within species (B), and pair-wise cluster enrichment between species (C).

Clusters above  $\pm 2 \log_2\text{FC}$  are highlighted (mean  $\pm$  SEM), with red numbers indicating statistical significance (p-value adj.  $< 0.05$ ). **(D)** Pseudotime and trajectory plot for the multispecies integrated UMAP, indicating the mitotic RGCs of origin (pink circles for RGC-As and red for RGC-Bs). **(E, F)** UMAPs highlighting the progenitor cell clusters involved in each of the three trajectories (colored lines as in Fig. 3B) identified in the integrated dataset (E), and summary of trajectories (F). **(G)** Pseudotime and trajectory plots for ferret, human and mouse cells within the integrated UMAP. All three trajectories were found in ferret and human, but only one in mouse. **(H)** Schematic drawings of summarized cell lineages found in human and ferret versus mouse.

### **7. Distinct maturation of newborn ENs in gyrus and sulcus linked to human malformations of cortical development**

Our analyses of microdissected GZs in ferret identified newborn ENs in addition to progenitor cells, in agreement with histological evidence (Reillo and Borrell, 2012). The multiple parallel trajectories and lineages of progenitor cells identified above did not derive into early neuronal diversification, as might be expected, but converged onto a single class of IPC-newborn ENs (cluster 3). This was in agreement with the notion that cortical neuron type diversity is defined postmitotically (Yuzwa et al., 2017; Di Bella et al., 2021). Subclustering of ferret late IPCs and newborn ENs distinguished two main cluster groups, which we identified as “immature-lower layer” and “mature-upper layer” neurons, owing to the expression of marker genes (Fig. 7A, B; Fig. S20). This was unexpected because at E34 and P1 only upper layer neurons are born (Jackson et al., 1989). Pseudotime analysis revealed that transcriptomic cell maturation progresses from “lower layer” to “upper layer” profiles, as in normal cortical histogenesis, and it was consistent with the former being enriched in VZ and the later enriched in OSVZ (Fig. 7B, C). This indicated that cortical neurons born at late stages and destined to upper cortical layers follow an early maturation process that recapitulates the transcriptomic progression of cortical neurogenesis. Remarkably, many EN subclusters were differentially enriched in SG or LS, suggesting that distinct neuron subtypes are produced in these closely related cortical areas (Fig. 7D). Furthermore, FISH analyses by means of RNAscope confirmed the higher levels of *NFIA* and *NFIX*, key regulators of neuronal differentiation and maturation (Campbell et al., 2008; Piper et al., 2010; Harris et al., 2015), in VZ of SG compared

## RESULTS

to LS (Fig. 7E). Cell clusters enriched in gyrus or sulcus segregated orthogonal to the pseudotime trajectory, thus following parallel but distinctive trajectories of maturation (Fig. 7C).

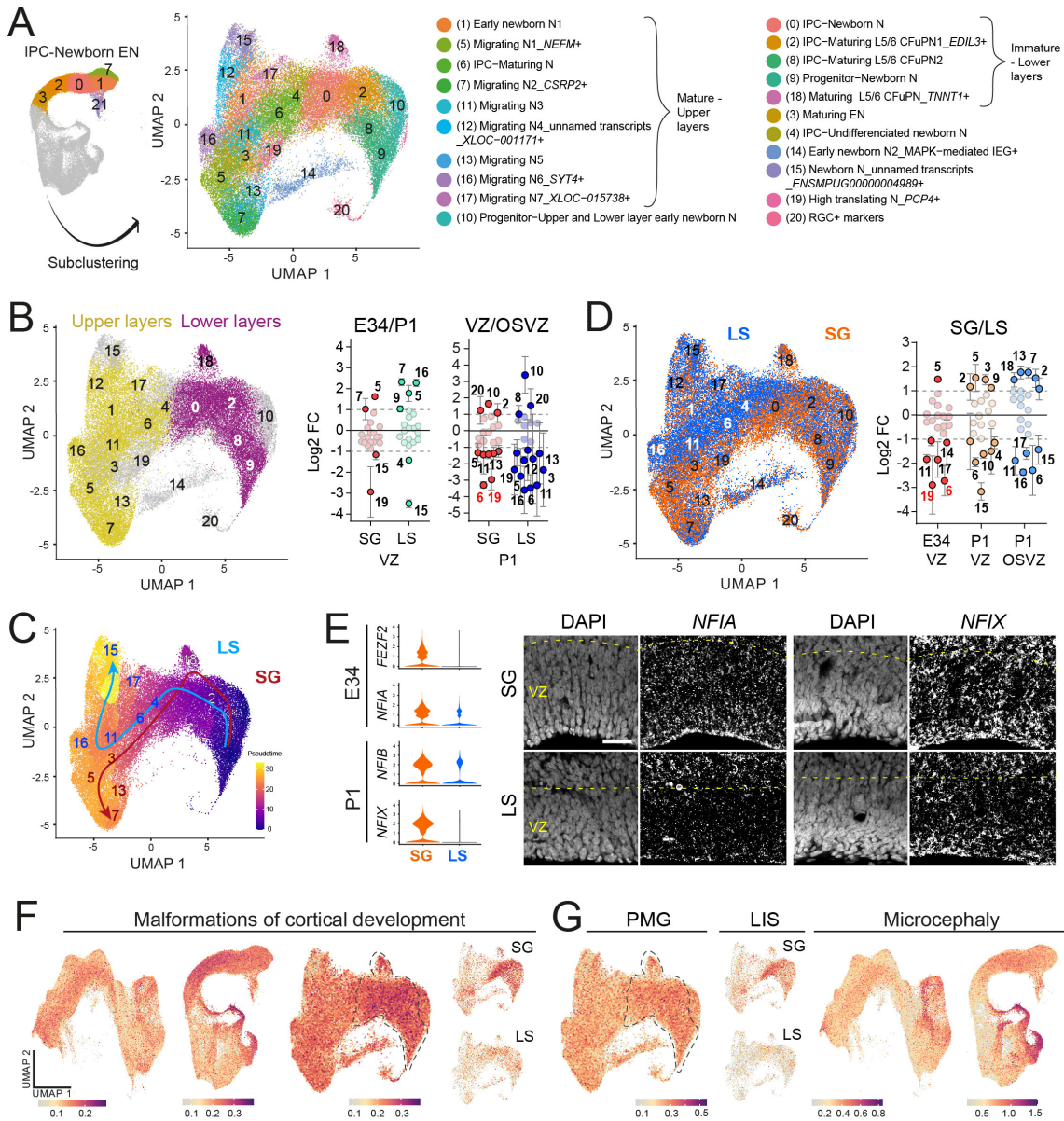


**FIGURE 7. Different newborn neuron classes in gyrus and sulcus and linked MCD.** (A) UMAP of subclustered IPC-newborn ENs from primary ferret dataset. (B-D) UMAPs highlighting “mature-upper layer” and “immature-lower layer” cluster sets (B), pseudotime (C) and cells coming from LS versus SG (D), and pair-wise cluster enrichment between conditions (B, D). Clusters above  $\pm 2$  log<sub>2</sub>FC are highlighted (mean  $\pm$  SEM), with red numbers indicating statistical significance (p-value adj.  $< 0.05$ ). In (C), cluster numbers indicated in blue are enriched in LS, in red are enriched in SG; arrows indicate estimated pseudotime trajectory of cells from each region. (E) Violin plots for DEGs between ENs in SG and LS, and RNAscope analysis at the corresponding ages. Adjusted p-values range from 2E-139 to 6.5E-25. Scale bar, 30  $\mu$ m. Dashed lines indicate borders of germinal layers.

**(F, G)** UMAPs showing enrichment values of genes linked to human MCD in general (F), or specifically in polymicrogyria (PMG), lissencephaly (LIS) or microcephaly (G). scRNAseq datasets from species integrated, primary ferret and neuronal ferret subset show gene score values from all conditions together. SG and LS plots show gene score values in VZ ENs at P1. Dashed lines delimitate lower layer clusters.

Human MCD are caused by mutations in developmentally relevant genes, but their expression and biological functions in normal development remain under debate ([Severino et al., 2020](#)). Analysis of our datasets revealed an overall enrichment of genes related to MCD in ENs and mitotic progenitors (Fig. 7F). More specifically, genes linked to lissencephaly (LIS) were higher in SG than LS of ENs at P1 VZ (Fig. 7G), supporting their executive role in cortex folding. Genes associated to microcephaly were highly enriched in mitotic RGCs and IPCs (not in G1), in agreement with their key role in mitotic spindle and neurogenesis (Fig. 7G). Genes related to polymicrogyria (PMG) were highly present across neuronal clusters, especially in immature lower layer neurons (Fig. 7G). Statistical analysis of MCD, PMG and LIS gene score values in the neuronal subset, confirmed their greater prevalence in SG compared to LS in P1 VZ, as well as their higher enrichment in lower versus upper layers (Fig. S21A-C).

## RESULTS



8. Supplementary figures

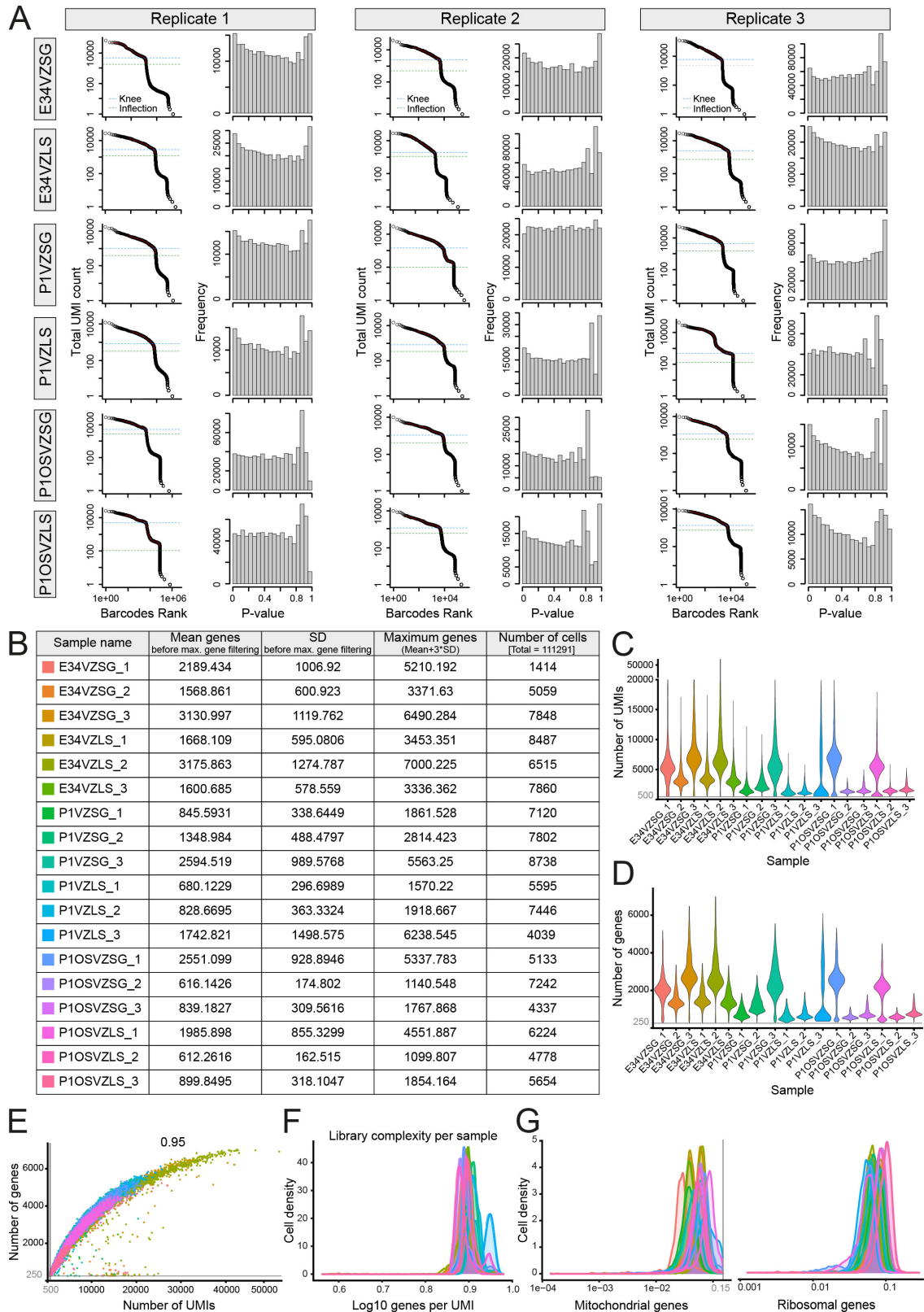


**FIGURE S1. Cell barcode filtering and high-quality cell parameters for each scRNAseq library.** (A) Knee plots to identify cell-containing droplets, and distribution of p-values from empty droplets. (B) Adaptive threshold for the maximum number of genes and cell outcome. SD, standard deviation. (C, D) Violin

## RESULTS - Supplementary

plots of fixed thresholds for minimum number of unique molecular identifiers (UMI) (C), and minimum number of genes (D). (E) Scatter plot of number of UMIs versus genes detected, with Pearson correlation value. (F, G) Cell density plots of log<sub>10</sub> genes identified per UMI (F), and ratio of mitochondrial and ribosomal genes per cell with maximum mitochondrial genes threshold (G). Number of libraries = 3 per condition, total n = 18.

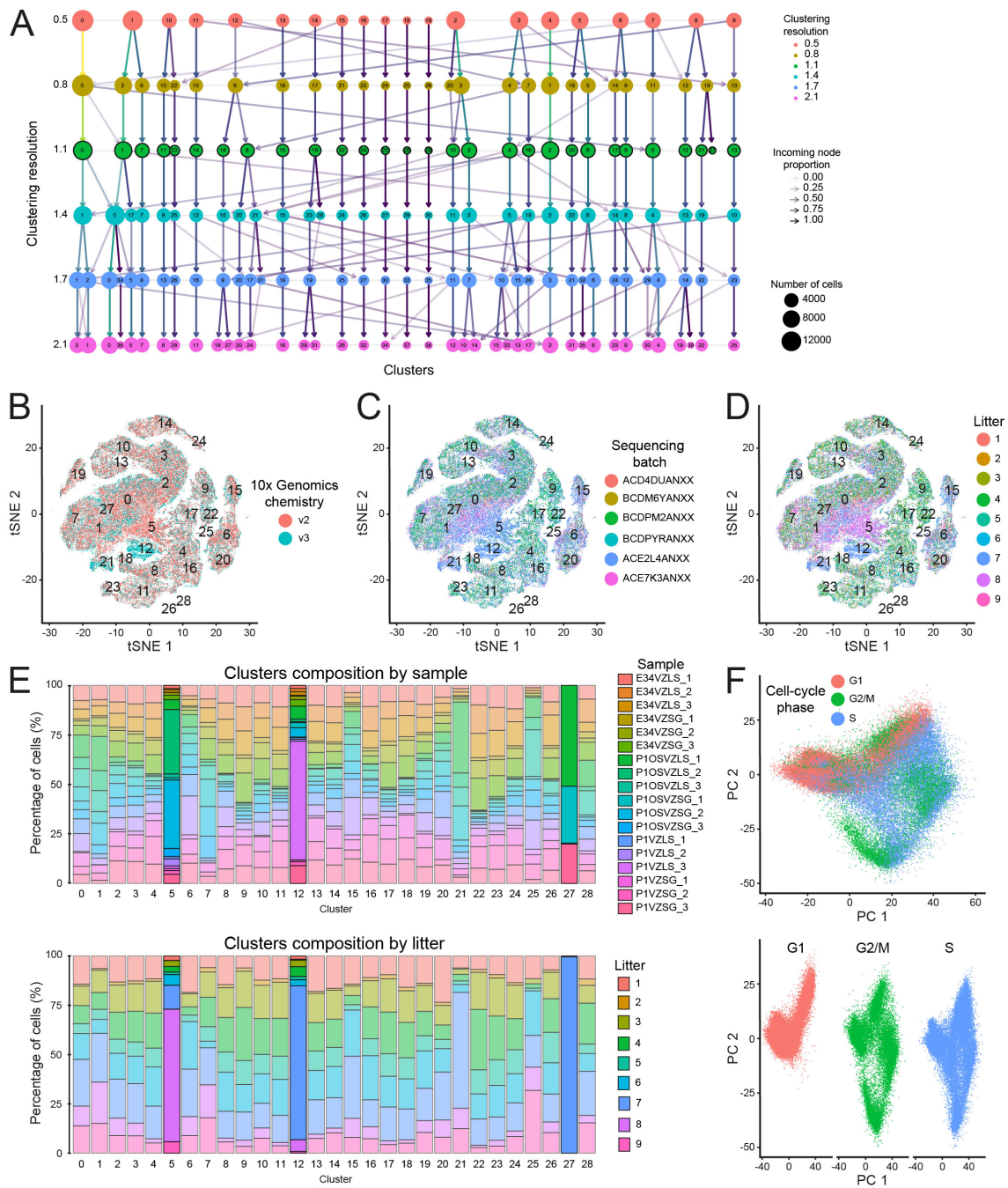


**FIGURE S2. Cluster resolution and evaluation after sample integration.** (A) Tree of relationship between clusters as resolution increases for 37PCs, highlighting the 1.1 resolution selected. (B-D) t-SNE plots of cells, identified by 10x Genomics chemistry (B), sequencing batch (C), and ferret litter of origin (D) to identify confounding sources of unwanted variation. (E) Normalized frequency distribution of cells per cluster, colored by sample or litter of origin, with litter-specific clusters 5, 12 and 27 highlighted. (F) PCA plot with cells color-coded according to their cell-cycle phase, after regressing out the difference between S and G2/M phases.

# RESULTS - Supplementary



**FIGURE S3. Ferret cell cluster characterization. (A)** t-SNE plot identifying cell clusters, with litter-specific clusters (5, 12, 27) in grey. **(B)** Dot-plot of canonical marker expression levels across clusters of the excitatory neuron lineage. **(C)** Top marker transcripts in each cell cluster used to define their individual identity and name.

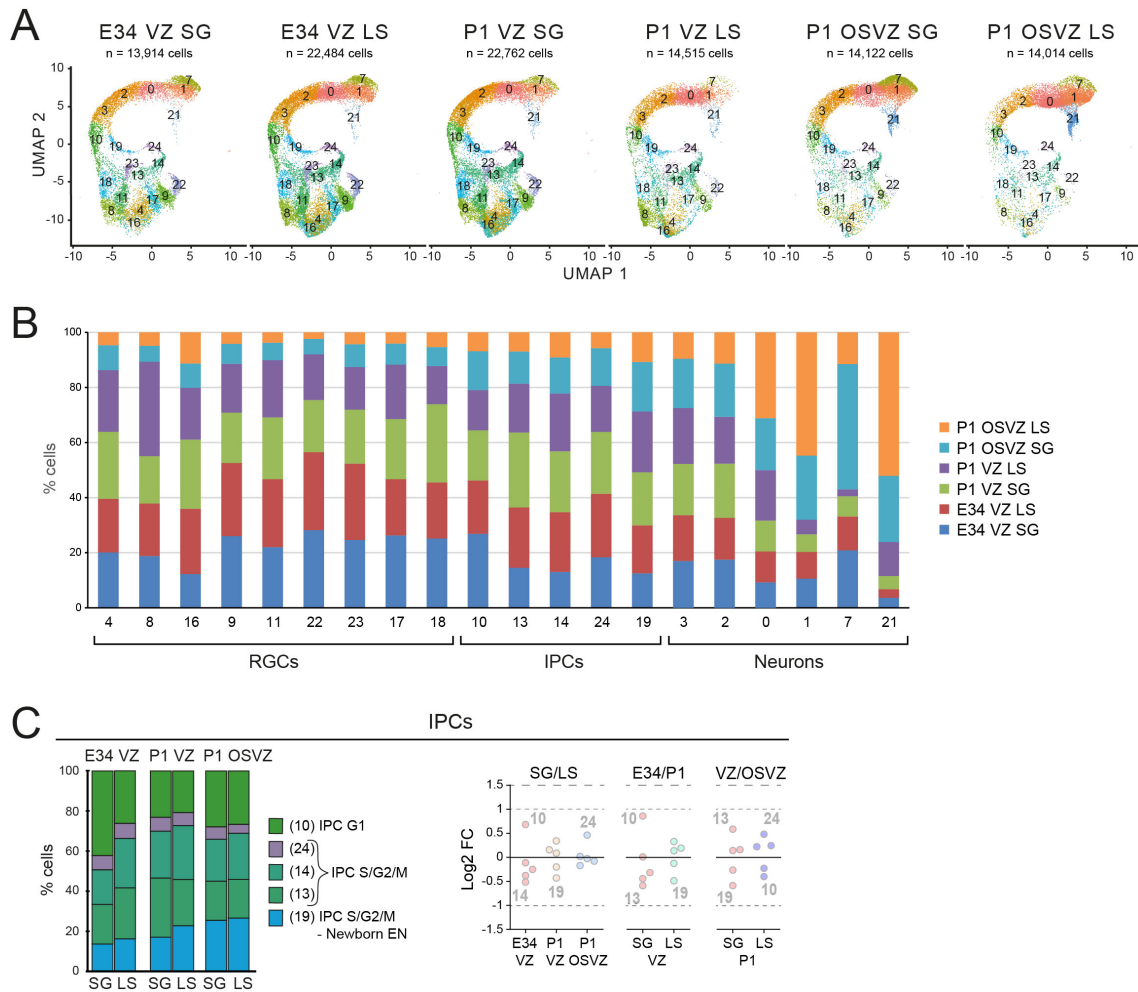


**FIGURE S4. Cluster composition across experimental conditions and IPC cluster enrichment.** (A) UMAPs showing the cell contribution of each experimental condition to clusters involved in the excitatory neuron lineage. The number of cells in each dataset is indicated. (B) Normalized frequency distribution of cells from each condition across clusters. (C) Normalized frequency distribution of IPC clusters across conditions, and pair-wise cluster enrichment between conditions. No cluster was enriched near or above  $\pm 2 \log_2FC$ .

RESULTS - Supplementary



**FIGURE S5. Differential gene expression between conditions in main cell types.** Violin plots for all DEGs identified between VZ versus OSVZ at P1, and SG versus LS at E34 and P1 in VZ, in the three main cell types. Adjusted p-values range from 2.2E-308 to 0.02. Genes without name are shown as shorten Ensembl ids (ENSMPUG00000XXXXX).

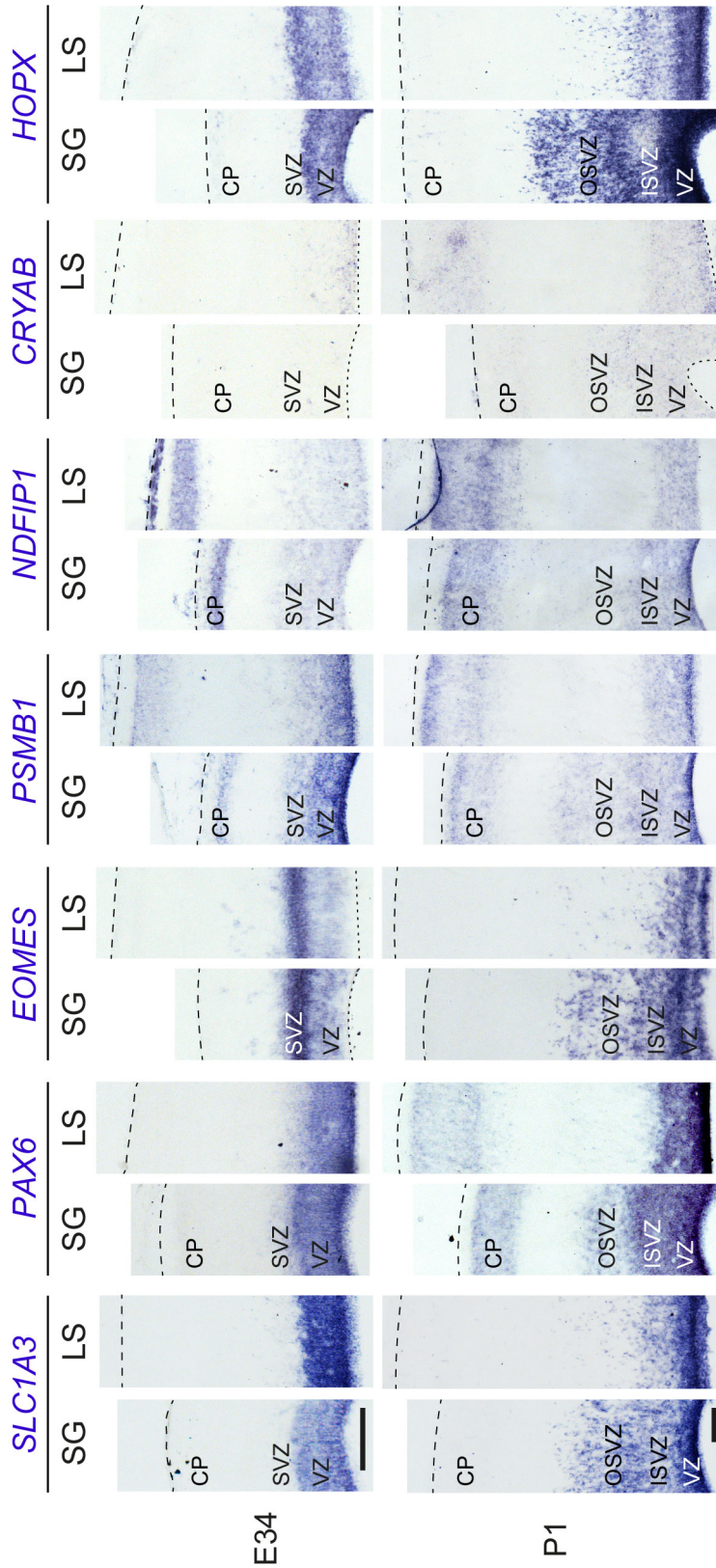


**FIGURE S6. Patterns of gene expression across experimental conditions.** Conventional ISH stains for canonical markers of cortical progenitor cells (*SLC1A3*, *PAX6*, *EOMES*, *HOPX*) and DEGs at P1 between VZ and OSVZ (*PSMB1*, *NDFIP1*, *CRYAB*) and between SG and LS (*CRYAB*). CP, cortical plate; SVZ, subventricular zone; ISVZ, inner subventricular zone; OSVZ, outer subventricular zone; VZ, ventricular zone. Dashed lines indicate basal pial surface and dotted lines indicate apical ventricular surface. Scale bars, 100 $\mu$ m.

## RESULTS - Supplementary

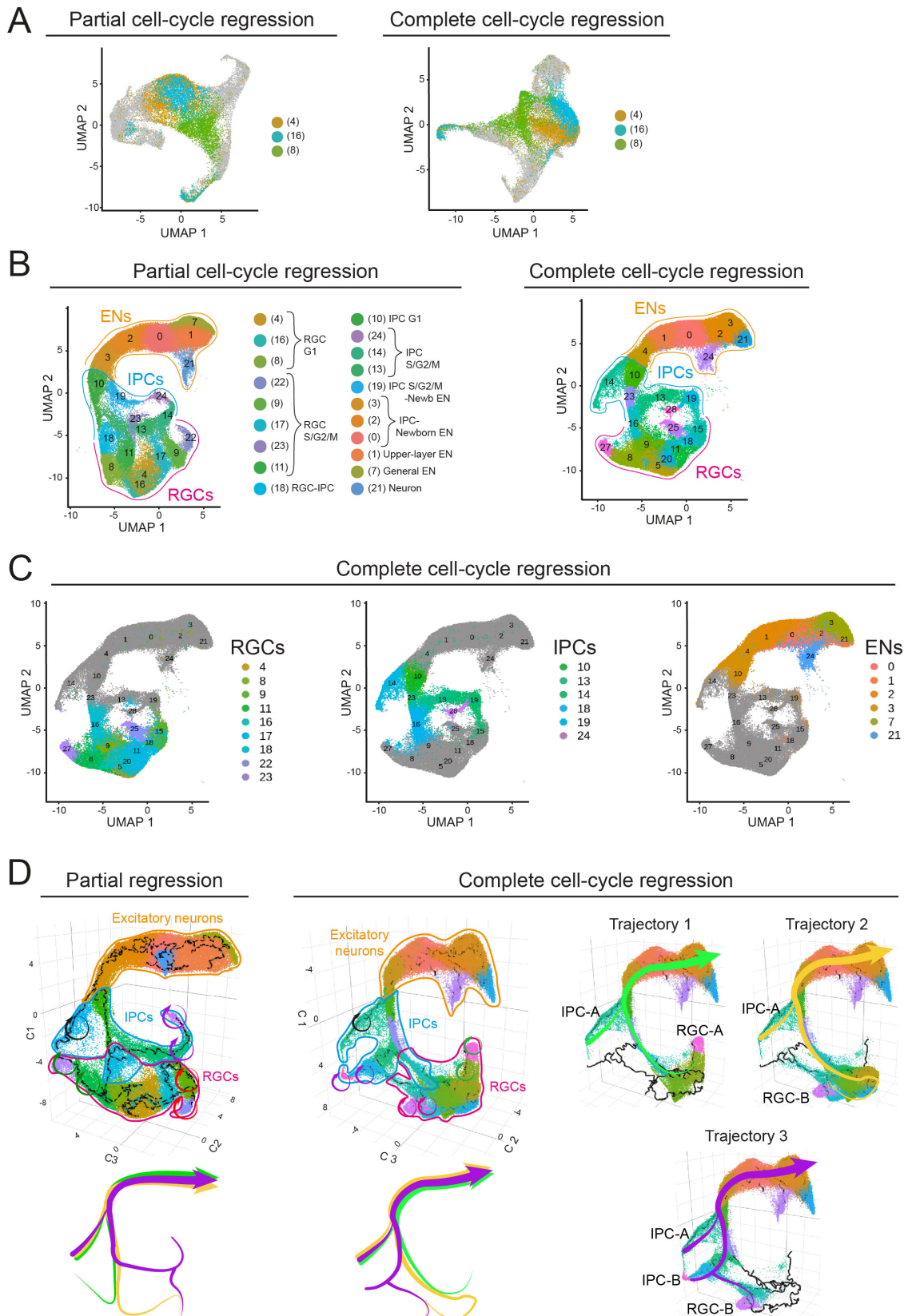


**FIGURE S7. High similarity in cell clustering and transcriptional trajectories between partial and complete cell-cycle regression of the ferret dataset. (A)** UMAPs of subclustered RGCs after partial or complete cell-cycle regression, as indicated. Cells in clusters 4, 8 and 16 are color-coded as in Fig. 1D. **(B)** UMAPs and cell clustering of the full ferret dataset after partial or complete cell-cycle

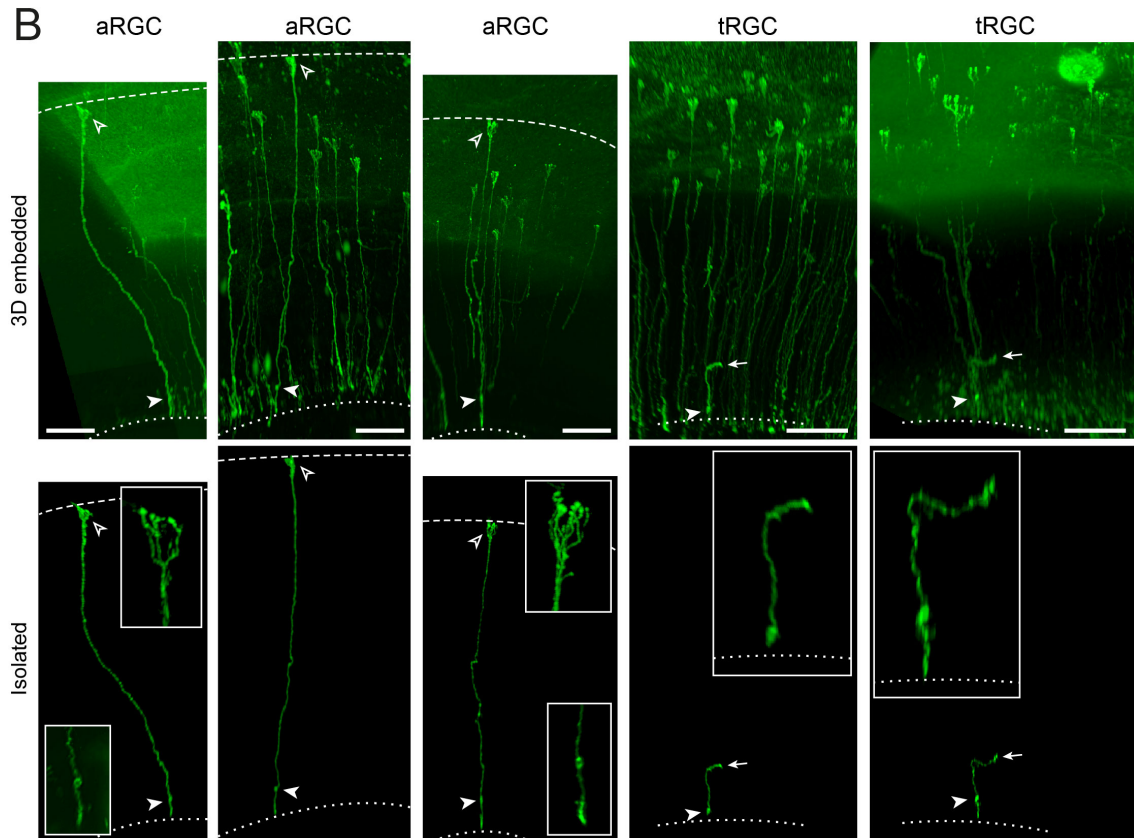


regression, as indicated. Clusters containing cells of the major cell types are indicated. **(C)** UMAPs after complete cell-cycle regression indicating the location of RGC (left), IPC (center) and EN (right) clusters, as identified after partial cell cycle regression (B). **(D)** 3-D UMAPs with trajectory reconstructions. Circular arrows indicate clusters of mitotic progenitors. Hand-drawn arrows indicate the three main trajectories identified, which involved the same cluster sequences with partial and complete cell-cycle regression (related to Fig. 3).

A

Cluster name	Top marker transcripts
8A <span style="color: orange;">●</span> (s4)	<i>TCF12, RYBP, XLOC-032047, RARRES2, ILKAP, Eif3f, SPARC, PKIA, GRIA2, RPS29, IGFBP5, PEA15, ENSMPUG00000014448, RPS25, XLOC-031135, XLOC-031140, Rpl36-ps3, ENSMPUG00000016488</i>
8B <span style="color: cyan;">●</span> (s6)	<i>CRYAB, GADD45B, PCP4, ENSMPUG00000010428, PKIA, PDLIM4, ITGB8, DNAJC1, XLOC-032047, ANXA5, CAP2, ENSMPUG00000019191, AZIN1, SDC2, CNN3, SPARC, ZFP36, CYR61, OGN, TPM1</i>
8B <span style="color: green;">●</span> (s2)	<i>CTHRC1, SCOC, MAD2L2, TFDP2, TOP2B, TPR, EIF4B, CORO1C, RND3, IGFBP5, NANS, PAK3, NCL, TOX3, ZEB1, PEG3, ELAVL4, RGS16, NEUROG2, ILKAP</i>
16A <span style="color: red;">●</span> (s3)	<i>HSPA1B, XLOC-006214, ID1, MGST1, BCAN, RASGRP2, NCAN, MFGE8, APOE, PTN, NTRK2, CSDC2, MMD, SERPINE2, TTYH1, GSDPD2, XLOC-032605, CLU, CST3, SMPDL3A</i>
16B <span style="color: teal;">●</span> (s1)	<i>TYMS, SDF2L1, HOPX, XLOC-006214, ENSMPUG00000010427, HELLS, DAB1, TUBB4B, CSDC2, PCNA, ENSMPUG00000016702, TUBB2B, XLOC-032605, DNMT1, FOS, MMD, SEC11C, XLOC-018857, SMPDL3A, TUBA1C</i>
16B <span style="color: green;">●</span> (s9)	<i>CDCA3, CENPF, SPC24, ENSMPUG00000008844, ENSMPUG00000014648, XLOC-036181, DNMT1, UHRF1, CKS1B, HMGB2, 2810417H13RIK, GINS1, H2AFZ, TUBA1C, CDK1, TOP2A, RRM2, GSE1, PCNA, DCK</i>

B



C

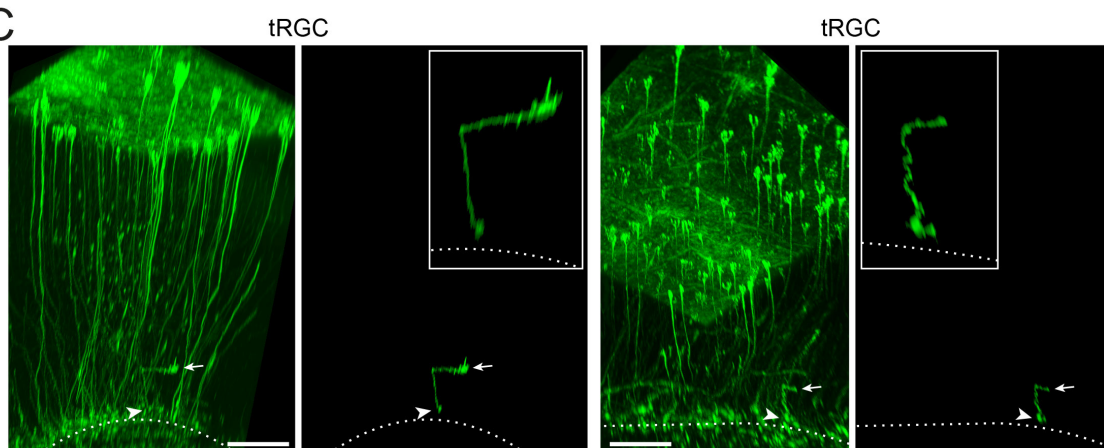


**FIGURE S8. RGC markers and morphologies in the neonatal ferret cerebral cortex. (A)** Top marker transcripts for subclusters of primary RGC classes 8 and 16 at P1, as indicated. **(B, C)** Images from brains of P2 (B) and P6 (C) ferrets clarified after EGFP-electroporation at P1, showing examples of RGC types, as indicated. Example EGFP+ RGCs are shown embedded in their 3-dimensional

context with other EGFP-labeled cells, and then digitally isolated. Insets show high magnifications of the digitally isolated tRGCs, or details of aRGCs. Arrows indicate tip of the truncated basal process in tRGCs, solid arrowheads indicate cell soma and open arrowheads indicate basal endfoot arbors of aRGCs. Dashed lines indicate basal pial surface and dotted lines indicate apical ventricular surface. Scale bars, 150  $\mu\text{m}$ .

## RESULTS - Supplementary

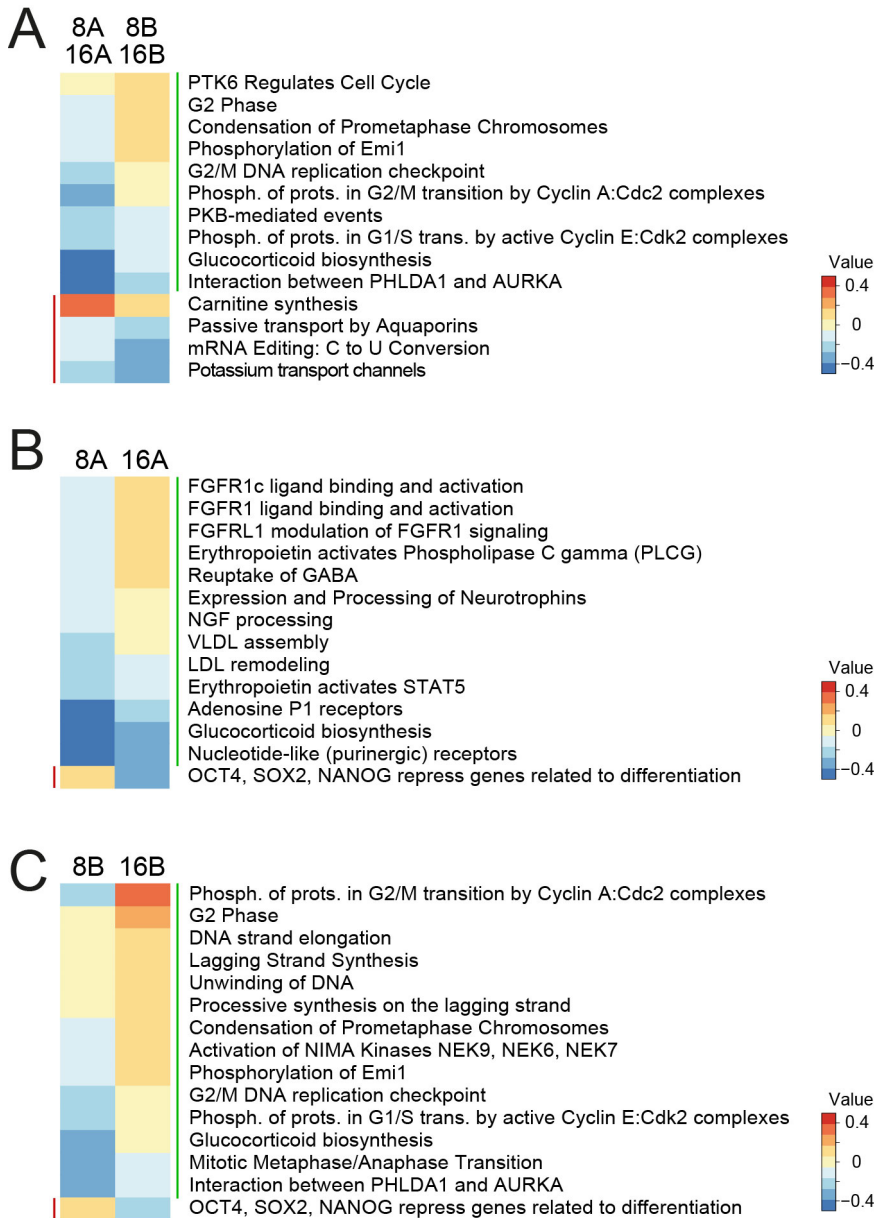


**FIGURE S9. Characterization of primary RGC classes 8 and 16 at P1.** Differential Reactome pathway analysis between P1 RGC classes (8A, 8B, 16A and 16B), as indicated. Red and green lines indicate Reactome terms differentially enriched in the left and right columns, respectively.

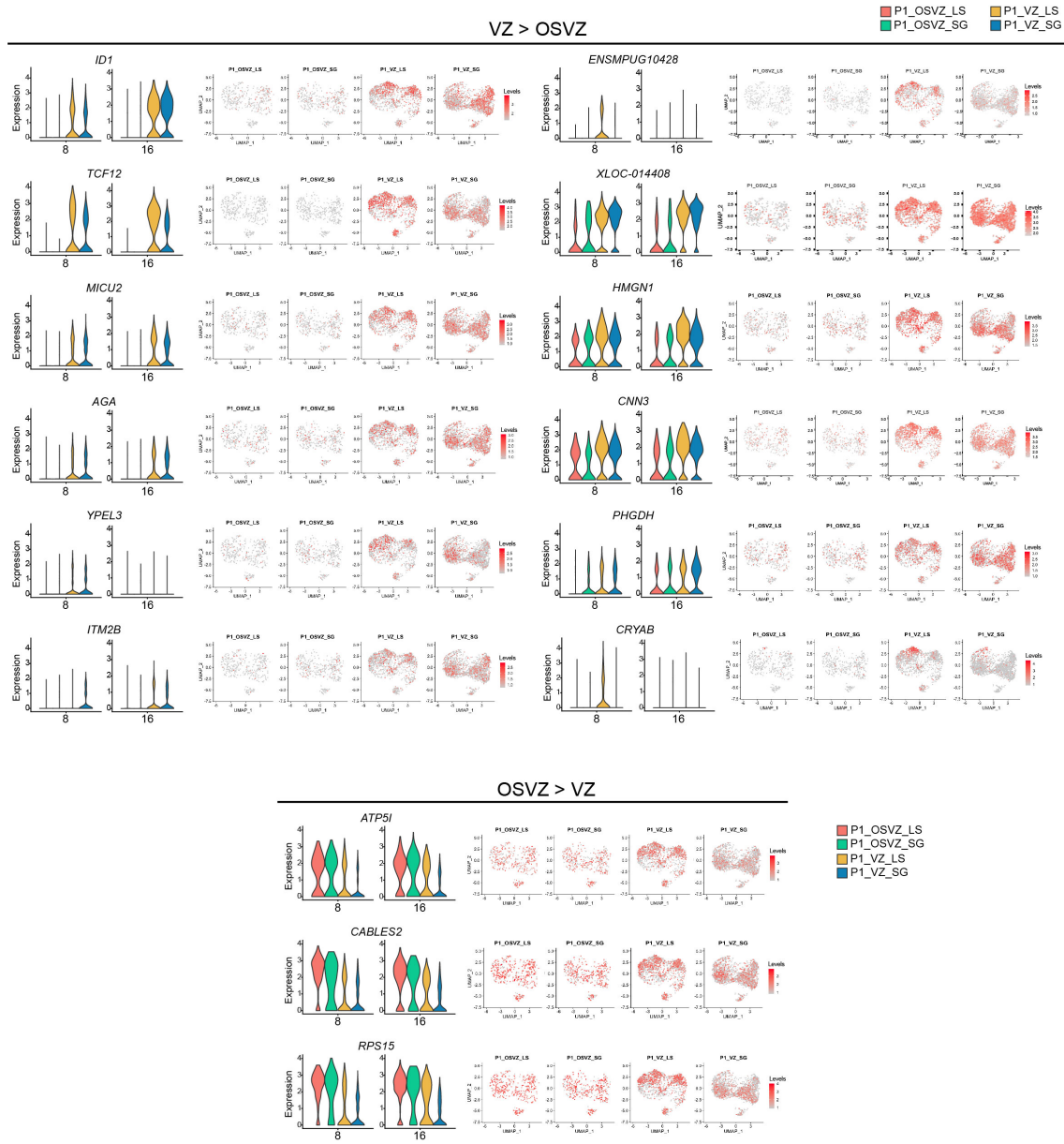


**FIGURE S10. Differential gene expression between germinal layers in primary RGC clusters 8 and 16 at P1.** Violin plots and expression UMAPs of DEGs between germinal layers in primary P1 RGC clusters 8 and 16, as indicated. Adjusted p-values range from 2.2E-308 to 0.03. Genes without name are shown as shorten Ensembl ids (ENSMYPUG00000XXXXX).

# RESULTS - Supplementary

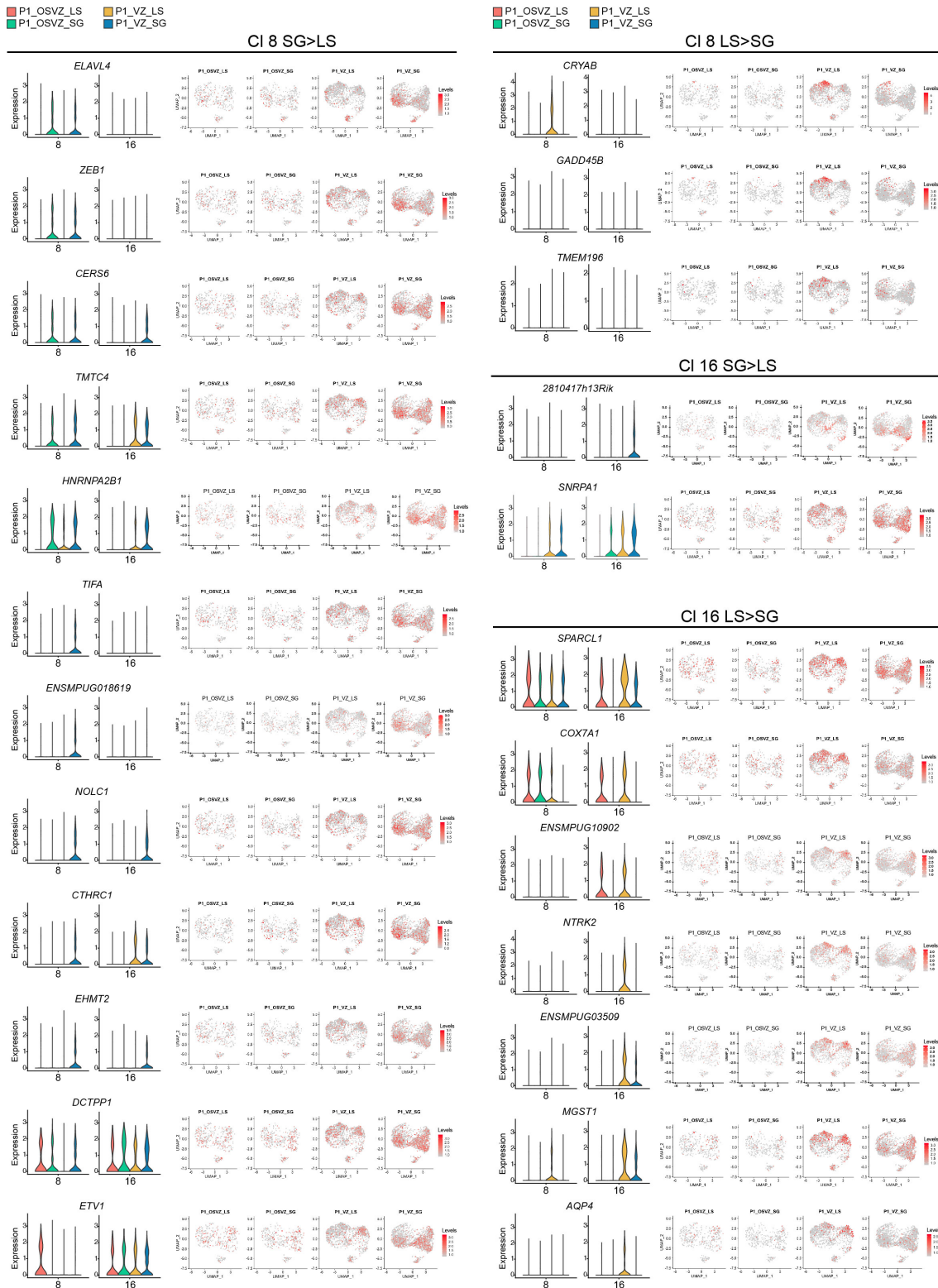


**FIGURE S11. Differential gene expression between cortical areas in primary RGC clusters 8 and 16 at P1.** Violin plots and expression UMAPs of DEGs between cortical areas in primary P1 RGC clusters 8 and 16, as indicated. Adjusted p-values range from  $2.1E-45$  to  $0.03$ . Genes without name are shown as shorten Ensembl ids (ENSMYPUG00000XXXXX). *TMEM196* does not appear as a DEG significantly in the indicated comparison, but has a specific distribution to define the tRGC cluster, similar to *CRYAB* and *GADD45B*.

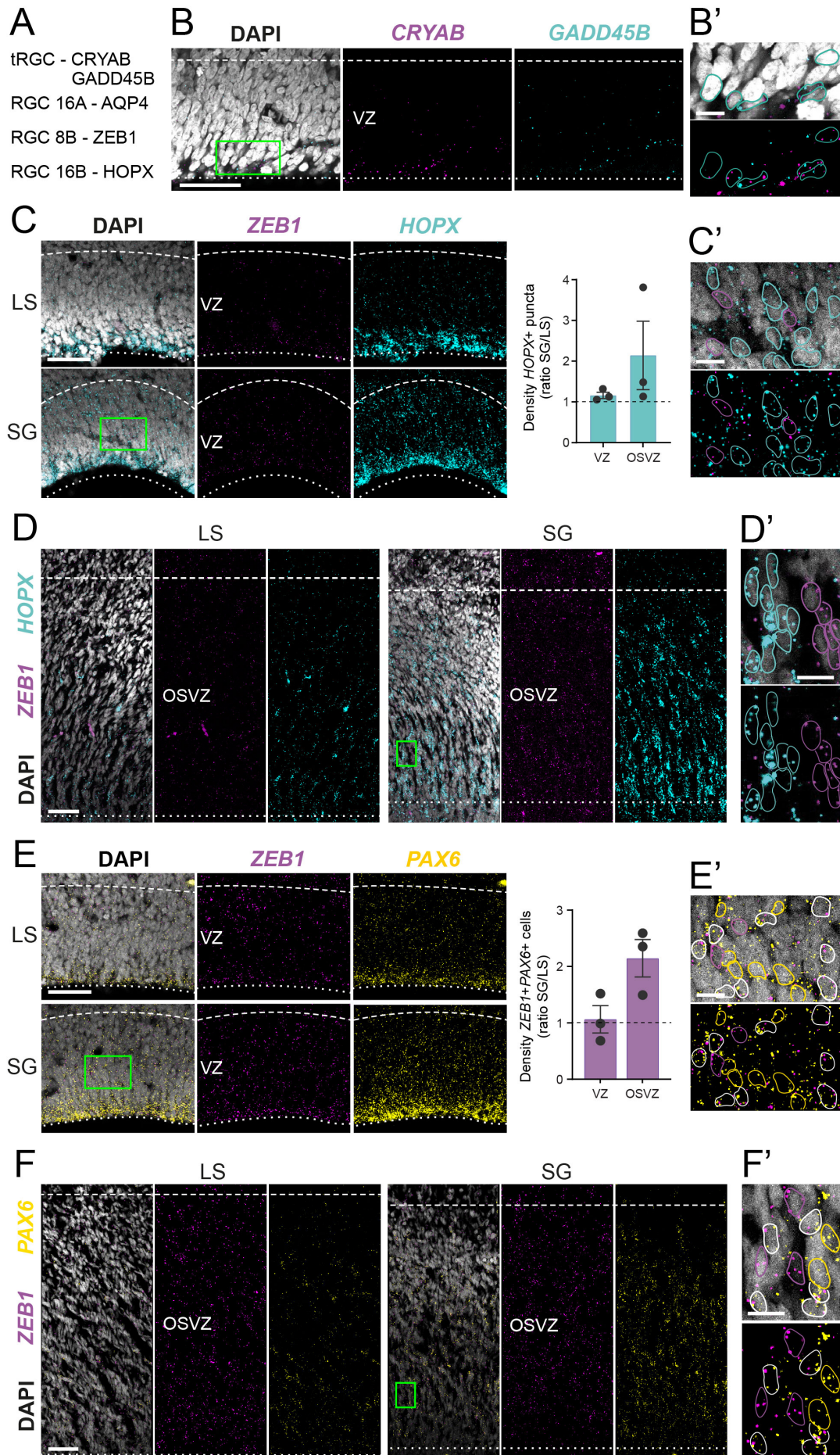


**FIGURE S12. RNAscope analysis of marker genes for RGC classes at P1.** (A) P1 RGC type and associated marker gene (related to Fig. 2). (B, B') Expression patterns of *CRYAB* and *GADD45B* in VZ of LS (B), and high magnification (green box in B) showing coexpression in individual cells (colored contours) (B'). (C-D') Expression patterns of *ZEB1* and *HOPX*, and quantification of *HOPX* in SG compared to LS in VZ (C) and OSVZ (D); and high magnifications showing absence of coexpression in individual cells (colored contours) in VZ (C') and OSVZ (D'). (E-F') Expression patterns of *ZEB1* and *PAX6* in VZ (E) and OSVZ (F), and quantification of density of *ZEB1*-expressing *PAX6*<sup>+</sup> cells in SG compared to LS; high magnifications showing coexpression in individual cells (white contours) in VZ (E') and OSVZ (F'). *PAX6* transcripts are present in primary RGC classes 8 and 16, as well as other RGC types (yellow contours) with an uneven distribution between them (see Fig. S3B) and between germinal layers (see Fig. S6). *ZEB1* transcripts are present also in non-RGCs. Scale bars 50µm low magnification and 10µm high magnification images. Dashed lines indicate basal borders and dotted lines apical borders of germinal layers.



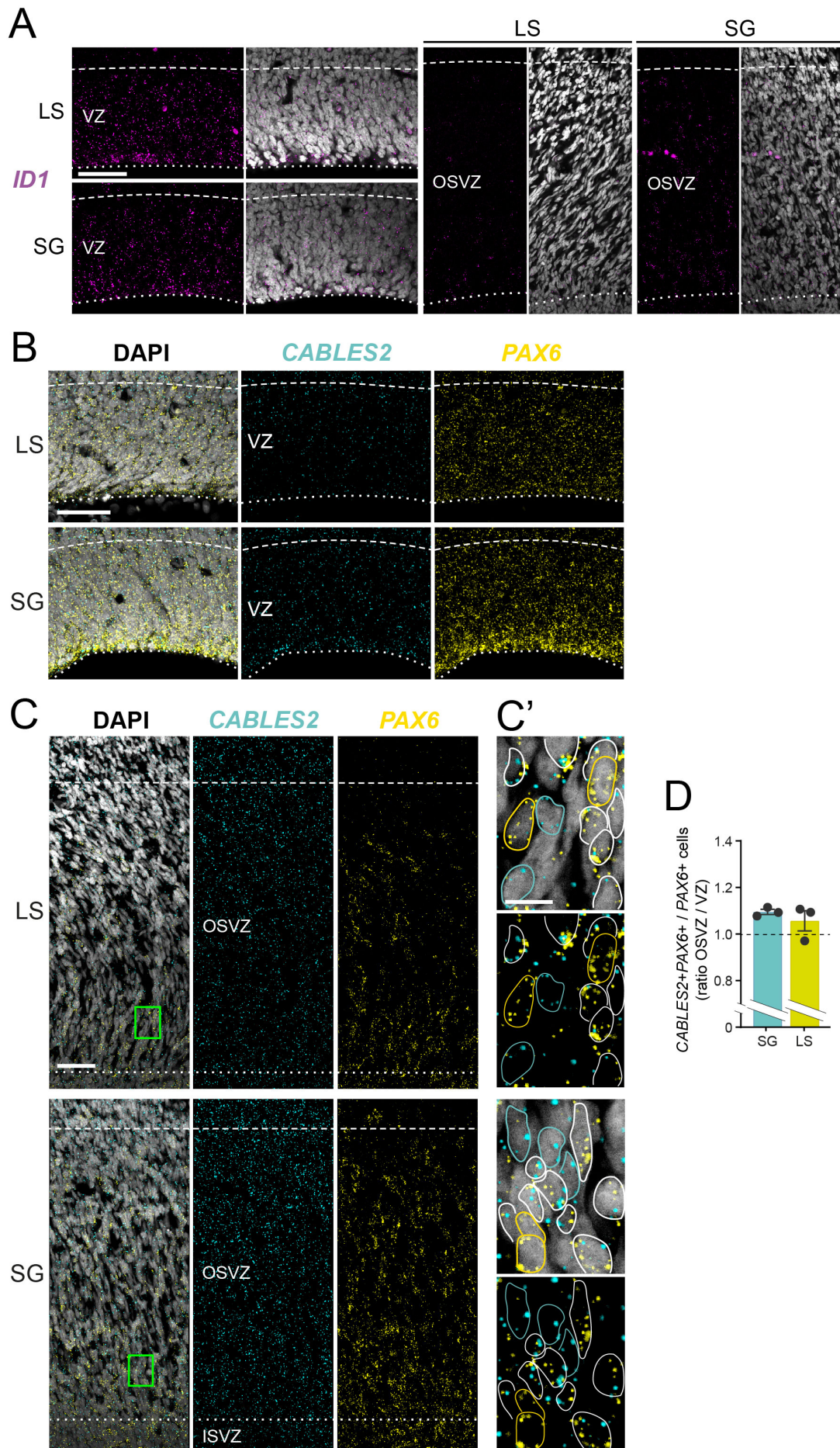


**FIGURE S13. RNAscope analysis of marker genes for microdissected layers at P1.** (A) Expression patterns of *ID1* in VZ compared to OSVZ in SG and LS, as indicated. (B-C') Expression patterns of *CABLES2* and *PAX6* in VZ (B) compared to OSVZ (C) in SG and LS, as indicated; and high magnifications from OSVZ (green boxes in C) showing coexpression in individual cells (white contours), as well as single *PAX6*<sup>+</sup> or *CABLES2*<sup>+</sup> cells (yellow and blue contours, respectively) (C'). (D) Quantification of the proportion of *PAX6*<sup>+</sup> cells expressing *CABLES2* in OSVZ compared to VZ. The low difference in *CABLES2*<sup>+</sup>*PAX6*<sup>+</sup> cells in LS is likely due to the uneven distribution of *PAX6* across RGC types (see Fig. S3B) and germinal layers (see Fig. S6). *CABLES2* transcripts are found also in non-RGCs. Scale bars 50µm low magnification and 10µm high magnification images. Dashed lines indicate basal borders and dotted lines apical borders of germinal layers.

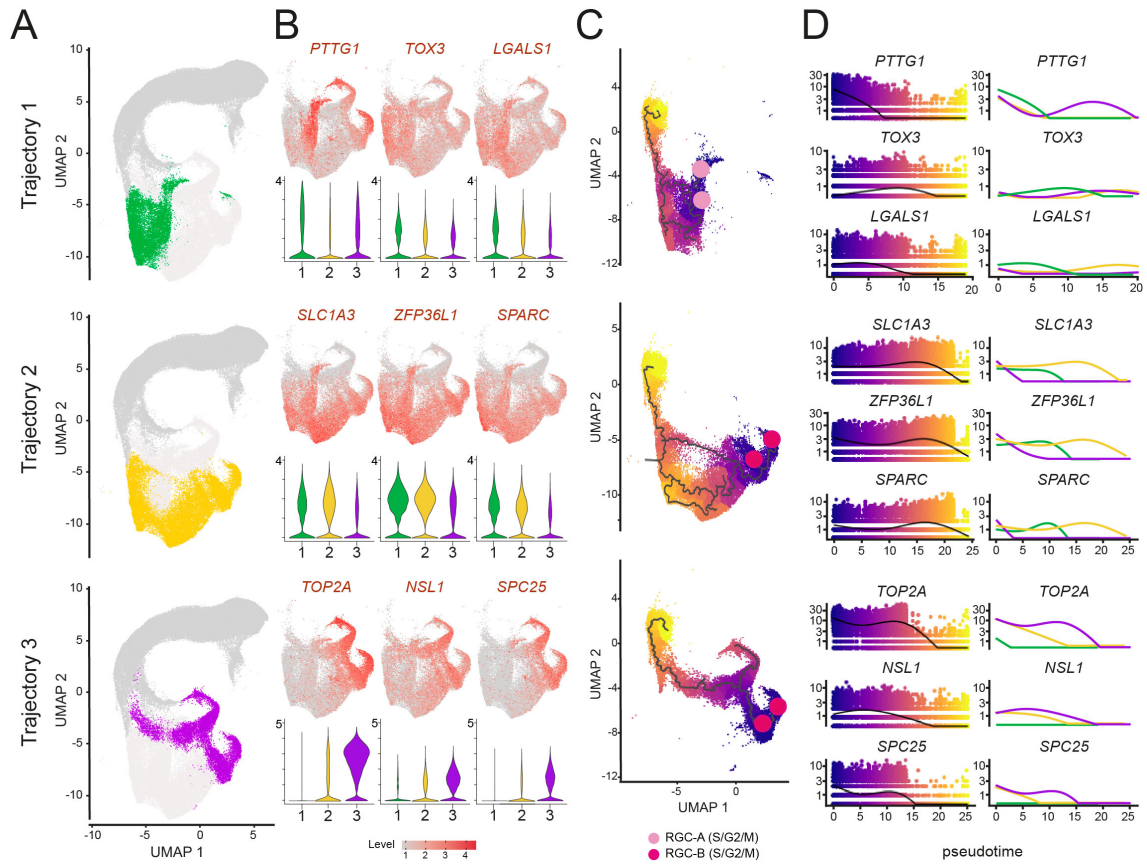


**FIGURE S14. Transcriptional profile of progenitor cell trajectories.** (A) UMAPs highlighting the distinct progenitor cell populations involved in each trajectory. (B) UMAPs and violin plots of the level of key genes defining the transcriptomic signatures of each trajectory. (C) Pseudotime and trajectories highlighting the mitotic RGCs of origin (pink circles for RGC-A and red for RGC-B). (D) Comparison of the dynamics of gene levels as a function of pseudotime across trajectories. Adjusted p-values range from  $2.2E-308$  to  $1.9E-57$ .

## RESULTS - Supplementary

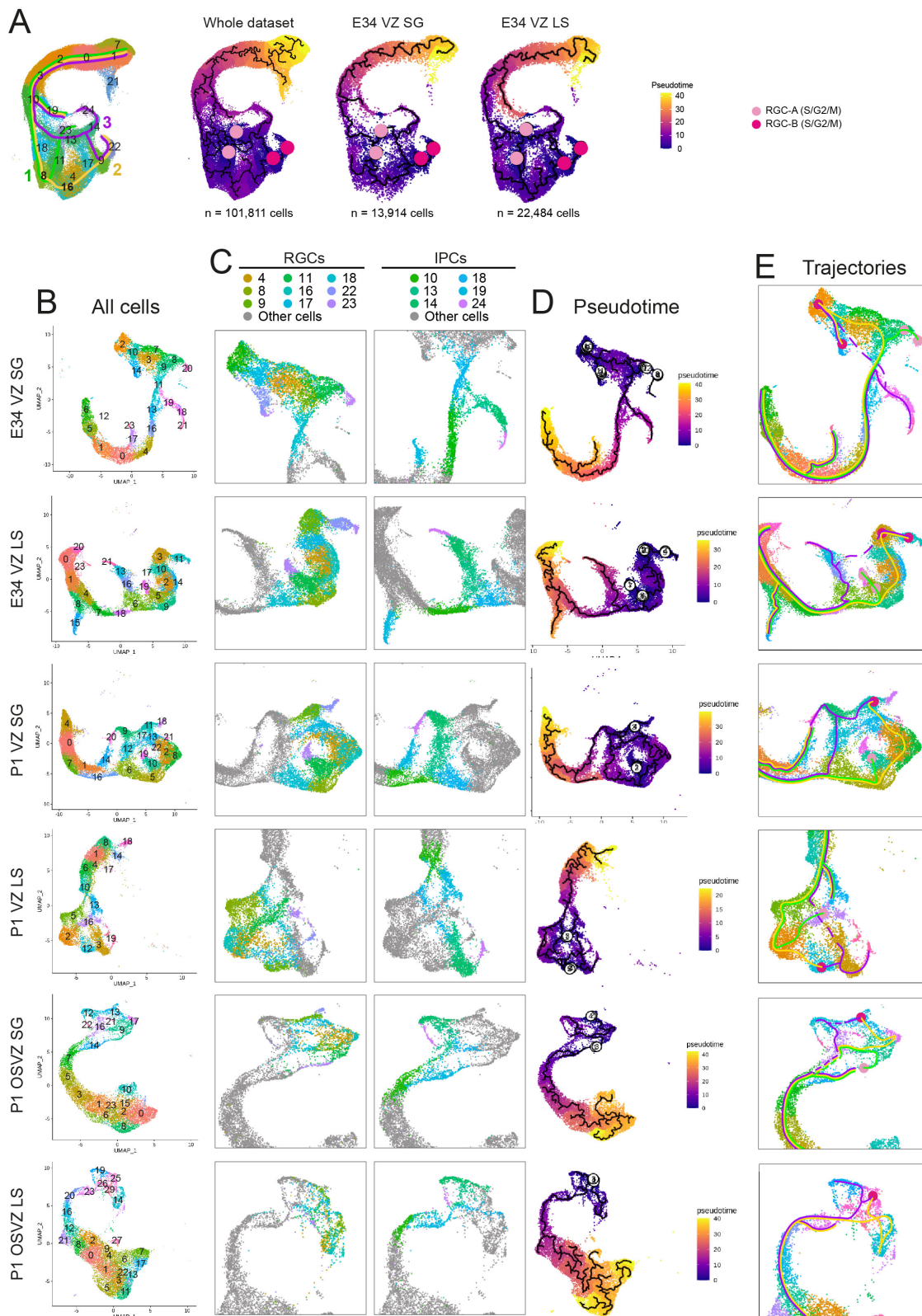


**FIGURE S15. Cell trajectories in the developing ferret cortex.** (A) UMAP of cell clusters showing the three trajectories identified in Fig. 3B, and pseudotime and trajectory plots of the complete ferret dataset and individual E34 conditions, indicating the RGCs of origin (pink circles for RGC-As and red for RGC-Bs). Total number of cells in each condition is specified. (B) UMAPs of integrated replicates for each individual experimental condition, showing cell clusters. (C) Distribution

of RGC and IPC clusters as identified in Fig. 1D, and involved in each of the three trajectories identified. **(D)** Pseudotime and trajectory plots for each integrated experimental condition. **(E)** Identification in each individual dataset of the trajectories found in the full dataset, as in Fig. 3B. Trajectories are schematically indicated as color-coded lines. Dashed segments indicate parts of the trajectory not identified by Monocle.

## RESULTS - Supplementary

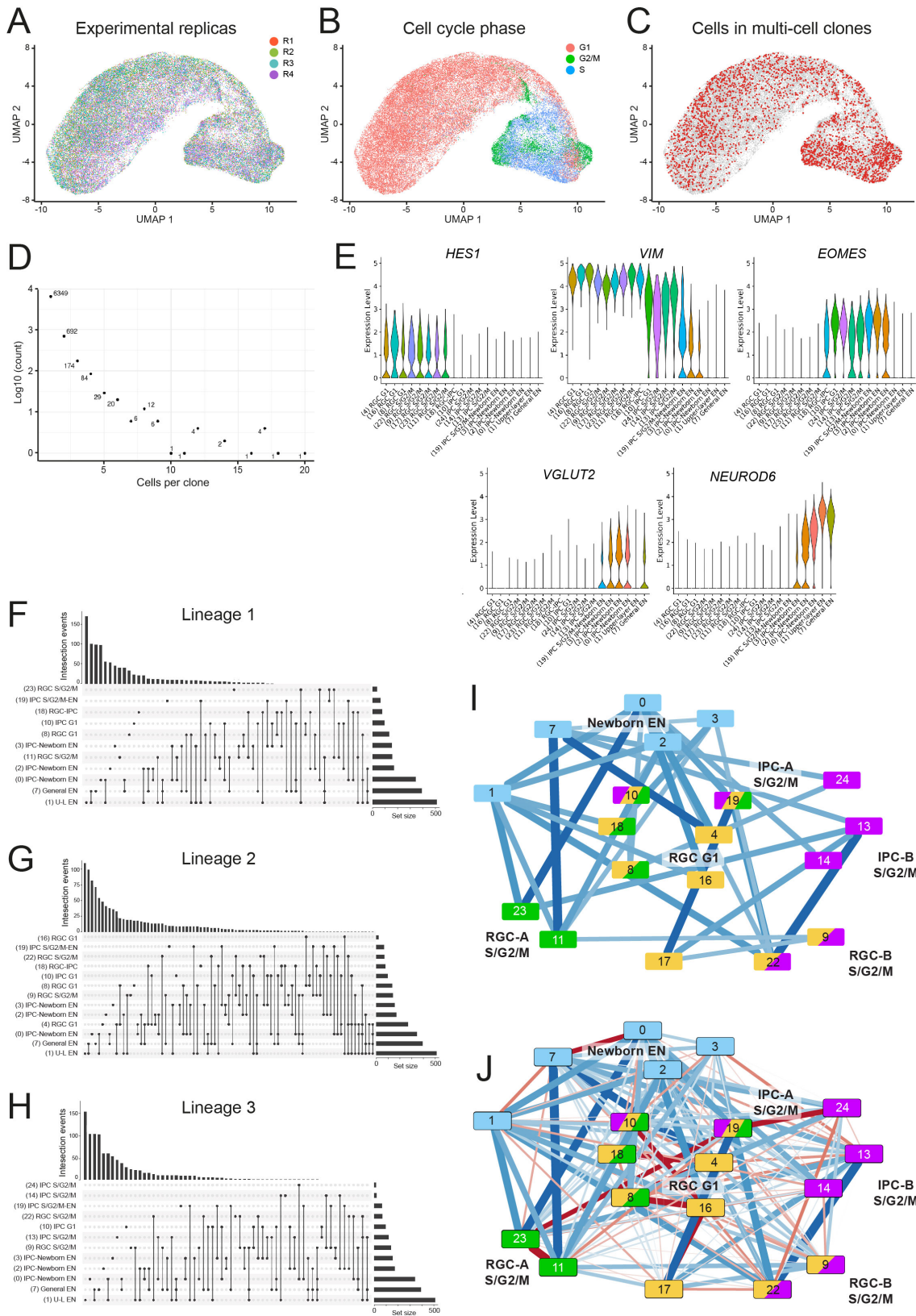


**FIGURE S16. Identification of cell lineages with barcode lineage tracing. (A-C)** UMAP-embedding of sampled cells colored by sequencing run (A), by cell-cycle phase (B) and if involved in multi-cell clones (C). **(D)** Abundance distribution of clones according to the number of cells per clone. **(E)** Expression levels of marker genes across label-transferred cell classes. **(F-H)** UpSet-plots of cell combinations

of clones from clusters that belong to each of the three lineages. Size of the interaction on top and absolute number of clones per cell cluster on the right. **(I, J)** Cell cluster network visualization, with edges representing negative (blue) (I, J) and positive (red) lineage coupling correlation scores. Position of nodes was set manually to facilitate reading.

## RESULTS - Supplementary

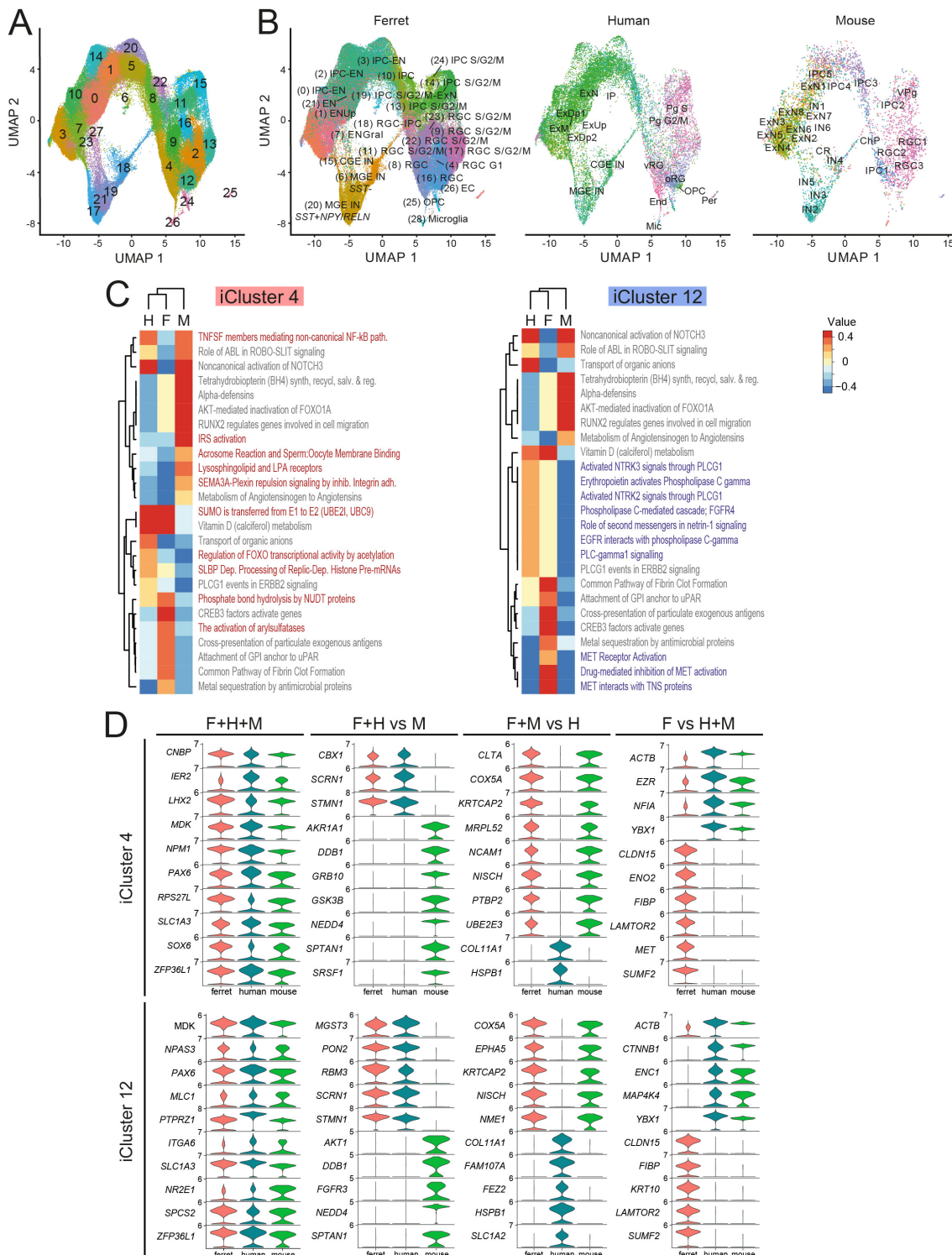


**FIGURE S17. Integration of ferret, human and mouse scRNAseq datasets, and analysis of similarities. (A, B)** UMAPs of cell clusters from the integrated multispecies dataset (A) showing the distribution of cells from each individual species with their original cluster names (B). **(C)** Differential Reactome pathway analysis between species in the integrated clusters (iCl.) 4 and 12, as indicated. Red and purple indicates pathways among top 25 that are specific for iCl.4 and iCl.12, respectively, and grey indicates common pathways. **(D)** Stacked violin plots for common and DEGs in the integrated clusters iCl.4 and iCl.12 across species. Adjusted p-values range from 2.2E-308 to 0.002.



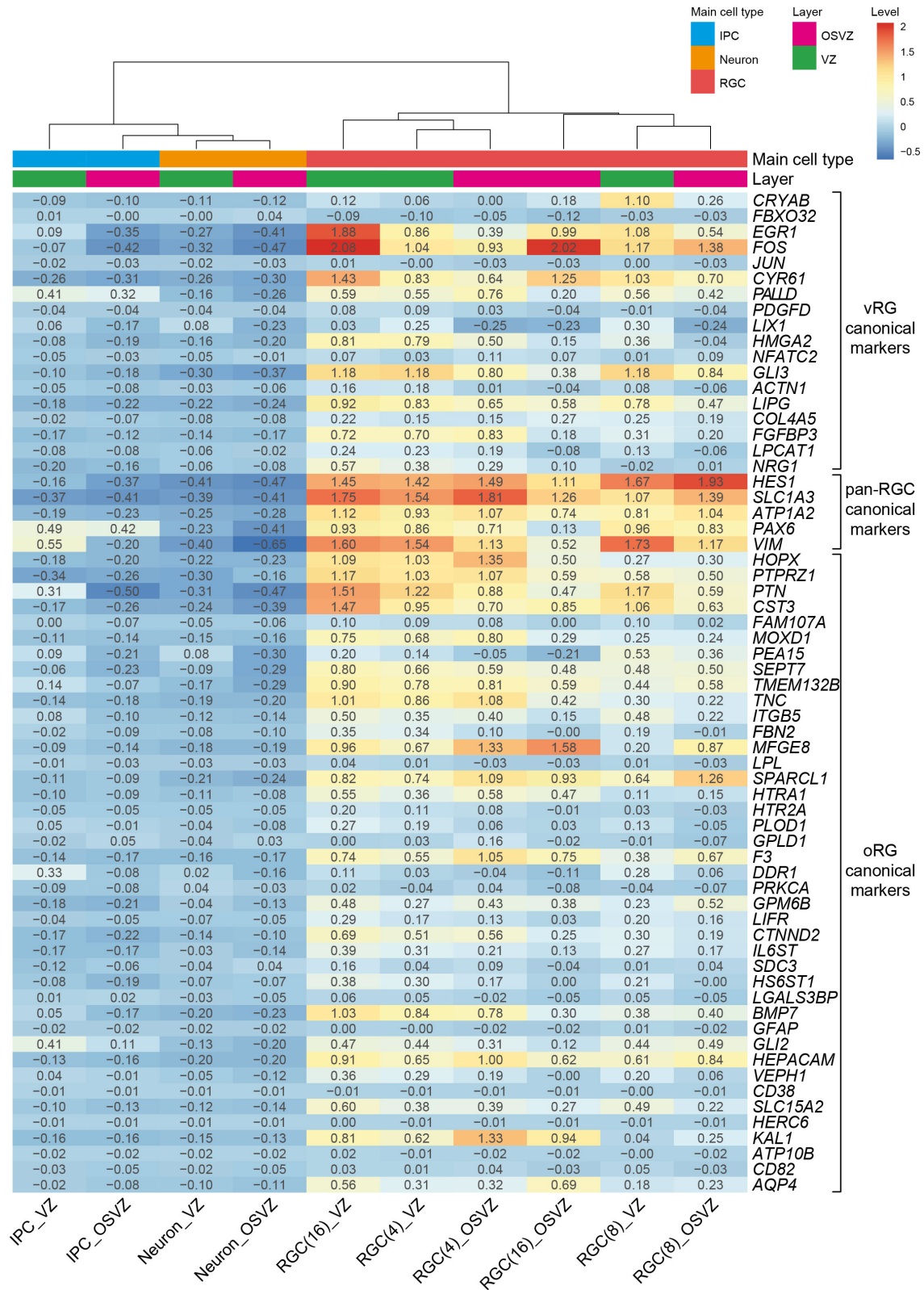


**FIGURE S18. Expression in ferret cells of canonical marker genes for human RGC types.** Heatmap of expression levels of canonical marker genes for human aRGC, bRGC and pan-RGC in the indicated ferret cell types, germinal layers and G1 RGC clusters. Color-code and numbers in heatmap cells indicate relative expression levels. Cladogram indicates similarity between samples.

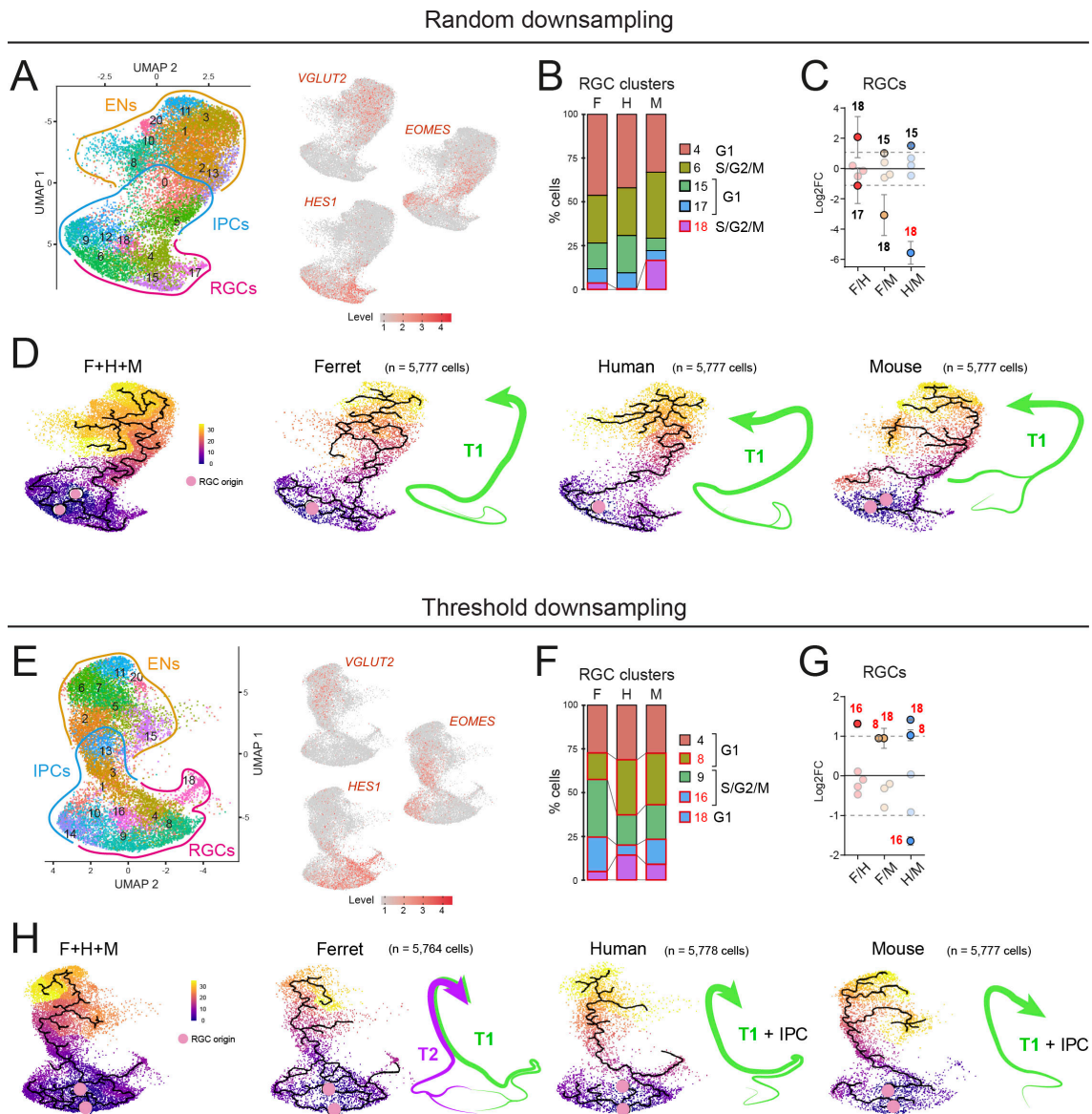
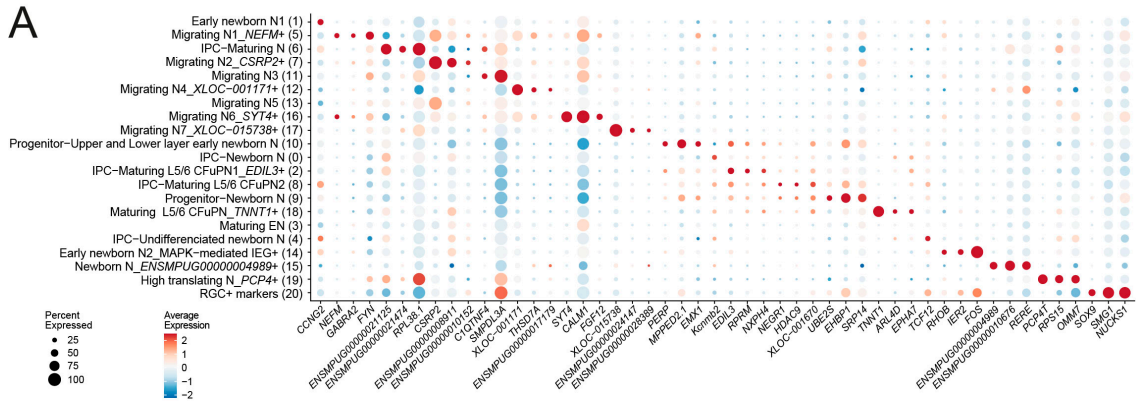


**FIGURE S19. Cell clustering and transcriptional trajectories of integrated multispecies datasets after equalizing cell numbers.** (A, E) UMAPs and clustering (showing only cells in the excitatory neuron lineage) and levels of marker genes for main cell types, after random (A) or threshold (E) downsampling of P1 ferret and human datasets to equalize the size of the available mouse dataset. (B, C, F, G) Normalized frequency distribution (B, F), and pair-wise cluster enrichment (C, G) of RGC classes after random or threshold downsampling, as indicated. Clusters above  $\pm 2$  log<sub>2</sub>FC are highlighted (mean  $\pm$  SEM), with red numbers indicating statistical significance (p-value adj. < 0.05). (D, H) Pseudotime and trajectory plots after random or threshold downsampling, as indicated, for the full downsampled dataset or by species. Mitotic RGCs of origin are highlighted (pink circles) and numbers of cells analyzed from each dataset are indicated. Green and purple arrows are interpretations of the trajectory results. After random downsampling (D), one similar single trajectory is identified in all species, with a minor variation in mouse. After threshold downsampling (H), two similar parallel trajectories are identified in ferret, but only one in human and mouse.



Cluster name	Top marker transcripts
(1) Early newborn N1	<i>XLOC-028896, STMN4.1</i>
(5) Migrating N1 _NEFM+	<i>CSRP2, NEFM, RUNX1T1, NEUROD6, XLOC-001171, DAB1, XLOC-018857, Shn1, NCAM1, THSD7A, KLHL5, SYT4, TENM2, GAP43, CELF2, INA, SCG3, CHL1, Nsg1, FEZF2</i>
(6) IPC-Maturing N	<i>ENSMYPUG00000010676, XLOC-011242, RPL38.1, MT-ND3, UNC5D, POU3F2, ENSMYPUG00000021474, FBXW7, XLOC-022239, XLOC-018446, ENSMYPUG00000021125, PCDH8, ARL4C, SEMA3C, BTG1, BASP1, MT-ND2, EPHA5, CENPV, NUDT4</i>
(7) Migrating N2 _CSRP2+	<i>CSRP2, XLOC-018857, RUNX1T1, NEUROD6, GAP43, TUBA1A, NCAM1, NTM, SYT4, Nsg1, KLHL5, PPP2R2B, THSD7A, CCSE1, Tubb3, BCL2, ABRACL, SOX5, ENSMYPUG00000010152, ENSMYPUG00000016045</i>
(11) Migrating N3	<i>SMPDL3A, Shn1.1, PID1, C1QTNF4, UNC5D, NEUROD6, NTM, XLOC-022229, JMJD1C, KLF6, BCL2, HS3ST1, SEMA3C, PLK2, XLOC-018446, LIMCH1, MT-ND3, BASP1, MT-ND2, POU3F2</i>
(12) Migrating N4 _unnamed transcripts_XLOC-001171+	<i>XLOC-001171, XLOC-022307, NTM, THSD7A, XLOC-018446, ENSMYPUG00000004989, ENSMYPUG00000029595, TENM2, XLOC-025818, EML6, CCSE1, LRR7, UNC5D, GRIN2B, LRR40, ENSMYPUG00000010902, ENSMYPUG00000001728, ENSMYPUG00000019825, ENSMYPUG00000010676, MYCBP2</i>
(13) Migrating N5	<i>CSRP2, XLOC-001171</i>
(16) Migrating N6 _SYT4+	<i>SYT4, DAB1, FGF12, CALM1, XLOC-018857, RUNX1T1, NEFM, Shn1.1, NEUROD6, XLOC-001171, NTM, CSRP2, ID2, TENM2, LIMCH1, CSRP3, CELF2, NCAM1, KLF6, KLHL5</i>
(17) Migrating N7 _XLOC-015738+	<i>XLOC-015738, ENSMYPUG00000024147, ENSMYPUG00000028389, PCDH7, INA, CUX2, XLOC-011242, MYT1L, MT-ND3, UNC5D, JMJD1C, POU3F2, PTBP2, EPHA5</i>
(10) Progenitor-Upper and Lower layer early newborn N	<i>EOMES, NEUROD4, MFAP2, VIM, MPPED2.1, ELAVL4, RND3, MDK, ENSMYPUG00000004181.1, PERP, PAX6, PTN, NHLH1, ENSMYPUG00000013479, ENSMYPUG00000030234, PCDH9, FAM110A, CD63, PAK3, IGFBP2</i>
(0) IPC-Newborn N	<i>CLIC1, ENSMYPUG00000009320, SLC25A5, FBXW7, NEUROD1, NRN1, ARHGAP20, Kcnmb2</i>
(2) IPC-Maturing L5/6 CFuPN1 _EDIL3+	<i>EOMES, RND3, ADRA2A, PCDH9, RASGRP1, NHLH1, FAM110A, NRN1, EDIL3, RPRM, ELAVL4, GABRB3, MFAP2, XLOC-028732, PAK3, ENSMYPUG00000030234, ENSMYPUG00000015996, AMPH, NEUROD1, XLOC-015136</i>
(8) IPC-Maturing L5/6 CFuPN2	<i>EOMES, RND3, NEUROD4, PCDH9, PAX6, MDK, XLOC-001670, CDK6, ENSMYPUG00000015996, ELAVL4, XLOC-003584, SLC25A5, ENSMYPUG00000004621, H2AFY2, EHPB1, DLGAP1, NEUROD1, GABRB3, DLL3, IGFBP2</i>
(9) Progenitor-Newborn N	<i>EOMES, MDK, NEUROD4, XLOC-003584, RND3, EHPB1, MFAP2, PAX6, CDK6, ELAVL4, NOTCH1, SRSF3, SOX6, ENSMYPUG00000004181.1, GAPDH, DUT, H2AFY2, H2AFV, XLOC-022270, IGFBP2</i>
(18) Maturing L5/6 CFuPN _TNNT1+	<i>TNNT1, ARL4D, XLOC-001670, SLC25A5, EPHA7, NEUROD1, PFAH1B3, RND2</i>
(3) Maturing EN	<i>XLOC-018857, GAP43</i>
(4) IPC-Undifferentiated newborn N	<i>FBXW7, TCF12, HIST2H2AA4</i>
(14) Early newborn N2 _MAPK-mediated IEG+	<i>FOS, EGR1, FOSB, IER2, JUN.1, DUSP1, TOB1, RHOB, KLF6, STMN4.1</i>
(15) Newborn N _unnamed transcripts_ ENSMYPUG00000004989+	<i>ENSMYPUG00000010676, ENSMYPUG00000004989, XLOC-022307, XLOC-018446, ENSMYPUG00000027726, ENSMYPUG00000019825, EML6, XLOC-025818, RERE, METTL7A, XLOC-035917, XLOC-020965, XLOC-023823, ENSMYPUG00000031951, SLC24A5, ENSMYPUG00000023331, ZCCHC11, LRR40, MYCBP2</i>
(19) High translating N _PCP4+	<i>PCP4, SMPDL3A, SNORD72, ENSMYPUG00000022567, RPL34, XLOC-030039, XLOC-031140, RPS15, CABLES2, ENSMYPUG00000019637, RPL19, Shn1, RPS29, UNC5D, ATP5i, C14orf2, ENSMYPUG00000031951.1, XLOC-020965, HS3ST1, MAP6D1</i>
(20) RGC+ markers	<i>VIM, HES1, ZFP36L1, PON2, SLC1A3, SOX9, BIRC5, 2810417H13Rik, CDCA3, ENSMYPUG00000014648, Pttg1, XLOC-032605, NUSAP, HMGB2, FOS, CENPF, PTN, XLOC-036181, XLOC-003584, TOP2A</i>

**FIGURE S20. Immature neuron markers.** (A) Dot-plot showing the expression of neuron-type specific marker genes across clusters, defining their identity. (B) Top marker transcripts for immature neuron clusters as indicated.

## RESULTS - Supplementary

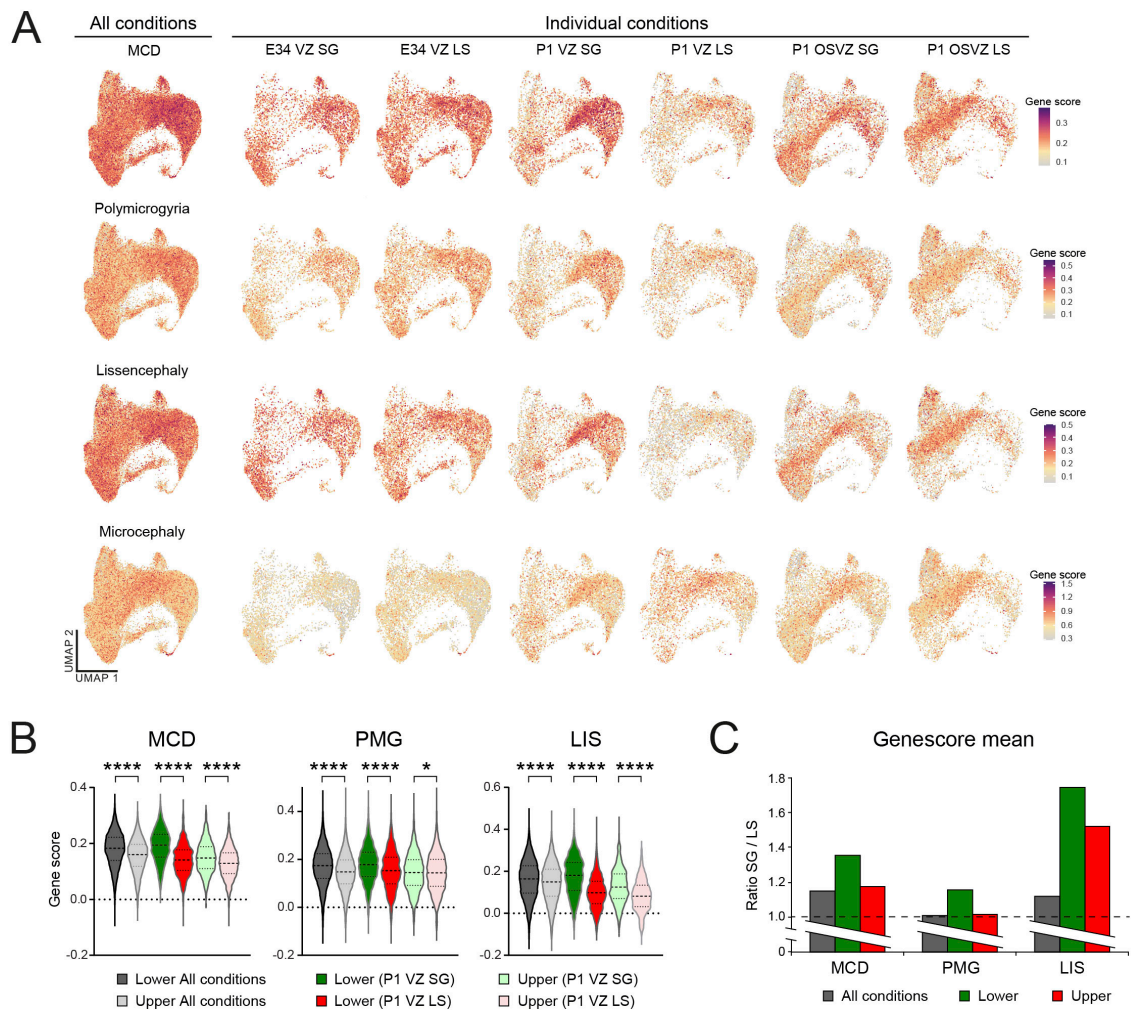


**FIGURE S21. Gene score of MCD.** (A) UMAPs of neuronal ferret subset showing enrichment values of genes linked to human malformations of cortical development for all malformations together (MCD), or separately for genes linked to polymicrogyria (PMG), lissencephaly (LIS) or microcephaly, in all conditions together and individually. (B) Violin plots of gene score values of MCD, PMG and LIS in cells belonging to the clusters identified as lower layer or upper layer neurons (related to Figure 7B) in the indicated conditions. Dotted lines within each violin indicate mode and quartiles. (C) Ratio between SG and LS cells of means of gene score values plotted in (B).

## **DISCUSSION**

The main objective of this Doctoral Thesis was to understand the mechanisms behind the expansion and folding of the cerebral cortex in mammals. To do this, we have analyzed different aspects of perinatal development of ferret, a small carnivore with a naturally folded cortex. Specifically, we microdissected the VZ and OSVZ individually from the prospective LS and SG from ferret cortex at E34 and P1 stages. scRNAseq experiments from such precise conditions allowed us to characterize the transcriptomic diversity of the ferret progenitor cells with a unprecedented spatial resolution. This led to a reconstruction of their developmental trajectories towards ENs and a solid identification of their lineage relationships. Furthermore, we found an enrichment of RGC types and trajectories in this carnivore comparable to the complexity found in the large folded cortex from primates ([Betizeau et al., 2013](#); [Nowakowski et al., 2016](#); [Kalebic et al., 2019](#)) This range of RGC types and trajectories is apparently not recapitulated in the smaller smooth rodent brain ([Pilz et al., 2013](#); [Kalebic et al., 2019](#)).

### **1. Increasing progenitor cell diversity in folds and fissures**

Previous research in ferret cortex showed the existence of the archetypal aRGC, IPC and bRGC in this species, as well as the presence of various RGC morphotypes ([Reillo et al., 2011](#); [Pilz et al., 2013](#); [Reillo et al., 2017](#); [Kalebic et al., 2019](#)). Hitherto, the described heterogeneity of progenitor cells has been mainly examined from the morphological point of view and/or by placing the emphasis on particular genes. RNAseq access at a single-cell level has expanded the amount of information obtained per cell and calls into question our current definition of what is a cell type.

The results of this Thesis reveal that apical and basal RGCs cannot be distinguished transcriptomically between using the canonical markers widely used currently. This absence of distinction is reminiscent of the largely overlapping landscape between cortical cells uncovered by previous scRNAseq work ([Telley et al., 2016](#); [Yuzwa et al., 2017](#); [Loo et al., 2019](#); [Polioudakis et al., 2019](#); [Telley et al., 2019](#); [Di Bella et al., 2021](#); [Li et al., 2020](#)). Despite this, we find 5 types of RGCs located in

## DISCUSSION

the VZ as aRGCs and in the OSVZ as bRGCs. We additionally identify tRGCs in ferret VZ, until now only demonstrated in human cortex (Nowakowski et al., 2016). The similarity of the newly characterized RGCs with previously defined human vRG and oRG clusters, combined with the presence of presumptive canonical markers of apical and basal RGCs in both RGC types at the transcriptome level, reveal that these 6 different classes of RGCs might represent a clearer transcriptomic distinction of RGC progenitors in cortical development than classical aRGCs and bRGCs. Considering the above, we propose that the 6 types of RGCs we uncovered in this Thesis correspond to *bona fide* types of RGCs.

A rise in the diversity of RGC has been associated to cortical development in gyrencephalic species (Rakic, 2009; Reillo et al., 2011; Pilz et al., 2013; Sun and Hevner, 2014; Florio and Huttner, 2014; Nowakowski et al., 2016; Matsumoto et al., 2020). While our new types of RGCs are found in the VZ as well as the OSVZ (with the exception of tRGCs), the majority of these cell types are segregated by their enrichment in the LS or SG at the visual cortex. The regional enrichment of RGC-types along the germinal layers prior to cortex folding recalls the concept of *protomap of cortical folding*. Therefore, we propose that these 5 cell types may underlie the imminent formation of sulci or gyri in the still smooth ferret cortex. It would be interesting and necessary to further study how these sulci or gyri-related RGCs evolve from P4 onwards, when folding starts visually taking place and progresses.

From the functional point of view, we group the new RGC types in 1) amplifying versus 2) those that differentiate into the next stage/neurogenic progenitor cells. Both functional profiles are represented in VZ and OSVZ from LS and SG areas, even though a greater capacity of proliferation has been associated to the gyrus, which is consistent with previous studies (Reillo et al., 2011; Sun and Hevner, 2014). The widespread presence of proliferative RGCs in our dataset may be explained by the stages analyzed in our study (E34 and P1), when the brain, either in LS or SG, has yet to grow massively in size.

By integrating our ferret dataset with publicly available databases from human and mouse (Polioudakis et al., 2019; Li et al., 2020), we obtain a new set of cells grouped by transcriptomic similarities between the three species. The previously isolated ferret RGCs with differentiating/neurogenic profile constitute a cluster together with many human and mouse cells. In the original publications, these human cells were identified as aRGCs, and those from mouse expressed aRGC canonical markers and *Eomes*, a classic IPC marker. On the other hand, ferret RGCs associated to an amplifying profile comprise another cluster shared with predefined human bRGCs and a small group of mouse cells without a previous distinction. The clustering together of differentiating/neurogenic RGCs in ferret and apical RGCs in human suggests that these cells correspond to the same cell types. The same is true for amplifying RGCs in ferret and basal RGCs in human. Knowing that these two profiles of RGCs in ferret are located in both VZ and OSVZ, it indicates the two germinal layers must be analyzed separately to clearly identify these cell types that are transcriptomically so similar. Additionally, this challenges the validity of using certain genes or proteins as cell type markers across all stages of development and species. For instance, bRGCs in the OSVZ from macaque coexpress PAX6/*EOMES* in 35% of archetypal bRGCs, 35% of bRGCs with apical-P and 50% with both-P (Betizeau et al., 2013). *Eomes* expression has also been reported in mouse progenitor cells with several morphotypes, including groups of aRGCs and bRGCs (Li et al., 2020). Similarly, *HOPX* is used as the main marker for bRGCs, however it profusely labels human VZ at GW 13.5 (Pollen et al., 2015). At GW 16, *HOPX* expression has been reported in cells with an apically anchored process (Thomsen et al., 2016). Gradually, *HOPX* decreases its presence in the VZ until GW 18.2-19, and it remains confined to the SVZ thereafter (Pollen et al., 2015; Thomsen et al., 2016). Interestingly, Thomsen and colleagues subclassified human bRGCs in OSVZ as HOPX+ and HOPX- cells (Thomsen et al., 2016). In ferret cortex, we show by ISH that *HOPX* is expressed in the VZ at E34 and P1, and in the SVZ at the latter stage. A recent study from Matsumoto and colleagues in ferret identified high levels of HOPX protein in the VZ at P1 (Matsumoto et al., 2020). Likewise, they characterized HOPX+ and HOPX- bRGC coexisting in the OSVZ, the first being more abundant in prospective gyri and the last in the future sulci (Matsumoto et al., 2020). Most importantly, HOPX+ bRGCs maintained a longer proliferative state,

## DISCUSSION

while HOPX- bRGCs were prone to differentiate ([Matsumoto et al., 2020](#)). In line with Thomsen and Matsumoto's studies, our findings indicate the existence of HOPX- bRGCs with a differentiating/neurogenic profile and the proposed functional profile of HOPX+ cells in progenitor cell amplification, particularly in SG.

### **2. Identical cell lineages emerge from distinct germinal layers**

In our study we identify three transcriptomic trajectories that give rise to newborn ENs. These originate from two sets of mitotic progenitor clusters. Pseudotime analyses show the presence of these two groups of progenitors and the three trajectories in VZ and OSVZ, with a slight tendency of increased proliferation in the gyrus compared to the sulcus. In parallel, our lineage barcoding experiments validate the three trajectories as cell lineages. There is a high number of clones per lineage, most notably in those with widely differing routes, which we named 1 and 3. Lineage 3 is composed by many more dividing progenitor cell clusters than the other lineages, including extra mitotic IPCs, while lineage 1 only contains one type of RGC in G1 (with a differentiating/neurogenic profile). Lineage 2 has a lower predominance, attributable to the short experimental time (3 days) between barcode delivery and cell lineage analysis. This is maybe because the dividing RGCs did not have enough time to generate the 3 types of RGCs in G1 that characterize this lineage. Furthermore, the clusters of origin in lineage 2 are shared with lineage 3, decreasing even further the probability of finding clones that belong to lineage 2. This leads us to speculate that in our period of study for cortex development, there may be a hierarchy among lineages. Lineages 1 and 3, which are more efficient in the generation of ENs, may expand the tissue rapidly, but to a limited extent. In contrast, lineage 2 contains amplifying RGCs, which may support cortex folding.

Surprisingly, the three trajectories of progenitor cells converge in a single cluster that leads to excitatory neuron production. This funnel-like pattern has been reported in other studies regarding telencephalic development ([Polioudakis et al., 2019](#); [Di Bella et al., 2021](#); [Bandler et al., 2022](#)). Furthermore, newborn ENs arising from each trajectory cannot be transcriptomically distinguished from the others, but rather mixed in a progressive maturation track. Once more, this has been validated by the lineage barcoding experiments, where ENs emerging from the two



sets of mitotic progenitors do not separate in isolated clusters. This seems to indicate that newborn ENs have a common immature identity, and acquire their distinctive status only postmitotically, during their radial migration towards the CP.

The mechanism of promoting neuronal diversity has always been a subject of debate in the field, and the use of scRNAseq currently supports both possibilities: the existence of fate-restricted progenitors (Telley et al., 2019; Bandler et al., 2022) and the progressive impact of postmitotic changes on newborn ENs (Yuzwa et al., 2017; Di Bella et al., 2021). From the perspective of this Thesis, which examines neurons residing at the dissected germinal layers and hence extremely immature, we only observe a small diversification towards the end of the trajectory when analyzing the neuronal subset. These newborn ENs have a slightly higher level of maturation and, for this reason, are segregated based on their prospective gyrus or sulcus location, further highlighting the effect of postmitotic changes. In any case, we cannot exclude the role of posttranscriptional modifications in refining neuronal identities earlier in development (Yuzwa et al., 2017).

By looking at human genes related to MCD, we detect that ferret orthologs are located at newborn excitatory neuronal clusters. They are enriched in the most immature clusters at the SG, in agreement with the protomap of cortical folding outlined by some of these genes in the developing human cortex (de Juan Romero et al., 2015). Future research on the clusters specifically involved may clarify the genetic network operating behind these disorders, where ferret might serve as a highly informative animal model (Del-Valle-Anton and Borrell, 2022).

### **3. Similar cell types and conserved trajectories between gyrencephalic species**

Our study depicts in depth the transcriptomic landscape of the developing ferret cortex. We have uncovered new types of RGCs in the prospective gyrus and sulcus that have different functional profiles, and different lineage relationships. This small carnivore is phylogenetically more distant from primates than rodents

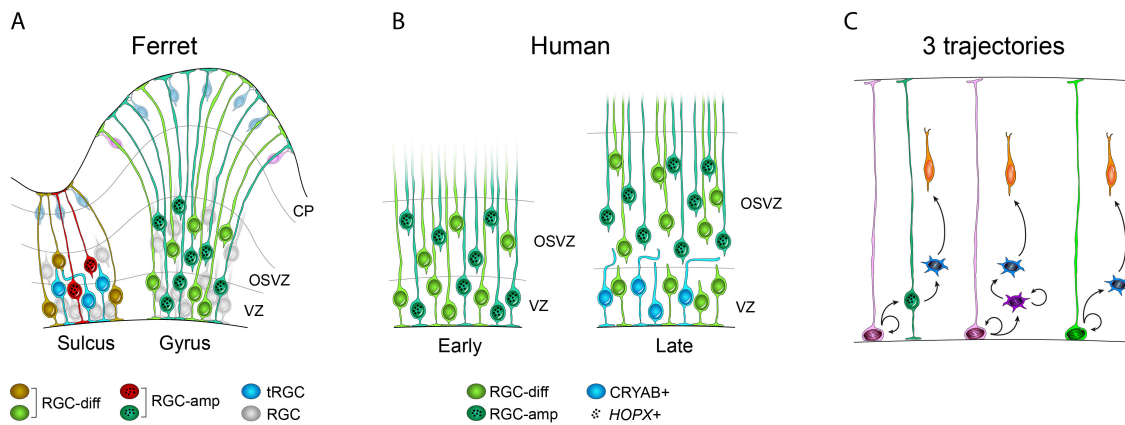
## DISCUSSION

([Franchini et al., 2021](#)). However, integration of our ferret dataset with public datasets from human and mouse embryonic cortex ([Polioudakis et al., 2019](#); [Li et al., 2020](#)) reveals a greater transcriptomic and functional similarity between ferret-human cells than between human-mouse.

Interestingly, we have identified a new aRGC morphotype in ferret, known as tRGC, previously observed in the human cortex but not in mouse ([Nowakowski et al., 2016](#)). Its short basal process, together with its presence in the LS of ferret, contribute to the modification of the radial fiber scaffold for migrating newborn neurons in the sulcus compared to the gyrus. The enrichment of tRGCs in LS occurs at P1, shortly before the sulcus starts being visible. Therefore, tRGCs might be directly contributing to the generation of the LS. Now that we have a good outline of the timing and location where we can find tRGCs, it would be interesting to study the involvement of these RGCs in neuronal migration by videomicroscopy.

RGC composition in ferret SG is likely conserved in human cortex at early stages of neurogenesis, but not later ([Pollen et al., 2015](#); [Thomsen et al., 2016](#)). tRGCs replace aRGCs in human cortex by mid-neurogenesis (GW 17-18) ([Nowakowski et al., 2016](#)). This coincides with HOPX restricted expression in the SVZ ([Pollen et al., 2015](#); [Thomsen et al., 2016](#)) and the expansion of upper layer neurons ([Sidman and Rakic, 1973](#)). Thus, we infer that tRGC might take over from HOPX+ aRGCs and this may be a human specialization to facilitate cortex folding.

Regarding ferret transcriptomic trajectories, the three are found in human but our analysis only identified one trajectory in mouse. This suggests that there is a phylogenetic conservation of RGC types and neuronal production between these gyrencephalic species compared to the lissencephalic species. RGCs heterogeneity and cell trajectory diversification might be a mechanism to ensure high neuronal production throughout neurogenesis, a necessary trait for cortical folding ([Hutsler et al., 2005](#)). The existence of this complex system at both germinal layers might further expand the neuronal output and drive a feedback regulation to fine-tune the process ([Nelson et al., 2013](#); [Betizeau et al., 2013](#)). All these features provide robustness to the system, which may favor its maintenance along phylogeny.



**Schematic summary and interpretations of key findings in this study.** (A) Strategic location and functional profiles of the six subclasses of RGCs found in postnatal ferret to promote cortical folding. (B) Replacement of RGC types along human neurogenesis to support cortex folding. (C) Summary of the three developmental trajectories reconstructed in the cortex of gyrencephalic human and ferret. CP, cortical plate; OSVZ, outer subventricular zone; VZ, ventricular zone; RGC, radial glia cell; tRGC, truncated radial glia cell; diff, differentiating/neurogenic; amp; amplifying.

The integration of ferret, human and mouse datasets provides a new level of understanding of the cellular and genetic mechanisms for cortical expansion and folding. All this is framed in the process of mammalian brain evolution, leading to the maintenance of this complex system in the case of gyrencephalic species, or its simplification in lissencephalic mammals. The integration of our results with similar datasets from other mammals will test this model and better reveal the evolutionary process of cortex folding.



**CONCLUSIONS/CONCLUSIONES**

1. Ferret apical and basal RGC are transcriptomically similar and cannot be discriminated using canonical marker genes. This may be conserved in early human embryo.
2. In early postnatal cortex 5 classes of RGCs populate the VZ and OSVZ, plus tRGCs that populate the VZ. *HOPX*<sup>+</sup> RGCs have an amplifying profile, particularly in the gyrus, whereas *HOPX*<sup>-</sup> RGCs have a differentiating/neurogenic profile.
3. The 6 classes of RGCs have a differential distribution in prospective gyrus and sulcus regions, suggesting a potential role in cortex folding.
4. There are 3 transcriptomic cell trajectories leading to ENs that emerge from 2 sets of mitotic RGCs. These trajectories are repeated in the VZ and OSVZ, and are validated as cell lineages by cell barcoding experiments.
5. Newborn ENs residing in the germinal layers comprise a single immature identity. This suggests an essential role for postmitotic changes during their radial migration in the definition of the final neuronal identity.
6. Human MCD gene transcripts accumulate in the least differentiated newborn ENs, particularly in gyrus.
7. RGCs exhibit a greater transcriptomic and functional similarity between gyrencephalic species than with lissencephalic species.
8. The 3 transcriptomic cell trajectories in ferret are conserved in human, but not identifiable in mouse, which suggests the maintenance of this complex system during human evolution.

## CONCLUSIONS/CONCLUSIONES

1. Las células de glia radial apical y basal de hurón son transcriptómicamente similares y no se pueden distinguir mediante el uso de genes marcadores canónicos. Esto podría estar conservado en los estadios tempranos del embrión humano.
2. En la corteza posnatal temprana 5 clases de células de glia radial pueblan la zona ventricular y la zona subventricular externa, además de células de glia radial truncadas que pueblan la zona ventricular. Las células de glia radial con presencia de *HOPX* tienen un perfil amplificador, especialmente en el giro, mientras que las células de glia radial carentes de *HOPX* tienen un perfil diferenciador/neurogénico.
3. Las 6 clases de células de glia radial tienen una distribución diferente en las regiones de los futuros giro y surco, sugiriendo un posible papel en el plegamiento de la corteza.
4. Hay 3 trayectorias transcriptómicas celulares que conducen a la producción de neuronas excitatorias que emergen de 2 conjuntos de células de glia radial mitóticas. Estas trayectorias están repetidas en la zona ventricular y la zona subventricular externa, y están validadas como linajes celulares mediante experimentos de marcaje celular.
5. Las neuronas excitatorias recién nacidas que residen en las capas germinativas constituyen una identidad inmadura única. Esto sugiere un papel esencial de los cambios posmitóticos a lo largo de su migración radial en la definición de la identidad neuronal final.
6. Los transcritos de los genes de las malformaciones del desarrollo cortical humanas se acumulan en las neuronas excitatorias recién nacidas menos diferenciadas, especialmente en el giro.
7. Las células de glia radial presentan una mayor similitud transcriptómica y funcional entre las especies girencefálicas que con la especie lisencefálica.

8. Las 3 trayectorias transcriptómicas celulares del hurón están conservadas en el humano, pero no son identificables en ratón, lo que sugiere el mantenimiento de este complejo sistema a lo largo de la evolución humana.





**REFERENCES**

1. Aiken, J., Buscaglia, G., Bates, E.A., and Moore, J.K. (2017). The  $\alpha$ -Tubulin gene TUBA1A in Brain Development: A Key Ingredient in the Neuronal Isotype Blend. *J Dev Biol* 5, 8. 10.3390/jdb5030008.
2. Altschul, S.F., Gish, W., Miller, W., Myers, E.W., and Lipman, D.J. (1990). Basic local alignment search tool. *Journal of Molecular Biology* 215, 403–410. 10.1016/S0022-2836(05)80360-2.
3. Amin, S., and Borrell, V. (2020). The Extracellular Matrix in the Evolution of Cortical Development and Folding. *Frontiers in Cell and Developmental Biology* 8.
4. Andrews, S (2010). FastQC: A Quality Control Tool for High Throughput Sequence Data [Online]. Available online at: <http://www.bioinformatics.babraham.ac.uk/projects/fastqc/>.
5. Angevine, J.B., and Sidman, R.L. (1961). Autoradiographic Study of Cell Migration during Histogenesis of Cerebral Cortex in the Mouse. *Nature* 192, 766–768. 10.1038/192766b0.
6. Angevine Jr., J.B., Bodian, D., Coulombre, A.J., Edds Jr., M.V., Hamburger, V., Jacobson, M., Lyser, K.M., Prestige, M.C., Sidman, R.L., Varon, S., et al. (1970). Embryonic vertebrate central nervous system: Revised terminology. *The Anatomical Record* 166, 257–261. 10.1002/ar.1091660214.
7. Arai, Y., and Taverna, E. (2017). Neural Progenitor Cell Polarity and Cortical Development. *Frontiers in Cellular Neuroscience* 11.
8. Attardo, A., Calegari, F., Haubensak, W., Wilsch-Bräuninger, M., and Huttner, W.B. (2008). Live Imaging at the Onset of Cortical Neurogenesis Reveals Differential Appearance of the Neuronal Phenotype in Apical versus Basal Progenitor Progeny. *PLOS ONE* 3, e2388. 10.1371/journal.pone.0002388.
9. Azzarelli, R., Guillemot, F., and Pacary, E. (2015). Function and regulation of Rnd proteins in cortical projection neuron migration. *Front Neurosci* 9, 19. 10.3389/fnins.2015.00019.
10. Baizabal, J.-M., Mistry, M., García, M.T., Gómez, N., Olukoya, O., Tran, D., Johnson, M.B., Walsh, C.A., and Harwell, C.C. (2018). The Epigenetic State of PRDM16-Regulated Enhancers in Radial Glia Controls Cortical Neuron Position. *Neuron* 98, 945-962.e8. 10.1016/j.neuron.2018.04.033.
11. Balamotis, M.A., Tamberg, N., Woo, Y.J., Li, J., Davy, B., Kohwi-Shigematsu, T., and Kohwi, Y. (2012). *Satb1* Ablation Alters Temporal Expression of Immediate Early Genes and Reduces Dendritic Spine Density during Postnatal Brain Development. *Molecular and Cellular Biology* 32, 333–347. 10.1128/MCB.05917-11.
12. Bandler, R.C., Vitali, I., Delgado, R.N., Ho, M.C., Dvoretzkova, E., Ibarra Molinas,

## REFERENCES

- J.S., Frazel, P.W., Mohammadkhani, M., Machold, R., Maedler, S., et al. (2022). Single-cell delineation of lineage and genetic identity in the mouse brain. *Nature* *601*, 404–409. 10.1038/s41586-021-04237-0.
13. Barnette, A.R., Neil, J.J., Kroenke, C.D., Griffith, J.L., Epstein, A.A., Bayly, P.V., Knutsen, A.K., and Inder, T.E. (2009). Characterization of Brain Development in the Ferret via Magnetic Resonance Imaging. *Pediatr Res* *66*, 80–84. 10.1203/PDR.0b013e3181a291d9.
  14. Bayer, S.A., and Altman, J. (1991). *Neocortical development* 1st ed. (Raven Press, Ltd.).
  15. Bedogni, F., and Hevner, R.F. (2021). Cell-Type-Specific Gene Expression in Developing Mouse Neocortex: Intermediate Progenitors Implicated in Axon Development. *Front Mol Neurosci* *14*, 686034. 10.3389/fnmol.2021.686034.
  16. Bentivoglio, M., and Mazzarello, P. (1999). The history of radial glia. *Brain Research Bulletin* *49*, 305–315. 10.1016/S0361-9230(99)00065-9.
  17. Bertacchi, M., Romano, A.L., Loubat, A., Tran Mau-Them, F., Willems, M., Faivre, L., Khau van Kien, P., Perrin, L., Devillard, F., Sorlin, A., et al. (2020). NR2F1 regulates regional progenitor dynamics in the mouse neocortex and cortical gyrification in BBSOAS patients. *EMBO J* *39*, e104163. 10.15252/embj.2019104163.
  18. Betizeau, M., Cortay, V., Patti, D., Pfister, S., Gautier, E., Bellemin-Ménard, A., Afanassieff, M., Huissoud, C., Douglas, R.J., Kennedy, H., et al. (2013). Precursor Diversity and Complexity of Lineage Relationships in the Outer Subventricular Zone of the Primate. *Neuron* *80*, 442–457. 10.1016/j.neuron.2013.09.032.
  19. Bizzotto, S., and Francis, F. (2015). Morphological and functional aspects of progenitors perturbed in cortical malformations. *Front Cell Neurosci* *9*, 30. 10.3389/fncel.2015.00030.
  20. Boekhoorn, K., van Dis, V., Goedknecht, E., Sobel, A., Lucassen, P.J., and Hoogenraad, C.C. (2014). The microtubule destabilizing protein stathmin controls the transition from dividing neuronal precursors to postmitotic neurons during adult hippocampal neurogenesis. *Developmental Neurobiology* *74*, 1226–1242. 10.1002/dneu.22200.
  21. Borrell, V. (2010). In vivo gene delivery to the postnatal ferret cerebral cortex by DNA electroporation. *Journal of Neuroscience Methods* *186*, 186–195. 10.1016/j.jneumeth.2009.11.016.
  22. Borrell, V., and Reillo, I. (2012). Emerging roles of neural stem cells in cerebral cortex development and evolution. *Developmental Neurobiology* *72*, 955–971. 10.1002/dneu.22013.
  23. Breuss, M., Morandell, J., Nimpf, S., Gstrein, T., Lauwers, M., Hochstoeger, T., Braun, A., Chan, K., Sánchez Guajardo, E.R., Zhang, L., et al. (2015). The expression of *tubb2b* undergoes a developmental transition in murine cortical

- neurons. *Journal of Comparative Neurology* 523, 2161–2186. 10.1002/cne.23836.
24. Breuss, M.W., Leca, I., Gstrein, T., Hansen, A.H., and Keays, D.A. (2017). Tubulins and brain development – The origins of functional specification. *Molecular and Cellular Neuroscience* 84, 58–67. 10.1016/j.mcn.2017.03.002.
  25. Brusés, J.L. (2010). Identification of gene transcripts expressed by postsynaptic neurons during synapse formation encoding cell surface proteins with presumptive synaptogenic activity. *Synapse* 64, 47–60. 10.1002/syn.20702.
  26. Budday, S., Steinmann, P., and Kuhl, E. (2015). Secondary instabilities modulate cortical complexity in the mammalian brain. *Philos Mag (Abingdon)* 95, 3244–3256. 10.1080/14786435.2015.1024184.
  27. Bushnell, B., Rood, J., and Singer, E. (2017). BBMerge – Accurate paired shotgun read merging via overlap. *PLOS ONE* 12, e0185056. 10.1371/journal.pone.0185056.
  28. Butler, A., Hoffman, P., Smibert, P., Papalexi, E., and Satija, R. (2018). Integrating single-cell transcriptomic data across different conditions, technologies, and species. *Nat Biotechnol* 36, 411–420. 10.1038/nbt.4096.
  29. Bystron, I., Blakemore, C., and Rakic, P. (2008). Development of the human cerebral cortex: Boulder Committee revisited. *Nature reviews. Neuroscience* 9, 110–122. 10.1038/nrn2252.
  30. Cadwell, C.R., Bhaduri, A., Mostajo-Radji, M.A., Keefe, M.G., and Nowakowski, T.J. (2019). Development and Arealization of the Cerebral Cortex. *Neuron* 103, 980–1004. 10.1016/j.neuron.2019.07.009.
  31. Camargo Ortega, G., Falk, S., Johansson, P.A., Peyre, E., Broix, L., Sahu, S.K., Hirst, W., Schlichthaerle, T., De Juan Romero, C., Draganova, K., et al. (2019). The centrosome protein AKNA regulates neurogenesis via microtubule organization. *Nature* 567, 113–117. 10.1038/s41586-019-0962-4.
  32. Campbell, C.E., Piper, M., Plachez, C., Yeh, Y.-T., Baizer, J.S., Osinski, J.M., Litwack, E.D., Richards, L.J., and Gronostajski, R.M. (2008). The transcription factor Nfix is essential for normal brain development. *BMC Developmental Biology* 8, 52. 10.1186/1471-213X-8-52.
  33. Cao, J., Spielmann, M., Qiu, X., Huang, X., Ibrahim, D.M., Hill, A.J., Zhang, F., Mundlos, S., Christiansen, L., Steemers, F.J., et al. (2019). The single-cell transcriptional landscape of mammalian organogenesis. *Nature* 566, 496–502. 10.1038/s41586-019-0969-x.
  34. Castellani, V., Yue, Y., Gao, P.-P., Zhou, R., and Bolz, J. (1998). Dual Action of a Ligand for Eph Receptor Tyrosine Kinases on Specific Populations of Axons during the Development of Cortical Circuits. *J. Neurosci.* 18, 4663–4672. 10.1523/JNEUROSCI.18-12-04663.1998.

## REFERENCES

35. Cauli, B., Zhou, X., Tricoire, L., Toussay, X., and Staiger, J.F. (2014). Revisiting enigmatic cortical calretinin-expressing interneurons. *Front Neuroanat* 8, 52. 10.3389/fnana.2014.00052.
36. Chai, X., Förster, E., Zhao, S., Bock, H.H., and Frotscher, M. (2009). Reelin acts as a stop signal for radially migrating neurons by inducing phosphorylation of n-cofilin at the leading edge. *Commun Integr Biol* 2, 375–377.
37. Chazarra-Gil, R., van Dongen, S., Kiselev, V.Y., and Hemberg, M. (2021). Flexible comparison of batch correction methods for single-cell RNA-seq using BatchBench. *Nucleic Acids Research* 49, e42. 10.1093/nar/gkab004.
38. Choi, L., and An, J.-Y. (2021). Genetic architecture of autism spectrum disorder: Lessons from large-scale genomic studies. *Neuroscience & Biobehavioral Reviews* 128, 244–257. 10.1016/j.neubiorev.2021.06.028.
39. Clark, E.A., Rutlin, M., Capano, L., Aviles, S., Saadon, J.R., Taneja, P., Zhang, Q., Bullis, J.B., Lauer, T., Myers, E., et al. Cortical ROR $\beta$  is required for layer 4 transcriptional identity and barrel integrity. *eLife* 9, e52370. 10.7554/eLife.52370.
40. Dahlin, A., Royall, J., Hohmann, J.G., and Wang, J. (2009). Expression Profiling of the Solute Carrier Gene Family in the Mouse Brain. *J Pharmacol Exp Ther* 329, 558–570. 10.1124/jpet.108.149831.
41. Dai, X., Cai, L., and He, F. (2022). Single-cell sequencing: expansion, integration and translation. *Briefings in Functional Genomics* 21, 280–295. 10.1093/bfpg/elac011.
42. de Cárcer, G., Manning, G., and Malumbres, M. (2011). From Plk1 to Plk5. *Cell Cycle* 10, 2255–2262. 10.4161/cc.10.14.16494.
43. De Juan Romero, C., and Borrell, V. (2015). Coevolution of radial glial cells and the cerebral cortex. *Glia* 63, 1303–1319. 10.1002/glia.22827.
44. de Juan Romero, C., Bruder, C., Tomasello, U., Sanz-Anquela, J.M., and Borrell, V. (2015). Discrete domains of gene expression in germinal layers distinguish the development of gyrencephaly. *The EMBO Journal* 34, 1859–1874. 10.15252/embj.201591176.
45. de Olmos, S., Bender, C., de Olmos, J.S., and Lorenzo, A. (2009). Neurodegeneration and prolonged immediate early gene expression throughout cortical areas of the rat brain following acute administration of dizocilpine. *Neuroscience* 164, 1347–1359. 10.1016/j.neuroscience.2009.09.022.
46. DeBoer, E.M., Kraushar, M.L., Hart, R.P., and Rasin, M.-R. (2013). Post-transcriptional regulatory elements and spatiotemporal specification of neocortical stem cells and projection neurons. *Neuroscience* 0, 499–528. 10.1016/j.neuroscience.2013.05.042.

47. Del-Valle-Anton, L., and Borrell, V. (2022). Folding brains: from development to disease modeling. *Physiological Reviews* *102*, 511–550. [10.1152/physrev.00016.2021](https://doi.org/10.1152/physrev.00016.2021).
48. Demyanenko, G.P., Schachner, M., Anton, E., Schmid, R., Feng, G., Sanes, J., and Maness, P.F. (2004). Close Homolog of L1 Modulates Area-Specific Neuronal Positioning and Dendrite Orientation in the Cerebral Cortex. *Neuron* *44*, 423–437. [10.1016/j.neuron.2004.10.016](https://doi.org/10.1016/j.neuron.2004.10.016).
49. Di Bella, D.J., Habibi, E., Stickels, R.R., Scalia, G., Brown, J., Yadollahpour, P., Yang, S.M., Abbate, C., Biancalani, T., Macosko, E.Z., et al. (2021). Molecular logic of cellular diversification in the mouse cerebral cortex. *Nature* *595*, 554–559. [10.1038/s41586-021-03670-5](https://doi.org/10.1038/s41586-021-03670-5).
50. Ding, S., Wu, X., Li, G., Han, M., Zhuang, Y., and Xu, T. (2005). Efficient Transposition of the piggyBac (PB) Transposon in Mammalian Cells and Mice. *Cell* *122*, 473–483. [10.1016/j.cell.2005.07.013](https://doi.org/10.1016/j.cell.2005.07.013).
51. Dobin, A., Davis, C.A., Schlesinger, F., Drenkow, J., Zaleski, C., Jha, S., Batut, P., Chaisson, M., and Gingeras, T.R. (2013). STAR: ultrafast universal RNA-seq aligner. *Bioinformatics* *29*, 15–21. [10.1093/bioinformatics/bts635](https://doi.org/10.1093/bioinformatics/bts635).
52. Durinck, S., Moreau, Y., Kasprzyk, A., Davis, S., De Moor, B., Brazma, A., and Huber, W. (2005). BioMart and Bioconductor: a powerful link between biological databases and microarray data analysis. *Bioinformatics* *21*, 3439–3440. [10.1093/bioinformatics/bti525](https://doi.org/10.1093/bioinformatics/bti525).
53. Durinck, S., Spellman, P.T., Birney, E., and Huber, W. (2009). Mapping identifiers for the integration of genomic datasets with the R/Bioconductor package biomaRt. *Nat Protoc* *4*, 1184–1191. [10.1038/nprot.2009.97](https://doi.org/10.1038/nprot.2009.97).
54. Englund, C., Fink, A., Lau, C., Pham, D., Daza, R.A.M., Bulfone, A., Kowalczyk, T., and Hevner, R.F. (2005). Pax6, Tbr2, and Tbr1 Are Expressed Sequentially by Radial Glia, Intermediate Progenitor Cells, and Postmitotic Neurons in Developing Neocortex. *J. Neurosci.* *25*, 247–251. [10.1523/JNEUROSCI.2899-04.2005](https://doi.org/10.1523/JNEUROSCI.2899-04.2005).
55. Eze, U.C., Bhaduri, A., Haeussler, M., Nowakowski, T.J., and Kriegstein, A.R. (2021). Single-cell atlas of early human brain development highlights heterogeneity of human neuroepithelial cells and early radial glia. *Nat Neurosci* *24*, 584–594. [10.1038/s41593-020-00794-1](https://doi.org/10.1038/s41593-020-00794-1).
56. Ferent, J., Zaidi, D., and Francis, F. (2020). Extracellular Control of Radial Glia Proliferation and Scaffolding During Cortical Development and Pathology. *Front Cell Dev Biol* *8*, 578341. [10.3389/fcell.2020.578341](https://doi.org/10.3389/fcell.2020.578341).
57. Fietz, S.A., and Huttner, W.B. (2011). Cortical progenitor expansion, self-renewal and neurogenesis—a polarized perspective. *Current Opinion in Neurobiology* *21*, 23–35. [10.1016/j.conb.2010.10.002](https://doi.org/10.1016/j.conb.2010.10.002).
58. Fietz, S.A., Kelava, I., Vogt, J., Wilsch-Bräuninger, M., Stenzel, D., Fish, J.L.,

## REFERENCES

- Corbeil, D., Riehn, A., Distler, W., Nitsch, R., et al. (2010). OSVZ progenitors of human and ferret neocortex are epithelial-like and expand by integrin signaling. *Nat Neurosci* 13, 690–699. 10.1038/nn.2553.
59. Fiorentino, A., Sharp, S.I., Kandaswamy, R., Gurling, H.M., Bass, N.J., and McQuillin, A. (2016). Genetic variant analysis of the putative regulatory regions of the LRRC7 gene in bipolar disorder. *Psychiatr Genet* 26, 99–100. 10.1097/YPG.0000000000000119.
60. Fleiss, B., Stolp, H., Mezger, V., and Gressens, P. (2018). 58 - Central Nervous System Development. In *Avery's Diseases of the Newborn (Tenth Edition)*, C. A. Gleason and S. E. Juul, eds. (Elsevier), pp. 852-856.e1. 10.1016/B978-0-323-40139-5.00058-9.
61. Florio, M., Heide, M., Pinson, A., Brandl, H., Albert, M., Winkler, S., Wimberger, P., Huttner, W.B., and Hiller, M. (2018). Evolution and cell-type specificity of human-specific genes preferentially expressed in progenitors of fetal neocortex. *eLife* 7, e32332. 10.7554/eLife.32332.
62. Florio, M., and Huttner, W.B. (2014). Neural progenitors, neurogenesis and the evolution of the neocortex. *Development* 141, 2182–2194. 10.1242/dev.090571.
63. Franchini, L.F. (2021). Genetic Mechanisms Underlying Cortical Evolution in Mammals. *Frontiers in Cell and Developmental Biology* 9.
64. Gal, J.S., Morozov, Y.M., Ayoub, A.E., Chatterjee, M., Rakic, P., and Haydar, T.F. (2006). Molecular and Morphological Heterogeneity of Neural Precursors in the Mouse Neocortical Proliferative Zones. *J. Neurosci.* 26, 1045–1056. 10.1523/JNEUROSCI.4499-05.2006.
65. Garcia, K.E., Kroenke, C.D., and Bayly, P.V. (2018). Mechanics of cortical folding: stress, growth and stability. *Philos Trans R Soc Lond B Biol Sci* 373, 20170321. 10.1098/rstb.2017.0321.
66. García-Moreno, F., Vasistha, N.A., Trevia, N., Bourne, J.A., and Molnár, Z. (2012). Compartmentalization of Cerebral Cortical Germinal Zones in a Lissencephalic Primate and Gyrencephalic Rodent. *Cerebral Cortex* 22, 482–492. 10.1093/cercor/bhr312.
67. Gertz, C.C., and Kriegstein, A.R. (2015). Neuronal Migration Dynamics in the Developing Ferret Cortex. *Journal of Neuroscience* 35, 14307–14315. 10.1523/JNEUROSCI.2198-15.2015.
68. Gertz, C.C., Lui, J.H., LaMonica, B.E., Wang, X., and Kriegstein, A.R. (2014). Diverse Behaviors of Outer Radial Glia in Developing Ferret and Human Cortex. *J Neurosci* 34, 2559–2570. 10.1523/JNEUROSCI.2645-13.2014.
69. Gilardi, C., and Kalebic, N. (2021). The Ferret as a Model System for Neocortex Development and Evolution. *Frontiers in Cell and Developmental Biology* 9.

70. Glatzle, M., Hoops, M., Kauffold, J., Seeger, J., and Fietz, S.A. (2017). Development of Deep and Upper Neuronal Layers in the Domestic Cat, Sheep and Pig Neocortex. *Anatomia, Histologia, Embryologia* 46, 397–404. 10.1111/ahe.12282.
71. Golgi, C. (1898). Intorno alla struttura delle cellule nervose. *Arch. Ital. Biol.* 30, 60–71.
72. Gory-Fauré, S., Windscheid, V., Brocard, J., Montessuit, S., Tsutsumi, R., Denarier, E., Fukata, Y., Bosc, C., Delaroche, J., Collomb, N., et al. (2014). Non-Microtubular Localizations of Microtubule-Associated Protein 6 (MAP6). *PLOS ONE* 9, e114905. 10.1371/journal.pone.0114905.
73. Götz, M., and Huttner, W.B. (2005). The cell biology of neurogenesis. *Nat Rev Mol Cell Biol* 6, 777–788. 10.1038/nrm1739.
74. Graczyk, A., and Leśniak, W. (2014). S100A6 expression in keratinocytes and its impact on epidermal differentiation. *The International Journal of Biochemistry & Cell Biology* 57, 135–141. 10.1016/j.biocel.2014.10.007.
75. Griss, J., Viteri, G., Sidiropoulos, K., Nguyen, V., Fabregat, A., and Hermjakob, H. (2020). ReactomeGSA - Efficient Multi-Omics Comparative Pathway Analysis. *Molecular & Cellular Proteomics* 19, 2115–2125. 10.1074/mcp.TIR120.002155.
76. Güven, A., Kalebic, N., Long, K.R., Florio, M., Vaid, S., Brandl, H., Stenzel, D., and Huttner, W.B. (2020). Extracellular matrix-inducing Sox9 promotes both basal progenitor proliferation and gliogenesis in developing neocortex. *eLife* 9, e49808. 10.7554/eLife.49808.
77. Hafemeister, C., and Satija, R. (2019). Normalization and variance stabilization of single-cell RNA-seq data using regularized negative binomial regression. *Genome Biology* 20, 296. 10.1186/s13059-019-1874-1.
78. Han, J.S., Hino, K., Li, W., Reyes, R.V., Canales, C.P., Miltner, A.M., Haddadi, Y., Sun, J., Chen, C.-Y., La Torre, A., et al. (2020). CRL5-dependent regulation of the small GTPases ARL4C and ARF6 controls hippocampal morphogenesis. *Proceedings of the National Academy of Sciences* 117, 23073–23084. 10.1073/pnas.2002749117.
79. Hansen, D.V., Lui, J.H., Parker, P.R.L., and Kriegstein, A.R. (2010). Neurogenic radial glia in the outer subventricular zone of human neocortex. *Nature* 464, 554–561. 10.1038/nature08845.
80. Hao, Y., Hao, S., Andersen-Nissen, E., Mauck, W.M., Zheng, S., Butler, A., Lee, M.J., Wilk, A.J., Darby, C., Zager, M., et al. (2021). Integrated analysis of multimodal single-cell data. *Cell* 184, 3573–3587.e29. 10.1016/j.cell.2021.04.048.
81. Harris, L., Genovesi, L.A., Gronostajski, R.M., Wainwright, B.J., and Piper, M. (2015). Nuclear factor one transcription factors: Divergent functions in

## REFERENCES

- developmental versus adult stem cell populations. *Developmental Dynamics* 244, 227–238. 10.1002/dvdy.24182.
82. Hartfuss, E., Galli, R., Heins, N., and Götz, M. (2001). Characterization of CNS Precursor Subtypes and Radial Glia. *Developmental Biology* 229, 15–30. 10.1006/dbio.2000.9962.
83. Hasenpusch-Theil, K., West, S., Kelman, A., Kozic, Z., Horrocks, S., McMahon, A.P., Price, D.J., Mason, J.O., and Theil, T. (2018). Gli3 controls the onset of cortical neurogenesis by regulating the radial glial cell cycle through Cdk6 expression. *Development* 145, dev163147. 10.1242/dev.163147.
84. Hashimshony, T., Wagner, F., Sher, N., and Yanai, I. (2012). CEL-Seq: Single-Cell RNA-Seq by Multiplexed Linear Amplification. *Cell Reports* 2, 666–673. 10.1016/j.celrep.2012.08.003.
85. Haubensak, W., Attardo, A., Denk, W., and Huttner, W.B. (2004). Neurons arise in the basal neuroepithelium of the early mammalian telencephalon: A major site of neurogenesis. *Proc Natl Acad Sci U S A* 101, 3196–3201. 10.1073/pnas.0308600100.
86. Hertel, N., and Redies, C. (2011). Absence of Layer-Specific Cadherin Expression Profiles in the Neocortex of the Reeler Mutant Mouse. *Cerebral Cortex* 21, 1105–1117. 10.1093/cercor/bhq183.
87. Heuer, K., Gulban, O.F., Bazin, P.-L., Osoianu, A., Valabregue, R., Santin, M., Herbin, M., and Toro, R. (2019). Evolution of neocortical folding: A phylogenetic comparative analysis of MRI from 34 primate species. *Cortex* 118, 275–291. 10.1016/j.cortex.2019.04.011.
88. Hevner, R.F., and Haydar, T.F. (2012). The (Not Necessarily) Convoluted Role of Basal Radial Glia in Cortical Neurogenesis. *Cerebral Cortex* 22, 465–468. 10.1093/cercor/bhr336.
89. Hoeck, J.D., Jandke, A., Blake, S.M., Nye, E., Spencer-Dene, B., Brandner, S., and Behrens, A. (2010). Fbw7 controls neural stem cell differentiation and progenitor apoptosis via Notch and c-Jun. *Nat Neurosci* 13, 1365–1372. 10.1038/nn.2644.
90. Hooke, R. (1665). *Micrographia, or some physiological descriptions of minute bodies made by magnifying glasses, with observations and inquiries thereupon.* By R. Hooke. (Printed by Jo. Martyn, and Ja. Allestry, printers to the Royal Society.).
91. Huang, W., Zhou, Z., Asrar, S., Henkelman, M., Xie, W., and Jia, Z. (2011). p21-Activated Kinases 1 and 3 Control Brain Size through Coordinating Neuronal Complexity and Synaptic Properties. *Mol Cell Biol* 31, 388–403. 10.1128/MCB.00969-10.
92. Hutsler, J.J., Lee, D.-G., and Porter, K.K. (2005). Comparative analysis of cortical layering and supragranular layer enlargement in rodent carnivore



- and primate species. *Brain Research* 1052, 71–81. 10.1016/j.brainres.2005.06.015.
93. Huttner, W.B., and Kosodo, Y. (2005). Symmetric versus asymmetric cell division during neurogenesis in the developing vertebrate central nervous system. *Current Opinion in Cell Biology* 17, 648–657. 10.1016/j.ceb.2005.10.005.
  94. Irvin, D.K., Zurcher, S.D., Nguyen, T., Weinmaster, G., and Kornblum, H.I. (2001). Expression patterns of Notch1, Notch2, and Notch3 suggest multiple functional roles for the Notch-DSL signaling system during brain development. *Journal of Comparative Neurology* 436, 167–181. 10.1002/cne.1059.
  95. Jackson, C., Peduzzi, J., and Hickey, T. (1989). Visual cortex development in the ferret. I. Genesis and migration of visual cortical neurons. *J. Neurosci.* 9, 1242–1253. 10.1523/JNEUROSCI.09-04-01242.1989.
  96. Jackson, V.A., Mehmood, S., Chavent, M., Roversi, P., Carrasquero, M., del Toro, D., Seyit-Bremer, G., Ranaivoson, F.M., Comoletti, D., Sansom, M.S.P., et al. (2016). Super-complexes of adhesion GPCRs and neural guidance receptors. *Nat Commun* 7, 11184. 10.1038/ncomms11184.
  97. Jeong, K.H., Kim, S.-K., Kim, S.Y., and Cho, K.-O. (2009). Immunohistochemical localization of Krüppel-like factor 6 in the mouse forebrain. *Neuroscience Letters* 453, 16–20. 10.1016/j.neulet.2009.02.002.
  98. Jia, Q., Chu, H., Jin, Z., Long, H., and Zhu, B. (2022). High-throughput single-cell sequencing in cancer research. *Sig Transduct Target Ther* 7, 1–20. 10.1038/s41392-022-00990-4.
  99. Johnson, M.B., Sun, X., Kodani, A., Borges-Monroy, R., Girsakis, K.M., Ryu, S.C., Wang, P.P., Patel, K., Gonzalez, D.M., Woo, Y.M., et al. (2018). *Aspm* knockout ferret reveals an evolutionary mechanism governing cerebral cortical size. *Nature* 556, 370–375. 10.1038/s41586-018-0035-0.
  100. Johnson, M.B., Wang, P.P., Atabay, K.D., Murphy, E.A., Doan, R.N., Hecht, J., and Walsh, C.A. (2015). Single Cell Analysis Reveals Transcriptional Heterogeneity of Neural Progenitors in the Human Cortex. *Nat Neurosci* 18, 637–646. 10.1038/nn.3980.
  101. Johnson-Delaney, C.A., and Orosz, S.E. (2011). Ferret Respiratory System: Clinical Anatomy, Physiology, and Disease. *Veterinary Clinics of North America: Exotic Animal Practice* 14, 357–367. 10.1016/j.cvex.2011.03.001.
  102. Kalebic, N., Gilardi, C., Stepien, B., Wilsch-Bräuninger, M., Long, K.R., Namba, T., Florio, M., Langen, B., Lombardot, B., Shevchenko, A., et al. (2019). Neocortical Expansion Due to Increased Proliferation of Basal Progenitors Is Linked to Changes in Their Morphology. *Cell Stem Cell* 24, 535–550.e9. 10.1016/j.stem.2019.02.017.

## REFERENCES

103. Kandel, E.R., Schwartz, J.H., and Jessell, T.M. (2000). Principles of Neural Science 4th ed. (McGraw-Hill Companies, Inc.).
104. Karlinski, M., and Reiner, O. (2018). Unfolding the Folds: How the Biomechanics of the Extracellular Matrix Contributes to Cortical Gyrification. In.
105. Kawasaki, H., Iwai, L., and Tanno, K. (2012). Rapid and efficient genetic manipulation of gyrencephalic carnivores using in utero electroporation. *Molecular Brain* 5, 24. 10.1186/1756-6606-5-24.
106. Kawasaki, H., Toda, T., and Tanno, K. (2012). In vivo genetic manipulation of cortical progenitors in gyrencephalic carnivores using in utero electroporation. *Biol Open* 2, 95–100. 10.1242/bio.20123160.
107. Kelava, I., Lewitus, E., and Huttner, W.B. (2013). The secondary loss of gyrencephaly as an example of evolutionary phenotypical reversal. *Frontiers in Neuroanatomy* 7.
108. Kelava, I., Reillo, I., Murayama, A.Y., Kalinka, A.T., Stenzel, D., Tomancak, P., Matsuzaki, F., Lebrand, C., Sasaki, E., Schwamborn, J.C., et al. (2012). Abundant Occurrence of Basal Radial Glia in the Subventricular Zone of Embryonic Neocortex of a Lissencephalic Primate, the Common Marmoset *Callithrix jacchus*. *Cerebral Cortex* 22, 469–481. 10.1093/cercor/bhr301.
109. Kent, W.J. (2002). BLAT—The BLAST-Like Alignment Tool. *Genome Res.* 12, 656–664. 10.1101/gr.229202.
110. Kent, W.J., Sugnet, C.W., Furey, T.S., Roskin, K.M., Pringle, T.H., Zahler, A.M., and Haussler, and D. (2002). The Human Genome Browser at UCSC. *Genome Res.* 12, 996–1006. 10.1101/gr.229102.
111. Kershman, J. (1938). The Medulloblast and Medulloblastoma: a study of human embryos. *Archives of Neurology & Psychiatry* 40, 937–967. 10.1001/archneurpsyc.1938.02270110091007.
112. Kester, L., and van Oudenaarden, A. (2018). Single-Cell Transcriptomics Meets Lineage Tracing. *Cell Stem Cell* 23, 166–179. 10.1016/j.stem.2018.04.014.
113. Khan, S., Lu, X., Huang, Q., Tang, J., Weng, J., Yang, Z., Lv, M., Xu, X., Xia, F., Zhang, M., et al. (2019). IGFBP2 Plays an Essential Role in Cognitive Development during Early Life. *Adv Sci (Weinh)* 6, 1901152. 10.1002/advs.201901152.
114. Kinoshita, Y., Okudera, T., Tsuru, E., and Yokota, A. (2001). Volumetric Analysis of the Germinal Matrix and Lateral Ventricles Performed Using MR Images of Postmortem Fetuses. *American Journal of Neuroradiology* 22, 382–388.
115. Kita, Y., Nishibe, H., Wang, Y., Hashikawa, T., Kikuchi, S.S., U, M., Yoshida, A.C., Yoshida, C., Kawase, T., Ishii, S., et al. (2021). Cellular-resolution gene

- expression profiling in the neonatal marmoset brain reveals dynamic species- and region-specific differences. *Proc. Natl. Acad. Sci. U.S.A.* *118*, e2020125118. 10.1073/pnas.2020125118.
116. Klingler, E., De la Rossa, A., Fièvre, S., Devaraju, K., Abe, P., and Jabaudon, D. (2019). A Translaminar Genetic Logic for the Circuit Identity of Intracortically Projecting Neurons. *Current Biology* *29*, 332-339.e5. 10.1016/j.cub.2018.11.071.
  117. Knoll, M., and Ruska, E. (1932). Das Elektronenmikroskop. *Z. Physik* *78*, 318–339. 10.1007/BF01342199.
  118. Kodali, V (2017) cthreepo (version 0.1.1) [Source code]. <https://github.com/vkkodali/cthreepo>.
  119. Kolde, R (2018) (version 1.0.12) [Source code]. <https://github.com/raivokolde/pheatmap>.
  120. Kölliker, A. (1896). *Handbuch der Gewebelehre des Menschen* (Leipzig Verlag Von Wilhelm Engelmann).
  121. Kotliar, D (2018) [Source code]. <https://github.com/Hoohm/dropSeqPipe/issues/30#issuecomment-385957912>.
  122. Kou, Z., Wu, Q., Kou, X., Yin, C., Wang, H., Zuo, Z., Zhuo, Y., Chen, A., Gao, S., and Wang, X. (2015). CRISPR/Cas9-mediated genome engineering of the ferret. *Cell Res* *25*, 1372–1375. 10.1038/cr.2015.130.
  123. Krajewska, M., Mai, J.K., Zapata, J.M., Ashwell, K.W., Schendel, S.L., Reed, J.C., and Krajewski, S. (2002). Dynamics of expression of apoptosis-regulatory proteins Bid, Bcl-2, Bcl-X, Bax and Bak during development of murine nervous system. *Cell Death Differ* *9*, 145–157. 10.1038/sj.cdd.4400934.
  124. Kriegstein, A., Noctor, S., and Martínez-Cerdeño, V. (2006). Patterns of neural stem and progenitor cell division may underlie evolutionary cortical expansion. *Nat Rev Neurosci* *7*, 883–890. 10.1038/nrn2008.
  125. Krishna-K, Nuernberger, M., Weth, F., and Redies, C. (2009). Layer-Specific Expression of Multiple Cadherins in the Developing Visual Cortex (V1) of the Ferret. *Cerebral Cortex* *19*, 388–401. 10.1093/cercor/bhn090.
  126. Kroenke, C.D., and Bayly, P.V. (2018). How Forces Fold the Cerebral Cortex. *J. Neurosci.* *38*, 767–775. 10.1523/JNEUROSCI.1105-17.2017.
  127. Kyrousi, C., O’Neill, A.C., Brazovskaja, A., He, Z., Kielkowski, P., Coquand, L., Di Giaimo, R., D’ Andrea, P., Belka, A., Forero Echeverry, A., et al. (2021). Extracellular LGALS3BP regulates neural progenitor position and relates to human cortical complexity. *Nat Commun* *12*, 6298. 10.1038/s41467-021-26447-w.

## REFERENCES

128. La Manno, G., Soldatov, R., Zeisel, A., Braun, E., Hochgerner, H., Petukhov, V., Lidschreiber, K., Kastrioti, M.E., Lönnerberg, P., Furlan, A., et al. (2018). RNA velocity of single cells. *Nature* *560*, 494–498. 10.1038/s41586-018-0414-6.
129. Lake, B.B., Ai, R., Kaeser, G.E., Salathia, N.S., Yung, Y.C., Liu, R., Wildberg, A., Gao, D., Fung, H.-L., Chen, S., et al. (2016). Neuronal subtypes and diversity revealed by single-nucleus RNA sequencing of the human brain. *Science* *352*, 1586–1590. 10.1126/science.aaf1204.
130. LaMonica, B.E., Lui, J.H., Hansen, D.V., and Kriegstein, A.R. (2013). Mitotic spindle orientation predicts outer radial glial cell generation in human neocortex. *Nat Commun* *4*, 1665. 10.1038/ncomms2647.
131. Lee, J.S., Koh, J.-Y., Yi, K., Kim, Y.-I., Park, S.-J., Kim, E.-H., Kim, S.-M., Park, S.H., Ju, Y.S., Choi, Y.K., et al. (2021). Single-cell transcriptome of bronchoalveolar lavage fluid reveals sequential change of macrophages during SARS-CoV-2 infection in ferrets. *Nat Commun* *12*, 4567. 10.1038/s41467-021-24807-0.
132. Legland, D., Arganda-Carreras, I., and Andrey, P. (2016). MorphoLibJ: integrated library and plugins for mathematical morphology with ImageJ. *Bioinformatics* *32*, 3532–3534. 10.1093/bioinformatics/btw413.
133. Lehtinen, M.K., and Walsh, C.A. (2011). Neurogenesis at the Brain–Cerebrospinal Fluid Interface. *Annual Review of Cell and Developmental Biology* *27*, 653–679. 10.1146/annurev-cellbio-092910-154026.
134. Lewitus, E., Kelava, I., Kalinka, A.T., Tomancak, P., and Huttner, W.B. (2014). An Adaptive Threshold in Mammalian Neocortical Evolution. *PLOS Biology* *12*, e1002000. 10.1371/journal.pbio.1002000.
135. Li, M., and Zhang, P. (2009). The function of APC/CCdh1 in cell cycle and beyond. *Cell Division* *4*, 2. 10.1186/1747-1028-4-2.
136. Li, Z., Tyler, W.A., Zeldich, E., Santpere Baró, G., Okamoto, M., Gao, T., Li, M., Sestan, N., and Haydar, T.F. (2020). Transcriptional priming as a conserved mechanism of lineage diversification in the developing mouse and human neocortex. *Sci Adv* *6*, eabd2068. 10.1126/sciadv.abd2068.
137. Li, Z., Sun, X., Chen, J., Liu, X., Wisely, S.M., Zhou, Q., Renard, J.-P., Leno, G.H., and Engelhardt, J.F. (2006). Cloned ferrets produced by somatic cell nuclear transfer. *Dev Biol* *293*, 439–448. 10.1016/j.ydbio.2006.02.016.
138. Lim, L., Mi, D., Llorca, A., and Marín, O. (2018). Development and Functional Diversification of Cortical Interneurons. *Neuron* *100*, 294–313. 10.1016/j.neuron.2018.10.009.
139. Lin, M.-J., and Lee, S.-J. (2016). Stathmin-like 4 is critical for the maintenance of neural progenitor cells in dorsal midbrain of zebrafish larvae. *Sci Rep* *6*, 36188. 10.1038/srep36188.
140. Lin-Hendel, E.G., McManus, M.J., Wallace, D.C., Anderson, S.A., and Golden, J.A.

- (2016). Differential mitochondrial requirements for radially and non-radially migrating cortical neurons: Implications for mitochondrial disorders. *Cell Rep* *15*, 229–237. 10.1016/j.celrep.2016.03.024.
141. Lindeberg, H. (2008). Reproduction of the Female Ferret (*Mustela putorius furo*). *Reproduction in Domestic Animals* *43*, 150–156. 10.1111/j.1439-0531.2008.01155.x.
  142. Liu, S.J., Nowakowski, T.J., Pollen, A.A., Lui, J.H., Horlbeck, M.A., Attenello, F.J., He, D., Weissman, J.S., Kriegstein, A.R., Diaz, A.A., et al. (2016). Single-cell analysis of long non-coding RNAs in the developing human neocortex. *Genome Biol* *17*, 67. 10.1186/s13059-016-0932-1.
  143. Lohmann, G., von Cramon, D.Y., and Colchester, A.C.F. (2008). Deep Sulcal Landmarks Provide an Organizing Framework for Human Cortical Folding. *Cerebral Cortex* *18*, 1415–1420. 10.1093/cercor/bhm174.
  144. Lohmann, G., von Cramon, D.Y., and Steinmetz, H. (1999). Sulcal Variability of Twins. *Cerebral Cortex* *9*, 754–763. 10.1093/cercor/9.7.754.
  145. Long, K.R., and Huttner, W.B. (2022). The Role of the Extracellular Matrix in Neural Progenitor Cell Proliferation and Cortical Folding During Human Neocortex Development. *Frontiers in Cellular Neuroscience* *15*.
  146. Loo, L., Simon, J.M., Xing, L., McCoy, E.S., Niehaus, J.K., Guo, J., Anton, E.S., and Zylka, M.J. (2019). Single-cell transcriptomic analysis of mouse neocortical development. *Nat Commun* *10*, 134. 10.1038/s41467-018-08079-9.
  147. Lui, J.H., Hansen, D.V., and Kriegstein, A.R. (2011). Development and Evolution of the Human Neocortex. *Cell* *146*, 18–36. 10.1016/j.cell.2011.06.030.
  148. Lun, A.T.L., Riesenfeld, S., Andrews, T., Dao, T.P., Gomes, T., Marioni, J.C., and participants in the 1st Human Cell Atlas Jamboree (2019). EmptyDrops: distinguishing cells from empty droplets in droplet-based single-cell RNA sequencing data. *Genome Biology* *20*, 63. 10.1186/s13059-019-1662-y.
  149. Macosko, E.Z., Basu, A., Satija, R., Nemes, J., Shekhar, K., Goldman, M., Tirosh, I., Bialas, A.R., Kamitaki, N., Martersteck, E.M., et al. (2015). Highly Parallel Genome-wide Expression Profiling of Individual Cells Using Nanoliter Droplets. *Cell* *161*, 1202–1214. 10.1016/j.cell.2015.05.002.
  150. Manganas, L.N., Durá, I., Osenberg, S., Semerci, F., Tosun, M., Mishra, R., Parkitny, L., Encinas, J.M., and Maletic-Savatic, M. (2021). BASP1 labels neural stem cells in the neurogenic niches of mammalian brain. *Sci Rep* *11*, 5546. 10.1038/s41598-021-85129-1.
  151. Marin-Padilla, M. (1971). Early prenatal ontogenesis of the cerebral cortex (neocortex) of the cat (*Felis domestica*). A Golgi study. I. The primordial neocortical organization. *Z Anat Entwicklungsgesch* *134*, 117–145. 10.1007/BF00519296.

## REFERENCES

152. Marin-Padilla, M. (1978). Dual origin of the mammalian neocortex and evolution of the cortical plate. *Anat Embryol (Berl)* 152, 109–126. 10.1007/BF00315920.
153. Marin-Padilla, M. (1983). Structural organization of the human cerebral cortex prior to the appearance of the cortical plate. *Anat Embryol* 168, 21–40. 10.1007/BF00305396.
154. Marin-Padilla, M., and Marin-Padilla, T.M. (1982). Origin, prenatal development and structural organization of layer I of the human cerebral (motor) cortex. *Anat Embryol* 164, 161–206. 10.1007/BF00318504.
155. Marsh, S (2021). scCustomize: An R package for custom visualization & analyses of single cell sequencing. <https://doi.org/10.5281/zenodo.5706430>.
156. Martínez-Cerdeño, V., Cunningham, C.L., Camacho, J., Antczak, J.L., Prakash, A.N., Cziep, M.E., Walker, A.I., and Noctor, S.C. (2012). Comparative Analysis of the Subventricular Zone in Rat, Ferret and Macaque: Evidence for an Outer Subventricular Zone in Rodents. *PLOS ONE* 7, e30178. 10.1371/journal.pone.0030178.
157. Martínez-Cerdeño, V., Noctor, S.C., and Kriegstein, A.R. (2006). The Role of Intermediate Progenitor Cells in the Evolutionary Expansion of the Cerebral Cortex. *Cerebral Cortex* 16, i152–i161. 10.1093/cercor/bhk017.
158. Martínez-Martínez, M.Á., Ciceri, G., Espinós, A., Fernández, V., Marín, O., and Borrell, V. (2019). Extensive branching of radially-migrating neurons in the mammalian cerebral cortex. *Journal of Comparative Neurology* 527, 1558–1576. 10.1002/cne.24597.
159. Martínez-Martínez, M.Á., De Juan Romero, C., Fernández, V., Cárdenas, A., Götz, M., and Borrell, V. (2016). A restricted period for formation of outer subventricular zone defined by *Cdh1* and *Trnp1* levels. *Nat Commun* 7, 11812. 10.1038/ncomms11812.
160. Masuda, K., Toda, T., Shinmyo, Y., Ebisu, H., Hoshiba, Y., Wakimoto, M., Ichikawa, Y., and Kawasaki, H. (2015). Pathophysiological analyses of cortical malformation using gyrencephalic mammals. *Sci Rep* 5, 15370. 10.1038/srep15370.
161. Matsumoto, N., Hoshiba, Y., Morita, K., Uda, N., Hirota, M., Minamikawa, M., Ebisu, H., Shinmyo, Y., and Kawasaki, H. (2017). Pathophysiological analyses of periventricular nodular heterotopia using gyrencephalic mammals. *Human Molecular Genetics* 26, 1173–1181. 10.1093/hmg/ddx038.
162. Matsumoto, N., Kobayashi, N., Uda, N., Hirota, M., and Kawasaki, H. (2018). Pathophysiological analyses of leptomeningeal heterotopia using gyrencephalic mammals. *Human Molecular Genetics* 27, 985–991. 10.1093/hmg/ddy014.
163. Matsumoto, N., Shinmyo, Y., Ichikawa, Y., and Kawasaki, H. (2017).

- Gyrification of the cerebral cortex requires FGF signaling in the mammalian brain. *eLife* 6, e29285. 10.7554/eLife.29285.
164. Matsumoto, N., Tanaka, S., Horiike, T., Shinmyo, Y., and Kawasaki, H. (2020). A discrete subtype of neural progenitor crucial for cortical folding in the gyrencephalic mammalian brain. *eLife* 9, e54873. 10.7554/eLife.54873.
  165. Matsumoto, S., Fujii, S., Sato, A., Ibuka, S., Kagawa, Y., Ishii, M., and Kikuchi, A. (2014). A combination of Wnt and growth factor signaling induces *Arl4c* expression to form epithelial tubular structures. *EMBO J* 33, 702–718. 10.1002/embj.201386942.
  166. McGinnis, C.S., Murrow, L.M., and Gartner, Z.J. (2019). DoubletFinder: Doublet Detection in Single-Cell RNA Sequencing Data Using Artificial Nearest Neighbors. *cels* 8, 329–337.e4. 10.1016/j.cels.2019.03.003.
  167. McNair, K., Spike, R., Guilding, C., Prendergast, G.C., Stone, T.W., Cobb, S.R., and Morris, B.J. (2010). A Role for RhoB in Synaptic Plasticity and the Regulation of Neuronal Morphology. *J Neurosci* 30, 3508–3517. 10.1523/JNEUROSCI.5386-09.2010.
  168. Mi, D., Li, Z., Lim, L., Li, M., Moissidis, M., Yang, Y., Gao, T., Hu, T.X., Pratt, T., Price, D.J., et al. (2018). Early emergence of cortical interneuron diversity in the mouse embryo. *Science* 360, 81–85. 10.1126/science.aar6821.
  169. Mi, D., Manuel, M., Huang, Y.-T., Mason, J.O., and Price, D.J. (2018). Pax6 Lengthens G1 Phase and Decreases Oscillating Cdk6 Levels in Murine Embryonic Cortical Progenitors. *Front Cell Neurosci* 12, 419. 10.3389/fncel.2018.00419.
  170. Miyata, T., Kawaguchi, A., Saito, K., Kawano, M., Muto, T., and Ogawa, M. (2004). Asymmetric production of surface-dividing and non-surface-dividing cortical progenitor cells. *Development* 131, 3133–3145. 10.1242/dev.01173.
  171. Mizrak, D., Levitin, H.M., Delgado, A.C., Crotet, V., Yuan, J., Chaker, Z., Silva-Vargas, V., Sims, P.A., and Doetsch, F. (2019). Single-Cell Analysis of Regional Differences in Adult V-SVZ Neural Stem Cell Lineages. *Cell Reports* 26, 394–406.e5. 10.1016/j.celrep.2018.12.044.
  172. Molnár, Z., Métin, C., Stoykova, A., Tarabykin, V., Price, D.J., Francis, F., Meyer, G., Dehay, C., and Kennedy, H. (2006). Comparative aspects of cerebral cortical development. *European Journal of Neuroscience* 23, 921–934. 10.1111/j.1460-9568.2006.04611.x.
  173. Molyneaux, B.J., Arlotta, P., Fame, R.M., MacDonald, J.L., MacQuarrie, K.L., and Macklis, J.D. (2009). Novel Subtype-Specific Genes Identify Distinct Subpopulations of Callosal Projection Neurons. *J. Neurosci.* 29, 12343–12354. 10.1523/JNEUROSCI.6108-08.2009.
  174. Moon, S., and Zhao, Y.-T. (2021). Spatial, temporal and cell-type-specific expression profiles of genes encoding heparan sulfate biosynthesis enzymes

## REFERENCES

- and proteoglycan core proteins. *Glycobiology* 31, 1308–1318. 10.1093/glycob/cwab054.
175. Moreau, M.X., Saillour, Y., Cwetsch, A.W., Pierani, A., and Causeret, F. (2021). Single-cell transcriptomics of the early developing mouse cerebral cortex disentangle the spatial and temporal components of neuronal fate acquisition. *Development* 148, dev197962. 10.1242/dev.197962.
176. Nelson, B.R., Hodge, R.D., Bedogni, F., and Hevner, R.F. (2013). Dynamic Interactions between Intermediate Neurogenic Progenitors and Radial Glia in Embryonic Mouse Neocortex: Potential Role in Dll1-Notch Signaling. *J Neurosci* 33, 9122–9139. 10.1523/JNEUROSCI.0791-13.2013.
177. Nemes, A.D., Ayasoufi, K., Ying, Z., Zhou, Q.-G., Suh, H., and Najm, I.M. (2017). Growth Associated Protein 43 (GAP-43) as a Novel Target for the Diagnosis, Treatment and Prevention of Epileptogenesis. *Sci Rep* 7, 17702. 10.1038/s41598-017-17377-z.
178. Noctor, S.C., Flint, A.C., Weissman, T.A., Wong, W.S., Clinton, B.K., and Kriegstein, A.R. (2002). Dividing Precursor Cells of the Embryonic Cortical Ventricular Zone Have Morphological and Molecular Characteristics of Radial Glia. *J Neurosci* 22, 3161–3173. 10.1523/JNEUROSCI.22-08-03161.2002.
179. Noctor, S.C., Martínez-Cerdeño, V., Ivic, L., and Kriegstein, A.R. (2004). Cortical neurons arise in symmetric and asymmetric division zones and migrate through specific phases. *Nat Neurosci* 7, 136–144. 10.1038/nn1172.
180. Nomura, T., Yamashita, W., Gotoh, H., and Ono, K. (2018). Species-Specific Mechanisms of Neuron Subtype Specification Reveal Evolutionary Plasticity of Amniote Brain Development. *Cell Reports* 22, 3142–3151. 10.1016/j.celrep.2018.02.086.
181. Nonaka-Kinoshita, M., Reillo, I., Artegiani, B., Ángeles Martínez-Martínez, M., Nelson, M., Borrell, V., and Calegari, F. (2013). Regulation of cerebral cortex size and folding by expansion of basal progenitors. *EMBO J* 32, 1817–1828. 10.1038/emboj.2013.96.
182. Nowakowski, T.J., Bhaduri, A., Pollen, A.A., Alvarado, B., Mostajo-Radji, M.A., Di Lullo, E., Haeussler, M., Sandoval-Espinosa, C., Liu, S.J., Velmeshev, D., et al. (2017). Spatiotemporal gene expression trajectories reveal developmental hierarchies of the human cortex. *Science* 358, 1318–1323. 10.1126/science.aap8809.
183. Nowakowski, T.J., Pollen, A.A., Sandoval-Espinosa, C., and Kriegstein, A.R. (2016). Transformation of the Radial Glia Scaffold Demarcates Two Stages of Human Cerebral Cortex Development. *Neuron* 91, 1219–1227. 10.1016/j.neuron.2016.09.005.
184. O’Leary, M.A., Bloch, J.I., Flynn, J.J., Gaudin, T.J., Giallombardo, A., Giannini, N.P., Goldberg, S.L., Kraatz, B.P., Luo, Z.-X., Meng, J., et al. (2013). The Placental Mammal Ancestor and the Post-K-Pg Radiation of Placentals. *Science* 339,



- 662–667. 10.1126/science.1229237.
185. O'Dell, R.S., Ustine, C.J.M., Cameron, D.A., Lawless, S.M., Williams, R.M., Zipfel, W.R., and Olson, E.C. (2012). Layer 6 cortical neurons require Reelin-Dab1 signaling for cellular orientation, Golgi deployment, and directed neurite growth into the marginal zone. *Neural Development* 7, 25. 10.1186/1749-8104-7-25.
  186. Oegema, R., Barakat, T.S., Wilke, M., Stouffs, K., Amrom, D., Aronica, E., Bahi-Buisson, N., Conti, V., Fry, A.E., Geis, T., et al. (2020). International consensus recommendations on the diagnostic work-up for malformations of cortical development. *Nat Rev Neurol* 16, 618–635. 10.1038/s41582-020-0395-6.
  187. Ohnuma, S., and Harris, W.A. (2003). Neurogenesis and the Cell Cycle. *Neuron* 40, 199–208. 10.1016/S0896-6273(03)00632-9.
  188. Oldham, M.C., Konopka, G., Iwamoto, K., Langfelder, P., Kato, T., Horvath, S., and Geschwind, D.H. (2008). Functional organization of the transcriptome in human brain. *Nat Neurosci* 11, 1271–1282. 10.1038/nn.2207.
  189. Ollion, J., Cochenec, J., Loll, F., Escudé, C., and Boudier, T. (2013). TANGO: a generic tool for high-throughput 3D image analysis for studying nuclear organization. *Bioinformatics* 29, 1840–1841. 10.1093/bioinformatics/btt276.
  190. Online Mendelian Inheritance in Man, OMIM® McKusick-Nathans Institute of Genetic Medicine, Johns Hopkins University (Baltimore, MD), {2020}. World Wide Web URL: <https://omim.org/>.
  191. Peng, X., Alföldi, J., Gori, K., Einfeld, A.J., Tyler, S.R., Tisoncik-Go, J., Brawand, D., Law, G.L., Skunca, N., Hatta, M., et al. (2014). The draft genome sequence of the ferret (*Mustela putorius furo*) facilitates study of human respiratory disease. *Nat Biotechnol* 32, 1250–1255. 10.1038/nbt.3079.
  192. Pickering, A (2020) [Source code]. <https://github.com/MarioniLab/DropletUtils/issues/36#issue-564741989>.
  193. Pilz, G.-A., Shitamukai, A., Reillo, I., Pacary, E., Schwausch, J., Stahl, R., Ninkovic, J., Snippert, H.J., Clevers, H., Godinho, L., et al. (2013). Amplification of progenitors in the mammalian telencephalon includes a new radial glial cell type. *Nat Commun* 4, 2125. 10.1038/ncomms3125.
  194. Piper, M., Barry, G., Hawkins, J., Mason, S., Lindwall, C., Little, E., Sarkar, A., Smith, A.G., Moldrich, R.X., Boyle, G.M., et al. (2010). NFIA Controls Telencephalic Progenitor Cell Differentiation through Repression of the Notch Effector Hes1. *J. Neurosci.* 30, 9127–9139. 10.1523/JNEUROSCI.6167-09.2010.
  195. Pizzagalli, F., Auzias, G., Yang, Q., Mathias, S.R., Faskowitz, J., Boyd, J.D., Amini, A., Rivière, D., McMahon, K.L., de Zubicaray, G.I., et al. (2020). The reliability and heritability of cortical folds and their genetic correlations across hemispheres. *Commun Biol* 3, 1–12. 10.1038/s42003-020-01163-1.

## REFERENCES

196. Polioudakis, D., Torre-Ubieta, L. de la, Langerman, J., Elkins, A.G., Shi, X., Stein, J.L., Vuong, C.K., Nichterwitz, S., Gevorgian, M., Opland, C.K., et al. (2019). A Single-Cell Transcriptomic Atlas of Human Neocortical Development during Mid-gestation. *Neuron* 103, 785-801.e8. 10.1016/j.neuron.2019.06.011.
197. Pollen, A.A., Nowakowski, T.J., Chen, J., Retallack, H., Sandoval-Espinosa, C., Nicholas, C.R., Shuga, J., Liu, S.J., Oldham, M.C., Diaz, A., et al. (2015). Molecular Identity of Human Outer Radial Glia During Cortical Development. *Cell* 163, 55–67. 10.1016/j.cell.2015.09.004.
198. Poluch, S., and Juliano, S.L. (2015). Fine-Tuning of Neurogenesis is Essential for the Evolutionary Expansion of the Cerebral Cortex. *Cerebral Cortex* 25, 346–364. 10.1093/cercor/bht232.
199. Popovitchenko, T., Park, Y., Page, N.F., Luo, X., Krsnik, Z., Liu, Y., Salamon, I., Stephenson, J.D., Kraushar, M.L., Volk, N.L., et al. (2020). Translational derepression of *Elavl4* isoforms at their alternative 5' UTRs determines neuronal development. *Nat Commun* 11, 1674. 10.1038/s41467-020-15412-8.
200. Pruitt, K.D., Brown, G.R., Hiatt, S.M., Thibaud-Nissen, F., Astashyn, A., Ermolaeva, O., Farrell, C.M., Hart, J., Landrum, M.J., McGarvey, K.M., et al. (2014). RefSeq: an update on mammalian reference sequences. *Nucleic Acids Research* 42, D756–D763. 10.1093/nar/gkt1114.
201. Pruitt, K.D., Tatusova, T., and Maglott, D.R. (2005). NCBI Reference Sequence (RefSeq): a curated non-redundant sequence database of genomes, transcripts and proteins. *Nucleic Acids Research* 33, D501–D504. 10.1093/nar/gki025.
202. Puelles, L., Harrison, M., Paxinos, G., and Watson, C. (2013). A developmental ontology for the mammalian brain using the prosomere model. *Trends in neurosciences* 36. 10.1016/j.tins.2013.06.004.
203. Purves, D., Augustine, G.J., Fitzpatrick, D., Hall, W.C., LaMantia, A.-S., McNamara, J.O., and Williams, S.M. eds. (2004). *Neuroscience* 3rd ed. (Sinauer Associates, Inc.).
204. Qiu, X., Mao, Q., Tang, Y., Wang, L., Chawla, R., Pliner, H.A., and Trapnell, C. (2017). Reversed graph embedding resolves complex single-cell trajectories. *Nat Methods* 14, 979–982. 10.1038/nmeth.4402.
205. Rakic, P. (1972). Mode of cell migration to the superficial layers of fetal monkey neocortex. *Journal of Comparative Neurology* 145, 61–83. 10.1002/cne.901450105.
206. Rakic, P. (1974). Neurons in Rhesus Monkey Visual Cortex: Systematic Relation between Time of Origin and Eventual Disposition. *Science* 183, 425–427. 10.1126/science.183.4123.425.
207. Rakic, P. (1988). Specification of Cerebral Cortical Areas. *Science* 241, 170–

176. 10.1126/science.3291116.
208. Rakic, P. (1995). A small step for the cell, a giant leap for mankind: a hypothesis of neocortical expansion during evolution. *Trends in Neurosciences* *18*, 383–388. 10.1016/0166-2236(95)93934-P.
209. Rakic, P. (2009). Evolution of the neocortex: Perspective from developmental biology. *Nat Rev Neurosci* *10*, 724–735. 10.1038/nrn2719.
210. Ramón y Cajal, S. (1890). Sobre la existencia de células nerviosas especiales en la primera capa de las circonvoluciones cerebrales. *Gac. Méd. Cat.* *13*, 737–739.
211. Ramsköld, D., Luo, S., Wang, Y.-C., Li, R., Deng, Q., Faridani, O.R., Daniels, G.A., Khrebtkova, I., Loring, J.F., Laurent, L.C., et al. (2012). Full-Length mRNA-Seq from single cell levels of RNA and individual circulating tumor cells. *Nat Biotechnol* *30*, 777–782. 10.1038/nbt.2282.
212. Rasmussen, A.H., Rasmussen, H.B., and Silaharoglu, A. (2017). The DLGAP family: neuronal expression, function and role in brain disorders. *Molecular Brain* *10*, 43. 10.1186/s13041-017-0324-9.
213. Reillo, I., and Borrell, V. (2012). Germinal Zones in the Developing Cerebral Cortex of Ferret: Ontogeny, Cell Cycle Kinetics, and Diversity of Progenitors. *Cerebral Cortex* *22*, 2039–2054. 10.1093/cercor/bhr284.
214. Reillo, I., de Juan Romero, C., Cárdenas, A., Clascá, F., Martínez-Martínez, M.Á., and Borrell, V. (2017). A Complex Code of Extrinsic Influences on Cortical Progenitor Cells of Higher Mammals. *Cerebral Cortex* *27*, 4586–4606. 10.1093/cercor/bhx171.
215. Reillo, I., de Juan Romero, C., García-Cabezas, M.Á., and Borrell, V. (2011). A Role for Intermediate Radial Glia in the Tangential Expansion of the Mammalian Cerebral Cortex. *Cerebral Cortex* *21*, 1674–1694. 10.1093/cercor/bhq238.
216. Renier, N., Wu, Z., Simon, D.J., Yang, J., Ariel, P., and Tessier-Lavigne, M. (2014). iDISCO: A Simple, Rapid Method to Immunolabel Large Tissue Samples for Volume Imaging. *Cell* *159*, 896–910. 10.1016/j.cell.2014.10.010.
217. Retzius, G. (1893). Die Cajal'schen Zellen der Grosshirnrinde beim Menschen und bei Säugetieren. *Biol. Untersuchungen Neue Folge* *5*, 1–8.
218. Richman, D.P., Stewart, R.M., Hutchinson, J., and Caviness, V.S. (1975). Mechanical Model of Brain Convolutional Development. *Science* *189*, 18–21. 10.1126/science.1135626.
219. Risi, E. (2014). Control of Reproduction in Ferrets, Rabbits and Rodents. *Reproduction in Domestic Animals* *49*, 81–86. 10.1111/rda.12300.
220. Romero, D.M., Bahi-Buisson, N., and Francis, F. (2018). Genetics and

## REFERENCES

- mechanisms leading to human cortical malformations. *Seminars in Cell & Developmental Biology* 76, 33–75. 10.1016/j.semcdb.2017.09.031.
221. Rowell, J.J., Mallik, A.K., Dugas-Ford, J., and Ragsdale, C.W. (2010). Molecular analysis of neocortical layer structure in the ferret. *J Comp Neurol* 518, 3272–3289. 10.1002/cne.22399.
222. Safran, M., Rosen, N., Twik, M., BarShir, R., Stein, T.I., Dahary, D., Fishilevich, S., and Lancet, D. (2022). The GeneCards Suite. In *Practical Guide to Life Science Databases*, I. Abugessaisa and T. Kasukawa, eds. (Springer Nature), pp. 27–56. 10.1007/978-981-16-5812-9\_2.
223. Sanger, F., Nicklen, S., and Coulson, A.R. (1977). DNA sequencing with chain-terminating inhibitors. *Proceedings of the National Academy of Sciences* 74, 5463–5467. 10.1073/pnas.74.12.5463.
224. Satija, R., Farrell, J.A., Gennert, D., Schier, A.F., and Regev, A. (2015). Spatial reconstruction of single-cell gene expression data. *Nat Biotechnol* 33, 495–502. 10.1038/nbt.3192.
225. SatijaLab (2007) `seurat-wrappers` (version 0.3.0) [Source code]. <https://github.com/satijalab/seurat-wrappers>.
226. Sato, H., Fukutani, Y., Yamamoto, Y., Tatara, E., Takemoto, M., Shimamura, K., and Yamamoto, N. (2012). Thalamus-Derived Molecules Promote Survival and Dendritic Growth of Developing Cortical Neurons. *J. Neurosci.* 32, 15388–15402. 10.1523/JNEUROSCI.0293-12.2012.
227. Sauer, F.C. (1935). Mitosis in the neural tube. *J. Comp. Neurol.* 62, 377–405. 10.1002/cne.900620207.
228. Sawada, K., and Watanabe, M. (2012). Development of cerebral sulci and gyri in ferrets (*Mustela putorius*). *Congenital Anomalies* 52, 168–175. 10.1111/j.1741-4520.2012.00372.x.
229. Schindelin, J., Arganda-Carreras, I., Frise, E., Kaynig, V., Longair, M., Pietzsch, T., Preibisch, S., Rueden, C., Saalfeld, S., Schmid, B., et al. (2012). Fiji: an open-source platform for biological-image analysis. *Nat Methods* 9, 676–682. 10.1038/nmeth.2019.
230. Sedmak, G., and Judaš, M. (2021). White Matter Interstitial Neurons in the Adult Human Brain: 3% of Cortical Neurons in Quest for Recognition. *Cells* 10, 190. 10.3390/cells10010190.
231. Severino, M., Geraldo, A.F., Utz, N., Tortora, D., Pogledic, I., Klonowski, W., Triulzi, F., Arrigoni, F., Mankad, K., Leventer, R.J., et al. (2020). Definitions and classification of malformations of cortical development: practical guidelines. *Brain* 143, 2874–2894. 10.1093/brain/awaa174.
232. Shannon, P., Markiel, A., Ozier, O., Baliga, N.S., Wang, J.T., Ramage, D., Amin, N., Schwikowski, B., and Ideker, T. (2003). Cytoscape: A Software Environment

- for Integrated Models of Biomolecular Interaction Networks. *Genome Res* 13, 2498–2504. 10.1101/gr.1239303.
233. Shimojo, H., Ohtsuka, T., and Kageyama, R. (2008). Oscillations in Notch Signaling Regulate Maintenance of Neural Progenitors. *Neuron* 58, 52–64. 10.1016/j.neuron.2008.02.014.
234. Shimozaki, K. (2014). Sox2 transcription network acts as a molecular switch to regulate properties of neural stem cells. *World J Stem Cells* 6, 485–490. 10.4252/wjsc.v6.i4.485.
235. Shinmyo, Y., Terashita, Y., Dinh Duong, T.A., Horiike, T., Kawasumi, M., Hosomichi, K., Tajima, A., and Kawasaki, H. (2017). Folding of the Cerebral Cortex Requires Cdk5 in Upper-Layer Neurons in Gyrencephalic Mammals. *Cell Reports* 20, 2131–2143. 10.1016/j.celrep.2017.08.024.
236. Shiraishi, N., Katayama, A., Nakashima, T., Yamada, S., Uwabe, C., Kose, K., and Takakuwa, T. (2015). Morphology and morphometry of the human embryonic brain: A three-dimensional analysis. *NeuroImage* 115, 96–103. 10.1016/j.neuroimage.2015.04.044.
237. Shitamukai, A., Konno, D., and Matsuzaki, F. (2011). Oblique Radial Glial Divisions in the Developing Mouse Neocortex Induce Self-Renewing Progenitors outside the Germinal Zone That Resemble Primate Outer Subventricular Zone Progenitors. *J. Neurosci.* 31, 3683–3695. 10.1523/JNEUROSCI.4773-10.2011.
238. Sidman, R.L., Miale, I.L., and Feder, N. (1959). Cell proliferation and migration in the primitive ependymal zone; An autoradiographic study of histogenesis in the nervous system. *Experimental Neurology* 1, 322–333. 10.1016/0014-4886(59)90024-X.
239. Sidman, R.L., and Rakic, P. (1973). Neuronal migration, with special reference to developing human brain: a review. *Brain Research* 62, 1–35. 10.1016/0006-8993(73)90617-3.
240. Smart, I.H., and McSherry, G.M. (1986). Gyrus formation in the cerebral cortex in the ferret. I. Description of the external changes. *J Anat* 146, 141–152.
241. Smart, I.H.M., Dehay, C., Giroud, P., Berland, M., and Kennedy, H. (2002). Unique morphological features of the proliferative zones and postmitotic compartments of the neural epithelium giving rise to striate and extrastriate cortex in the monkey. *Cereb Cortex* 12, 37–53.
242. Smith, T., Heger, A., and Sudbery, I. (2017). UMI-tools: modeling sequencing errors in Unique Molecular Identifiers to improve quantification accuracy. *Genome Res* 27, 491–499. 10.1101/gr.209601.116.
243. Sokpor, G., Brand-Saberi, B., Nguyen, H.P., and Tuoc, T. (2022). Regulation of Cell Delamination During Cortical Neurodevelopment and Implication for Brain Disorders. *Frontiers in Neuroscience* 16.

## REFERENCES

244. Sousa, A.M.M., Meyer, K.A., Santpere, G., Gulden, F.O., and Sestan, N. (2017). Evolution of the Human Nervous System Function, Structure, and Development. *Cell* *170*, 226–247. 10.1016/j.cell.2017.06.036.
245. Stancik, E.K., Navarro-Quiroga, I., Sellke, R., and Haydar, T.F. (2010). Heterogeneity in Ventricular Zone Neural Precursors Contributes to Neuronal Fate Diversity in the Postnatal Neocortex. *J. Neurosci.* *30*, 7028–7036. 10.1523/JNEUROSCI.6131-09.2010.
246. Stensaas, L.J. (1967). The development of hippocampal and dorsolateral pallial regions of the cerebral hemisphere in fetal rabbits IV. Forty-one millimeter stage, intermediate lamina. *Journal of Comparative Neurology* *131*, 409–421. 10.1002/cne.901310402.
247. Stepien, B.K., Naumann, R., Holtz, A., Helppi, J., Huttner, W.B., and Vaid, S. (2020). Lengthening Neurogenic Period during Neocortical Development Causes a Hallmark of Neocortex Expansion. *Current Biology* *30*, 4227–4237.e5. 10.1016/j.cub.2020.08.046.
248. Stepien, B.K., Vaid, S., and Huttner, W.B. (2021). Length of the Neurogenic Period—A Key Determinant for the Generation of Upper-Layer Neurons During Neocortex Development and Evolution. *Frontiers in Cell and Developmental Biology* *9*.
249. Stuart, T., Butler, A., Hoffman, P., Hafemeister, C., Papalexi, E., Mauck, W.M., Hao, Y., Stoeckius, M., Smibert, P., and Satija, R. (2019). Comprehensive Integration of Single-Cell Data. *Cell* *177*, 1888–1902.e21. 10.1016/j.cell.2019.05.031.
250. Sun, T., and Hevner, R.F. (2014). Growth and folding of the mammalian cerebral cortex: from molecules to malformations. *Nat Rev Neurosci* *15*, 217–232. 10.1038/nrn3707.
251. Sun, X., Yan, Z., Yi, Y., Li, Z., Lei, D., Rogers, C.S., Chen, J., Zhang, Y., Welsh, M.J., Leno, G.H., et al. (2008). Adeno-associated virus–targeted disruption of the *CFTR* gene in cloned ferrets. *J Clin Invest* *118*, 1578–1583. 10.1172/JCI34599.
252. Svensson, V., Vento-Tormo, R., and Teichmann, S.A. (2018). Exponential scaling of single-cell RNA-seq in the past decade. *Nat Protoc* *13*, 599–604. 10.1038/nprot.2017.149.
253. Tanaka, M., DeLorey, T.M., Delgado-Escueta, A., and Olsen, R.W. (2012). GABRB3, Epilepsy, and Neurodevelopment (National Center for Biotechnology Information (US)).
254. Tang, F., Barbacioru, C., Wang, Y., Nordman, E., Lee, C., Xu, N., Wang, X., Bodeau, J., Tuch, B.B., Siddiqui, A., et al. (2009). mRNA-Seq whole-transcriptome analysis of a single cell. *Nat Methods* *6*, 377–382. 10.1038/nmeth.1315.
255. Tang, M (2020) [Source code].

<https://divingintogeneticsandgenomics.rbind.io/post/stacked-violin-plot-for-visualizing-single-cell-data-in-seurat/>.

256. Tarabykin, V., Britanova, O., Fradkov, A., Voss, A., Katz, L.S., Lukyanov, S., and Gruss, P. (2000). Expression of PTTG and *prc1* genes during telencephalic neurogenesis. *Mechanisms of Development* 92, 301–304. 10.1016/S0925-4773(00)00243-4.
257. Telley, L., Agirman, G., Prados, J., Amberg, N., Fièvre, S., Oberst, P., Bartolini, G., Vitali, I., Cadilhac, C., Hippenmeyer, S., et al. (2019). Temporal patterning of apical progenitors and their daughter neurons in the developing neocortex. *Science* 364, eaav2522. 10.1126/science.aav2522.
258. Telley, L., Govindan, S., Prados, J., Stevant, I., Nef, S., Dermitzakis, E., Dayer, A., and Jabaudon, D. (2016). Sequential transcriptional waves direct the differentiation of newborn neurons in the mouse neocortex. *Science* 351, 1443–1446. 10.1126/science.aad8361.
259. Thomsen, E.R., Mich, J.K., Yao, Z., Hodge, R.D., Doyle, A.M., Jang, S., Shehata, S.I., Nelson, A.M., Shapovalova, N.V., Levi, B.P., et al. (2016). Fixed single-cell transcriptomic characterization of human radial glial diversity. *Nat Methods* 13, 87–93. 10.1038/nmeth.3629.
260. Toda, T., Shinmyo, Y., Dinh Duong, T.A., Masuda, K., and Kawasaki, H. (2016). An essential role of SVZ progenitors in cortical folding in gyrencephalic mammals. *Sci Rep* 6, 29578. 10.1038/srep29578.
261. Toma, K., and Hanashima, C. (2015). Switching modes in corticogenesis: mechanisms of neuronal subtype transitions and integration in the cerebral cortex. *Front Neurosci* 9, 274. 10.3389/fnins.2015.00274.
262. Toro, D. del, Ruff, T., Cederfjäll, E., Villalba, A., Seyit-Bremer, G., Borrell, V., and Klein, R. (2017). Regulation of Cerebral Cortex Folding by Controlling Neuronal Migration via FLRT Adhesion Molecules. *Cell* 169, 621–635.e16. 10.1016/j.cell.2017.04.012.
263. Tran, H.T.N., Ang, K.S., Chevrier, M., Zhang, X., Lee, N.Y.S., Goh, M., and Chen, J. (2020). A benchmark of batch-effect correction methods for single-cell RNA sequencing data. *Genome Biology* 21, 12. 10.1186/s13059-019-1850-9.
264. Trapnell, C., Cacchiarelli, D., Grimsby, J., Pokharel, P., Li, S., Morse, M., Lennon, N.J., Livak, K.J., Mikkelsen, T.S., and Rinn, J.L. (2014). Pseudo-temporal ordering of individual cells reveals dynamics and regulators of cell fate decisions. *Nat Biotechnol* 32, 381–386. 10.1038/nbt.2859.
265. Trapnell, C., Cacchiarelli, D., Grimsby, J., Pokharel, P., Li, S., Morse, M., Lennon, N.J., Livak, K.J., Mikkelsen, T.S., and Rinn, J.L. (2014). The dynamics and regulators of cell fate decisions are revealed by pseudotemporal ordering of single cells. *Nat Biotechnol* 32, 381–386. 10.1038/nbt.2859.
266. Trapnell, C., Williams, B.A., Pertea, G., Mortazavi, A., Kwan, G., van Baren, M.J.,

## REFERENCES

- Salzberg, S.L., Wold, B.J., and Pachter, L. (2010). Transcript assembly and quantification by RNA-Seq reveals unannotated transcripts and isoform switching during cell differentiation. *Nat Biotechnol* 28, 511–515. 10.1038/nbt.1621.
267. Tutukova, S., Tarabykin, V., and Hernandez-Miranda, L.R. (2021). The Role of Neurod Genes in Brain Development, Function, and Disease. *Front Mol Neurosci* 14, 662774. 10.3389/fnmol.2021.662774.
268. Uittenbogaard, M., and Chiaramello, A. (2002). Expression of the bHLH transcription factor Tcf12 (ME1) gene is linked to the expansion of precursor cell populations during neurogenesis. *Brain Res Gene Expr Patterns* 1, 115–121. 10.1016/s1567-133x(01)00022-9.
269. Vaid, S., Camp, J.G., Hersemann, L., Eugster Oegema, C., Heninger, A.-K., Winkler, S., Brandl, H., Sarov, M., Treutlein, B., Huttner, W.B., et al. (2018). A novel population of Hopx-dependent basal radial glial cells in the developing mouse neocortex. *Development* 145, dev169276. 10.1242/dev.169276.
270. Vaid, S., and Huttner, W.B. (2020). Transcriptional Regulators and Human-Specific/Primate-Specific Genes in Neocortical Neurogenesis. *Int J Mol Sci* 21, E4614. 10.3390/ijms21134614.
271. Vallès, A., Boender, A.J., Gijsbers, S., Haast, R.A.M., Martens, G.J.M., and Weerd, P. de (2011). Genomewide Analysis of Rat Barrel Cortex Reveals Time- and Layer-Specific mRNA Expression Changes Related to Experience-Dependent Plasticity. *J. Neurosci.* 31, 6140–6158. 10.1523/JNEUROSCI.6514-10.2011.
272. van den Berg, D.L.C., Azzarelli, R., Oishi, K., Martynoga, B., Urbán, N., Dekkers, D.H.W., Demmers, J.A., and Guillemot, F. (2017). Nipbl Interacts with Zfp609 and the Integrator Complex to Regulate Cortical Neuron Migration. *Neuron* 93, 348–361. 10.1016/j.neuron.2016.11.047.
273. Vertesy, A (2007) Seurat.Utils [Source code]. <https://github.com/vertesy/Seurat.utils>.
274. Wagner, D.E., and Klein, A.M. (2020). Lineage tracing meets single-cell omics: opportunities and challenges. *Nat Rev Genet* 21, 410–427. 10.1038/s41576-020-0223-2.
275. Wagner, D.E., Weinreb, C., Collins, Z.M., Briggs, J.A., Megason, S.G., and Klein, A.M. (2018). Single-cell mapping of gene expression landscapes and lineage in the zebrafish embryo. *Science* 360, 981–987. 10.1126/science.aar4362.
276. Wang, X., Tsai, J.-W., LaMonica, B., and Kriegstein, A.R. (2011). A new subtype of progenitor cell in the mouse embryonic neocortex. *Nat Neurosci* 14, 555–561. 10.1038/nn.2807.
277. Wang, Z., Mehra, V., Simpson, M.T., Maunze, B., Chakraborty, A., Holan, L., Eastwood, E., Blackmore, M.G., and Venkatesh, I. (2018). KLF6 and STAT3 co-occupy regulatory DNA and functionally synergize to promote axon growth in



- CNS neurons. *Sci Rep* 8, 12565. 10.1038/s41598-018-31101-5.
278. Welker, W. (1990). Why Does Cerebral Cortex Fissure and Fold? In *Cerebral Cortex Cerebral Cortex*, E. G. Jones and A. Peters, eds. (Springer US), pp. 3–136. 10.1007/978-1-4615-3824-0\_1.
279. Wickham, H., Averick, M., Bryan, J., Chang, W., McGowan, L.D., François, R., Grolemund, G., Hayes, A., Henry, L., Hester, J., et al. (2019). Welcome to the Tidyverse. *Journal of Open Source Software* 4, 1686. 10.21105/joss.01686.
280. Willems, E., Dedobbeleer, M., Digregorio, M., Lombard, A., Lumapat, P.N., and Rogister, B. (2018). The functional diversity of Aurora kinases: a comprehensive review. *Cell Division* 13, 7. 10.1186/s13008-018-0040-6.
281. Wonders, C.P., and Anderson, S.A. (2006). The origin and specification of cortical interneurons. *Nat Rev Neurosci* 7, 687–696. 10.1038/nrn1954.
282. Yamada, M., Clark, J., and Iulianella, A. (2014). MLLT11/AF1q is differentially expressed in maturing neurons during development. *Gene Expression Patterns* 15, 80–87. 10.1016/j.gep.2014.05.001.
283. Yu, M., Sun, X., Tyler, S.R., Liang, B., Swatek, A.M., Lynch, T.J., He, N., Yuan, F., Feng, Z., Rotti, P.G., et al. (2019). Highly Efficient Transgenesis in Ferrets Using CRISPR/Cas9-Mediated Homology-Independent Insertion at the ROSA26 Locus. *Sci Rep* 9, 1971. 10.1038/s41598-018-37192-4.
284. Yuzwa, S.A., Borrett, M.J., Innes, B.T., Voronova, A., Ketela, T., Kaplan, D.R., Bader, G.D., and Miller, F.D. (2017). Developmental Emergence of Adult Neural Stem Cells as Revealed by Single-Cell Transcriptional Profiling. *Cell Rep* 21, 3970–3986. 10.1016/j.celrep.2017.12.017.
285. Zahr, S.K., Yang, G., Kazan, H., Borrett, M.J., Yuzwa, S.A., Voronova, A., Kaplan, D.R., and Miller, F.D. (2018). A Translational Repression Complex in Developing Mammalian Neural Stem Cells that Regulates Neuronal Specification. *Neuron* 97, 520-537.e6. 10.1016/j.neuron.2017.12.045.
286. Zappia, L., and Oshlack, A. (2018). Clustering trees: a visualization for evaluating clusterings at multiple resolutions. *GigaScience* 7, giy083. 10.1093/gigascience/giy083.
287. Zecevic, N., Chen, Y., and Filipovic, R. (2005). Contributions of cortical subventricular zone to the development of the human cerebral cortex. *Journal of Comparative Neurology* 491, 109–122. 10.1002/cne.20714.
288. Zeng, H., Shen, E.H., Hohmann, J.G., Oh, S.W., Bernard, A., Royall, J.J., Glattfelder, K.J., Sunkin, S.M., Morris, J.A., Guillozet-Bongaarts, A.L., et al. (2012). Large-Scale Cellular-Resolution Gene Profiling in Human Neocortex Reveals Species-Specific Molecular Signatures. *Cell* 149, 483–496. 10.1016/j.cell.2012.02.052.
289. Zhang, C., Cui, L., He, W., Zhang, X., and Liu, H. (2021). Dl-3-n-butylphthalide promotes neurite outgrowth of primary cortical neurons by Sonic Hedgehog

## REFERENCES

- signaling via upregulating Gap43. *Experimental Cell Research* 398, 112420. 10.1016/j.yexcr.2020.112420.
290. Zhang, M., Zhou, J., Jiao, L., Xu, L., Hou, L., Yin, B., Qiang, B., Lu, S., Shu, P., and Peng, X. (2021). Long Non-coding RNA T-uc.189 Modulates Neural Progenitor Cell Fate by Regulating Srsf3 During Mouse Cerebral Cortex Development. *Front Neurosci* 15, 709684. 10.3389/fnins.2021.709684.
291. Zhang, Y., Huang, Y., Hu, L., and Cheng, T. (2022). New insights into Human Hematopoietic Stem and Progenitor Cells via Single-Cell Omics. *Stem Cell Rev and Rep* 18, 1322–1336. 10.1007/s12015-022-10330-2.
292. Zheng, G.X.Y., Terry, J.M., Belgrader, P., Ryvkin, P., Bent, Z.W., Wilson, R., Ziraldo, S.B., Wheeler, T.D., McDermott, G.P., Zhu, J., et al. (2017). Massively parallel digital transcriptional profiling of single cells. *Nat Commun* 8, 14049. 10.1038/ncomms14049.
293. Zilles, K., Palomero-Gallagher, N., and Amunts, K. (2013). Development of cortical folding during evolution and ontogeny. *Trends in Neurosciences* 36, 275–284. 10.1016/j.tins.2013.01.006.
294. Nucleotide [Internet]. Bethesda (MD): National Library of Medicine (US), National Center for Biotechnology Information; [1988] – . Accession No. NC\_020638.1, *Mustela putorius furo* mitochondrion gff3, annotation release 101, assembly MusPutFur1.0/GCF\_000215625.1 [2019 Dec 16]. Available from: [https://www.ncbi.nlm.nih.gov/nucore/NC\\_020638.1](https://www.ncbi.nlm.nih.gov/nucore/NC_020638.1)
295. Gene [Internet]. Bethesda (MD): National Library of Medicine (US), National Center for Biotechnology Information; 2004 – [2022 Aug 17]. Available from: <https://www.ncbi.nlm.nih.gov/gene/101691950>
296. National Center for Biotechnology Information (NCBI) [Internet]. Bethesda (MD): National Library of Medicine (US), National Center for Biotechnology Information; [1988] – [2022 Aug 17]. Available from: <https://www.ncbi.nlm.nih.gov/>
297. UCSC Genome Bioinformatics Group (2022). UCSC Genome Browser [Online]. Available online at: <http://genome.ucsc.edu>. Genome assembly musFur1, release date Apr. 2011.
298. Protein [Internet]. Bethesda (MD): National Library of Medicine (US), National Center for Biotechnology Information; [1988] – . Accession AAH14225, *Homo sapiens* HOPX protein; [cited 2022 Aug 17]. Available from: <https://www.ncbi.nlm.nih.gov/protein/AAH14225.1>
299. R Core Team (2022). R: A language and environment for statistical computing. R Foundation for Statistical Computing, Vienna, Austria. URL <https://www.R-project.org/>.
300. Wickham, H., Averick, M., Bryan, J., Chang, W., McGowan, L. D., François, R., Grolemund, G., Hayes, A., Henry, L., Hester, J., Kuhn, M., Pedersen, T. L., Miller,

- E., Bache, S. M., Müller, K., Ooms, J., Robinson, D., Seidel, D. P., Spinu, V., ... Yutani, H. (2019). Welcome to the Tidyverse. *Journal of Open Source Software*, 4(43), 1686. <https://doi.org/10.21105/joss.01686>
301. McBain, M (2017) datapasta (version 3.1.0) [Source code]. <https://github.com/MilesMcBain/datapasta>.
302. Ooms J (2022). writexl: Export Data Frames to Excel 'xlsx' Format. <https://docs.ropensci.org/writexl/> (website) <https://github.com/ropensci/writexl> (devel) <https://libxlsxwriter.github.io> (upstream).



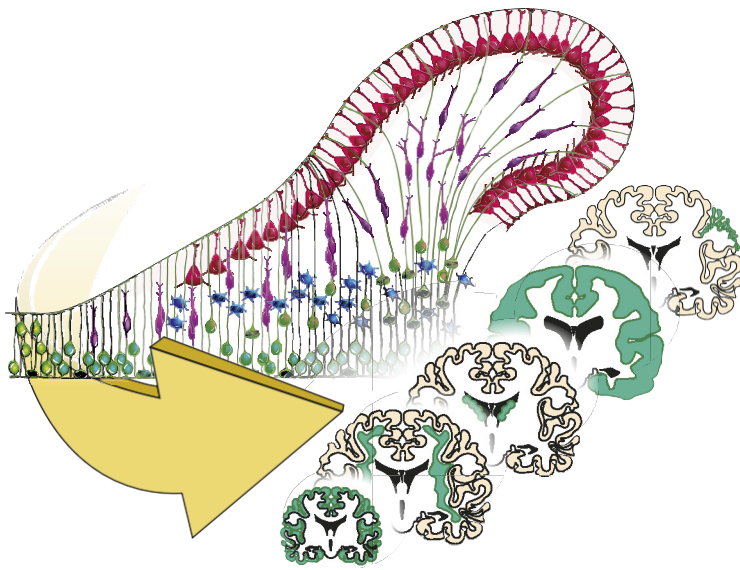
**APPENDIX: Author's published scientific contribution**

From Development To Disease Modeling. *Physiol. Rev.* 102, 511–550 (2022).

DOI: [10.1152/physrev.00016.2021](https://doi.org/10.1152/physrev.00016.2021)



# FOLDING BRAINS: FROM DEVELOPMENT TO DISEASE MODELING



## AUTHORS

Lucia Del-Valle-Anton, Víctor Borrell

## CORRESPONDENCE

vborrell@umh.es

## KEY WORDS

evolution; gyrencephaly; human; malformation; neurogenesis


## CLINICAL HIGHLIGHTS

The size and folding of the human cerebral cortex are critical for our higher cognition and result from a combination of developmental processes during embryonic and early postnatal life.

Human cortex folding disorders are linked to learning and cognitive deficits and emerge from impaired cellular and molecular mechanisms of development during specific time windows, frequently resulting in complex combinations of malformations.

Animal models and human-based in vitro culture systems are becoming increasingly powerful to illuminate the causes of developmental defects in human cortical malformations and to find potential therapeutic targets.

# FOLDING BRAINS: FROM DEVELOPMENT TO DISEASE MODELING

Lucia Del-Valle-Anton and  Víctor Borrell

Instituto de Neurociencias, Consejo Superior de Investigaciones Científicas and Universidad Miguel Hernández, Sant Joan d'Alacant, Spain

## Abstract

The human brain is characterized by the large size and intricate folding of its cerebral cortex, which are fundamental for our higher cognitive function and frequently altered in pathological dysfunction. Cortex folding is not unique to humans, nor even to primates, but is common across mammals. Cortical growth and folding are the result of complex developmental processes that involve neural stem and progenitor cells and their cellular lineages, the migration and differentiation of neurons, and the genetic programs that regulate and fine-tune these processes. All these factors combined generate mechanical stress and strain on the developing neural tissue, which ultimately drives orderly cortical deformation and folding. In this review we examine and summarize the current knowledge on the molecular, cellular, histogenic, and mechanical mechanisms that are involved in and influence folding of the cerebral cortex, and how they emerged and changed during mammalian evolution. We discuss the main types of pathological malformations of human cortex folding, their specific developmental origin, and how investigating their genetic causes has illuminated our understanding of key events involved. We close our review by presenting the animal and in vitro models of cortex folding that are currently used to study these devastating developmental brain disorders in children, and what are the main challenges that remain ahead of us to fully understand brain folding.

*evolution; gyrencephaly; human; malformation; neurogenesis*

1.	INTRODUCTION	511
2.	BASIC FACTS OF CORTICAL DEVELOPMENT	512
4.	PROGENITOR CELL AND LINEAGE DIVERSITY	515
3.	NEUROEPITHELIAL CELLS AND THE...	512
7.	RADIAL MIGRATION OF NEURONS	523
8.	CORTEX FOLDING	523
9.	EVOLUTION OF CORTICAL FOLDING	530
5.	MOLECULAR REGULATION OF CORTICAL...	518
6.	GENETIC SPECIALIZATIONS TO MAKE...	522
10.	HUMAN MALFORMATIONS OF CORTEX ...	533
11.	UNDERSTANDING MALFORMATIONS...	536
12.	CONCLUSIONS AND FUTURE DIRECTIONS	537
13.	APPENDIX	538

## CLINICAL HIGHLIGHTS

The size and folding of the human cerebral cortex are critical for our higher cognition and result from a combination of developmental processes during embryonic and early postnatal life.

Human cortex folding disorders are linked to learning and cognitive deficits and emerge from impaired cellular and molecular mechanisms of development during specific time windows, frequently resulting in complex combinations of malformations.

Animal models and human-based in vitro culture systems are becoming increasingly powerful to illuminate the causes of developmental defects in human cortical malformations and to find potential therapeutic targets.

## 1. INTRODUCTION

The cerebral cortex is the largest part of the brain in humans, with central roles in our higher cognitive abilities. One of the most characteristic features of the human brain is its wrinkled external appearance, due to the folding and fissuring of the cerebral cortex. With a remarkably precise organization in layers, and subject to dramatic expansion during evolution, the development of the human cerebral cortex has been an object of curiosity and intense scientific study for many decades. Much has

been learned about the histogenesis, cellular, and molecular mechanisms of cortex development, but much less about its folding. This is in part because cortical folding is a rather complex mechanism that involves many different biological and physical aspects of brain development, but also because most of our knowledge in this field comes from studies in mouse, which has a smooth cortex, with no folds. The advent of new and refined methods for the genetic and experimental manipulation of animal models traditionally considered “nongenetic” has sparked a renewed interest in understanding cortex folding over the last decade. This review comes from the necessity of bringing together and articulating our current knowledge



on the expansion and folding of the mammalian cerebral cortex, during development and evolution, with a particular focus on human. We present this issue in an accessible and yet comprehensive manner, including gaps of knowledge and aspects that are currently controversial in the field, such that it may serve as reference for researchers with expertise in other areas and for teaching purposes. Our journey starts with a basic description of cortical development, the characteristic features of the different cell types involved, and the mechanisms of their interrelationship. Then we move on to the elements and developmental mechanisms specifically involved in cortex folding, including the evolutionary adaptations and specializations that led cortical expansion and folding in mammals. We end this review recapitulating human developmental malformations of cortex folding, and how the basic knowledge covered in the previous sections allows modeling these diseases *in vivo* and *in vitro*, both to understand them better and to envisage potential future diagnostic and therapeutic strategies.

## 2. BASIC FACTS OF CORTICAL DEVELOPMENT

The development of the cerebral cortex has been a primary subject of intensive and extensive study for decades. At the onset of corticogenesis, the cortex is primarily composed by a primary germinal or ventricular zone (VZ), containing the primary type of cortical progenitor cells and limiting with the lateral telencephalic ventricle. Shortly after neurogenesis begins, newborn neurons begin accumulating above the VZ in a transient layer called preplate (PP). The PP contains two populations of excitatory neurons: generated in the underlying VZ, and at the borders of the

cortical primordium, the latter known as Cajal-Retzius cells (1, 2). As development proceeds and additional cohorts of neurons are generated, they migrate into the PP, splitting it in two layers: subplate (SP) and marginal zone (MZ). This way, a new layer forms between SP and MZ, called cortical plate (CP), where the successive generations of neurons will finish their migration and begin differentiating the dendritic and axonal arbors. The MZ is located externally from the CP and is mainly composed by Cajal-Retzius cells and migrating inhibitory interneurons (1, 3, 4).

The organization of cortical neurons in layers follows an inside-out gradient with respect to their time of origin (FIGURE 1). The discovery of this inside-out order of corticogenesis was a major cornerstone in our understanding of this process (5). In the adult cerebral cortex, neurons are organized in six main layers, which are generated in an orderly fashion during embryonic development. Neurons that occupy the deepest layer (VI) are generated first. The next generation of neurons migrate through and past layer VI, now transiently forming the CP, and are destined to form layer V, immediately superficial to layer VI (6). The same process repeats for neurons destined to progressively more superficial layers, until the neurons destined to the most superficial layer (II) are generated last (5). Exceptionally, layer I is constituted by the earliest-born cortical neurons, named Cajal-Retzius cells, but these have different origin and characteristics from the rest of cortical excitatory neurons (2, 7, 8).

## 3. NEUROEPITHELIAL CELLS AND THE CORTICAL PRIMORDIUM

The cerebral cortex stems from the cortical primordium in the early central nervous system (CNS), a monolayer

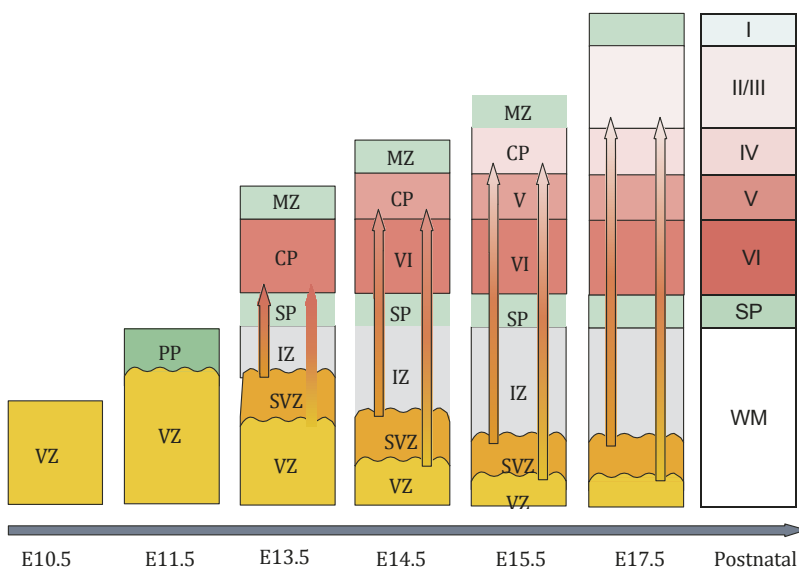


FIGURE 1. Inside-out model of cortical lamination. Neurons generated at the germinal layers (VZ and SVZ) migrate through the IZ and SP to accumulate forming the CP. The 6 layers that compose the mature neocortex are orderly produced from inside (layer VI) to outside (layer I). VZ, ventricular zone; PP, preplate; SVZ, subventricular zone; IZ, intermediate zone; SP, subplate; CP, cortical plate; MZ, marginal zone; WM, white matter; E, embryonic day.



of neural stem cells known as neuroepithelial cells (NECs) (9). NECs are highly polarized cells extending two thin processes perpendicular to the cortical plane, one apical and one basal, that contact the apical surface and the basal lamina of the telencephalic vesicle, respectively (10). At the apical side, NECs are bound to each other by forming tight junctions and adherent junctions, constituting an adherens junction belt. This preserves the polarity and structural integrity of the neuroepithelium, prevents the lateral diffusion of membrane components and regulates the trafficking of the cerebrospinal fluid (CSF) (11–13). The cell nucleus of NECs moves along the thickness of the neuroepithelium in perfect synchrony with the phases of the cell cycle, a process known as interkinetic nuclear migration (INM)

(FIGURE 2A). During G<sub>1</sub> phase, the nucleus migrates from the apical to the basal sides of the cortical primordium, S phase takes place near the basal side, during G<sub>2</sub> the nucleus descends to the apical side, and mitosis (M phase) takes place at the apical surface (10, 14). This movement is completely asynchronous between neighboring cells, such that at any given moment nuclei of NECs are found across the thickness of the neuroepithelium, conferring it a false layered or pseudostratified appearance. NECs are highly proliferative, dividing symmetrically into two progenitor cells to self-amplify. The starting number of NECs in the cortical primordium, the length of their cell cycle and of their proliferative period determine the cortical neurogenic capacity, and so the final number of neurons produced and, eventually, the

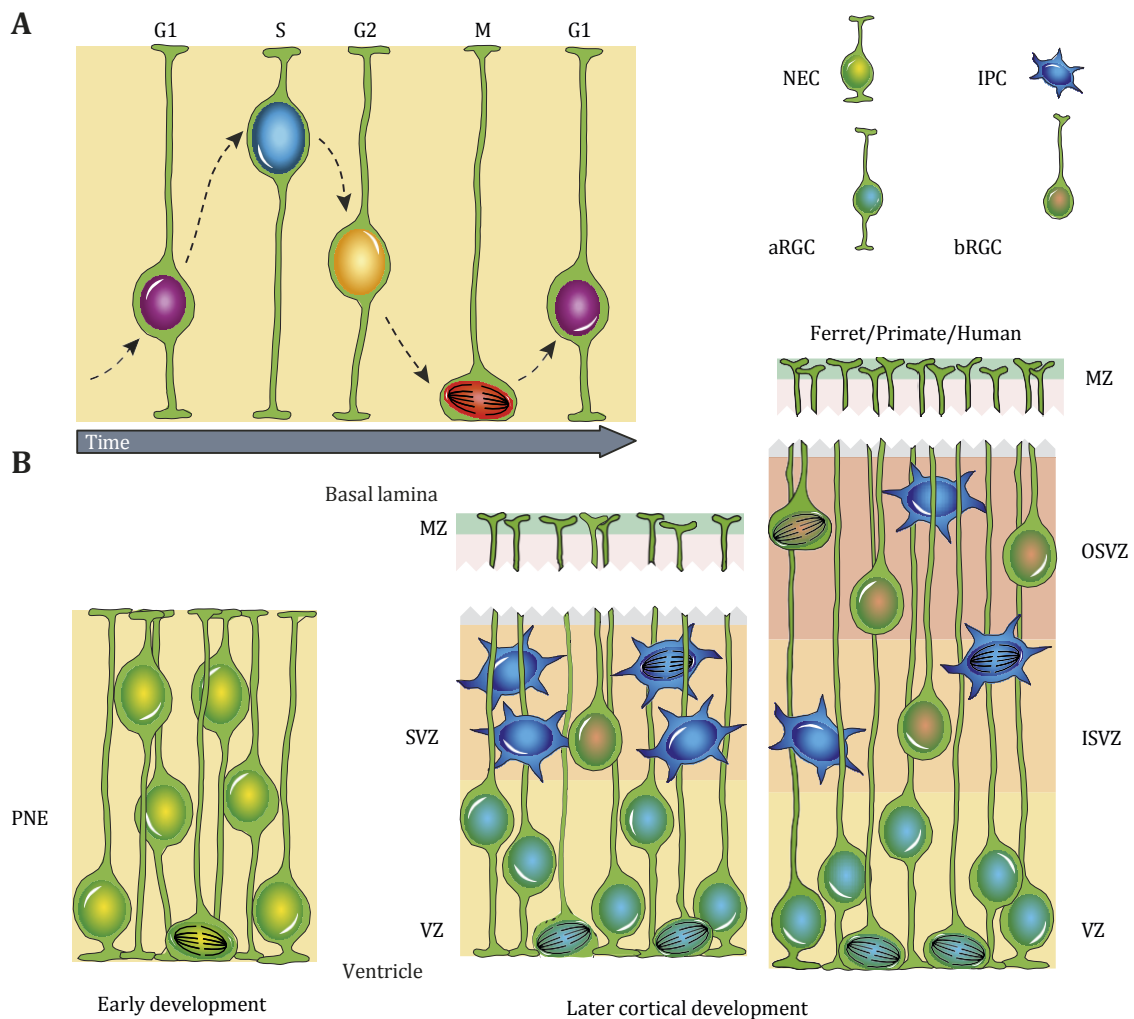


FIGURE 2. Progenitor cell diversity. *A*: apical-basal movement of the nucleus of neuroepithelial (NEC) and apical radial glia cells (aRGCs) along the thickness of the ventricular zone (VZ) during the stages of cell cycle, known as interkinetic nuclear migration. *B*: progenitor cell composition of germinal layers. At early phases of cortical development, the pseudostratified neuroepithelium (PNE) is populated by neuroepithelial cells (NECs) with the nuclei at different vertical positions depending on interkinetic nuclear migration. At subsequent stages, NECs are substituted by aRGCs with the soma in VZ and by basal radial glia cells (bRGCs) and intermediate progenitor cells (IPCs) forming the subventricular zone (SVZ). In mouse, the SVZ is thin compared with gyrencephalic species such as ferret, primates or human, where this is further subdivided in inner and outer SVZ (ISVZ, OSVZ). MZ, marginal zone.

degree of cortical folding (15). Accordingly, the telencephalic vesicles are particularly large in species possessing a large and highly folded cerebral cortex, such as humans and macaque monkeys compared with mouse. The duration of the cell cycle is longer in species with bigger cortices, such as carnivores and primates, compared with mice (16–18), which might suggest fewer cycles of NEC amplificative divisions. However, their neurogenic period is also much longer than in small-brained species, allowing for a larger number of amplificative divisions and the development of larger brains (19).

As cortical development progresses, immediately before the onset of neurogenesis [10 days postconception in rodents (E10), 5–6 gestation weeks (GW5–6) in humans], NECs gradually transform into apical radial glia cells (aRGCs) (FIGURE 2). These neural progenitor cells maintain several features from NECs, including their bipolar shape with apical and basal process, INM, and expression of neuroepithelial marker genes, such as Nestin (20). However, they also start acquiring distinctive astroglial characteristics, such as accumulation of glycogen granules in the endfeet, extension of lamellate

protrusions along the basal process, and expression of new marker genes: paired box 6 (Pax6), vimentin (Vim), glial fibrillary acidic protein (GFAP), astrocyte-specific glutamate transporter (GLAST), Ca<sup>2+</sup>-binding protein S100b, and brain-lipid-binding protein (BLBP) (21) (FIGURE 3). RGCs also lose tight junctions, but the adherens junction belt is maintained (22). The balance between NEC amplification and the transition to RGCs is the first key turning point in cortical development. In a groundbreaking experiment in 2002, Chenn and Walsh (23) generated transgenic mice where a constitutively active b-catenin (key component of the canonical Wnt signaling pathway) was expressed in NECs. This caused a dramatic increase in NEC amplification and tangential growth of the neuroepithelium, which folded onto itself in contrast to the normally smooth mouse neuroepithelium and cortex (23). Similarly, treatment of mouse cerebral hemispheres *ex vivo* with lysophosphatidic acid (LPA) caused a significant increase in cell-cycle reentry and decreased progenitor cell death, leading to cortical folding (24). Another gene fundamentally involved in NEC self-renewal is Lis1 Lissencephaly 1 (Lis1), with a critical role in the orientation of the mitotic spindle of NECs that enables their



	NECs	aRGCs	bRGCs	IPCs
<b>Morphology</b>	Bipolar	Bipolar	Unipolar	Multipolar
<b>Apical-basal contact</b>	Apical-basal contact	Apical-basal contact	Basal contact	No contact
<b>Period</b>	Pre-neurogenesis	Onset of neurogenesis	Late neurogenesis	Late neurogenesis
<b>Layer of somal location</b>	NE	VZ	SVZ	SVZ
<b>INM</b>	Apical-basal	Apical-basal (within VZ)	No INM	No INM
<b>Presence of tight junctions/ adherens junctions</b>	Tight junctions/ Adherens junctions	Adherens junctions	Adherens junctions	No
<b>Protein expression</b>	Nestin+, Sox2	Nestin+ (early stages), Pax6+, Vim+, GFAP+, GLAST+, BLBP+	Pax6+, Vim+, GFAP+, GLAST+, BLBP+, Eomes+ (primates and carnivores)	Eomes+
<b>Self-renewing capacity</b>	High	High	High (primate and carnivores)/ Low (rodents)	Low

symmetric, amplificative division. Impaired *Lis1* drastically disrupts mitosis, with arrest in metaphase and other proliferative deficiencies, leading to increased apoptosis (25).

Other signaling pathways important for the steady progression of NECs toward aRGC identity include Notch signaling (26). Loss-of-function mutations in signaling components of the Notch pathway stimulate the precocious differentiation of NECs, such as the Notch receptor 1 (*Notch1*) and the recombination signal binding protein for immunoglobulin-kappa J region (*RBPJk*; a Notch transcriptional regulator) (27, 28), as well as the depletion of Notch effectors like Hes family BHLH transcription factors 1, 3, and 5 (*Hes1*, *Hes3*, and *Hes5*) (29) or the C-promoter binding factor 1 (*CBF1*) (30). Similarly, the morphogen fibroblast growth factor 10 (*FGF10*) defines the period of NEC expansion, where its overexpression drives their transition to the RGC fate (31). MicroRNAs (miRNAs) add an additional level of complexity in the transition from NECs to aRGCs, by regulating the translation and cleavage of specific messenger RNAs (mRNAs) during early cortex development (32). For example, the early loss of *let-7* miRNAs in the cortical neuroepithelium of conditional *Dicer1* mutant mouse embryos drives the neuroepithelium to overgrow, losing the adherens junction belt and culminating in the formation of rosettes (33).

#### 4. PROGENITOR CELL AND LINEAGE DIVERSITY

Apical RGCs (aRGCs) bear a strong resemblance to NECs, as mentioned in sect. 3. aRGCs maintain the highly polarized morphology with an apical and a basal process, and undergo INM and mitosis at the apical surface. As the PP begins to form and neurons accumulate, the thickness of the developing cortex will increase and the basal process will concomitantly increase in length (10). However, INM will not occur along the entire length of these processes, but only within a short distance from the apical surface, hence defining the primary germinal layer for the rest of cortical development, where the cell body of aRGCs will remain confined: the ventricular zone (VZ) (34) (FIGURE 2B). Initially, aRGCs divide symmetrically to self-amplify and expand as a pool, but after a brief period they progressively begin dividing asymmetrically to produce one aRGC plus a different daughter cell. In these asymmetric divisions, the mitotic spindle is frequently oblique to the ventricular surface, such that the daughter cell that retains the apical process, and hence the cellular components associated to it such as the primary cilium, remain as the aRGC (35–38). Two additional types of progenitor cells are produced by asymmetric aRGC divisions, depending on the orientation of the cleavage plane, their cell morphology,

and final germinal layer of residence (FIGURE 2B). Basal RGCs (bRGCs) are born from oblique or horizontal aRGC divisions (with respect to the ventricular surface) (16, 35, 39, 40). This leads to the loss of adherens junctions and the delamination from the apical surface, moving the cell body basally from the VZ and forming the secondary cortical germinal layer: subventricular zone (SVZ). bRGCs maintain the long basal process of their mother aRGC but do not undergo INM (40–43). Instead, in primates, they perform mitotic somal translocation (39, 43, 44). The second additional type of progenitor cell produced by aRGCs is the intermediate progenitor cell (IPC) (FIGURE 2B). These are multipolar cells that emerge from oblique or horizontal apical divisions and also delaminate to the SVZ, where they undergo one or multiple neurogenic divisions (45–48). IPCs do not have apical nor basal process but only some short processes sprouting from the cell soma, thus lacking distinct polarity, and do not undergo INM (49). Whereas aRGCs and bRGCs may be self-renewing, and thus maintain their pool of progenitor cells and sustain continued cortex growth, IPCs are mostly neurogenic, with a limited capacity for self-renewal before they terminally divide to produce neurons, even in primates (44, 45, 49) (FIGURE 3).

##### 4.1. Progenitor Cell Classes, Germinal Layers, and Cortex Folding

The relative and absolute abundance of the different types of cortical progenitor cells varies significantly between species according to cortex size, which is related to the different outcome of their divisions. In animals with a smooth cortex, like mouse and rat, the abundance of IPCs vastly predominates over bRGCs, possibly due to a need of producing all cortical neurons in a relatively short gestational period, while also not requiring their tangential dispersion nor folding (45, 46, 48). This is also reflected in the low abundance of bRGCs in mouse, which after being born from aRGCs do not self-amplify but directly enter into self-consuming neurogenic division (35, 36, 50). In contrast, in gyrencephalic species like ferret, macaque, or human, the abundance of founder aRGCs before the onset of neurogenesis is already much greater than in small rodents (as for NECs; see sect. 3) and they have greater capacity for self-amplification. These two features underlie a greater production and accumulation of IPCs and bRGCs, populating a much thicker SVZ compared with mouse (16, 41–43, 51). This enlarged SVZ further splits in two distinct layers: inner and outer SVZ (ISVZ and OSVZ, respectively; FIGURE 2B). Both ISVZ and OSVZ contain bRGCs and IPCs, but while the ISVZ has a high and homogeneous cell density similar to the rodent SVZ, the OSVZ has a low density of cells radially organized in ribbons (16, 41, 51, 52). A key

distinction between ISVZ and OSVZ, due to their different location and structure, is the interaction of their constituent progenitor cells with extrinsic elements. In the developing ferret cerebral cortex, IPCs and bRGCs in ISVZ and OSVZ are exposed to different sets of inputs and external cues, such as axon fibers and migrating interneurons, with the potential of influencing their proliferation and fate (53). The potential interaction between progenitor cell types and external cues is particularly evident and striking in the macaque visual cortex, where geniculostriate and corticogeniculate axon fibers run through the outer fiber layer (OFL) located basally from the OSVZ, and the inner fiber layer (IFL) separating ISVZ from OSVZ (51). At the functional level, *in vitro* studies demonstrate that thalamic axons promote the proliferation of cortical progenitor cells, possibly via secretion of factors stimulating cell division (54).

The specific presence of OSVZ in species with a folded cortex, its large size in highly folded species, and its high content in self-amplificative progenitors at late stages of neurogenesis, sparked the hypothesis that the OSVZ might play important roles in cortical expansion and folding (41–43, 55–58). Indeed, the OSVZ is greatly expanded in primates and is the major source of upper-layer cortical neurons in macaque monkeys (18, 42, 44, 51). Importantly, bRGCs and OSVZ are not a primate-unique feature, but they are also very relevant in nonprimate gyrencephalic species like sheep, cat and ferret, a small carnivore with a folded cortex (42). In ferret, for example, the OSVZ proliferates massively at the end of embryogenesis to nearly double the size of the ISVZ, preceding the formation of cortical folds (16, 42). Comparative studies have revealed that the proportion of cortical progenitor cells found in the OSVZ during embryogenesis correlates with the degree of cortex folding in that species, as observed across rodents, carnivores, ungulates, and primates (42) (for further details, please see sect. 8.2, on cellular mechanisms of cortex folding). This further prompts the notion that OSVZ is key in cortex folding. OSVZ and bRGCs have also been observed in species with a nearly smooth cortex, like the marmoset monkey, indicating that these may be necessary but not sufficient for gyrencephaly to emerge (59–61). However, the abundance of OSVZ progenitors in general, and of bRGCs in particular, is far smaller in the embryonic marmoset cortex than in ferret, sheep, or human, where bRGC abundance is a robust predictor of cortex size and degree of folding (62).

#### 4.2. Specialized Progenitor Morphotypes

The increased size and complexity of the cortical germinal

layers in primates is also accompanied by increased progenitor cell diversity. In addition to the common bRGCs and IPCs, found in variable abundance across mammalian phylogeny, distinct morphotype variants of bRGCs have been described in carnivores and primates (FIGURE 4). bRGCs-both-P display the defining basal process and also an apically directed process (44, 62); bRGC-apical-P display only an apically directed process but not a basal process; and tbRGC transiently display either an apical and/or a basal process (44). In the human cortex, yet additional morphotypes have been observed, namely bRGCs with two basal processes (bRGC-2-basal-P), and bRGCs with two basal processes and one apically directed process (bRGC-apical-2-basal-P) (63). The number of these cellular processes in bRGCs and IPCs seem to improve their capacity for proliferation, potentially by exposing these cells to pro-proliferative extrinsic signals from the developing cortex (64). This correlates well with the fact that the human cortex contains a greater percentage of basal progenitors with two or more processes than ferret, and this more than mouse (63). The multiple classes of bRGCs and IPCs have been observed to transition between each other (44), prompting the possibility that they represent different cell states rather than progenitor cell types.

Cellular morphotypes have also been observed related to aRGCs. Subapical progenitors (SAPs) share morphology with aRGCs but undergo mitosis basally within the VZ, at a distance from the apical surface in contrast to the typical apical divisions of aRGCs. SAPs tend to rapidly self-amplify before giving rise to two neurons by self-consuming symmetric divisions, hence are highly productive neurogenic progenitors. While they are very scarce in the mouse cortex, SAPs are abundant in gyrencephalic species like ferret and sheep (62). Finally, there is one aRGC morphotype only observed in the human cerebral cortex at late stages of development, described as truncated aRGC (taRGC)

(65). This morphotype has an apical process and a basal process that does not reach through the pial surface but prematurely ends (hence truncated) wrapping endothelial cells with the basal end-feet. These progenitor cells substitute the classical aRGCs by gestational week (GW) 17 and by doing this they set a gap between VZ and OSVZ without RGC fibers. This would allow bRGCs to expand, and neurons massively generated in the OSVZ to migrate dispersing tangentially, as they reach their final position in the CP using the basal process of bRGCs (65). This model has been proposed to explain the massive increase in surface area of upper cortical layers (II–IV) compared with lower layers (V and VI) observed in humans, which would contribute to cortex folding (58).

#### 4.3. Distinguishing Progenitor Cell Types

Single-cell RNA sequencing (scRNAseq) is a high-throughput technique to characterize the transcriptomic landscape of thousands of individual cells. This is

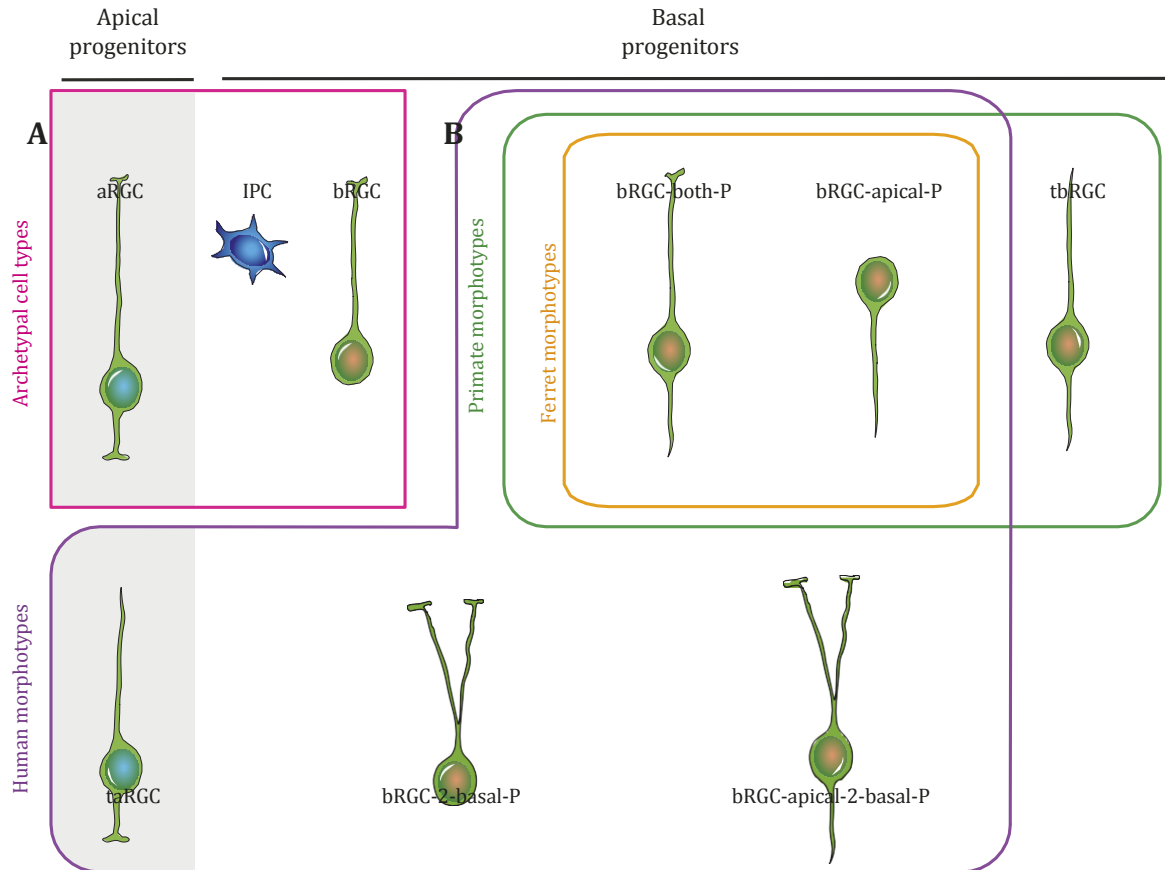


FIGURE 4. Specialized progenitor morphotypes. *A*: archetypal progenitor cell types found in the great majority of mammals, albeit at varying abundance. *B*: specialized morphotypes of apical (gray background) or basal (white background) RGCs found in ferret, primates, and/or human. aRGC, apical radial glia cell; IPC, intermediate progenitor cell; bRGC, basal radial glia cell; bRGC-both-P, basal radial glia cell with a basal process and an apically directed process; bRGC-apical-P, basal radial glia cell with only 1 apically directed process; tbRGC, truncated basal radial glia cell; taRGC, truncated apical radial glia cell; bRGC-2-basal-P, basal radial glia cell with 2 basal processes; bRGC-apical-2-basal-P, basal radial glia cell with 2 basal processes and one apically directed process.

achieved by the encapsulation of individual cells from a suspension into an oily emulsion of gel beads, where the full transcriptome of individual cells is tagged before sequencing, which then can be analyzed quantitatively. The simultaneous transcriptomic profiling of thousands of individual cortical cells by means of scRNAseq is enabling researchers to define their heterogeneity and establish similarity relationships based on transcriptomic signatures (66–68). For example, these studies have enabled discovering developmental similarities and trajectories across apical and basal progenitors of the mouse cerebral cortex (69). The transcriptomic profiles of individual cortical progenitor cells identify consecutive transcriptional waves of neuronal maturation in a dynamic process that runs through the duration of cortical neurogenesis. While transmission of the conserved transcriptomic landscape from aRGCs to their cell lineage is a key point at early development, extrinsic signals seem to modulate the final neuronal cell fate at later stages

(69). Importantly, the disruption of these orderly primed progenitors by the premature expression of a late-wave mRNA accelerates neuronal differentiation and disorganizes cortical layering (70).

scRNAseq studies have demonstrated an important transcriptomic similarity between progenitor cells in the developing mouse and human cortex, with an apparent greater diversity of IPCs in mouse (5 subtypes in mouse vs. 3 in human) and for aRGCs in human (2 subtypes in mouse vs. 3 in human) (71). Interestingly, ferret and human RGCs are more similar than those in mouse, with a greater neuronal commitment in human RGCs (72). This high correlation between ferret and human cortical progenitor cells allows improved modeling in ferret of human disorders of cortical development such as microcephaly, lissencephaly or polymicrogyria (see sect. 10) (73). Sorting of progenitor cells, or microdissection of germinal layers before scRNAseq has allowed increasing the sequencing depth of single cortical progenitor cells, which in turn has led to deciphering an unsuspected diversity of bRGCs in

the fetal human cortex, specifically enriched on a number of genes related to stemness and extracellular matrix (ECM) (72, 74). Renewed efforts using scRNAseq at greater sequencing depth and with improved analytical methods raise the seminal question of how to distinguish cell types from cell states (75).

## 5. MOLECULAR REGULATION OF CORTICAL CELL LINEAGES

In order for the cerebral cortex to expand and then fold, cortical stem and progenitor cells must be first amplified and later their lineages must be finely regulated. In this section, we summarize the current knowledge on the molecular mechanisms regulating the different types of cortical progenitor cells and their different lineage decisions (FIGURE 5).

### 5.1. Apical Radial Glia Cells

As introduced above in sect. 4, aRGCs follow multiple lineage behaviors depending on developmental stage: self-amplification, self-renewal, generation of basal progenitors, neurogenesis, and gliogenesis.

#### 5.1.1. RGC self-amplification.

At early stages of cortical development, aRGCs self-amplify to increase their pool before giving rise to the rest of cortical cell lineages. The Notch pathway is a primary signaling mechanism to promote the transition from NECs to aRGCs (26–30), but it is also key later on, stimulating aRGC proliferation via interaction with other signaling pathways. For example, activation of Janus kinase-signal transducer and activator of transcription (Jak-Stat) pathway through Stat3 phosphorylation regulates the transcription of delta-like 1 (Dll1), a canonical Notch ligand, and boosts cortical aRGC maintenance via a noncell-autonomous mechanism (76). Other factors promoting aRGC expansion include members of the fibroblast growth factor (FGF) family. Blockade of FGF receptors (FGFRs) early in development disrupts Notch signaling and produces the premature differentiation of aRGCs into neurons, leading to their early depletion and a drastic decrease in cortical thickness and surface area (77). Similarly, blockade of FGF2 strongly reduces the pool of progenitor cells, accompanied by a very dramatic decrease in cortical neuron numbers by the end of neurogenesis (78, 79). Accordingly, overexpression of FGF2 or FGF8b lead to the overproliferation and growth of the cerebral cortex, including the formation of folds (80). Similarly, overexpression of FGF8 in the gyrencephalic ferret further increases cortex folding (81).

The self-amplification of aRGCs also involves insulin-like growth factor (IGF) signaling. In the developing cortex, IGF1 activates phosphoinositide 3-kinase/Akt signaling, which sequentially activates cyclin D1/D3/E and represses the cyclin-dependent kinase (Cdk) inhibitor p27KIP1/ p57KIP2, ultimately favoring G<sub>1</sub> progression (82). Similarly, IGF2 in the CSF interacts directly with aRGCs through the apical domain promoting their proliferation (12). Overexpression of the cell-cycle proteins Cdk4 and cyclin D1 in the developing mouse cerebral cortex directly favors cell-cycle progression and progenitor cell self-amplification, which results in megacephaly and increased cortical surface (83). This manipulation has the same effect in the ferret cortex, which when applied to OSVZ progenitors leads to an aberrant increase in cortical folding (84).

The proliferation and self-amplification of cortical progenitor cells is also regulated by the Wnt/b-catenin pathway. b-Catenin is both a key downstream component of Wnt signaling acting as a transcription factor and a structural component of the apical adherens junctions. Conditional disruption of b-catenin in the developing cerebral cortex perturbs INM and causes loss of adherens junctions, resulting in decreased aRGC proliferation, which demonstrates the importance of VZ integrity in this process (85). Retinoic acid is secreted by the meninges surrounding the cerebral cortex and sensed by aRGCs via their basal endfeet, which respond limiting their self-amplification. Genetic loss of meningeal RA causes a massive proliferation and self-amplification of aRGCs at the expense of neurogenesis and IPC production, leading to the aberrant folding of the VZ (86).

The lissencephaly gene *Lis1*, which is essential for NEC proliferation, also regulates mitotic spindle orientation in aRGCs, which leads to the premature reduction of the aRGC progenitor pool and therefore to decreased neuron production and brain size (25). Finally, the proliferation of aRGCs is also modulated by microRNAs, as in the case of NECs. In early cortical development, *miR-9* and *let-7* miRNAs favor aRGC amplification and inhibit neuronal differentiation (32, 87).

#### 5.1.2. RGC self-renewal.

After an initial period of self-amplification, aRGCs begin dividing asymmetrically to self-renew and produce neurons or IPCs, before they proceed with terminally symmetric divisions that produce two neurons (88). The Notch signaling pathway is also involved in this fate decision of aRGCs, through Slit/Robo signaling. Activation of the cell surface receptors Roundabout (Robo) 1 and Robo2 in cortical aRGCs promotes Notch1 activity and expression of the Notch effector *Hes1*, hence promoting aRGC self-renewal and decreased neurogenesis (89).



Similarly, the Ras-mitogen-activated protein kinase (Ras-MAPK) pathway promotes aRGC self-renewal, as demonstrated by loss-of-function manipulations overexpressing the inhibitor Sprouty-related EVH1 domain containing 1 (Spred1) protein, which prevents proliferation and leads to early neuronal differentiation (90).

Another important aspect that regulates aRGCs self-renewal is the preservation of their characteristic apical-basal polarity. aRGCs carry out mitosis only at the apical surface, which is regulated by polarity proteins such as Par3 or Par6, members of the apical Par complex that define cell polarity in dividing cells (91, 92), and its regulator cell division cycle 42 (cdc42) (93). Likewise, glycogen synthase kinase 3 (Gsk3) is indirectly regulated by cdc42 and necessary for proper microtubule dynamics (94). Disruption or downregulation of these proteins impairs RGC polarity and undermines the apical proliferation of cortical progenitors.

### 5.1.3. Generation of basal progenitors.

One of the primary roles of aRGCs is to produce basal progenitors, namely IPCs and bRGCs, so that their neurogenic potential is amplified. The generation of basal progenitors by aRGCs is boosted by Cdk4/cyclinD1, similar to its effects in the self-amplification of aRGCs mentioned above, causing the SVZ to increase in thickness (83). Similarly, attenuation of Notch signaling in mouse favors the production of IPCs from aRGCs (30, 89, 95). Furthermore, the severe reduction of Dll1-Notch signaling levels caused by high Robo signaling drives neurogenesis directly from aRGCs, skipping IPC production altogether. This has been shown to be an evolutionary ancient mechanism to regulate the mode and abundance of cortical neurogenesis, from reptiles to mammals (96). The transcription factor Pax6, best known as a hallmark of RGC identity, also promotes the generation of bRGCs when expressed at high levels (97).

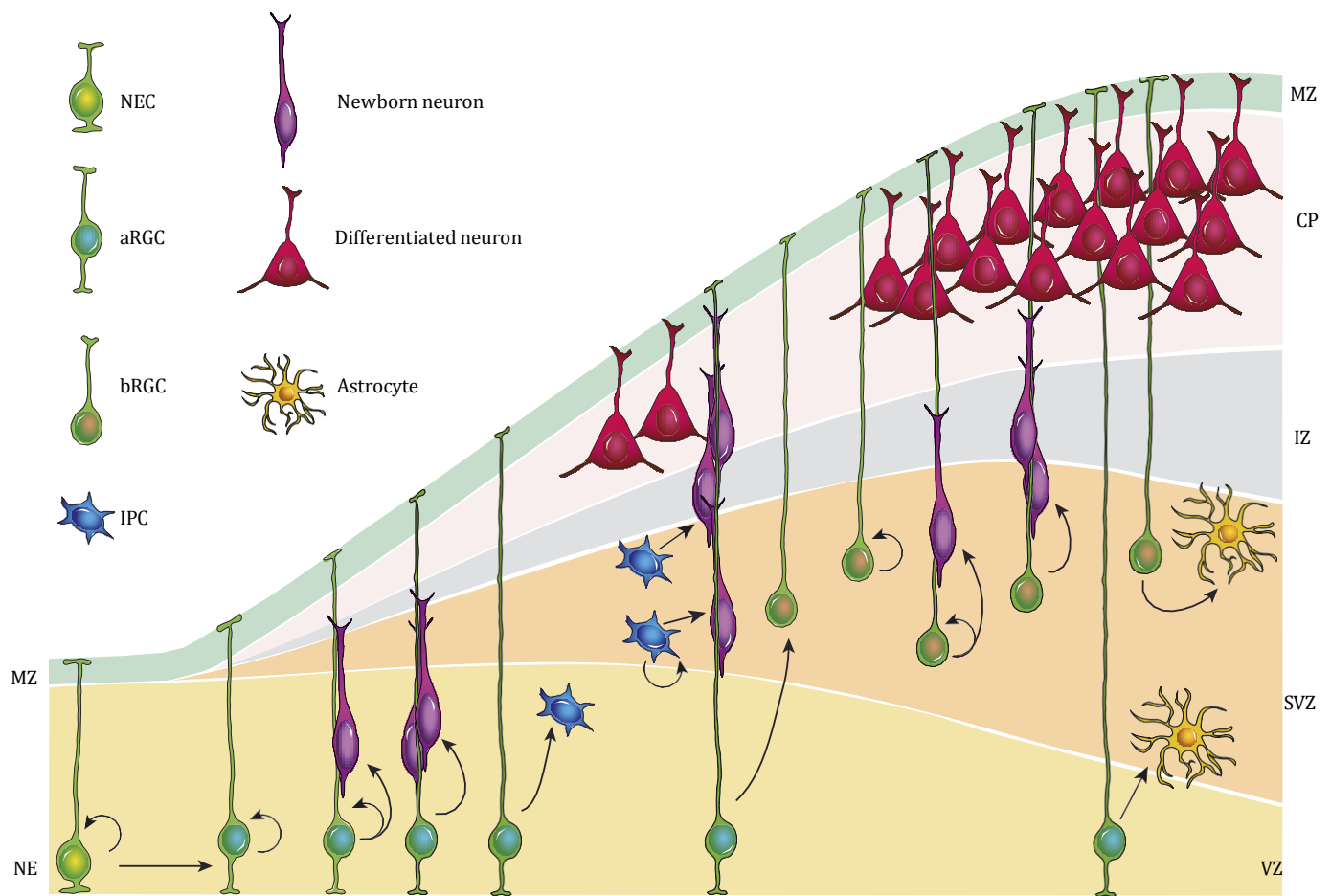
A key step following the birth of basal progenitors at the apical surface is their delamination from VZ to SVZ while avoiding neuronal differentiation. In fact, the loss of proteins that maintain the integrity of the apical adherens junction belt, like pleckstrin homology domain containing A7 (Plekha7), driven by insulinoma-associated protein 1 (Insm1) is sufficient to promote the generation of basal progenitor cells (98). In a similar manner, the centrosomal microtubule organizing protein Akna drives microtubule destabilization at the adherens junctions, followed by cell delamination from VZ and their retention in the SVZ (99). Likewise, leucine zipper tumor suppressor 1 (Lzts1) forces aRGC delamination by retraction of the apical process and quick translocation of the cell soma to basal positions, a process observed in ferret during the formation of bRGCs (100).

The type of basal progenitor produced is also determined by the orientation of the mitotic spindle. The mouse homolog of *Drosophila* Inscuteable (Insc) shifts the mitotic spindle orientation from horizontal to oblique or vertical, favoring the formation of IPCs (101). The formation of bRGCs is favored by the overactivation of Sonic hedgehog (Shh) signaling, as well as by disruption of G protein-signaling modulator 2 (LGN), both of which regulate the orientation of the mitotic spindle in the developing cortex (35, 102).

### 5.1.4. Direct neurogenesis from aRGCs.

The capacity of aRGCs to divide symmetrically and generate neurons is enhanced by several proteins. Neurotrophin3 (NT3) promotes neurogenic mitoses instead of new progenitor cells, which is the opposite effect of FGF signals (see sect. 5.1.1). This is achieved by NT3 signaling upregulating p27KIP1 and decreasing cyclinD2 in aRGCs, which lengthens G<sub>1</sub> and favors cell-cycle exit and neurogenesis (79). On the other hand, Slit/Robo and Notch signaling interact in aRGCs, such that high levels of Robo decrease Dll1 expression and promote expression of Jagged (Jag1/2 a canonical Notch ligand), which forces direct neurogenesis from aRGCs (96). Notch signaling regulates the balance between progenitor self-renewal and neurogenesis by means of lateral inhibition. The bHLH proneural transcription regulators Neurogenin 2 (Neurog2) and Achaete-scute family bHLH transcription factor 1 (Ascl1) drive Dll1 expression, a transmembrane ligand that binds the Notch receptor on neighboring cells. This activates Notch signaling, which triggers a transcriptional program that promotes progenitor self-renewal, including the downregulation of Dll1 expression. Due to the absence of Dll1 ligand expression in this progenitor cell, Notch is not activated in its neighboring cells, which hence unleash the proneural gene program and enter neuronal differentiation (103).

Premature cell-cycle exit and direct neurogenesis from aRGCs is also promoted by the loss of Wnt signaling at early developmental stages, via b-catenin suppression (104) or elimination of the low density lipoprotein receptor-related protein 6 (LPR6) (105). This ultimately translates into a reduced size of the cerebral cortex, as expected, but with no severe layering defects. In contrast, activation of Wnt signaling at later stages of development, either by the Wnt family member secreted factors 3a (Wnt3a) or 7a (Wnt7a), or by b-catenin, also drives neuronal differentiation (106, 107), demonstrating that the fine-tuned regulation of Wnt signaling along development is essential in controlling the lineage and fate of cortical progenitor cells. Activation of bone morphogenetic protein (BMP) signaling during



NECs	aRGCs	bRGCs/IPCs
<p><b>Self-amplification</b></p> <p>Wnt <math>\beta</math>-catenin; LPA; Lis1; absence of miRNA let-7</p>	<p><b>Self-amplification</b></p> <p>Notch signaling pathway; Jak/Stat3; Fgf2/8b; Igf1/2; Cdk4/CyclinD1; Wnt <math>\beta</math>-catenin; Lis1; miRNA miR-9</p>	<p><b>Self-amplification</b></p> <p>Sox9 (Laminin <math>\alpha</math>2-<math>\beta</math>1-<math>\gamma</math>1); Integrin <math>\alpha</math>V-<math>\beta</math>3R; Palmd, Pdgfr; FgfRs; <b>ARHGAP11B; NOTCH2NL; TBC1D3</b></p>
<p><b>Transition to aRGCs</b></p> <p>Notch signaling pathway (Notch1, Rbpjk, Hes1/3/5, Cbf1); Fgf10</p>	<p><b>Self-renewal</b></p> <p>Robo1/2; Ras/Mapk; Par3/6; Cdc42-Gsk3</p>	<p><b>Self-renewal</b></p> <p>Notch; Shh</p>
	<p><b>Neurogenesis</b></p> <p>Nt3; high Robo1/2 and low Dll1; Neurog2/Ascl1; low Wnt (early stages); absence of Lpr6 (early stages); high Wnt3a/7a and <math>\beta</math>-catenin (later stages); RA; Bmp, Ece2</p>	<p><b>Neurogenesis</b></p> <p>Shh; Sox9; Palmd; FgfRs; Pax6</p>
	<p><b>Genesis of basal progenitors (IPCs, bRGCs)</b></p> <p>Cdk4/CyclinD1; Notch signaling attenuation (blockade of Cbf1; low Robo1/2 and high Dll1); Pax6; Insm1 repression of Plekha7; Akna; Lzts1; Insc; Shh; absence of Lgn; <b>absence of Trnp1; ARHGAP11B; TBC1D3</b></p>	<p><b>Gliogenesis</b></p> <p>Sox9</p>
	<p><b>Gliogenesis</b></p> <p>Cntf; absence of Wnt <math>\beta</math>-catenin; Bmp (later stages)</p>	

development also negatively regulates cell-cycle reentry and promotes neuronal differentiation (108). The endothelin-converting enzyme 2 (ECE2) is a newly described neurogenic factor that regulates neurogenesis, apical adhesion, cytoskeletal organization and ECM secretion, altogether leading to the mislocalization of cortical neurons (109).

### 5.1.5. Gliogenesis.

At the end of cortical development neurogenesis declines and is replaced by the generation of glial cells (gliogenesis). Apical RGCs undergo severe morphological changes, growing lamellate processes and losing their apical and basal processes, becoming star shaped (110). At the molecular level, the ciliary neurotrophic factor signals via Jak-Stat3 driving the astrocytic differentiation of cortical aRGCs in mouse (111, 112). Similarly, the loss of b-catenin induces the premature differentiation of aRGCs into astrocytes (85). Similar to Wnt and Notch signaling, BMP signaling exerts very different outputs depending on its temporal and spatial expression in the developing cerebral cortex. While at early stages BMP ligands in the VZ induce neurogenesis, at later stages they facilitate astroglialogenesis and inhibit oligodendroglialogenesis in the SVZ (113).

## 5.2. Basal Progenitors

Similar to aRGCs, basal progenitor cells undergo a variety of lineage decisions (FIGURE 5), which are finely regulated at the molecular level.

### 5.2.1. Neurogenesis.

One of the main roles of basal progenitors is to amplify the number of cortical neurons produced during the neurogenic period, as the main characters of indirect neurogenesis (45, 58, 96, 114). Basal progenitors were initially identified in small rodents as cells expressing the T-box transcription factor *Tbr2* (also known as *Eomes*) and dividing at basal position to produce neurons (45–47) (FIGURE 3). Their greater abundance at late stages of cortex development led to suggest that they are of particular importance to generate late-born neurons, destined to upper cortical layers. However, more detailed analyses showed that they produce neurons to

all layers of the mammalian cerebral cortex (48). Basal progenitors are fundamental in the evolutionary expansion and folding of the cerebral cortex for two main reasons: they are directly implicated in amplifying cortical neuron production, and specifically bRGCs expand the scaffold of radial fibers and sculpt the radial migration of cortical neurons (55, 57, 87, 115–117) (see also sect. 7). Recent studies have identified a number of factors and signaling pathways driving cortical upper-layer neurogenesis from bRGCs, already mentioned above. These include the *Shh* signaling pathway (102, 118), proteins regulating the expression of ECM components (*Sox9*, *Palmd*, and *FGFRs*) (63, 119, 120), and *Pax6* (97).

### 5.2.2. Self-amplification.

In small rodents like mouse, basal progenitors have a very limited self-amplificative capacity, as they mostly undergo neurogenic divisions (45, 46, 49). However, mammals with large brains have a high abundance of basal progenitors with significant self-renewing and self-amplificative activity (40, 42–44). This self-amplification implies following a lineage independent from apical progenitors (namely aRGCs) and thus also the establishment of a basal progenitor niche in the SVZ that promotes cell proliferation. ECM components such as integrins, laminins, collagens, and proteoglycans promote cortical progenitor cell expansion and are differentially enriched in the human ISVZ and OSVZ compared with mouse SVZ (41, 121). This is also the case for the transcription factor *Sox9*, which in fact promotes the expression of ECM proteins, notably laminin- $\alpha$ 2 $\beta$ 1 $\gamma$ 1, followed by increased IPC proliferation and the generation of upper-layer neurons in mouse (119). Similarly, pharmacological activation of the integrin- $\alpha$ V $\beta$ 3 receptor in mouse IPCs promotes their cell-cycle reentry and proliferation (122), while its disruption in ferret drastically reduces bRGC abundance in the OSVZ (41).

*Palmd* (*Palmdelphin*) is a protein enriched in human SVZ that regulates the morphology and number of processes in basal progenitor cells, as shown in an elegant study by Kalebic et al. (63). When overexpressed, *PALMD* prompts basal progenitor mitosis in mouse, ferret and human by means of integrin- $\beta$ 1 signaling, which finally leads to increased number of upper-layer neurons (63). In a similar way, Lui et al. (123) showed that the local

FIGURE 5. Progenitor cell lineages and their molecular regulation. During early stages of cortical development, NECs self-amplify by symmetric divisions, after which they produce apical radial glia cells (aRGCs). These newly formed cells start self-amplifying by symmetric divisions. At the onset of neurogenesis, aRGCs begin to divide asymmetrically to directly produce neurons while self-renewing. They can also generate neurons indirectly via producing IPCs, which are essentially neurogenic in rodents. aRGCs in gyrencephalic species like ferret, primates or human generate large numbers of basal radial glia cells (bRGCs), which in the outer SVZ self-amplify forming an independent pool of progenitors; they can produce vast amounts of neurons. At the end of neurogenesis, aRGCs and bRGCs transform into proper glial cells. All these lineages are strictly regulated by specific molecules and signaling pathways, depicted in the table. Names in red refer to specializations of expanded brains. MZ, marginal zone; VZ, ventricular zone; SVZ, sub-ventricular zone; IZ, intermediate zone; CP, cortical plate; IPC, intermediate progenitor cell; NEC, neuroepithelial cell; NE, neuroepithelium.

expression of platelet-derived growth factor D (PDGFD) and its putative receptor PDGFR- $\beta$ , which is expressed in the developing human but not mouse cortex, increase proliferation and dispersion of RGCs in the SVZ in mouse (123). FGFRs have also been found specifically expressed in bRGCs in the OSVZ but not in IPCs. Inhibition of FGF signaling by FGFR blockade reduces the proliferation of bRGCs in the OSVZ without affecting RGC abundance in ISVZ nor VZ, and this ultimately decreases the thickness of the upper neuronal layers (120).

### 5.2.3. Self-renewal.

The Notch signaling pathway is important for aRGC maintenance as detailed above (sect. 5.1.2). In addition, this pathway is also necessary for the self-renewal of bRGCs in the human OSVZ, where blockade of Notch signaling in cortical slices decreases bRGCs in favor of increasing IPCs and neurons (43). Another pathway bound to bRGC self-renewal is Shh. Overactivation of Shh signaling inhibits differentiation and promotes the proliferation and self-renewal of basal progenitors in the mouse cortex, ultimately inducing cortical folding (102). Shh signaling may also increase proliferation of a particular type of bRGC in ferret, located in prospective gyri during cortical development and characterized by the expression of the Hop homeobox gene (*Hopx*) (118). Disruption of Shh signaling in the developing ferret cortex reduces the size of folds and fissures and the amount of upper-layer neurogenesis. These observations, together with the fact that Shh signaling is more active in the ferret cortex than in mouse, strongly support the significant importance of this mechanism in cortex folding.

### 5.2.4. Gliogenesis.

Basal progenitors, and particularly bRGCs, also generate glial cells in the cerebral developing cortex (110). Early studies in ferret already showed that bRGCs transform into astroglial cells at late developmental stages, and a recent study in macaque reveals that bRGCs in OSVZ, a layer particularly relevant in cortex folding (see sect. 8.2.1), becomes gliogenic at E92, just before the onset of cortex folding at E100–E125 (124). Mouse studies also demonstrate that overexpression of *Sox9* in the embryonic cortex from E13.5 to E15.5 decreases the abundance of IPCs and anticipates the generation of oligodendrocytes (119).

## 6. GENETIC SPECIALIZATIONS TO MAKE BIG BRAINS

In the previous sections, we have carefully described the basic cellular and molecular mechanisms of cortical development, and how the initial number of progenitor

cells, their cellular morphology and laminar distribution, their proliferative capacity, and the length of the neurogenic period determine brain size. Most importantly, comparative studies across mammalian phylogeny have revealed that genes regulating these features of cortical development are expressed at significantly different levels between species, consistent with the involvement of these genes and pathways in regulating cortical size and expansion during evolution (FIGURE 5). TMF-regulated nuclear protein 1 (*Trnp1*) is a DNA-binding protein expressed at high levels in self-renewing aRGCs of the mouse cortex, which gradually decreases as these cells progress toward neurogenesis and self-consumption (125). *Trnp1* operates in several key events during cortical development, influencing aRGC proliferation, mitotic spindle orientation and delamination, and neuronal migration (125). The sequence of *Trnp1* is well conserved among mammals, with an 86% similarity between human-mouse orthologs. However, in contrast to mouse, *Trnp1* is expressed at low levels in the ferret and human cortical germinal layers, particularly in cortical regions that experience significant expansion along development (126). In agreement with these observations, knockdown of *Trnp1* in mouse increases the abundance of IPCs and, particularly, of the otherwise scarce bRGCs. This results in thickening the SVZ and enabling a faster and more divergent radial migration of neurons, which ultimately results in cortical folding (125). This artificial folding of the mouse cortex recapitulates all the major characteristics of natural gyrencephaly (16, 51, 52, 127). Altogether, the spatial and temporal modulation of *Trnp1* expression appears critical in driving cortex folding across mammalian phylogeny (see also sect. 8 on cortex folding, below).

Another gene with fundamental relevance for cortex folding is the hominin-specific *ARHGAP11B* (Rho GTPase-activating protein 11B), specifically enriched in apical and basal RGCs. This gene emerged very recently in the human lineage by partial duplication of *ARHGAP11A* followed by mutation of a splicing site, causing a partial deletion which now encoded for a protein with an entirely new biological function (128). *ARHGAP11B* is a mitochondrial protein that promotes glutaminolysis, a particular type of cellular metabolism that seems important to produce the abundant amount of energy required by highly proliferative cells like the amplifying cortical progenitor cells (129). The artificial expression of *ARHGAP11B* in mouse cortex causes the delamination of aRGCs and the substantial IPC self-amplification, altogether enlarging the SVZ and leading to folding of the otherwise smooth mouse cortex (130). Similarly, expression of *ARHGAP11B* in ferret causes a massive increase of self-renewing bRGCs and lengthening of neurogenic period, significantly increasing the abundance

of upper-layer cortical neurons, all hallmarks of cortical expansion, but without additional folding of the already gyrated ferret cortex (131). Intriguingly, expression of *ARHGAP11B* in the embryonic marmoset cortex (a small primate with a near lissencephalic cortex) not only increases the abundance of OSVZ bRGCs and upper-layer neurons, but it also leads to significant growth in cortex size and folding in vivo (132). Hence, hominin specific *ARHGAP11B* sustains critical hallmarks of cortical expansion during evolution.

Similarly to *ARHGAP11B*, *NOTCH2NL* (Notch homolog 2 NH<sub>2</sub>-terminal-like protein) is a hominid-specific gene generated by genome duplication that translates into novel segregated Notch-like proteins (NOTCH2NLA, B, and C). These proteins strengthen Notch signaling, or block Dll1, in progenitor cells with varying efficiency, leading in both cases to an extensive period of progenitor amplification and a delay in neuronal differentiation (133–135). In patients, duplications in *NOTCH2NL* are linked to megalencephaly (pathological enlargement of brain volume) and autism, while its loss is linked to microcephaly and schizophrenia (134). Finally, the hominid-specific gene *TBC1D3* induces aRGC delamination and bRGC self-amplification when expressed in mouse, likely by reducing *Trnp1* expression, which finally results in cortex folding (136). Taken together, it seems clear that the emergence of these genes during the recent history of human evolution was part of the genetic changes responsible for the dramatic expansion and folding of the human cortex. However, this is not the end of the story, as additional new genes that also evolved in the recent human lineage by gene duplication are likely to also have been relevant in the evolutionary expansion and folding of the human cortex (133, 137).

## 7. RADIAL MIGRATION OF NEURONS

Once neurons are generated in the cortical germinal layers by a variety of mechanisms, as described in the preceding sections, they must travel or migrate in the radial axis from those deep layers to the vicinity of the cortical surface, in the CP, where they coalesce into definitive neuronal layers and begin differentiating their dendritic and axonal arbors (10, 138). This process, called radial migration, requires the existence a scaffold of radial fibers, which provide the necessary substrate and guidance (10, 139). This scaffolding necessary to support the radial migration of cortical neurons is provided by the basal fibers of RGCs and defines the final location of neurons along the cortical surface (15, 139). In mouse, neurons originated from adjacent aRGCs migrate close

to each other and end-up in close vicinity at the CP by the end of migration (140, 141) (FIGURE 6A).

At the onset of neurogenesis, when VZ and CP are close to each other, newborn neurons must travel radially only a short distance, and they do so by translocating their cell soma along their inherited basal process (142, 143). As the cortex gets thicker and the radial distance between VZ and CP increases, migrating neurons display a more complex migration process, based on four stages: 1) first, as neurons exit the VZ they transiently display a bipolar shape; 2) this is followed by a brief phase of multipolar migration within the SVZ and lower intermediate zone (IZ), when neurons acquire a multipolar morphology and move laterally (144); 3) neurons reacquire bipolarity and resume radial migration by locomotion (10, 139, 143); and 4) neurons finish radial migration with a final step of somal translocation as they make contact with the MZ (145, 146). The bipolar shape of neurons during locomotion includes their extension of a leading process that steers the direction of migration and pulls the cell forwards, while retracting a short trailing process (139, 147). The whole process involves a highly dynamic coordination of cell-to-cell adhesion interactions between migrating neurons and the basal fibers of radial glia, a balance between adhesion, de-adhesion, and motility under tight molecular regulation (145, 148–152).

The importance of intercellular adhesion in the neuronal migratory process becomes evident from studies on fibronectin leucine-rich transmembrane protein 1/3 (*Flrt1/3*) cell adhesion molecules. *Flrt1/3* are expressed in radially migrating neurons of the embryonic mouse cortex, and their loss leads to decreased adhesion between migrating neurons and increased radial migration speed toward the CP, where neurons cluster together giving rise to sulci (153–155) (FIGURE 6B). In agreement with these results, endogenous expression of *Flrt1/3* in the developing ferret cortex is low in prospective fissures and high in prospective folds. Importantly, cortical folding caused by the loss of *Flrt1/3* occurs without increases progenitor cell proliferation, indicating that cortex folding involves multiple nonoverlapping developmental mechanisms (156).

## 8. CORTEX FOLDING

Cortex folding is the process occurring during brain development whereby the cortical mantle, a two-dimensional sheet of neural tissue containing all cortical neurons and glial cells, acquires a three-dimensional conformation and a characteristic wrinkled or folded appearance, with rounded crests on the outside and deep valleys on the inside. Cortex folding is exclusive to

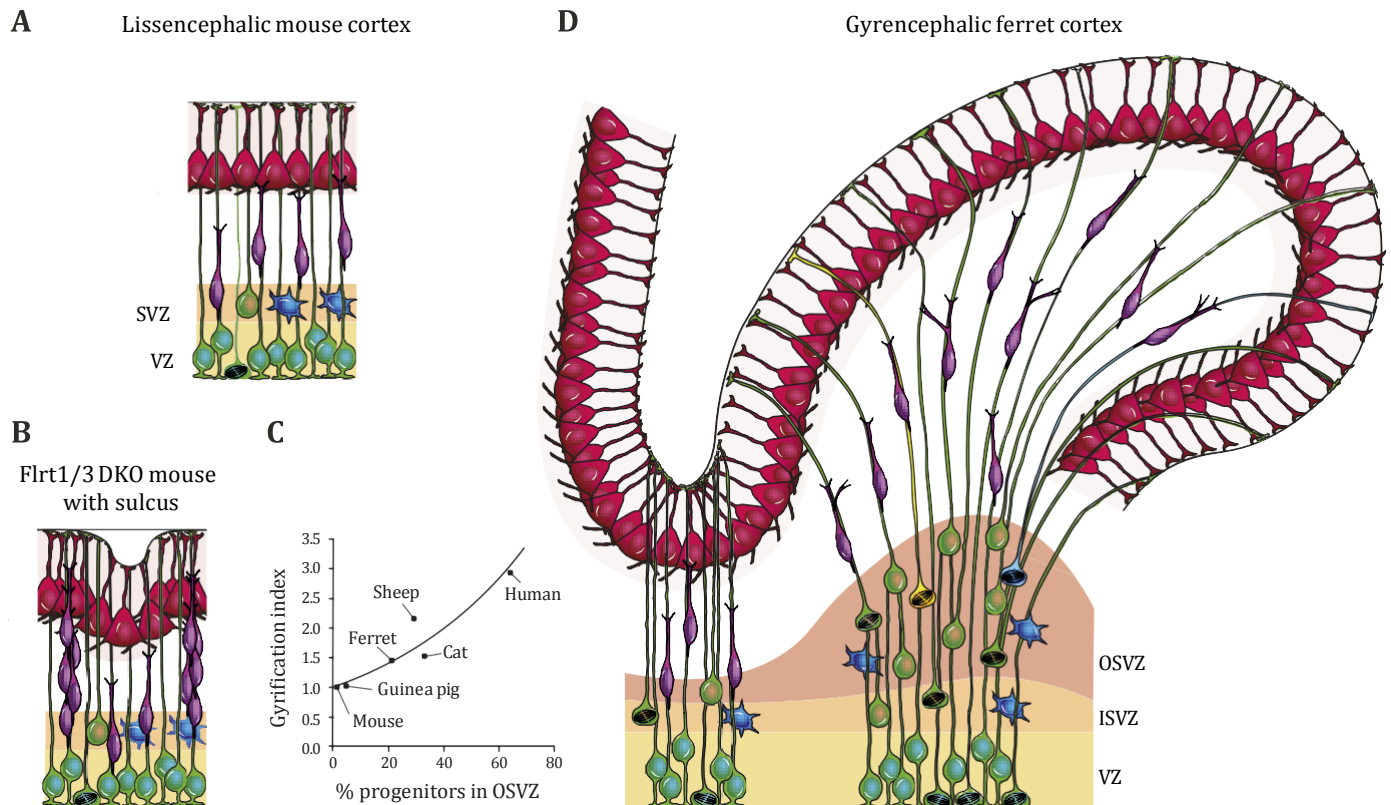


**FIGURE 6.** Cellular mechanisms that regulate cortical folding. *A*: the developing lissencephalic mouse cortex contains a high proportion of apical radial glia cells (aRGCs) (green) and intermediate progenitor cells (IPCs) (blue), while basal radial glia cells (bRGCs) (light green) are scarce. Neurons (purple) generated in the VZ and SVZ radially migrate using the parallel RGC fibers to their final position in the cortical plate (CP). *B*: deletion of *Flrt1/3* adhesion molecules drives the formation of sulci in the mouse cortex, due to a decrease in adhesion between migrating neurons that allows them to move faster toward the CP, where they cluster together. *C*: dot plot of exponential growth of the gyrification index with respect to the relative abundance of progenitor cells in the OSVZ (for gyrencephalic species) and IZ (for lissencephalic species). *D*: in the gyrencephalic ferret, cellular mechanisms become specialized along the cortex in prospective areas of gyri or sulci. In sulci there is a smaller proportion of bRGCs than in gyri, with thinner ISVZ and OSVZ. In sulci, the scaffold of radial glia fibers is parallel, while in gyri it acquires a fan-like organization due to the abundant presence of bRGC processes. As a result, radially migrating neurons follow divergent trajectories and end up in very distant positions along the CP. Migrating neurons in gyri elaborate branches in their leading process, which allows them to switch between radial fibers and disperse tangentially. In gyri, cell proliferation (mitotic figures) is greater compared with sulci, which in turn is greater than in the mouse cortex. VZ, ventricular zone; SVZ, subventricular zone; ISVZ, inner subventricular zone; OSVZ, outer subventricular zone; DKO, double knockout.

mammals and typical of species with large brains. Species with a folded cortex are called gyrencephalic (folded brain) and include elephants, dolphins, whales, cattle, dogs, cats, and particularly old-world primates, including humans. In contrast, small mammals typically have a small and smooth cortex, hence called lissencephalic (smooth brain), including rabbits, rats, and mice. Small primates, typically new-world monkeys, usually are nearly lissencephalic, displaying only one or two main fissures. There are a few exceptions to this general rule, and for a number of species with intermediate brain sizes the correlation between size and folding does not fully apply.

Folding of the cerebral cortex has fascinated naturalists and scientists for centuries, and yet only recently we have begun to see some light on the mechanisms that underlie and lead to cortex folding. The mature mammalian cerebral cortex is composed of six main neuronal

layers on the outside (gray matter), plus an underlying white matter, a thick layer of outgoing and incoming myelinated axonal fibers that connect the overlying neurons with the rest of the brain. In lissencephalic species, gray and white matter are smooth and have a relatively constant thickness along the entire cortex. In contrast, in the cortex of gyrencephalic species the six neuronal layers of the gray matter bend in each fold and fissure, changing their thickness from maximal in the gyral crowns to minimal in the sulcal fundi. The white matter, on the other hand, is only folded in its outer surface, limiting with the gray matter, while it is smooth in its inner surface, limiting with the telencephalic ventricle. These detailed characteristics distinguish true, bona fide cortex folding from pseudofolding, as in some experimental or animal models, or pathological cal situations, where folding involves either only part of the gray matter (subset of neuronal layers), the

entire cortical thickness including white matter, or a largely undifferentiated cortex (23, 86).

Cortical folding serves at least two main purposes: 1) to compact a big cerebral cortex with a massively enlarged surface area into a reduced cranial volume; 2) to bring into proximity cortical areas that have strong functional links, thus minimizing the distance between neurons and optimizing neural network efficiency (157). Indeed, neurons on either side of a gyrus have a strong bias to connect with each other, whereas the connectivity between neurons of opposite sides of a sulcus is biasedly weak (158). The notion that cortex folding optimizes brain function is consistent with clinical observations from human patients, where cortical malformations are linked to severe learning and cognitive disabilities and frequently drug-resistant epilepsy (see sect. 10). Remarkably, however, the specific physiological role that normal folding plays in cortex function remains completely unknown.

Cerebral cortex folding takes place during late stages of brain development and it involves the combined action of a complex series of molecular, cellular, and mechanical events, which we are just beginning to identify. Our understanding of this process is still very immature and incomplete, but some key aspects have been elucidated.

### 8.1. Physical Forces

Cortex folding fundamentally implies the mechanical buckling of neural tissue, so understanding this process involves elucidating the physical forces involved, their nature, origin, and mode of action.

#### 8.1.1. Confinement pressure.

Intuitively, it might seem that cortex folding is simply a question of packing a disproportionately enlarged flat tissue into a confined cranial space: the cortex grows in surface area more than the cranium can handle and so pressure causes it to fold onto itself as it develops. This was one of the first hypotheses proposed to explain cortex folding, but it was refuted by experimental testing, which demonstrated that alleviating cranial pressure (or reducing brain volume) during development does not preclude cortex folding (159). On the contrary, development of the cranial cavity appears to be strongly influenced by brain growth. In certain human pathologies like hydrocephalus, an abnormally high internal pressure of the cerebrospinal fluid drives the enlargement of the brain, and this is accompanied by a significant enlargement of the endocranial volume, not by further cortex folding (160). Thus folding of the cerebral cortex is

developmentally programmed and independent from cranial constraints.

#### 8.1.2. Pulling tension.

The basal process of radial glia cells, and the long axons of cortical projection neurons, are thin cellular extensions with viscoelastic properties subject to tension. The pulling force of this tension may impose mechanical deformation on the soft developing cortical tissue and hence lead to the formation of folds (161, 162). Some cortical areas are more profusely interconnected than others (157, 158), so a greater axonal tension in areas highly connected may pull them together forming a gyrus, whereas poorly connected areas occupy the opposite banks of fissures. While simple, attractive, and convincing, the axon tension hypothesis has been proven wrong by experimental testing in ferret brain slices (163). If an elastic cable is under tension, cutting the cable causes its retraction, and the amount of retraction is proportional to the tension sustained. According to the axonal tension model, cutting the white matter parallel to the banks of a gyrus (across the interconnecting axons) should cause significant axonal retraction, whereas cutting it perpendicular should not. However, this very simple experiment demonstrated that in fact, there is axonal tension in the developing cortex, but it is not within gyri pulling them together (163). The axonal tension hypothesis (162) has been recently reviewed and updated, incorporating our increasing knowledge on the complexity of cellular components and events in the developing cortex (see sect. 2), including new progenitor cell types, cellular interactions, and the influence of the extracellular matrix (161).

#### 8.1.3. Tissue compression due to differential tangential growth.

An alternative view to the tension hypothesis takes into consideration that cortical gray and white matter grow tangentially at different speeds, and that soft tissues growing nonuniformly are under mechanical instability. Mathematical models of cortex growth and folding show that the compressive mechanical forces generated in such a system suffice to generate folds and fissures (164, 165). These conclusions are supported by experimental testing using hydrogels, where folding emerges spontaneously upon expansion of a compound hydrogel with two layers of distinct viscoelasticity and expansion rate (166, 167). Importantly, differential tangential growth explains many features of cortex folding, including folding wavelength, which is determined by cortical thickness, relative stiffness differences, initial shape of cortical surface, and growth rate of cortex relative to subcortical layers (168, 169).

Differences in tissue stiffness along and across cortical layers may have multiple causes, among which the extracellular matrix (ECM) appears to be particularly relevant. Specific sets of ECM components are expressed at very different levels between layers of the developing cortex, and between prospective gyrus and sulcus (121, 126). Slice cultures of fetal human cortex treated with a cocktail of ECM components acquire stiffness heterogeneity along the cortical plate, concomitant with the formation of folds *in vitro* (170, 171). In parallel to determinants of tissue stiffness, neuronal differentiation and maturation may provide a primary mechanism of tangential cortical growth, as this is coincident in developmental time with cortical folding (164, 169, 172–174). An additional mechanism that seems to be key for cortical expansion is the intercalation of neurons within the cortical plate at late stages of development (55, 175). This contributes dramatically to the differential tangential growth of the cortex and to the generation of tissue compression forces, and thus it is likely to contribute significantly in favoring cortex folding. As we will see in sect. 8.2, neuron intercalation is related to modifications in radial neuronal migration found specifically in gyrencephalic species.

## 8.2. Cellular Mechanisms

Folding takes place at late stages of cortical development, well after neurogenesis and neuron migration are over (169, 176, 177). Therefore, these early events do not drive tissue buckling directly, but they set the stage necessary for cortical expansion and folding.

### 8.2.1. Progenitor proliferation and neurogenesis.

As mentioned above, cortex folding occurs in species with large brains, linked to a high abundance of cortical neurons and, thus, to high rates of neurogenesis. In agreement with this notion, comparison of germinal layers between gyrencephalic and lissencephalic species evidences that the abundance of basal progenitor cells (source of most cortical neurons) is massively larger in the former than the latter, which translates in a much thicker SVZ. This thickening is accompanied by the distinction of two sublayers in the SVZ: inner (ISVZ) and outer (OSVZ). Indeed, although the OSVZ was first identified in primates (51) it is present in gyrencephalic species across mammalian phylogeny, from primates to rodents, carnivores, and ungulates, supporting a conserved role in cortex folding, and/or in cortex size (42, 61, 178). The percentage of cortical progenitor cells found in the OSVZ at a given developmental stage varies significantly between species, and it is strongly correlated with their gyrification index (GI) (42) (FIGURE

6C). This index measures the degree of cortex folding independent from absolute size (179), so a positive correlation with OSVZ progenitor abundance strongly supports the notion that this layer is relevant for the eventual formation of folds. Seen in more detail, the density of cell proliferation in the OSVZ is not homogeneous along the developing cortex, but it may be several-fold greater in regions that will undergo surface area expansion and folding compared with those becoming a sulcus. This has been shown in ferret, cat, and human embryos (42), supporting even further the direct involvement of the OSVZ in setting the stage for cortex folding. Experimental support for this notion first came from studies in ferret, where genetic manipulations promoting OSVZ proliferation led to increased cortex folding and GI (84), whereas folding was impaired upon reducing or blocking OSVZ proliferation (42, 180, 181). Remarkably, even in the smooth mouse cortex, experimental enhancement of proliferation specifically in the SVZ is also sufficient to induce folding (80, 130).

However, cortex folding involves more than just generating a large number of neurons (55), as shown by clinical evidence. For example, microcephaly is malformation of brain development defined by a significant reduction in the size of the brain and the cerebral cortex, which is namely due to a defective generation of neurons (as in the Zika virus outburst) (182, 183). However, microcephalic patients may display folds with remarkably normal appearance, demonstrating that cortex folding does not depend on producing a critical number of neurons. Similarly, lissencephaly is characterized by a significant (sometimes, complete) loss or simplification of cortical folds, and yet some patients display normal brain size with an approximately normal number of cortical neurons. This shows that generating a normal number of cortical neurons is not strictly necessary, nor sufficient, to drive cortex folding (55). The key to this question lies in the specific composition of basal progenitor cell types. In lissencephalic species, like mouse, the vast majority of basal progenitors in SVZ are IPCs, cells with no specific polarity and multiple short processes. In contrast, in the ISVZ and OSVZ of gyrencephalic species bRGCs are very abundant, cells with very strong apical-basal polarity and morphologically similar to apical RGCs, usually with one long basal process extended radially all the way to the pial surface (16, 41–44, 50). Whereas both IPCs and bRGCs produce neurons (40–43, 50), only bRGCs, via their basal process, serve the additional function of acting as substrate and guide for the radial migration of immature neurons, from the neurogenic layers to the cortical surface. Due to their strategic location in ISVZ/OSVZ, the basal process of bRGCs intercalates within the scaffold of basal fibers of aRGCs (radial fiber scaffold), modifying the parallel arrangement



of this scaffold and transforming it into a fanned array (FIGURE 6D) (55, 57, 60). Due to this modification, cortical neurons migrating radially along the divergent radial glia fiber scaffold become progressively separated from each other as they approach the brain's surface, thus expanding tangentially the cortical surface area, which sets the stage for the formation of folds (FIGURE 6D)

(87). Indeed, tangential or horizontal dispersion of neuronal clones is a landmark feature of large and highly folded brains (184, 185). Importantly, this model of radial glia scaffold divergence also explains how during embryonic development the pial surface becomes much larger than the ventricular surface in gyrencephalic species but not in lissencephalic species.

Multiple lines of evidence support the model and role of radial glia fiber divergence on cortex folding. First, this model predicts that the greater abundance of bRGCs in the developing cortex, the more tangential dispersion of cortical neurons, the larger cortical surface area, and the more folding. The relative abundance of bRGCs among cortical progenitors in each species correlates with their degree of cortex folding (44, 60–62), fully supporting the above prediction and that this type of basal progenitor cell is central for the development of gyrencephaly (56). This notion is further supported by experimental manipulations of the folded ferret cortex, where specifically reducing the abundance of bRGCs leads to smaller cortical surface area and fold size (42). Conversely, genetic manipulations of the embryonic smooth mouse cortex that increase the abundance of bRGCs (otherwise very scarce) drive the formation of cortical folds, as, for example, with the loss-of-function of the nuclear protein *Trnp1*, or the overactivation of *Shh* signaling (102, 125). Second, the model predicts that if the abundance of bRGCs is not homogeneous along the mantle of the developing cerebral cortex, regions with greater bRGC abundance should have greater radial fiber divergence and eventually expand more in surface area and fold more than regions with fewer bRGCs. Measurements of the density and divergence of the radial fiber scaffold along the developing cortex of ferrets confirm this prediction (42).

If the abundance of bRGCs and the size of the OSVZ are critical in determining the degree of cortex folding, how are they established during development? Similar to the spatial differences in bRGC abundance along the developing cortex, there are temporal differences in bRGC generation. As mentioned above, basal progenitors are initially generated by aRGCs and later they may self-amplify, especially in gyrencephalic species (see sect. 5.2.2) (40, 43, 44). However, a study in ferrets discovered that bRGCs populating the OSVZ are produced by aRGCs only during a very brief period of time during embryonic development, neither before nor after (40).

During this short time window, or critical period, a large proportion of aRGCs undergo self-consuming mitotic divisions to produce massive amounts of bRGCs that are destined to initiate (seed) the OSVZ. After this period, aRGCs restore their self-renewal capacity and switch to producing bRGCs at a much lower pace, which from then on are destined exclusively to the ISVZ, not to OSVZ anymore. As for the OSVZ, the number of founder bRGCs produced during the critical period will increase exclusively by self-amplification (FIGURE 5). Therefore, the size of the OSVZ and the abundance of its bRGCs, which are key factors in cortex folding, depend on the dynamics of this critical period and the posterior rate of self-amplification of bRGCs. The longer the critical period, the more founder bRGCs will be generated to seed the OSVZ (but also the fewer aRGCs left to continue with VZ and ISVZ development). The earlier in development the critical period occurs, the more time founder bRGCs will have to self-amplify and grow a large OSVZ before neurogenesis ends and cortex buckling takes place. Variations in these parameters are expected to occur across species with different degree of cortex folding (87, 156).

### 8.2.2. Neuronal migration.

According to the radial divergence model (see sect. 8.2.1), cortex folding depends on the abundant presence of bRGCs in a thick and highly proliferative OSVZ (16, 42, 87). In this model, the role of bRGCs is to provide additional radial fibers for the migration of cortical neurons, and to create divergence in the radial fiber scaffold to disperse laterally these radially migrating neurons, thus expanding the cortical surface area (FIGURE 6D). In radial glia-guided neuronal migration, neurons are intimately associated and closely apposed to one radial glia fiber via cell surface adhesion molecules (10, 139, 149) and move toward the cortical surface by crawling along this fiber (141, 186). In order for migrating neurons to disperse laterally in the divergent radial fiber scaffold, they must switch between radial fibers as they migrate. This is achieved thanks to a cellular specialization of migrating neurons particular to folded brains: branching of their leading process. Analyses of the detailed morphology of migrating cortical neurons revealed that their leading process is not simple and unbranched, as traditionally viewed (10), but it runs through cycles of making lateral branches (187). In smooth cortices like in mouse, radially migrating neurons display only one branch that is frequently parallel to the main process. However, in folded cortices like in ferret, these neurons display up to three branches, and frequently form at wide angles from the main process. On the one hand, these side branches allow migrating neurons to reach out to neighbor radial

fibers without losing attachment to their parent fiber. On the other hand, by selecting one of the side branches and retracting all the others, migrating neurons steer their trajectory of migration, including switching between radial fibers (187). Similar migration behaviors have been observed in the developing cortex of macaque monkeys (188), supporting that this is a common mechanism for the development of folded cortices.

Neurons undergoing radial migration sustain cell contact-dependent attractive and repulsive forces, both with radial glia fibers and with other migrating neurons. The dynamic balance between attraction and repulsion during neuronal migration is of key importance during cortical development, and it also plays a central role in cortex folding. A family of cell adhesion proteins called Flrt (Flrt1-3) expressed by subpopulations of migrating cortical neurons are necessary for the intercellular adhesion between them. In mouse, these proteins are expressed at high levels, and the absence of Flrt1 and Flrt3 in mutants causes a loss of intercellular adhesion, leading to an increase in migration speed and, ultimately, to the formation of cortical fissures (153) (FIGURE 6B) (see also sect. 7 on radial migration). Notably, *FLRT1/3* expression is low in the embryonic human cortex and in future sulcus areas of ferrets, supporting that intercellular adhesion is another key regulator of cortical folding across species, independent from progenitor proliferation and neurogenesis.

### 8.3. Folding Patterns

Folds and fissures are hierarchically organized, similar to branches in a tree. Primary folds form the earliest during development, where primary fissures are the deepest in the cortex, forming always at the same, highly conserved positions between individuals (189–191). Some species like ferret and cat only develop primary folds, thus exhibiting a relatively simple and much conserved pattern of cortical folding (159). Secondary folds form next in between primary fissures and are less conserved, more variable between individuals. Folds of even higher order form at subsequent epochs and exhibit the greatest interindividual variability. The fact that primary folds are so well conserved within a species reflects that cortex folding is a process under strong genetic regulation. Although the overall pattern of cortex folding is highly variable between individuals in species with large and profoundly convoluted brains, like humans, monozygotic twins have significantly greater similarity between them than with people not genetically related (192), again indicating that these patterns have a strong genetic basis. Finally, species belonging to the same phylogenetic clade (i.e., carnivores) share the same

basic patterns of cortex folding (even secondary folds) (55), supporting the idea that not only cortex folding is genetically regulated but that the genetic and developmental programs defining the folding patterns were strongly conserved during evolution.

#### 8.3.1. Regional variations in progenitor cell proliferation.

Detailed analyses of cortical development in ferret, cat, and human show that the patterns of primary folding and fissuring are linked to regional variations in progenitor cell proliferation. Regions with high proliferation rates undergo significant expansion and develop to become primary folds (or lobes, in human), whereas regions with low proliferation expand much less and develop to become fissures (42, 177). This correlation has been observed in all three germinal layers (VZ, ISVZ, and OSVZ) but is particularly striking in the OSVZ, where differences in proliferation between regions are greater (16, 42) (FIGURE 6D). Cell proliferation and cell cycle are processes under very tight genetic regulation, consistent with these being at the core of the genetic regulation of cortex folding.

#### 8.3.2. Genetic protomaps of cortex folding.

Classical genetic screening studies in neurological patients have identified a long list of genes whose mutation alters the development of cortical folds (160). However, this list is neither complete nor does it illuminate the mechanisms defining the pattern of cortical folds. A key experiment to identify genetic programs involved in the patterning of cortical folds was performed in developing ferret kits using next generation sequencing (RNAseq) (126). The underlying idea is that genes controlling the patterned formation of cortical folds must have different levels of activity between areas developing as folds from those developing as fissures, and thus they may be expressed at different levels between these regions. The experiment also took advantage of the fact that the pattern of cortex folding in ferrets is perfectly conserved, such that regions eventually giving rise to folds or fissures are clearly identifiable before folding takes place. Hence, the individual cortical germinal layers of newborn ferrets (VZ, ISVZ, and OSVZ) were microdissected out of living brain slices, while distinguishing the area that gives rise to the splenial gyrus (the most prominent gyrus in ferret) from that giving rise to the adjacent lateral sulcus. Thousands of genes were found differentially expressed between the prospective gyrus and sulcus (>2-fold), particularly in OSVZ, in agreement with this layer being key in cortex folding and with these genes being relevant in the process

(126). As predicted, the genes found differentially expressed are known to be important in regulating progenitor cell proliferation, cortical patterning, neurogenesis, and neuron differentiation. In further support of the main hypothesis, differentially expressed genes included >80% of genes mutated in human cortical malformations. Some of these genes were selected for analysis of their expression pattern in tissue by in situ hybridization, revealing an expression in stripes, where segments of germinal layers with high gene expression levels alternate with segments of low levels. Strikingly, similar gene expression patterns also occur in the embryonic human cortex, but not in mouse, consistent with this being linked to cortex folding (126). Most importantly, the alignment of gene expression stripes across the developing ferret

cortical surface area outlines a map of expression levels that strongly correlates with the distribution map of prospective folds and fissures, thus defining a genetic proto-map of cortex folding (FIGURE 7) (193).

The notion of a cortical proto-map has been under debate for decades in the context of the definition of functional cortical areas (reviewed in Refs. 194–196). Whereas this controversy may not be fully settled, the notion that a genetic proto-map of cortex folding exists has not been challenged so far. The existence of similar stripes or blocks of gene expression in the developing cerebral cortex of human fetuses is particularly revealing, especially for genes linked to cortical malformations. Most frequently, human malformations of cortical development do not affect the entire cortex but only one

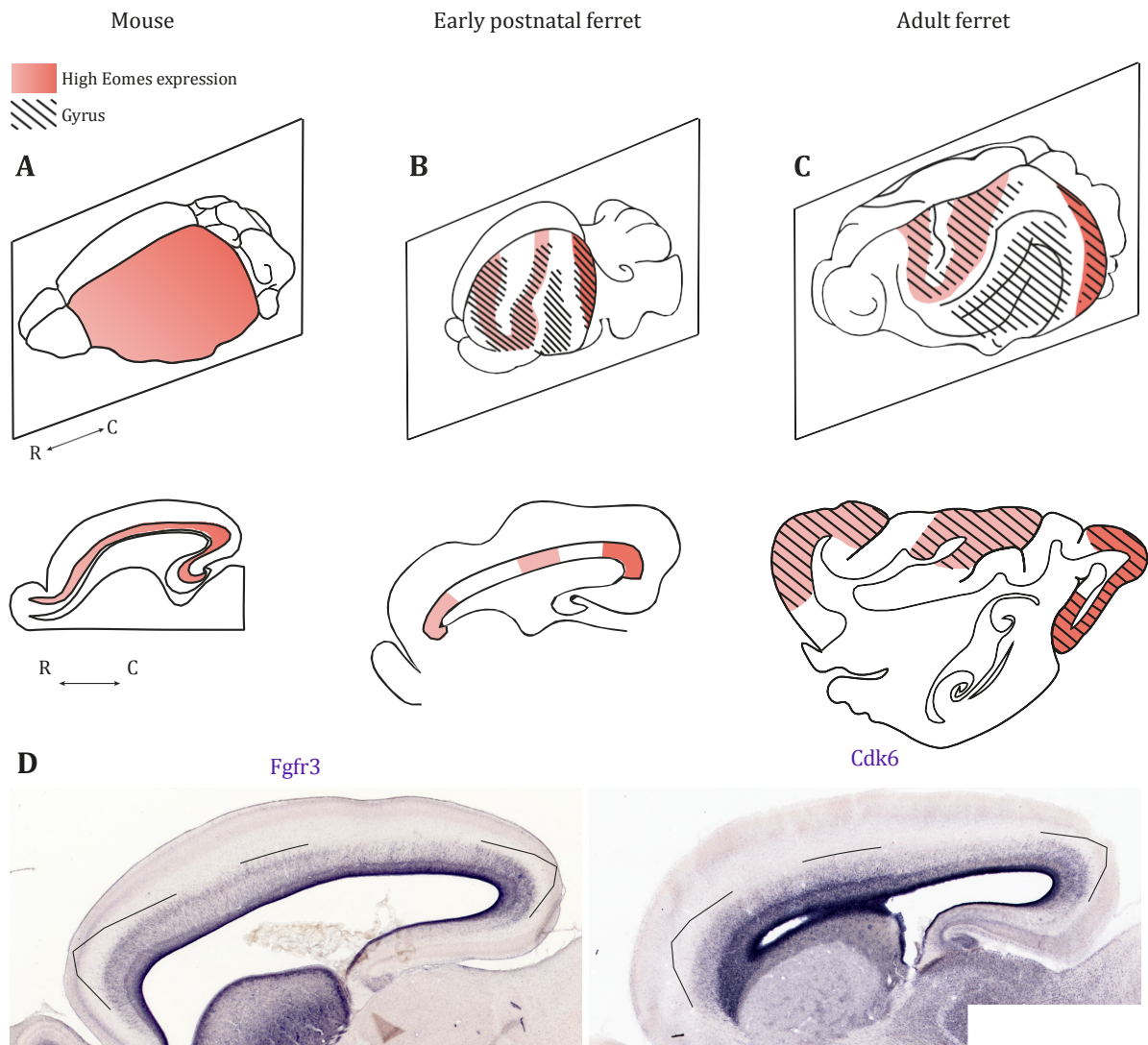


FIGURE 7. Differential pattern of expression of protomap genes along cortical germinal layers in mouse and ferret. *A*: schematic of a sagittal section through the mouse brain where *Eomes* mRNA displays a rostral-caudal gradient. *B*: in the early postnatal ferret, *Eomes* mRNA displays a modular or block-wise pattern, where regions of high expression correspond with prospective gyri (striped pattern), as shown in the adult cortex (*C*). *D*: in situ hybridization stains of the newborn ferret cortex revealing the expression pattern of *Fgfr3* and *Cdk6* mRNA, with alternating modules of low and high (lines) expression levels along the outer subventricular zone. R, rostral; C, caudal.

region, even if the genetic mutation is germline (affecting all brain cells). In fact, specific malformations like nodular heterotopia or polymicrogyria affect only small portions of the cortex or may even alternate between normal and affected regions (160). The occurrence of these local phenotypes from germline mutations (global) has remained a mystery for decades, but it may be explained by the expression of the linked genes following a protomap pattern.

Functional validation of the genetic protomap of cortex folding came from experimental manipulations. One of the genes differentially expressed in ferret VZ (low levels in prospective gyrus) encodes for the nuclear protein *Trnp1*, expressed homogeneously and at high levels along the mouse cortical VZ. Local loss of *Trnp1* expression in the embryonic mouse cortex by in utero electroporation led to a high production of bRGCs and the formation of folds in the otherwise smooth cortex (125). Conversely, overexpression of *Trnp1* in ferret embryos led to reduced genesis of bRGCs (40). The two folding protomap genes *Flrt1* and *Flrt3* (low levels in prospective sulcus) encode for cell adhesion proteins and are expressed homogeneously in a salt-and-pepper fashion along the embryonic mouse cortex. Double mutant mouse embryos, missing both *Flrt1/3*, develop conspicuous cortical fissures (153). Other protomap genes have been tested in ferrets, such as PALMD and FGFR, for example, both of which have differentially high expression in OSVZ of prospective gyrus and promote basal progenitor proliferation and cortical folding (63, 120).

## 9. EVOLUTION OF CORTICAL FOLDING

### 9.1. Phylogenetic Origin of Cortex Folding

The traditional, naïve view of mammalian brain evolution, and cortex evolution in particular, is that the stem ancestor to all mammals had a small brain with a smooth cortex and that this progressively increased in size, folding, and complexity until the modern human configuration. However, evolutionary biology tells a different story. Close attention to the latest revisions of the mammalian phylogenetic tree (based on genetic similarity), combined with the morphological brain characteristics of species, provides irrefutable evidence that cortex folding is a widespread phenomenon across mammalian phylogeny (FIGURE 8) (198). Although frequently considered a primate trait, cortex folding occurs in all major clades of placental mammals, including primates, carnivores, ungulates, afrotherids (elephant), and even rodents (capybara) and xenarthra (anteater, sloth) (<http://neurosciencelibrary.org>). Phylogenetically interspersed in between gyrencephalic species, we also find

numerous examples of lissencephalic species (FIGURE 8), posing the question of whether gyrencephaly was the original and default state, or it was lissencephaly. A parsimonious view of the extraordinary complexity of molecular, cellular, and mechanical factors involved in cortex folding suggests the former. This is supported by studies of cerebral size and neocortical folding in old- and new-world primates using phylogenetic comparative methods, which conclude that the common ancestor of primates may have had a folded cerebrum similar to that of a small lemur (60, 199) (FIGURE 8). At a more global level, and considering the conclusions from primate studies, the most parsimonious explanation for the widespread occurrence of cortex folding across placental mammals is that their common ancestor was gyrencephalic, at least to some degree. In support of this view, a polyphenomic character analysis of fossil and living species suggested that the ancestor to placental mammals resembled a large, long-tailed rodent with a mildly folded cortex (200). Even more remarkable is the observation that cortex folding occurs also in marsupials (gray kangaroo, wallaby, wombat) and even in a monotreme species (equidna) (FIGURE 8). Being these the most ancient mammalian clades, which diverged from placentals more than 160 million years ago (201), it seems likely that the cerebral cortex of an early mammalian ancestor was already folded (202).

### 9.2. Divergences in the Evolution of Cortex Folding

Cortex folding is widespread across mammalian phylogeny, with significant similarities between species and clades. For example, a study across 34 primate species, including new-world and old-world monkeys, revealed that the wavelength of cortical folds (that is, the periodicity or distance between adjacent crests) is extremely constant in species with relatively large brains, despite a 20-fold variation in their cerebral volume (199). Another constant across species, particularly within clades, is the proportion between brain weight and the degree of cortical folding, measured as GI (203–205). Not surprisingly, bigger brains have higher GIs. However, cetaceans (dolphins, whales) display a significant deviation from this norm. Cetaceans not only have the highest GIs among mammals (the most convoluted cortical folding), but their GI is also disproportionate to the size of their brains, having the highest GI-brain weight ratios among mammals by very far (204). The reasons behind the extreme cortical folding in cetaceans remains unclear, but it may be related to their particular cytoarchitecture. The cetacean cortex is the thinnest of all mammals, it has fewer neurons and lower cell densities than primates with similar brain size, and it lacks layer IV, all of which may

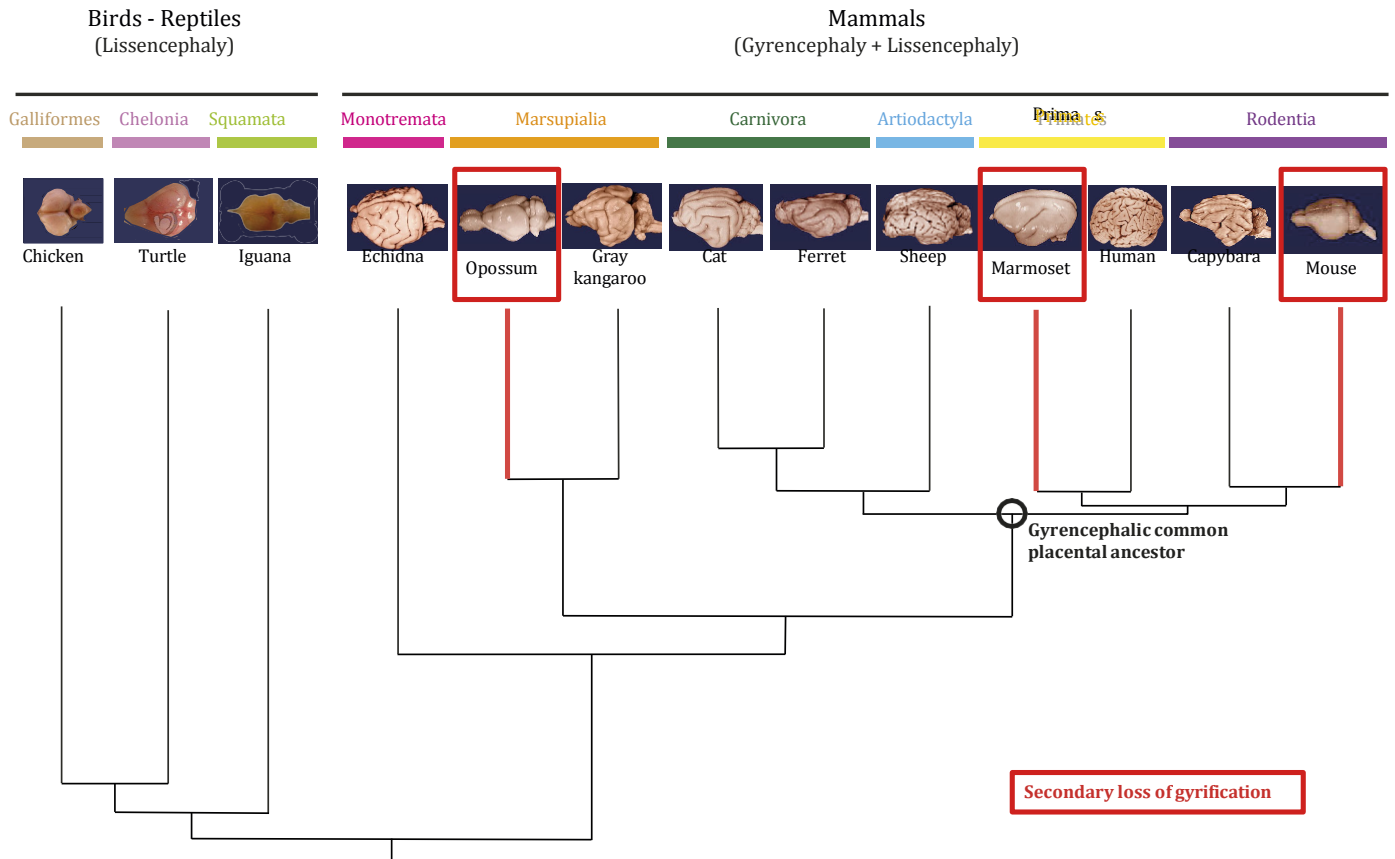


FIGURE 8. Cortical folding across vertebrate phylogeny. Simplified phylogenetic tree showing the brains of a selection of species belonging to major orders of amniotes. Red lines indicate lissencephalic species found within an order containing gyrencephalic species. The ancestor common to all placental mammals has been predicted to be gyrencephalic (see text), so lissencephaly is thought to be an adaptive secondary loss of gyrification. Images for chicken and iguana are from [www.global.anato.cl](http://www.global.anato.cl) (code: 6cAgc00004) and used with permission; turtle is from Ref. 197 and used with permission; mammalian images are from <http://brainmuseum.org> (specimens from the Defense Health Agency Neuroanatomical Collections Division of the National Museum of Health and Medicine, the University of Wisconsin, and Michigan State Comparative Mammalian Brain Collections supported by the U.S. National Science Foundation).

contribute to their extraordinary folding (204, 206). Under the simple perspective of how much cortical tissue can fold while still preserving its laminar composition (cell types, density, and connectivity), thinner cortices allow for smaller and more numerous gyri, which results in more intense cortical folding relative to brain weight. The converse is also reflected in some other species like the beaver and the manatee, two unrelated species with large but smooth brains, both with an unusually thick white matter and cortex (159).

The evolution of cortical folding involved in many cases an increase in the degree of folding (GI) from the initial ancestor, but in others it involved a decrease of folding, or secondary loss (FIGURE 8). Cortical folding is very prominent in humans and other large primates, namely great apes and old-world monkeys. However, the smaller new-world monkeys have small brains and near-smooth cortices. Mathematical analyses of cortical folding and phylogeny show that two different trajectories emerged from the common ancestor to extant primates: one that increased GI, the most dramatic

examples being modern human, chimpanzee and gorilla; and a second that decreased GI, leading to lemurs and marmosets (60, 199, 202). This demonstrates that secondary loss of gyrencephaly was an important aspect of primate brain evolution. A similar example is found in marsupials, where folded and smooth brained species are interspersed across the phylogenetic tree, as well as in the two extinct monotremes, the gyrencephalic echidna and the lissencephalic platypus (FIGURE 8). However, the paramount example of secondary loss of cortex folding occurred in rodents and lagomorphs (rabbits). About 100 million years ago, an ancestral placental mammal diverged in two lineages: one giving rise to modern carnivores and ungulates, all highly folded, and the other giving rise to primates and rodents. Only 10 million years later the common ancestor to primates and rodents would diverge, following independent evolution ever since (201). From that point, whereas most carnivores and ungulates, and many primates evolved to ever-increase cortex folding, the entire rodent and lagomorph lineage evolved to reduce cortex size and

folding to the minimum. Intriguingly, one extant rodent species has remarkable cortex folding, the large south-american Capybara, which may have spared this secondary loss or re-gained folding from a smooth brained ancestor (FIGURE 8). Secondary loss is more likely to have occurred independently in multiple lineages than by evolutionary convergence, because a loss of bRGCs, neurogenesis, and the genetic mechanisms regulating them is evolutionarily much more economical than their generation de novo. The differential changes and reversals in the cortical phenotype during the evolution of mammalian brains reflects their remarkable adaptability in this process (207).

### 9.3. Ongoing Evolution of Cortex Folding and Human Uniqueness

The genetic mechanisms underlying the evolutionary expansion and folding of the human cerebral cortex are beginning to be elucidated (208), while much less is known about mechanisms involved in their secondary loss in rodents. Human cortical malformations most frequently result from developmental defects of genetic origin. A number of genes have been identified as critical in cortical development and folding, whose mutation is linked to specific malformations, but when these same genetic mutations have been introduced in transgenic mice, cortical defects fail to occur in most cases (160, 209). This strongly suggests that those genes, although encoded in both genomes, were coopted during human brain evolution to participate in key processes of cortical development, including the emergence of gyrencephaly (210). Indeed, genes involved in key aspects of brain development, notably protein-coding genes regulating cortical size and folding (i.e., *ASPM*, *MCPH1*, *LIS1*) and nonprotein-coding genes, have evolved considerably faster in primates compared with lissencephalic rodents (211–214), especially in the recent primate lineage leading to humans (134, 135, 208, 215, 216). Patterns of gene expression in the fetal human brain seem to have also evolved rapidly, as for example genes involved in the cortical folding protomap (126, 217, 218). In summary, the rapid evolution of genes and mechanisms regulating their expression seem to have driven the evolution of primate brain size and complexity, especially the dramatic increases in gyrencephaly that occurred in the recent human evolutionary history (60, 208, 219).

#### 9.3.1. Novel protein-coding genes.

One of the obvious mechanisms to introduce new biological functions into a system under evolution is by selecting and incorporating newly created genes. Integrative analyses of gene expression datasets from

multiple laboratories identified 50 genes that exist only in primate genomes and that are highly expressed in embryonic cortical progenitor cells, strongly suggesting a specific relevance in the evolution of the primate cerebral cortex (133). A set of 15 of these genes emerged in the most recent human lineage, after splitting from the chimpanzee lineage but already present in the ancient genomes of Neanderthal and Denisovan humans (128, 133–135, 220–222). These new genes originated mostly by partial or complete gene duplication from the ancestral genome, frequently combined with small indels that shifted reading frames or changed RNA splice sites, creating new genetic functionalities (133). Importantly, expression of some of these human-specific genes such as *ARHGAP11B* (see sect. 6) in the developing cortex of nonhuman species, such as mouse or marmoset monkey, causes the expansion of basal progenitor cells and cortical folding, otherwise naturally smooth (130, 132).

#### 9.3.2. Changes in gene regulatory elements.

In addition to the emergence of new protein-coding genes, cortical evolution was also driven by changes in the regulation of gene expression. Most of the mammalian genome does not code for protein. Once considered useless or junk DNA, it is now clear that the noncoding part of the genome plays very important roles in regulating expression of the coding part. Most of the noncoding DNA is intronic (between exons) or intergenic (between genes), and it contains a wide diversity of types of gene regulatory elements: promoters, proximal and distal enhancers, topologically associating domains, untranslated regions, etc. (223). Unlike protein-coding genes, where function depends on the strict conservation of the protein amino acid sequence encoded in the DNA, the function of gene regulatory elements tends to accept much more sequence flexibility. In other words, single spontaneous changes in the sequence of noncoding regions are much less deleterious than in coding sequences, and thus the former are more susceptible to be fixed in evolution. As a result, genetic evolution tends to occur much more frequently in gene regulatory elements than in protein-coding parts, and therefore, changes in those elements become a driving mechanism of brain evolution. A team of scientists searched for gene regulatory elements involved in the rapid evolution of the human brain from its ancestors, by comparing the human and chimpanzee genomes at high resolution (224). They identified hundreds of small DNA fragments exhibiting highly divergent sequences, with rapid nucleotide substitutions in the human lineage. These small elements, named human accelerated regions (HARs), were proposed to regulate gene expression, and therefore contribute to

human-specific brain expansion and complexity (213, 224, 225). Not surprisingly, >30% of HARs encode active developmental enhancers, making them good candidates as regulatory elements that define human-specific spatiotemporal patterns of gene expression, hence regulating human cortical expansion and folding.

Gene expression is also regulated by multiple classes of noncoding RNAs, which have central roles in cortical development (226). In particular, long noncoding RNAs have been proposed to be important in the evolution of gene regulation (226–228). On the other hand, hundreds of primate-specific miRNAs target genes regulating the cell cycle and neurogenesis and are expressed in progenitor cells of the developing macaque cortex but not in mouse. These miRNAs have been proposed to contribute to primate cortical complexification and possibly folding, although this remains poorly explored (18, 214, 229, 230). In summary, variations in enhancers, promoters, HARs, noncoding RNAs and other gene regulatory elements were likely central in the evolution of the spatiotemporal patterns of gene expression that determine cortical size and folding patterns during fetal development (40, 193, 198).

## 10. HUMAN MALFORMATIONS OF CORTEX FOLDING

Folding of the cerebral cortex has a profound influence on higher brain function. In humans, alterations in cortical folding are usually by loss or excess of folds and typically are associated with severe intellectual disability and intractable epilepsy (160, 231, 232). These defects result from pathological modifications of the normal program of cortical development, described in the above sections, which have an irreversible impact on key events of cortical histogenesis and, eventually, on the cortical phenotype. In patients, defects of cortical folding rarely appear isolated, but usually as part of compound phenotypes of human malformations of cortical development. Alterations of cortical folding are most frequently linked to defects in brain size, either by reduction (i.e., microcephaly), excess (i.e., megalencephaly), or imbalanced growth (dysplasia). The causes and clinical characteristics of the full diversity of these malformations of human cortical development have been reviewed at length elsewhere (160). In this section, we focus on defects of cortical folding.

Alterations of human cortical folding have been traditionally related to defects in neuronal migration (233). Our current better understanding of the cellular and molecular mechanisms of cortical development and folding confirm and support this notion and also highlight the

key implications of cortical progenitor cells (209) (FIGURE 9).

### 10.1. Lissencephaly (Smooth Brain)

The absence or simplification of the folding pattern of the cerebral cortex is clinically referred to as lissencephaly, or smooth brain. This includes several disorders classified depending on the severity of changes in cortex folding: agyria, complete absence of folds; pachygyria, simplified pattern of folds; or subcortical band heterotopia, where the gyral pattern is simplified with broad folds and thickened gray matter (234). Under a histological perspective, lissencephalies are classified in two main types: type I, or classic, is caused by genetic mutations related to the cytoskeleton of migrating neurons and that affect their movement. As detailed previously in sects. 2 and 7, cortical neurons are not born in their final layer of residence, but in the cortical germinal zones deep in the embryonic brain, so they need to migrate from their birthplace to their final position (10, 15). The first genetic mutations discovered to be linked to defects in cortex folding (type I lissencephaly) affected genes related to the cytoskeleton of migrating neurons. These mutations severely impaired the forward displacement of cortical newborn neurons to the cortical surface, thus failing to form the characteristic six main neuronal layers but instead accumulating in a highly disorganized, thickened and smooth cortex (233, 235–239). This demonstrated that the movement of radially migrating neurons, and their correct final location, are essential for cortical folding. Unfortunately, these discoveries did not readily provide a mechanism for cerebral cortex folding, because the same proteins and cytoskeletal mechanisms are key for neuronal migration in mouse, and this has a smooth cerebral cortex (240). Type II lissencephaly, or cobblestone, is typically caused by the defective interaction between the basal end-feet of RGCs and the pial surface, with disruption of the latter. This causes a characteristic overflow of radially migrating neurons past their termination zone below the marginal zone, which traverse through and above the meninges, which confers the appearance of having cobblestones on the cortical surface (241).

Most frequently, type I lissencephaly is due to mutations in the cytoskeleton-interacting proteins LIS1 and Doublecortin (DCX) (235, 236). The interaction of these proteins with the tubulin cytoskeleton allows its polymerization and stability (242, 243), as is also the case for tubulin b3 (*TUBB3*) and tubulin a1a (*TUBA1A*), mutated in type I lissencephaly with impaired growth of the cerebellum (244, 245). Autosomal recessive type I lissencephaly with cerebellar defects is also caused by mutations in Reelin (*RELN*) in a small number of patients (246). This

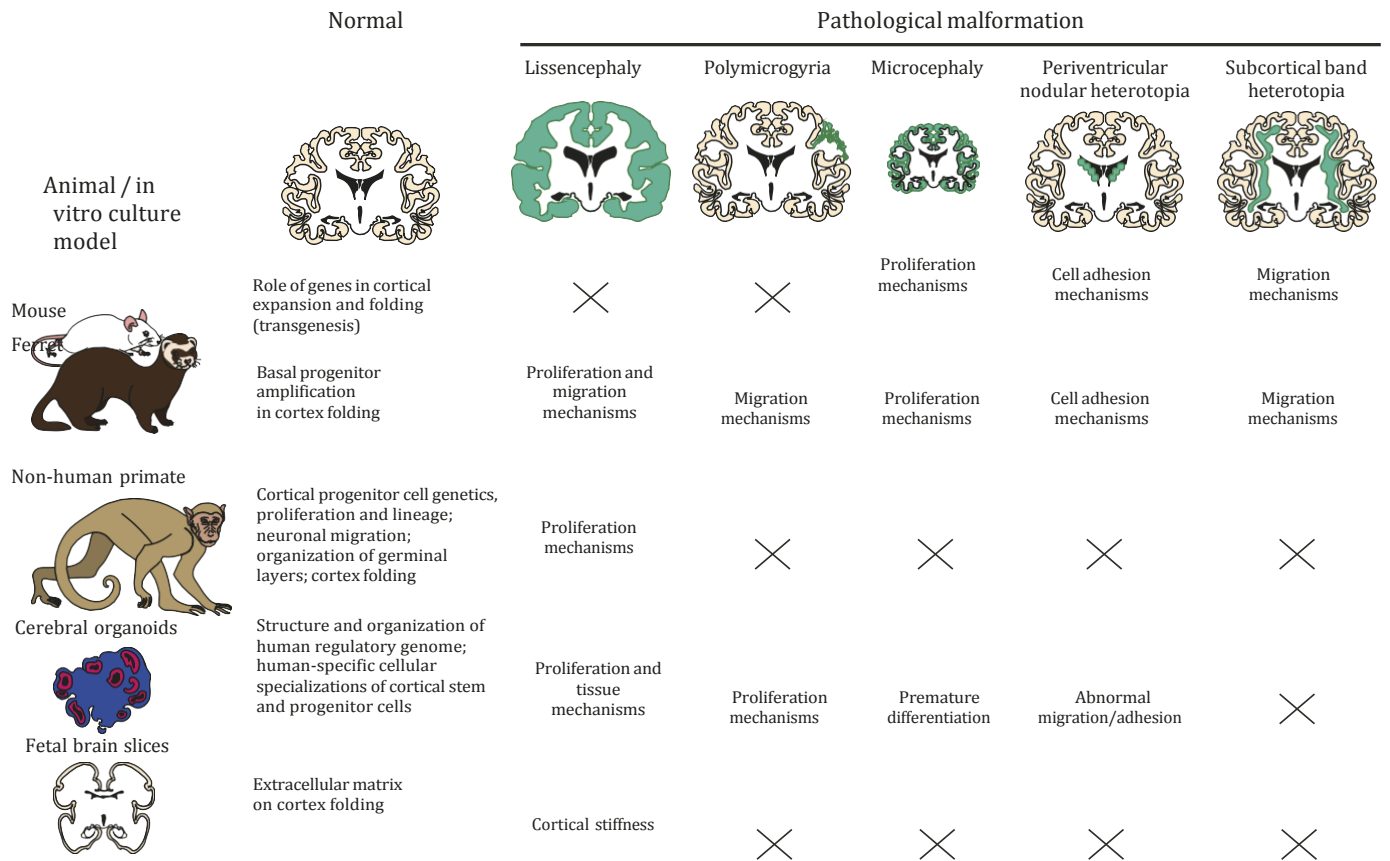


FIGURE 9. Human cortex in health and disease and its modeling in vivo and in vitro. Schematic of coronal sections through the normal or pathologically malformed human cortex and features that can be studied with each animal or in vitro culture model, based on their intrinsic characteristics. The extent of the malformation in the cortex is depicted in green. Mouse is an extremely useful genetic model due to the large number of genetic tools available, but their naturally smooth cortex limits the study of specific malformations like lissencephaly or polymicrogyria. On the contrary, the gyrencephalic cortex of ferret recapitulates the developmental mechanisms underlying most human cortical malformations. Nonhuman primates, while very important to unravel pathomechanisms of cortical malformations, the ethical limitations prevent their extensive use. In vitro modeling of early human cortex development with cerebral organoids and fetal brain slices enable studying characteristics only present in human cells.

gene encodes for an extracellular protein secreted by Cajal-Retzius cells at the marginal zone of the developing cortex (below the pia), which is essential for radial migration and lamination of cortical neurons in both mouse and human (3, 247, 248). When migrating neurons reach the top of the cortical plate and encounter Reln, they stop moving, detach from the basal fiber of RGCs, and begin differentiation (249). Whereas all the above proteins and their cellular effects are key for the radial migration of cortical neurons both in human and mouse (247, 250), the mouse cortex is already smooth, so none of the downstream mechanisms leading to deficient cortex folding observed in patients can be studied in mouse mutants (251).

Type II lissencephaly, also known as cobblestone, is most frequently caused by the overshooting of migrating neurons as a result of alterations in the cortical basement membrane and its anchoring to RGCs (252, 253). Due to this defective anchoring, neurons fail to stop migrating when they reach the top of the cortical plate

and surpass the basal lamina, overmigrating into the meningeal space. This results in the formation of ectopic clusters of neurons on the cortical surface that resemble cobblestones (254).

### 10.2. Polymicrogyria (Many Small Folds)

One of the less well understood and most enigmatic malformations of cortical folding is polymicrogyria (PMG). This is characterized by the developmental formation of an excessive number of small and superficial folds, usually involving the interdigitation of white matter that results in abnormal layering (255, 256) (FIGURE 9). Defects in the formation of cortical layers range from a reduction to four abnormal layers, to a complete disorganization of the laminar arrangement. Frequently, PMG is part of a complex phenotype that also includes other alterations, such as microcephaly (257, 258). The phenotypic presentation of PMG per se is also very diverse: it may be unilateral or bilateral; it may affect only one



cerebral lobe (partially or completely) or the entire cerebral hemisphere. Due to this complexity of phenotypes, understanding PMG remains extremely elusive and appropriate, faithful experimental models are nearly nonexistent (see sect. 11). This phenotypic complexity is also translated to the genetic level, where for example mutations in phosphoinositide 3 kinase regulatory subunit 2 (PIK3R2), a component of the mechanistic target of rapamycin kinase (mTOR) pathway, cause either severe or very mild PMG depending on the degree of genetic mosaicism (259, 260). PMG may also occur as a result of insults during embryogenesis, including hypoxia, hypoperfusion, or infection (261, 262).

### 10.3. Cellular Causes of Folding Defects

Based on current knowledge of basic mechanisms of cerebral cortex development and folding, a number of hypotheses have been proposed to explain the cellular and histogenetic bases of cortical folding defects in human pathology.

#### 10.3.1. Defects in neuron movement.

Cortical folding involves buckling of the gray matter, where neurons reside organized in distinct layers, so neurons are main characters in these malformations. Details on how the abnormal migration of cortical neurons causes folding defects have been presented in the previous section.

#### 10.3.2. Defects in the radial fiber scaffold.

The radial migration of cortical neurons depends on the scaffold of radial glia fibers. Migrating neurons use these thin cellular extensions as their guide and physical substrate for their movement to the cortical surface (10, 139, 186). Even if neurons have the appropriate cellular machinery in working order for movement (see sect. 7), defects in this fiber scaffold will have an incapacitating effect on their radial migration, as they literally serve as railways for neuron migration. The most dramatic defect is the loss of integrity of radial glia fibers, for example, due to their loss of attachment to the pial surface [as in *RELN* mutations (263) or in cobblestone lissencephaly], loss of aRGC polarity, or their premature delamination and differentiation (93, 264). A significant change in the structural organization of an, otherwise normal, radial fiber scaffold may also cause cortical folding defects. As presented above (see sect. 8.2), a major feature of cortical development that leads to folding is the divergence of the radial fiber scaffold (55). This drives radially migrating neurons to separate laterally and disperse tangentially in the developing cortex, thus expanding the

cortical surface area and prompting tissue buckling (156). The radial fiber scaffold acquires divergence from the presence of bRGCs in the OSVZ, which extend their own basal process perfectly intercalated among the basal processes of aRGCs, while maintaining the equidistance between radial fibers (42). Therefore, the more bRGCs the greater the divergence of the radial fiber scaffold, the greater the cortical surface area and the more folding. In contrast, the fewer bRGCs the smaller cortical surface area. Based on this simple principle, given a fixed amount of migrating neurons, increases or decreases in the relative abundance of bRGCs will drive equivalent changes in cortical folding. For example, lissencephaly may result from a disproportionately reduced number of bRGCs, and polymicrogyria from a disproportional excess, as demonstrated in experimental animal models (42, 55, 84, 125).

#### 10.3.3. Defects in the interaction between migrating neurons and radial glia fibers.

All the above factors remaining unaltered, defects in the physical-chemical interaction between migrating neurons and radial glia fibers still result in altered cortical folding. The intimate association between migrating neurons and the basal process of radial glia depends on the expression of cell surface adhesion molecules, including integrins and connexins (149, 150, 249, 265). Defects in expression or in functional binding (for example, due to point mutations in the protein binding domain) may impair neuronal migration or termination of migration, causing type I lissencephaly or cobblestone, respectively. Migrating neurons also exert adhesive and repulsive interactions between them, and changes in these interactions also may be a source of cortical folding defects. For example, loss of two such cell-adhesion proteins, *Flrt1* and *Flrt3*, alters the adhesive-repulsive interaction between cortical migrating neurons and drives folding of the otherwise smooth mouse cortex (153). The balance between adhesion and repulsion during neuronal migration is particularly critical in the context of a divergent radial fiber scaffold, as in folded cortices. In order for the radial divergence to be effective, migrating neurons must switch laterally between radial fibers, hence dispersing tangentially (56). As mentioned above (sect. 8.2), the formation of side branches in the leading process of migrating neurons greatly facilitates switching between radial fibers, and hence their tangential dispersion (187). Defects in the formation and/or retraction of these side branches, as shown in mice mutant for *Dcx*, may severely impair the proper tangential dispersion of migrating neurons, and consequently impair cortex folding.

## 11. UNDERSTANDING MALFORMATIONS OF HUMAN CORTEX FOLDING

Genetic linkage studies of human cortical malformations have been fundamental to identify specific genes that are critical for cortical folding in humans, as well as the genetic mutations that perturb their normal function in this process (160). Unfortunately, these studies do not reveal the physiological function of those genes in normal cortical development, nor the contribution of this function to cortical folding. To illuminate the developmental mechanisms directly affected by pathogenic mutations, and to understand the cellular and histogenetic bases of malformations of human cortex folding, a variety of animal models and in vitro culture systems are becoming increasingly useful (FIGURE 9).

### 11.1. Animal Models

#### 11.1.1. Mouse.

Due to the amenability of the mouse for transgenesis, and its widely common use in basic research, this was the first animal model used to investigate the role of genes mutated in human malformations of cortex folding. Demonstration of the basic concept that high progenitor cell proliferation drives cortex expansion and folding (15) came from transgenic mouse lines that constitutively activate key signaling pathways such as Wnt/b-catenin (23), FGF (80), or Shh (102). Similarly, mouse studies have demonstrated that blockade of developmental apoptosis promotes cortical expansion and folding (24, 266, 267). Targeted genetic manipulation of the developing mouse cortex has allowed investigators to systematically test (and confirm) emerging hypotheses on cellular mechanisms that drive cortical expansion and folding (125), to identify new mechanisms that promote cortical progenitor cell amplification (86), and to discover new and unsuspected mechanisms that promote cortex folding (153). Most importantly, specific genetic mutations that drive cortical malformations in humans have been introduced by transgenesis in mouse models. This approach has been extraordinarily useful to understand the pathomechanisms of disease when mutant mice reproduce similar cortical malformations as patients, such as for subcortical band heterotopia, periventricular nodular heterotopia or microcephaly (268–272). Unfortunately, however, human malformations of cortical folding have mostly not been recapitulated in transgenic mice carrying the same genetic mutation, such as in doublecortex (240) or lissencephaly (273). These negative results make sense considering that the mutations introduced cause a loss of folds in the human cortex, and the mouse cortex is naturally smooth already.

This has recently led researchers to look out for new and more appropriate models to understand human malformations of cortex folding.

#### 11.1.2. Ferret.

This small carnivore (*Mustela putorius furo*) has been used for many decades in biomedical research, particularly neuroscience (274, 275). A renewed interest for ferret has awakened in recent years due to the simple and highly stereotyped pattern of cortical folds that it develops naturally, and particularly due to pioneering work that demonstrated its amenability for experimental and genetic manipulation (276, 277). This holds the promise to bring light in understanding cortical folding and human malformations (55, 178, 278). Indeed, the existence outside of primates of bRGCs, OSVZ, and the associated transient fiber layers IFL and OFL, was first discovered in ferret (16, 41, 42, 279). Since then, the ferret has continued being a reference model in this field of research (87, 156). At the level of genetic manipulation, in utero electroporation or viral vector delivery of DNA constructs in developing ferrets is widely exploited for gene overexpression (40, 63, 84, 178, 276) and combined with CRISPR/Cas9 for genome editing (280). With the use of these strategies, ferret studies have revealed the central importance in cortex folding of specific cellular mechanisms such as basal progenitor amplification (84, 181), and the deleterious effects on normal cortical development of genetic mutations linked to human cortical malformations (81). For example, the ferret has been uniquely useful to elucidate specific defects in developmental mechanisms behind thanatophoric dysplasia (81, 120), cobblestone lissencephaly (281), double cortex (282), microcephaly (73, 282), type I lissencephaly (180), polymicrogyria (84), and periventricular nodular heterotopia (283). While much remains to be learned, and the ferret is only a model organism for human disease, it is currently one of the most relevant tools to dissect the pathomechanisms of human malformations of cortex folding (FIGURE 9).

#### 11.1.3. Nonhuman primates.

Model organisms are only as good as their resemblance to the human condition, and a key limitation of nonprimate species to understand human disease of cortical development is their genomic and phylogenetic distance from human. While nonhuman primates are ideally suited, the obvious ethical implications make them a very limiting resource. Nevertheless, biomedical research is making very significant progress on this front by focusing on a reduced number of nonhuman primate species that reproduce well in captivity and are susceptible to

genetic modification (284). One such example is the marmoset (*Callithrix jacchus*), a small new world monkey with a small and smooth cortex, displaying a single sulcus. Recent technological developments now allow generating transgenic marmosets, and this is being used to understand genetic pathomechanisms of human malformations of cortical development, and genetic mechanisms of human brain evolution (285). For example, expression of the human-specific gene *ARHGAP11B* in marmoset progenitor cells causes significant folding of the otherwise near-lissencephalic marmoset cerebral cortex (132) (see sects. 6 and 9.3). A second example is the macaque (*Macaca mulatta*), an old-world monkey with a large and folded cortex historically used as a model in systems and developmental neuroscience. Experimental analyses and manipulations of the developing macaque cerebral cortex have unraveled fundamental primate-specific mechanisms of cortical progenitor cell genetics, proliferation and lineage, organization of germinal layers, neuronal migration, and cortex folding (18, 44, 51, 214, 286–290). The advent of macaque transgenesis (291) open a new window of opportunities to study and model complex human brain diseases like Huntington’s and Parkinson’s (292, 293), and efforts are underway to generate transgenic macaques to understand human developmental brain disease (FIGURE 9).

## 11.2. In Vitro Culture Models

### 11.2.1. Cerebral organoids.

Nonhuman primates are excellent models to recapitulate primate-specific features of brain development. Ferret is a fantastic model to study natural mechanisms of cortex expansion and folding in vivo, and mouse is the reference model to understand the molecular and cellular mechanisms of brain development, with an unmatched repertoire of available experimental tools. However, human brain development and its disease involves certain aspects that cannot yet be modeled. These include, but are not limited to, the structure and organization of the regulatory genome (proximal and distal regulatory elements, 3-dimensional chromatin organization), and distinct cellular specializations of neural stem and progenitor cells (length of mitotic phases, morphology of neuroepithelial cells) (294–296). Human cerebral organoids were developed from human induced pluripotent stem cells (hiPSCs) to study brain development in the context of some of these human-unique features (297). Since then, they have become the reference system for this purpose and to understand human brain development, evolution and disease (298–301). Among the many emergent uses of cerebral organoids, they are

being utilized to understand human-specific principles of cortical stem cells in normal development (295, 302), and how these are affected by genetic mutations of human developmental disease (FIGURE 9). For example, cerebral organoids grown from hiPSCs produced from skin fibroblasts of neurological patients are used to understand glioblastoma (303), microcephaly (297), and ventricular heterotopia (304) but also lissencephaly (305, 306) and polymicrogyria (307, 308).

### 11.2.2. Human cortex slices.

This is a second in vitro system recently emerged as useful in studying cortex folding. Fresh cortical tissue from human fetuses is sliced and maintained in culture for a few days, while it can be treated with protein solutions, drugs or by acute genetic manipulation (170). This system has been used to test the involvement of the extracellular matrix on cortex folding. Application of a mixture of extracellular matrix component proteins onto cultured human fetal cortex slices induces changes in tissue mechanics and the rapid folding of the cortical plate, a response altered in slices obtained from neurological patients with known defects in cortex folding (FIGURE 9) (170, 171).

While cerebral organoids and brain slices are far from modeling bona fide cortex folding, the fact that assemblies of human neural stem cells carrying exactly the disease-causing genomic defects can be studied represents an unmatched opportunity to approach some understanding of the original pathomechanisms (299), and to measure the fitness of the nonhuman models available. All in all, both these in vitro systems also have limitations that cannot rival with intact animals, including accurate reproducibility of developmental events, integration of intrinsic and extrinsic cues (i.e., hormones and maternal influence), and full completion of development that allows testing the consequences of experimental alterations on brain function and animal behavior.

## 12. CONCLUSIONS AND FUTURE DIRECTIONS

Folding of the cerebral cortex is a complex and multifactorial process occurring in the latest period of cortical development. A renewed interest in the fundamental question of how the cerebral cortex folds has led to an upsurge of research in this topic over the last decade, unravelling some of the key cellular and mechanical principles of this process, and some of their gene regulatory mechanisms (156). As summarized in this review, folding of the cerebral cortex is essentially based on modifications of the basic process of cortical

development, including diversification and expansion of progenitor cell types and their lineages, lengthening of the neurogenic period, modifications of the radial migration of neurons and their distribution along the cortical surface, and finally neuronal differentiation, altogether leading to the occurrence of mechanical forces in the developing cortex that cause neural tissue deformation and folding (FIGURE 10). Some of our knowledge comes from studying human malformations of cortex folding, which has identified genes and cellular mechanisms key in this process. Although our current knowledge seems to set the grounds of cortex folding mechanisms, much remains to be learned. Not only at the level of genetic regulation, but even more fundamentally at the level of how all these developmental events come together to cause tissue deformation and cortex folding. What determines the highly conserved periodicity and wavelength of cortex folds, how specific cellular mechanisms translate into particular mechanical forces, which aspects of genome evolution primed the phylogenic variations in folding, and what gene regulatory mechanisms define the genetic protomaps of cortex folding are just a few of

the many key questions that remain for future research in our quest to understand brain folding in health, and its alterations in disease.

### 13. APPENDIX

#### 13.1. Controversies and Gaps of Knowledge

##### 13.1.1. Related to sect. 4.1 (Progenitor Cell Classes, Germinal Layers, and Cortex Folding).

Mounting evidence supports the notion that the existence of OSVZ, and bRGCs populating it, are central in cortex folding. However, both bRGCs and OSVZ have been described also in lissencephalic species with large brains like the marmoset monkey. Moreover, experimental folding of the otherwise smooth mouse cortex is achieved by modification of neuronal migration and their adhesive properties, without an abundant presence of bRGCs nor OSVZ. This raises the controversy that OSVZ and bRGCs may be necessary but not sufficient for

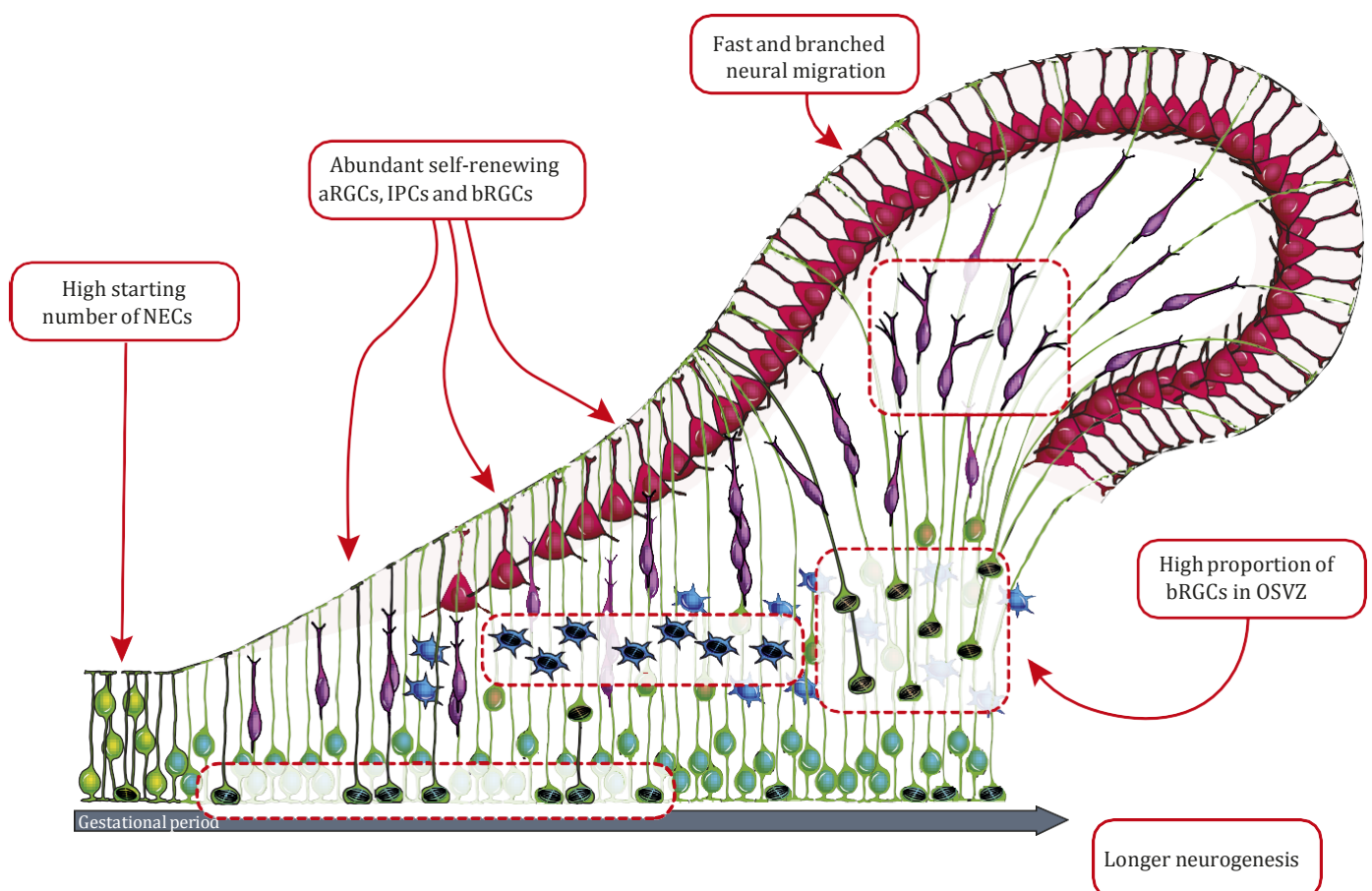


FIGURE 10. Main aspects of normal cortical development involved in cortical folding. This is an extraordinarily complex mechanism implicating a large diversity of fine-tuned cellular processes unfolding simultaneously in a time- and space-dependent manner. Characteristics necessary for cortex folding, although not sufficient, are indicated in red outlines. NECs, neuroepithelial cells; aRGCs, apical radial glia cells; bRGCs, basal radial glia cells; IPCs, intermediate progenitor cells; OSVZ, outer subventricular zone.

gyrencephaly. This conflict may be resolved by looking into the normal development of additional species with strategic characteristics (i.e., primates with small but folded brains, species with large but smooth brains), and very importantly also in the cortex of human embryos with diagnosed folding malformations, and by manipulating the expression and function of genes causative of these human malformations in experimental *in vivo* and *in vitro* models.

### 13.1.2. Related to sect. 4.2 (Specialized Progenitor Morphotypes).

Morphotypes of bRGCs and IPCs occur frequently in the developing cortex of gyrencephalic species, especially in primates, raising the key question of whether these are distinct cell types or rather simply different states of a single cell type, which has fundamental implications both on our understanding of normal and pathological cortical development and on potential therapeutic treatment of these diseases. Exhaustive and comprehensive multiomic single cell analyses, combined with analyses of cell lineage, will be key to resolve this controversial question.

### 13.1.3. Related to sect. 4.3 (Distinguishing Progenitor Cell Types).

Related to the previous point, existing single cell RNAseq analyses identify multiple transcriptomic clusters of RGCs, and of IPCs, in each of several species, including mouse, ferret and human. The specific phase of the cell cycle is clearly one of the main traits distinguishing these clusters: cells of a given cell type are clustered separately if they are in mitosis, S-phase, or interphase. This demonstrates that different cell states may be mistaken as different cell types. Again, multiomic single cell analysis, carefully filtered by existing knowledge on the biology of identified cell types, should bring light into distinguishing progenitor cell types and more generally into defining what is a cell type.

### 13.1.4. Related to sect. 8.1 (Physical Forces).

There is still a hot debate on what are the physical/mechanical forces that drive cortex folding, whether it is axonal tension, tissue compression, or the result of passive accommodation of overgrown layered tissue, with the pattern and wavelength of folds depending on tissue thickness. While experimental measurement and manipulation of physical forces during the development of cortex folds are improving, they must be combined with mathematical modelling of physical properties of

biological tissue, with the promise of solving this long-standing controversy.

### 13.1.5. Related to sect. 11 (Understanding Malformations of Human Cortex Folding).

Polymicrogyria is one of the most salient developmental malformations of cortical folding in children. Whereas multiple genes have been identified as causative of this clinical condition, our understanding of even the most basic aspects of cortical development leading to this highly incapacitating condition is unacceptably scarce, nearly anecdotic. This is fundamentally due to the lack of suitable animal or experimental models, and so renewed efforts must be placed on developing such much needed models of study. This may come from a combination of animal and *in vitro* models, each bringing a particular aspect relevant to the malformation, for example, human cerebral organoids *in vitro* for cell biological mechanisms, brain slices from macaque for layer-specific progenitor cell behavior and neuronal migration features, and ferret to test the *in vivo* consequences of identified alterations.

## CORRESPONDENCE

V. Borrell (vborrell@umh.es).

## ACKNOWLEDGMENTS

The authors thank members of the Borrell laboratory for insightful discussions on this topic and also M. Villarroel and A. Fobbs for use of brain images in [FIGURE 8](#).

## GRANTS

L.D-V-A. is funded by a predoctoral fellowship from the Spanish State Research Agency (AEI). Work in our laboratory is supported by grants from AEI (PGC2018-102172-B-I00, as well as through the “Severo Ochoa” Programme for Centers of Excellence in R&D (Ref. SEV-2017-0723).

## DISCLOSURES

No conflicts of interest, financial or otherwise, are declared by the authors.

## AUTHOR CONTRIBUTIONS

L.D-V-A. and V.B. conceived the manuscript and designed the figures; L.D-V-A. prepared the figures; L.D-V-A. and V.B. wrote the manuscript.

## REFERENCES

- ▶ 1. Marin-Padilla M. Cajal-Retzius cells and the development of the neocortex. *Trends Neurosci* 21: 64–71, 1998. doi:[10.1016/s0166-2236\(97\)01164-8](https://doi.org/10.1016/s0166-2236(97)01164-8).
- ▶ 2. Bielle F, Griveau A, Narboux-Neme N, Vigneau S, Sigrist M, Arber S, Wassef M, Pierani A. Multiple origins of Cajal-Retzius cells at the borders of the developing pallium. *Nat Neurosci* 8: 1002–1012, 2005. doi:[10.1038/nn1511](https://doi.org/10.1038/nn1511).
- ▶ 3. Soriano E, Del Rio JA. The cells of cajal-retzius: still a mystery one century after. *Neuron* 46: 389–394, 2005. doi:[10.1016/j.neuron.2005.04.019](https://doi.org/10.1016/j.neuron.2005.04.019).
- ▶ 4. Marin O, Rubenstein JL. A long, remarkable journey: tangential migration in the telencephalon. *Nat Rev Neurosci* 2: 780–790, 2001. doi:[10.1038/35093564](https://doi.org/10.1038/35093564), [10.1038/35097509](https://doi.org/10.1038/35097509). doi:[10.1038/35097509](https://doi.org/10.1038/35097509).
- ▶ 5. Rakic P. Neurons in rhesus monkey visual cortex: Systematic relation between time of origin and eventual disposition. *Science* 183: 425–427, 1974. doi:[10.1126/science.183.4123.425](https://doi.org/10.1126/science.183.4123.425).
- ▶ 6. Gupta A, Tsai LH, Wynshaw-Boris A. Life is a journey: a genetic look at neocortical development. *Nat Rev Genet* 3: 342–355, 2002. doi:[10.1038/nrg799](https://doi.org/10.1038/nrg799).
- ▶ 7. Borrell V, Marin O. Meninges control tangential migration of hem-derived Cajal-Retzius cells via CXCL12/CXCR4 signaling. *Nat Neurosci* 9: 1284–1293, 2006. doi:[10.1038/nn1764](https://doi.org/10.1038/nn1764).
- ▶ 8. Marin-Padilla M, Marin-Padilla TM. Origin, prenatal development and structural organization of layer I of the human cerebral (motor) cortex. A Golgi study. *Anat Embryol (Berl)* 164: 161–206, 1982. doi:[10.1007/BF00318504](https://doi.org/10.1007/BF00318504).
9. Bayer SA, Altman J. *Neocortical Development*. New York: Raven Press, 1991, vol 1.
- ▶ 10. Sidman RL, Rakic P. Neuronal migration, with special reference to developing human brain: a review. *Brain Res* 62: 1–35, 1973. doi:[10.1016/0006-8993\(73\)90617-3](https://doi.org/10.1016/0006-8993(73)90617-3).
- ▶ 11. Gumbiner BM. Cell adhesion: the molecular basis of tissue architecture and morphogenesis. *Cell* 84: 345–357, 1996. doi:[10.1016/S0092-8674\(00\)81279-9](https://doi.org/10.1016/S0092-8674(00)81279-9).
- ▶ 12. Lehtinen MK, Zappaterra MW, Chen X, Yang YJ, Hill AD, Lun M, Maynard T, Gonzalez D, Kim S, Ye P, D'Ercole AJ, Wong ET, LaMantia AS, Walsh CA. The cerebrospinal fluid provides a proliferative niche for neural progenitor cells. *Neuron* 69: 893–905, 2011. doi:[10.1016/j.neuron.2011.01.023](https://doi.org/10.1016/j.neuron.2011.01.023).
- ▶ 13. Lehtinen MK, Walsh CA. Neurogenesis at the brain–cerebrospinal fluid interface. *Annu Rev Cell Dev Biol* 27: 653–679, 2011. doi:[10.1146/annurev-cellbio-092910-154026](https://doi.org/10.1146/annurev-cellbio-092910-154026).
- ▶ 14. Takahashi T, Nowakowski RS, Caviness VS Jr. The cell cycle of the pseudostratified ventricular epithelium of the embryonic murine cerebral wall. *J Neurosci* 15: 6046–6057, 1995. doi:[10.1523/JNEUROSCI.15-09-06046.1995](https://doi.org/10.1523/JNEUROSCI.15-09-06046.1995).
- ▶ 15. Rakic P. A small step for the cell, a giant leap for mankind: a hypothesis of neocortical expansion during evolution. *Trends Neurosci* 18: 383–388, 1995. doi:[10.1016/0166-2236\(95\)93934-P](https://doi.org/10.1016/0166-2236(95)93934-P).
- ▶ 16. Reillo I, Borrell VV. Germinal zones in the developing cerebral cortex of ferret: ontogeny, cell cycle kinetics, and diversity of progenitors. *Cereb Cortex* 22: 2039–2054, 2012. doi:[10.1093/cercor/bhr284](https://doi.org/10.1093/cercor/bhr284).
- ▶ 17. Kornack DR, Rakic P. Changes in cell-cycle kinetics during the development and evolution of primate neocortex. *Proc Natl Acad Sci US A* 95: 1242–1246, 1998. doi:[10.1073/pnas.95.3.1242](https://doi.org/10.1073/pnas.95.3.1242).
- ▶ 18. Lukaszewicz A, Savatier P, Cortay V, Giroud P, Huissoud C, Berland M, Kennedy H, Dehay C. G1 phase regulation, area-specific cell cycle control, and cytoarchitectonics in the primate cortex. *Neuron* 47: 353–364, 2005. doi:[10.1016/j.neuron.2005.06.032](https://doi.org/10.1016/j.neuron.2005.06.032).
- ▶ 19. Borrell V, Calegari F. Mechanisms of brain evolution: regulation of neural progenitor cell diversity and cell cycle length. *Neurosci Res* 86: 14–24, 2014. doi:[10.1016/j.neures.2014.04.004](https://doi.org/10.1016/j.neures.2014.04.004).
- ▶ 20. Hartfuss E, Galli R, Heins N, Götz M. Characterization of CNS precursor subtypes and radial glia. *Dev Biol* 229: 15–30, 2001. doi:[10.1006/dbio.2000.9962](https://doi.org/10.1006/dbio.2000.9962).
- ▶ 21. Götz M, Huttner WB. The cell biology of neurogenesis. *Nat Rev Mol Cell Biol* 6: 777–788, 2005. doi:[10.1038/nrm1739](https://doi.org/10.1038/nrm1739).
- ▶ 22. Aaku-Saraste E, Hellwig A, Huttner WB. Loss of occludin and functional tight junctions, but not ZO-1, during neural tube closure–remodeling of the neuroepithelium prior to neurogenesis. *Dev Biol* 180: 664–679, 1996. doi:[10.1006/dbio.1996.0336](https://doi.org/10.1006/dbio.1996.0336).
- ▶ 23. Chenn A, Walsh CA. Regulation of cerebral cortical size by control of cell cycle exit in neural precursors. *Science* 297: 365–369, 2002. doi:[10.1126/science.1074192](https://doi.org/10.1126/science.1074192).
- ▶ 24. Kingsbury MA, Rehen SK, Contos JJ, Higgins CM, Chun J. Non-proliferative effects of lysophosphatidic acid enhance cortical growth and folding. *Nat Neurosci* 6: 1292–1299, 2003. doi:[10.1038/nn1157](https://doi.org/10.1038/nn1157).
- ▶ 25. Yingling J, Youn YH, Darling D, Toyo-Oka K, Pramparo T, Hirotsune S, Wynshaw-Boris A. Neuroepithelial stem cell proliferation requires LIS1 for precise spindle orientation and symmetric division. *Cell* 132: 474–486, 2008. doi:[10.1016/j.cell.2008.01.026](https://doi.org/10.1016/j.cell.2008.01.026).
- ▶ 26. Gaiano N, Nye JS, Fishell G. Radial glial identity is promoted by Notch1 signaling in the murine forebrain. *Neuron* 26: 395–404, 2000. doi:[10.1016/S0896-6273\(00\)81172-1](https://doi.org/10.1016/S0896-6273(00)81172-1).
- ▶ 27. de la Pompa JL, Wakeham A, Correia KM, Samper E, Brown S, Aguilera RJ, Nakano T, Honjo T, Mak TW, Rossant J, Conlon RA. Conservation of the Notch signalling pathway in mammalian neurogenesis. *Development* 124: 1139–1148, 1997. doi:[10.1242/dev.124.6.1139](https://doi.org/10.1242/dev.124.6.1139).
- ▶ 28. Imayoshi I, Sakamoto M, Yamaguchi M, Mori K, Kageyama R. Essential roles of Notch signaling in maintenance of neural stem cells in developing and adult brains. *J Neurosci* 30: 3489–3498, 2010. doi:[10.1523/JNEUROSCI.4987-09.2010](https://doi.org/10.1523/JNEUROSCI.4987-09.2010).
- ▶ 29. Hatakeyama J, Bessho Y, Katoh K, Ookawara S, Fujioka M, Guillemot F, Kageyama R. Hes genes regulate size, shape and histogenesis of the nervous system by control of the timing of neural stem cell differentiation. *Development* 131: 5539–5550, 2004. doi:[10.1242/dev.01436](https://doi.org/10.1242/dev.01436).
- ▶ 30. Mizutani KI, Yoon K, Dang L, Tokunaga A, Gaiano N. Differential Notch signalling distinguishes neural stem cells from intermediate progenitors. *Nature* 449: 351–355, 2007. doi:[10.1038/nature06090](https://doi.org/10.1038/nature06090).
- ▶ 31. Sahara S, O'Leary DD. Fgf10 regulates transition period of cortical stem cell differentiation to radial glia controlling generation of neurons and basal progenitors. *Neuron* 63: 48–62, 2009. doi:[10.1016/j.neuron.2009.06.006](https://doi.org/10.1016/j.neuron.2009.06.006).
32. Mora-Bermúdez F, García MT, Huttner WB. In: *Neuroscience in the 21st Century*. New York: Springer, 2015, p. 1–25. doi:[10.1007/978-1-4614-6434-1\\_7-3](https://doi.org/10.1007/978-1-4614-6434-1_7-3).

- ▶ 33. Fernández V, Martínez-Martínez MÁ, Prieto-Colomina A, Cárdenas A, Soler R, Dori M, Tomasello U, Nomura Y, Lopez-Atalaya JP, Calegari F, Borrell V. Repression of *Irs2* by *let-7* miRNA is essential for homeostasis of the telencephalic neuroepithelium. *EMBO J* 39: e105479, 2020. doi:10.15252/embj.2020105479.
- ▶ 34. Angevine JB Jr, Bodian D, Coulombre AJ, Edds MV Jr, Hamburger V, Jacobson M, Lyser KM, Prestige MC, Sidman RL, Varon S, Weiss PA. Embryonic vertebrate central nervous system: revised terminology. *Anat Rec* 166: 257–261, 1970. doi:10.1002/ar.1091660214.
- ▶ 35. Shitamukai A, Konno D, Matsuzaki F. Oblique radial glial divisions in the developing mouse neocortex induce self-renewing progenitors outside the germinal zone that resemble primate outer subventricular zone progenitors. *J Neurosci* 31: 3683–3695, 2011. doi:10.1523/JNEUROSCI.4773-10.2011.
- ▶ 36. Matsuzaki F, Shitamukai A. Cell division modes and cleavage planes of neural progenitors during mammalian cortical development. *Cold Spring Harb Perspect Biol* 7: a015719, 2015. doi:10.1101/cshperspect.a015719.
- ▶ 37. Vessey JP, Amadei G, Burns SE, Kiebler MA, Kaplan DR, Miller FD. An asymmetrically localized *Staufen2*-dependent RNA complex regulates maintenance of mammalian neural stem cells. *Cell Stem Cell* 11: 517–528, 2012. doi:10.1016/j.stem.2012.06.010.
- ▶ 38. Kusek G, Campbell M, Doyle F, Tenenbaum SA, Kiebler M, Temple S. Asymmetric segregation of the double-stranded RNA binding protein *Staufen2* during mammalian neural stem cell divisions promotes lineage progression. *Cell Stem Cell* 11: 505–516, 2012. doi:10.1016/j.stem.2012.06.006.
- ▶ 39. LaMonica BE, Lui JH, Hansen DV, Kriegstein AR. Mitotic spindle orientation predicts outer radial glial cell generation in human neocortex. *Nat Commun* 4: 1665, 2013. doi:10.1038/ncomms2647.
- ▶ 40. Martínez-Martínez MÁ, De Juan Romero C, Fernández V, Cárdenas A, Goetz M, Borrell V. A restricted period for formation of outer subventricular zone defined by *Cdh1* and *Trnp1* levels. *Nat Commun* 7: 11812, 2016. doi:10.1038/ncomms11812.
- ▶ 41. Fietz SA, Kelava I, Vogt J, Wilsch-Brauninger M, Stenzel D, Fish JL, Corbeil D, Riehn A, Distler W, Nitsch R, Huttner WB. OSVZ progenitors of human and ferret neocortex are epithelial-like and expand by integrin signaling. *Nat Neurosci* 13: 690–699, 2010. doi:10.1038/nn.2553.
- ▶ 42. Reillo I, De Juan Romero C, García-Cabezas MÁ, Borrell V. A Role for intermediate radial glia in the tangential expansion of the mammalian cerebral cortex. *Cereb Cortex* 21: 1674–1694, 2011. doi:10.1093/cercor/bhq238.
- ▶ 43. Hansen DV, Lui JH, Parker PR, Kriegstein AR. Neurogenic radial glia in the outer subventricular zone of human neocortex. *Nature* 464: 554–561, 2010. doi:10.1038/nature08845.
- ▶ 44. Betzeau M, Cortay V, Patti D, Pfister S, Gautier E, Bellemin-Menard A, Afanassieff M, Huissoud C, Douglas RJ, Kennedy H, Dehay C. Precursor diversity and complexity of lineage relationships in the outer subventricular zone of the primate. *Neuron* 80: 442–457, 2013. doi:10.1016/j.neuron.2013.09.032.
- ▶ 45. Noctor SC, Martínez-Cerdeño V, Ivic L, Kriegstein AR, Martínez-Cerdeño V, Ivic L, Kriegstein AR. Cortical neurons arise in symmetric and asymmetric division zones and migrate through specific phases. *Nat Neurosci* 7: 136–144, 2004. doi:10.1038/nn1172.
- ▶ 46. Miyata T, Kawaguchi A, Saito K, Kawano M, Muto T, Ogawa M. Asymmetric production of surface-dividing and non-surface-dividing cortical progenitor cells. *Development* 131: 3133–3145, 2004. doi:10.1242/dev.01173.
- ▶ 47. Haubensak W, Attardo A, Denk W, Huttner WB. Neurons arise in the basal neuroepithelium of the early mammalian telencephalon: a major site of neurogenesis. *Proc Natl Acad Sci U S A* 101: 3196–3201, 2004. doi:10.1073/pnas.0308600100.
- ▶ 48. Kowalczyk T, Pontious A, Englund C, Daza RA, Bedogni F, Hodge R, Attardo A, Bell C, Huttner WB, Hevner RF. Intermediate neuronal progenitors (basal progenitors) produce pyramidal-projection neurons for all layers of cerebral cortex. *Cereb Cortex* 19: 2439–2450, 2009. doi:10.1093/cercor/bhn260.
- ▶ 49. Noctor SC, Martínez-Cerdeño V, Kriegstein AR. Distinct behaviors of neural stem and progenitor cells underlie cortical neurogenesis. *J Comp Neurol* 508: 28–44, 2008. doi:10.1002/cne.21669.
- ▶ 50. Wang X, Tsai JW, LaMonica B, Kriegstein AR. A new subtype of progenitor cell in the mouse embryonic neocortex. *Nat Neurosci* 14: 555–561, 2011. doi:10.1038/nn.2807.
- ▶ 51. Smart IH, Dehay C, Giroud P, Berland M, Kennedy H. Unique morphological features of the proliferative zones and postmitotic compartments of the neural epithelium giving rise to striate and extrastriate cortex in the monkey. *Cereb Cortex* 12: 37–53, 2002. doi:10.1093/cercor/12.1.37.
- ▶ 52. Martínez-Cerdeño V, Cunningham CL, Camacho J, Antczak JL, Prakash AN, Cziep ME, Walker AI, Noctor SC. Comparative analysis of the subventricular zone in rat, ferret and macaque: evidence for an outer subventricular zone in rodents. *PLoS One* 7: e30178, 2012. doi:10.1371/journal.pone.0030178.
- ▶ 53. Reillo I, de Juan Romero C, Cárdenas A, Clascá F, Martínez-Martínez MÁ, Borrell V. A complex code of extrinsic influences on cortical progenitor cells of higher mammals. *Cereb Cortex* 27: 4586–4606, 2017. doi:10.1093/cercor/bhx171.
- ▶ 54. Dehay C, Savatier P, Cortay V, Kennedy H. Cell-cycle kinetics of neocortical precursors are influenced by embryonic thalamic axons. *J Neurosci* 21: 201–214, 2001. doi:10.1523/JNEUROSCI.21-01-00201.2001.
- ▶ 55. Borrell V, Reillo I. Emerging roles of neural stem cells in cerebral cortex development and evolution. *Dev Neurobiol* 72: 955–971, 2012. doi:10.1002/dneu.22013.
- ▶ 56. Borrell V, Goetz M. Role of radial glial cells in cerebral cortex folding. *Curr Opin Neurobiol* 27: 39–46, 2014. doi:10.1016/j.conb.2014.02.007.
- ▶ 57. Lui JH, Hansen DV, Kriegstein AR. Development and evolution of the human neocortex. *Cell* 146: 18–36, 2011. doi:10.1016/j.cell.2011.06.030.
- ▶ 58. Kriegstein A, Noctor S, Martínez-Cerdeño V. Patterns of neural stem and progenitor cell division may underlie evolutionary cortical expansion. *Nat Rev Neurosci* 7: 883–890, 2006. doi:10.1038/nrn2008.
- ▶ 59. Hevner RF, Haydar TF. The (not necessarily) convoluted role of basal radial glia in cortical neurogenesis. *Cereb Cortex* 22: 465–468, 2012. doi:10.1093/cercor/bhr336.
- ▶ 60. Kelava I, Reillo I, Murayama AY, Kalinka AT, Stenzel D, Tomancak P, Matsuzaki F, Lebrand C, Sasaki E, Schwamborn JC, Okano H, Huttner WB, Borrell V. Abundant Occurrence of basal radial glia in the subventricular zone of embryonic neocortex of a lissencephalic primate, the common marmoset *Callithrix jacchus*. *Cereb Cortex* 22: 469–481, 2012. doi:10.1093/cercor/bhr301.
- ▶ 61. Garcia-Moreno F, Vasistha NA, Trevia N, Bourne JA, Molnar Z. Compartmentalization of cerebral cortical germinal zones in a

- lissencephalic primate and gyrencephalic rodent. *Cereb Cortex* 22: 482–492, 2012. doi:[10.1093/cercor/bhr312](https://doi.org/10.1093/cercor/bhr312).
- ▶ 62. Pilz GA, Shitamukai A, Reillo I, Pacary E, Schwausch J, Stahl R, Ninkovic J, Snippert HJ, Clevers H, Godinho L, Guillemot F, Borrell V, Matsuzaki F, Götz M. Amplification of progenitors in the mammalian telencephalon includes a new radial glial cell type. *Nat Commun* 4: 2125, 2013. doi:[10.1038/ncomms3125](https://doi.org/10.1038/ncomms3125).
- ▶ 63. Kalebic N, Gilardi C, Stepien B, Wilsch-Braeuning M, Long KR, Namba T, Florio M, Langen B, Lombardot B, Shevchenko A, Kilimann MW, Kawasaki H, Wimberger P, Huttner WB. Neocortical expansion due to increased proliferation of basal progenitors is linked to changes in their morphology. *Cell Stem Cell* 24: 535–550.e9, 2019. doi:[10.1016/j.stem.2019.02.017](https://doi.org/10.1016/j.stem.2019.02.017).
- ▶ 64. Kalebic N, Huttner WB. Basal progenitor morphology and neocortex evolution. *Trends Neurosci* 43: 843–853, 2020. doi:[10.1016/j.tins.2020.07.009](https://doi.org/10.1016/j.tins.2020.07.009).
- ▶ 65. Nowakowski TJ, Pollen AA, Sandoval-Espinosa C, Kriegstein AR. Transformation of the radial glia scaffold demarcates two stages of human cerebral cortex development. *Neuron* 91: 1219–1227, 2016. doi:[10.1016/j.neuron.2016.09.005](https://doi.org/10.1016/j.neuron.2016.09.005).
- ▶ 66. Pollen AA, Nowakowski TJ, Shuga J, Wang X, Leyrat AA, Lui JH, et al. Low-coverage single-cell mRNA sequencing reveals cellular heterogeneity and activated signaling pathways in developing cerebral cortex. *Nat Biotechnol* 32: 1053–1058, 2014. doi:[10.1038/nbt.2967](https://doi.org/10.1038/nbt.2967).
- ▶ 67. Mayer C, Hafemeister C, Bandler RC, Machold R, Batista Brito R, Jaglin X, Allaway K, Butler A, Fishell G, Satija R. Developmental diversification of cortical inhibitory interneurons. *Nature* 555: 457–462, 2018. doi:[10.1038/nature25999](https://doi.org/10.1038/nature25999).
- ▶ 68. Yao Z, Van Velthoven CT, Nguyen N, Smith KA, Tasic B, Zeng H. A taxonomy of transcriptomic cell types across the isocortex and hippocampal formation. *Cell* 184: 3222–3241.e26, 2021. doi:[10.1016/j.cell.2021.04.021](https://doi.org/10.1016/j.cell.2021.04.021).
- ▶ 69. Tolley L, Agirman G, Prados J, Amberg N, Fie'vre S, Oberst P, Bartolini G, Vitali I, Cadilhac C, Hippenmeyer S, Nguyen L, Dayer A, Jabaudon D. Temporal patterning of apical progenitors and their daughter neurons in the developing neocortex. *Science* 364: eaav2522, 2019. doi:[10.1126/science.aav2522](https://doi.org/10.1126/science.aav2522).
- ▶ 70. Tolley L, Govindan S, Prados J, Stevant I, Nef S, Dermitzakis E, Dayer A, Jabaudon D. Sequential transcriptional waves direct the differentiation of newborn neurons in the mouse neocortex. *Science* 351: 1443–1446, 2016. doi:[10.1126/science.aad8361](https://doi.org/10.1126/science.aad8361).
- ▶ 71. Li Z, Tyler WA, Zeldich E, Santpere Baro, G, Okamoto M, Gao T, Li M, Sestan N, Haydar TF. Transcriptional priming as a conserved mechanism of lineage diversification in the developing mouse and human neocortex. *Sci Adv* 6: eabd2068, 2020. doi:[10.1126/sciadv.abd2068](https://doi.org/10.1126/sciadv.abd2068).
- ▶ 72. Johnson MB, Wang PP, Atabay KD, Murphy EA, Doan RN, Hecht JL, Walsh CA. Single-cell analysis reveals transcriptional heterogeneity of neural progenitors in human cortex. *Nat Neurosci* 18: 637–646, 2015. doi:[10.1038/nn.3980](https://doi.org/10.1038/nn.3980).
- ▶ 73. Johnson MB, Sun X, Kodani A, Borges-Monroy R, Girsakis KM, Ryu SC, Wang PP, Patel K, Gonzalez DM, Woo YM, Yan Z, Liang B, Smith RS, Chatterjee M, Coman D, Papademetris X, Staib LH, Hyder F, Mandeville JB, Grant PE, Im K, Kwak H, Engelhardt JF, Walsh CA, Bae BI. Aspm knockout ferret reveals an evolutionary mechanism governing cerebral cortical size. *Nature* 556: 370–375, 2018. doi:[10.1038/s41586-018-0035-0](https://doi.org/10.1038/s41586-018-0035-0).
- ▶ 74. Pollen AA, Nowakowski TJ, Chen J, Retallack H, Sandoval-Espinosa C, Nicholas CR, Shuga J, Liu SJ, Oldham MC, Diaz A, Lim DA, Leyrat AA, West JA, Kriegstein AR. Molecular identity of human outer radial glia during cortical development. *Cell* 163: 55–67, 2015. doi:[10.1016/j.cell.2015.09.004](https://doi.org/10.1016/j.cell.2015.09.004).
- ▶ 75. Nowakowski TJ, Bhaduri A, Pollen AA, Alvarado B, Mostajo-Radji MA, Lullo ED, Haeussler M, Sandoval-Espinosa C, Liu SJ, Velmeshev D, Ounadjela JR, Shuga J, Wang X, Lim DA, West JA, Leyrat AA, Kent WJ, Kriegstein AR. Spatiotemporal gene expression trajectories reveal developmental hierarchies of the human cortex. *Science* 358: 1318–1323, 2017. doi:[10.1126/science.aap8809](https://doi.org/10.1126/science.aap8809).
- ▶ 76. Yoshimatsu T, Kawaguchi D, Oishi K, Takeda K, Akira S, Masuyama N, Gotoh Y. Non-cell-autonomous action of STAT3 in maintenance of neural precursor cells in the mouse neocortex. *Development* 133: 2553–2563, 2006. doi:[10.1242/dev.02419](https://doi.org/10.1242/dev.02419).
- ▶ 77. Rash BG, Lim HD, Breunig JJ, Vaccarino FM, Lim HD, Breunig JJ, Vaccarino FM. FGF signaling expands embryonic cortical surface area by regulating notch-dependent neurogenesis. *J Neurosci* 31: 15604–15617, 2011. doi:[10.1523/JNEUROSCI.4439-11.2011](https://doi.org/10.1523/JNEUROSCI.4439-11.2011).
- ▶ 78. Raballo R, Rhee J, Lyn-Cook R, Leckman JF, Schwartz ML, Vaccarino FM. Basic fibroblast growth factor (Fgf2) is necessary for cell proliferation and neurogenesis in the developing cerebral cortex. *J Neurosci* 20: 5012–5023, 2000. doi:[10.1523/JNEUROSCI.20-13-05012.2000](https://doi.org/10.1523/JNEUROSCI.20-13-05012.2000).
- ▶ 79. Lukaszewicz A, Savatier P, Cortay V, Kennedy H, Dehay C. Contrasting effects of basic fibroblast growth factor and neurotrophin 3 on cell cycle kinetics of mouse cortical stem cells. *J Neurosci* 22: 6610–6622, 2002. doi:[10.1523/JNEUROSCI.22-15-06610.2002](https://doi.org/10.1523/JNEUROSCI.22-15-06610.2002).
- ▶ 80. Rash BG, Tomasi S, Lim HD, Suh CY, Vaccarino FM. Cortical gyrification induced by fibroblast growth factor 2 in the mouse brain. *J Neurosci* 33: 10802–10814, 2013. doi:[10.1523/JNEUROSCI.3621-12.2013](https://doi.org/10.1523/JNEUROSCI.3621-12.2013).
- ▶ 81. Masuda K, Toda T, Shinmyo Y, Ebisu H, Hoshiba Y, Wakimoto M, Ichikawa Y, Kawasaki H. Pathophysiological analyses of cortical malformation using gyrencephalic mammals. *Sci Rep* 5: 15370, 2015. doi:[10.1038/srep15370](https://doi.org/10.1038/srep15370).
- ▶ 82. Mairet-Coello G, Tury A, DiCicco-Bloom E. Insulin-like growth factor-1 promotes G(1)/S cell cycle progression through bidirectional regulation of cyclins and cyclin-dependent kinase inhibitors via the phosphatidylinositol 3-kinase/Akt pathway in developing rat cerebral cortex. *J Neurosci* 29: 775–788, 2009. doi:[10.1523/JNEUROSCI.1700-08.2009](https://doi.org/10.1523/JNEUROSCI.1700-08.2009).
- ▶ 83. Lange C, Huttner WB, Calegari F. Cdk4/CyclinD1 overexpression in neural stem cells shortens G1, delays neurogenesis, and promotes the generation and expansion of basal progenitors. *Cell Stem Cell* 5: 320–331, 2009. doi:[10.1016/j.stem.2009.05.026](https://doi.org/10.1016/j.stem.2009.05.026).
- ▶ 84. Nonaka-Kinoshita M, Reillo I, Artegiani B, Ángeles Martínez-Martínez M, Nelson M, Borrell VV, Calegari F. Regulation of cerebral cortex size and folding by expansion of basal progenitors. *EMBO J* 32: 1817–1828, 2013. doi:[10.1038/emboj.2013.96](https://doi.org/10.1038/emboj.2013.96).
- ▶ 85. Machon O, van den Bout CJ, Backman M, Kemler R, Krauss S. Role of beta-catenin in the developing cortical and hippocampal neuroepithelium. *Neuroscience* 122: 129–143, 2003. doi:[10.1016/S0306-4522\(03\)00519-0](https://doi.org/10.1016/S0306-4522(03)00519-0).
- ▶ 86. Siegenthaler JA, Ashique AM, Zarbalis K, Patterson KP, Hecht JH, Kane MA, Folias AE, Choe Y, May SR, Kume T, Napoli JL, Peterson AS, Pleasure SJ. Retinoic acid from the meninges regulates cortical neuron generation. *Cell* 139: 597–609, 2009. doi:[10.1016/j.cell.2009.10.004](https://doi.org/10.1016/j.cell.2009.10.004).
- ▶ 87. Fernandez V, Llinares-Benadero C, Borrell V, Fernández V, Llinares-Benadero C, Borrell V. Cerebral cortex expansion and folding: what



- have we learned? *EMBO J* 35: 1021–1044, 2016. doi:[10.15252/embj.201593701](https://doi.org/10.15252/embj.201593701).
- ▶ 88. Taverna E, Goetz M, Huttner WB. The cell biology of neurogenesis: toward an understanding of the development and evolution of the neocortex. *Annu Rev Cell Dev Biol* 30: 465–502, 2014. doi:[10.1146/annurev-cellbio-101011-155801](https://doi.org/10.1146/annurev-cellbio-101011-155801).
- ▶ 89. Borrell V, Cárdenas A, Ciceri G, Galcerán J, Flames N, Pla R, No, brega-Pereira S, García-Frigola C, Peregrín S, Zhao Z, Ma L, Tessier-Lavigne M, Marín O. Slit/Robo signaling modulates the proliferation of central nervous system progenitors. *Neuron* 76: 338–352, 2012. doi:[10.1016/j.neuron.2012.08.003](https://doi.org/10.1016/j.neuron.2012.08.003).
- ▶ 90. Phoenix TN, Temple S. Spred1, a negative regulator of Ras-MAPK-ERK, is enriched in CNS germinal zones, dampens NSC proliferation, and maintains ventricular zone structure. *Genes Dev* 24: 45–56, 2010. doi:[10.1101/gad.1839510](https://doi.org/10.1101/gad.1839510).
- ▶ 91. Bultje RS, Castaneda-Castellanos DR, Jan LY, Jan YN, Kriegstein AR, Shi SH. Mammalian Par3 regulates progenitor cell asymmetric division via notch signaling in the developing neocortex. *Neuron* 63: 189–202, 2009. doi:[10.1016/j.neuron.2009.07.004](https://doi.org/10.1016/j.neuron.2009.07.004).
- ▶ 92. Costa MR, Wen G, Lepier A, Schroeder T, Goetz M. Par-complex proteins promote proliferative progenitor divisions in the developing mouse cerebral cortex. *Development* 135: 11–22, 2008. doi:[10.1242/dev.009951](https://doi.org/10.1242/dev.009951).
- ▶ 93. Cappello S, Attardo A, Wu X, Iwasato T, Itohara S, Wilsch-Brauninger M, Eilken HM, Rieger MA, Schroeder TT, Huttner WB, Brakebusch C, Goetz M. The Rho-GTPase cdc42 regulates neural progenitor fate at the apical surface. *Nat Neurosci* 9: 1099–1107, 2006. doi:[10.1038/nn1744](https://doi.org/10.1038/nn1744).
- ▶ 94. Yokota Y, Eom TY, Stanco A, Kim WY, Rao S, Snider WD, Anton ES. Cdc42 and Gsk3 modulate the dynamics of radial glial growth, inter-radial glial interactions and polarity in the developing cerebral cortex. *Development* 137: 4101–4110, 2010. doi:[10.1242/dev.048637](https://doi.org/10.1242/dev.048637).
- ▶ 95. Ohata S, Aoki R, Kinoshita S, Yamaguchi M, Tsuruoka-Kinoshita S, Tanaka H, Wada H, Watabe S, Tsuboi T, Masai I, Okamoto H. Dual roles of Notch in regulation of apically restricted mitosis and apico-basal polarity of neuroepithelial cells. *Neuron* 69: 215–230, 2011. doi:[10.1016/j.neuron.2010.12.026](https://doi.org/10.1016/j.neuron.2010.12.026).
- ▶ 96. Cárdenas A, Villalba A, de Juan Romero C, Pico, E, Kyrousi C, Tzika AC, Tessier-Lavigne M, Ma L, Drukker M, Cappello S, Borrell V. Evolution of cortical neurogenesis in amniotes controlled by robo signaling levels. *Cell* 174: 590–606.e21, 2018. doi:[10.1016/j.cell.2018.06.007](https://doi.org/10.1016/j.cell.2018.06.007).
- ▶ 97. Wong FK, Fei JF, Mora-Bermudez F, Taverna E, Haffner C, Fu J, Anastassiadis K, Stewart AF, Huttner WB. Sustained Pax6 expression generates primate-like basal radial glia in developing mouse neocortex. *PLoS Biol* 13: e1002217, 2015. doi:[10.1371/journal.pbio.1002217](https://doi.org/10.1371/journal.pbio.1002217).
- ▶ 98. Tavano S, Taverna E, Kalebic N, Haffner C, Namba T, Dahl A, Wilsch-Brauninger M, Paridaen JT, Huttner WB. Insm1 induces neural progenitor delamination in developing neocortex via downregulation of the adherens junction belt-specific protein Plekha7. *Neuron* 97: 1299–1314.e8, 2018. doi:[10.1016/j.neuron.2018.01.052](https://doi.org/10.1016/j.neuron.2018.01.052).
- ▶ 99. Camargo Ortega G, Falk S, Johansson PA, Peyre E, Broix L, Sahu SK, Hirst W, Schlichthaerle T, De Juan Romero C, Draganova K, Vinopal S, Chinnappa K, Gavranovic A, Karakaya T, Steininger T, Merl-Pham J, Feederle R, Shao W, Shi SH, Hauck SM, Jungmann R, Bradke F, Borrell V, Geerlof A, Reber S, Tiwari VK, Huttner WB, Wilsch-Brauninger M, Nguyen L, Goetz M. The centrosome protein AKNA regulates neurogenesis via microtubule organization. *Nature* 567: 113–117, 2019. doi:[10.1038/s41586-019-0962-4](https://doi.org/10.1038/s41586-019-0962-4).
- ▶ 100. Kawae T, Shitamukai A, Nagasaka A, Tsunekawa Y, Shinoda T, Saito K, Terada R, Bilgic M, Miyata T, Matsuzaki F, Kawaguchi A. Lzts1 controls both neuronal delamination and outer radial glial-like cell generation during mammalian cerebral development. *Nat Commun* 10: 2780, 2019. doi:[10.1038/s41467-019-10730-y](https://doi.org/10.1038/s41467-019-10730-y).
- ▶ 101. Postiglione MP, Jueschke C, Xie Y, Haas GA, Charalambous C, Knoblich JA. Mouse inscuteable induces apical-basal spindle orientation to facilitate intermediate progenitor generation in the developing neocortex. *Neuron* 72: 269–284, 2011. doi:[10.1016/j.neuron.2011.09.022](https://doi.org/10.1016/j.neuron.2011.09.022).
- ▶ 102. Wang L, Hou S, Han YG. Hedgehog signaling promotes basal progenitor expansion and the growth and folding of the neocortex. *Nat Neurosci* 19: 888–896, 2016. doi:[10.1038/nn.4307](https://doi.org/10.1038/nn.4307).
- ▶ 103. Guillemot F. Spatial and temporal specification of neural fates by transcription factor codes. *Development* 134: 3771–3780, 2007. doi:[10.1242/dev.006379](https://doi.org/10.1242/dev.006379).
- ▶ 104. Woodhead GJ, Mutch CA, Olson EC, Chenn A. Cell-autonomous beta-catenin signaling regulates cortical precursor proliferation. *J Neurosci* 26: 12620–12630, 2006. doi:[10.1523/JNEUROSCI.3180-06.2006](https://doi.org/10.1523/JNEUROSCI.3180-06.2006).
- ▶ 105. Zhou CJ, Borello U, Rubenstein JL, Pleasure SJ. Neuronal production and precursor proliferation defects in the neocortex of mice with loss of function in the canonical Wnt signaling pathway. *Neuroscience* 142: 1119–1131, 2006. doi:[10.1016/j.neuroscience.2006.07.007](https://doi.org/10.1016/j.neuroscience.2006.07.007).
- ▶ 106. Hirabayashi Y, Itoh Y, Tabata H, Nakajima K, Akiyama T, Masuyama N, Gotoh Y. The Wnt/b-catenin pathway directs neuronal differentiation of cortical neural precursor cells. *Development* 131: 2791–2801, 2004. doi:[10.1242/dev.01165](https://doi.org/10.1242/dev.01165).
- ▶ 107. Munji RN, Choe Y, Li G, Siegenthaler JA, Pleasure SJ. Wnt signaling regulates neuronal differentiation of cortical intermediate progenitors. *J Neurosci* 31: 1676–1687, 2011. doi:[10.1523/JNEUROSCI.5404-10.2011](https://doi.org/10.1523/JNEUROSCI.5404-10.2011).
- ▶ 108. Li W, Cogswell CA, LoTurco JJ. Neuronal differentiation of precursors in the neocortical ventricular zone is triggered by BMP. *J Neurosci* 18: 8853–8862, 1998. doi:[10.1523/JNEUROSCI.18-21-08853.1998](https://doi.org/10.1523/JNEUROSCI.18-21-08853.1998).
- ▶ 109. Buchsbaum IY, Kielkowski P, Giorgio G, O’Neill AC, Di Giaimo R, Kyrousi C, Khattak S, Sieber SA, Robertson SP, Cappello S. ECE2 regulates neurogenesis and neuronal migration during human cortical development. *EMBO Rep* 21: e48204, 2020. doi:[10.15252/embr.201948204](https://doi.org/10.15252/embr.201948204).
- ▶ 110. Voigt T. Development of glial cells in the cerebral wall of ferrets: direct tracing of their transformation from radial glia into astrocytes. *J Comp Neurol* 289: 74–88, 1989. doi:[10.1002/cne.902890106](https://doi.org/10.1002/cne.902890106).
- ▶ 111. Bonni A, Sun Y, Nadal-Vicens M, Bhatt A, Frank DA, Rozovsky I, Stahl N, Yancopoulos GD, Greenberg ME. Regulation of gliogenesis in the central nervous system by the JAK-STAT signaling pathway. *Science* 278: 477–483, 1997. doi:[10.1126/science.278.5337.477](https://doi.org/10.1126/science.278.5337.477).
- ▶ 112. Rajan P, McKay RD. Multiple routes to astrocytic differentiation in the CNS. *J Neurosci* 18: 3620–3629, 1998. doi:[10.1523/JNEUROSCI.18-10-03620.1998](https://doi.org/10.1523/JNEUROSCI.18-10-03620.1998).
- ▶ 113. Gross RE, Mehler MF, Mabie PC, Zang Z, Santschi L, Kessler JA. Bone morphogenetic proteins promote astroglial lineage commitment by mammalian subventricular zone progenitor cells. *Neuron* 17: 595–606, 1996. doi:[10.1016/S0896-6273\(00\)80193-2](https://doi.org/10.1016/S0896-6273(00)80193-2).

- ▶ 114. Martinez-Cerdeno V, Noctor SC, Kriegstein AR. The role of intermediate progenitor cells in the evolutionary expansion of the cerebral cortex. *Cereb Cortex* 16, *Suppl 1*: i152–61, 2006. doi:[10.1093/cercor/bhk017](https://doi.org/10.1093/cercor/bhk017).
- ▶ 115. Villalba A, Goetz M, Borrell V. In: *Current Topics in Developmental Biology*. New York: Academic Press Inc, vol 142, p. 1–66, 2021.
- ▶ 116. Sousa AM, Meyer KA, Santpere G, Gulden FO, Sestan N. Evolution of the human nervous system function, structure, and development. *Cell* 170: 226–247, 2017. doi:[10.1016/j.cell.2017.06.036](https://doi.org/10.1016/j.cell.2017.06.036).
- ▶ 117. Molnár Z, Meitner C, Stoykova A, Tarabykin V, Price DJ, Francis F, Meyer G, Dehay C, Kennedy H. Comparative aspects of cerebral cortical development. *Eur J Neurosci* 23: 921–934, 2006. doi:[10.1111/j.1460-9568.2006.04611.x](https://doi.org/10.1111/j.1460-9568.2006.04611.x).
- ▶ 118. Matsumoto N, Tanaka S, Horiike T, Shinmyo Y, Kawasaki H. A discrete subtype of neural progenitor crucial for cortical folding in the gyrencephalic mammalian brain. *Elife* 9: 1–26, 2020. doi:[10.7554/eLife.54873](https://doi.org/10.7554/eLife.54873).
- ▶ 119. Guven A, Kalebic N, Long KR, Florio M, Vaid S, Brandl H, Stenzel D, Huttner WB. Extracellular matrix-inducing Sox9 promotes both basal progenitor proliferation and gliogenesis in developing neocortex. *Elife* 9: e49808, 2020. doi:[10.7554/eLife.49808](https://doi.org/10.7554/eLife.49808).
- ▶ 120. Matsumoto N, Shinmyo Y, Ichikawa Y, Kawasaki H. Gyrification of the cerebral cortex requires FGF signaling in the mammalian brain. *Elife* 6: 1–20, 2017. doi:[10.7554/eLife.29285](https://doi.org/10.7554/eLife.29285).
- ▶ 121. Fietz SA, Lachmann R, Brandl H, Kircher M, Samusik N, Schroeder R, Lakshmanaperumal N, Henry I, Vogt J, Riehn A, Distler W, Nitsch R, Enard W, Paabo S, Huttner WB. Transcriptomes of germinal zones of human and mouse fetal neocortex suggest a role of extracellular matrix in progenitor self-renewal. *Proc Natl Acad Sci U S A* 109: 11836–11841, 2012. doi:[10.1073/pnas.1209647109](https://doi.org/10.1073/pnas.1209647109).
- ▶ 122. Stenzel D, Wilsch-Brauninger M, Wong FK, Heuer H, Huttner WB. Integrin avb3 and thyroid hormones promote expansion of progenitors in embryonic neocortex. *Development* 141: 795–806, 2014. doi:[10.1242/dev.101907](https://doi.org/10.1242/dev.101907).
- ▶ 123. Lui JH, Nowakowski TJ, Pollen AA, Javaherian A, Kriegstein AR, Oldham MC. Radial glia require PDGFR signaling in human but not mouse neocortex. *Nature* 515: 264–268, 2014. doi:[10.1038/nature13973](https://doi.org/10.1038/nature13973).
- ▶ 124. Rash BG, Duque A, Morozov YM, Arellano JI, Micali N, Rakic P. Gliogenesis in the outer subventricular zone promotes enlargement and gyrification of the primate cerebrum. *Proc Natl Acad Sci U S A* 116: 7089–7094, 2019. doi:[10.1073/pnas.1822169116](https://doi.org/10.1073/pnas.1822169116).
- ▶ 125. Stahl R, Walcher T, De Juan Romero C, Pilz GA, Cappello S, Irmeler M, Sanz-Aguela JM, Beckers J, Blum R, Borrell V, Goetz M. Trnp1 regulates expansion and folding of the mammalian cerebral cortex by control of radial glial fate. *Cell* 153: 535–549, 2013. doi:[10.1016/j.cell.2013.03.027](https://doi.org/10.1016/j.cell.2013.03.027).
- ▶ 126. De Juan Romero C, Bruder U, Tomasello JM, Sanz-Aguela VV, Borrell JM. Discrete domains of gene expression in germinal layers distinguish the development of gyrencephaly. *EMBO J* 34: 1859–1874, 2015. doi:[10.15252/embj.201591176](https://doi.org/10.15252/embj.201591176).
- ▶ 127. Bayatti N, Moss JA, Sun L, Ambrose P, Ward JF, Lindsay S, Clowry GJ. A molecular neuroanatomical study of the developing human neocortex from 8 to 17 postconceptional weeks revealing the early differentiation of the subplate and subventricular zone. *Cereb Cortex* 18: 1536–1548, 2008. doi:[10.1093/cercor/bhm184](https://doi.org/10.1093/cercor/bhm184).
- ▶ 128. Florio M, Namba T, Paabo S, Hiller M, Huttner WB. A single splice site mutation in human-specific ARHGAP11B causes basal progenitor amplification. *Sci Adv* 2: e1601941, 2016. doi:[10.1126/sciadv.1601941](https://doi.org/10.1126/sciadv.1601941).
- ▶ 129. Namba T, Do, czi J, Pinson A, Xing L, Kalebic N, Wilsch-Brauninger M, Long KR, Vaid S, Lauer J, Bogdanova A, Borgonovo B, Shevchenko A, Keller P, Drechsel D, Kurzchalia T, Wimberger P, Chinopoulos C, Huttner WB. Human-specific ARHGAP11B acts in mitochondria to expand neocortical progenitors by glutaminolysis. *Neuron* 105: 867–881.e9, 2020. doi:[10.1016/j.neuron.2019.11.027](https://doi.org/10.1016/j.neuron.2019.11.027).
- ▶ 130. Florio M, Albert M, Taverna E, Namba T, Brandl H, Lewitus E, Haffner C, Sykes A, Wong FK, Peters J, Guhr E, Klemroth S, Pruffer K, Kelso J, Naumann R, Nusslein I, Dahl A, Lachmann R, Paabo S, Huttner WB. Human-specific gene ARHGAP11B promotes basal progenitor amplification and neocortex expansion. *Science* 347: 1465–1470, 2015. doi:[10.1126/science.aaa1975](https://doi.org/10.1126/science.aaa1975).
- ▶ 131. Kalebic N, Gilardi C, Albert M, Namba T, Long KR, Kostic M, Langen B, Huttner WB. Human-specific ARHGAP11B induces hallmarks of neocortical expansion in developing ferret neocortex. *Elife* 7: e41241, 2018. doi:[10.7554/elife.41241](https://doi.org/10.7554/elife.41241).
- ▶ 132. Heide M, Haffner C, Murayama A, Kurotaki Y, Shinohara H, Okano H, Sasaki E, Huttner WB. Human-specific ARHGAP11B increases size and folding of primate neocortex in the fetal marmoset. *Science* 369: 546–550, 2020. doi:[10.1126/science.abb2401](https://doi.org/10.1126/science.abb2401).
- ▶ 133. Florio M, Heide M, Pinson A, Brandl H, Albert M, Winkler S, Wimberger P, Huttner WB, Hiller M. Evolution and cell-type specificity of human-specific genes preferentially expressed in progenitors of fetal neocortex. *Elife* 7: e32332, 2018. doi:[10.7554/elife.32332](https://doi.org/10.7554/elife.32332).
- ▶ 134. Fiddes IT, Lodewijk GA, Mooring M, Bosworth CM, Ewing AD, Mantalas GL, Novak AM, van den Bout A, Bishara A, Rosenkrantz JL, Lorig-Roach R, Field AR, Haeussler M, Russo L, Bhaduri A, Nowakowski TJ, Pollen AA, Dougherty ML, Nuttle X, Addor MC, Zwolinski S, Katzman S, Kriegstein A, Eichler EE, Salama SR, Jacobs FM, Haussler D. Human-specific NOTCH2NL genes affect notching and cortical neurogenesis. *Cell* 173: 1356–1369.e22, 2018. doi:[10.1016/j.cell.2018.03.051](https://doi.org/10.1016/j.cell.2018.03.051).
- ▶ 135. Suzuki IK, Gacquer D, Van Heurck R, Kumar D, Wojno M, Bilheu A, Herpoel A, Lambert N, Cheron J, Polleux F, Detours V, Vanderhaeghen P. Human-specific NOTCH2NL genes expand cortical neurogenesis through Delta/Notch regulation. *Cell* 173: 1370–1384.e16, 2018. doi:[10.1016/j.cell.2018.03.067](https://doi.org/10.1016/j.cell.2018.03.067).
- ▶ 136. Ju XC, Hou QQ, Sheng AL, Wu KY, Zhou Y, Jin Y, Wen T, Yang Z, Wang X, Luo ZG. The hominoid-specific gene TBC1D3 promotes generation of basal neural progenitors and induces cortical folding in mice. *Elife* 5: e18197, 2016. doi:[10.7554/elife.18197](https://doi.org/10.7554/elife.18197).
- ▶ 137. Dennis MY, Eichler EE. Human adaptation and evolution by segmental duplication. *Curr Opin Genet Dev* 41: 44–52, 2016. doi:[10.1016/j.gde.2016.08.001](https://doi.org/10.1016/j.gde.2016.08.001).
- ▶ 138. Marin O, Rubenstein JL. Cell migration in the forebrain. *Annu Rev Neurosci* 26: 441–483, 2003. doi:[10.1146/annurev.neuro.26.041002.131058](https://doi.org/10.1146/annurev.neuro.26.041002.131058).
- ▶ 139. Rakic P. Mode of cell migration to the superficial layers of fetal monkey neocortex. *J Comp Neurol* 145: 61–83, 1972. doi:[10.1002/cne.901450105](https://doi.org/10.1002/cne.901450105).
- ▶ 140. O’Leary DD, Borngasser D. Cortical ventricular zone progenitors and their progeny maintain spatial relationships and radial patterning during preplate development indicating an early Protomap. *Cereb Cortex* 16: i46–i56, 2006. doi:[10.1093/cercor/bhk019](https://doi.org/10.1093/cercor/bhk019).
- ▶ 141. Gupta A, Sanada K, Miyamoto DT, Rovelstad S, Nadarajah B, Pearlman AL, Brunstrom J, Tsai LH. Layering defect in p35 deficiency

- is linked to improper neuronal-glia interaction in radial migration. *Nat Neurosci* 6: 1284–1291, 2003. doi:[10.1038/nn1151](https://doi.org/10.1038/nn1151).
- ▶ 142. Miyata T, Kawaguchi A, Okano H, Ogawa M. Asymmetric inheritance of radial glial fibers by cortical neurons. *Neuron* 31: 727–741, 2001. doi:[10.1016/S0896-6273\(01\)00420-2](https://doi.org/10.1016/S0896-6273(01)00420-2).
- ▶ 143. Nadarajah B, Brunstrom JE, Grutzendler J, Wong RO, Pearlman AL. Two modes of radial migration in early development of the cerebral cortex. *Nat Neurosci* 4: 143–150, 2001. doi:[10.1038/83967](https://doi.org/10.1038/83967).
- ▶ 144. Tabata H, Nakajima K. Multipolar migration: the third mode of radial neuronal migration in the developing cerebral cortex. *J Neurosci* 23: 9996–10001, 2003. doi:[10.1523/JNEUROSCI.23-31-09996.2003](https://doi.org/10.1523/JNEUROSCI.23-31-09996.2003).
- ▶ 145. Silva CG, Peyre E, Nguyen L. Cell migration promotes dynamic cellular interactions to control cerebral cortex morphogenesis. *Nat Rev Neurosci* 20: 318–329, 2019. doi:[10.1038/s41583-019-0148-y](https://doi.org/10.1038/s41583-019-0148-y).
- ▶ 146. Nadarajah B, Parnavelas JG. Modes of neuronal migration in the developing cerebral cortex. *Nat Rev Neurosci* 3: 423–432, 2002. doi:[10.1038/nrn845](https://doi.org/10.1038/nrn845).
- ▶ 147. Lambert de Rouvroit C, Goffinet AM. Neuronal migration. *Mech Dev* 105: 47–56, 2001. doi:[10.1016/S0925-4773\(01\)00396-3](https://doi.org/10.1016/S0925-4773(01)00396-3).
- ▶ 148. Xie Z, Sanada K, Samuels BA, Shih H, Tsai LH. Serine 732 phosphorylation of FAK by Cdk5 is important for microtubule organization, nuclear movement, and neuronal migration. *Cell* 114: 469–482, 2003. doi:[10.1016/S0092-8674\(03\)00605-6](https://doi.org/10.1016/S0092-8674(03)00605-6).
- ▶ 149. Anton ES, Kreidberg JA, Rakic P. Distinct functions of alpha3 and alpha(v) integrin receptors in neuronal migration and laminar organization of the cerebral cortex. *Neuron* 22: 277–289, 1999. doi:[10.1016/S0896-6273\(00\)81089-2](https://doi.org/10.1016/S0896-6273(00)81089-2).
- ▶ 150. Elias LA, Wang DD, Kriegstein AR. Gap junction adhesion is necessary for radial migration in the neocortex. *Nature* 448: 901–907, 2007. doi:[10.1038/nature06063](https://doi.org/10.1038/nature06063).
- ▶ 151. Rakic P. Neuronal migration and contact guidance in the primate telencephalon. *Postgr Med J* 54: 25–40, 1978.
- ▶ 152. Anton ES, Marchionni MA, Lee KF, Rakic P. Role of GGF/neuregulin signaling in interactions between migrating neurons and radial glia in the developing cerebral cortex. *Development* 124: 3501–3510, 1997. doi:[10.1242/dev.124.18.3501](https://doi.org/10.1242/dev.124.18.3501).
- ▶ 153. del Toro D, Ruff T, Cederfjäll E, Villalba A, Seyit-Bremer G, Borrell V, Klein R. Regulation of cerebral cortex folding by controlling neuronal migration via FLRT adhesion molecules. *Cell* 169: 621–635.e16, 2017. doi:[10.1016/j.cell.2017.04.012](https://doi.org/10.1016/j.cell.2017.04.012).
- ▶ 154. Seiradake E, del Toro D, Nagel D, Cop F, Hartl R, Ruff T, Seyit-Bremer G, Harlos K, Border EC, Acker-Palmer A, Jones EY, Klein R. FLRT structure: balancing repulsion and cell adhesion in cortical and vascular development. *Neuron* 84: 370–385, 2014. doi:[10.1016/j.neuron.2014.10.008](https://doi.org/10.1016/j.neuron.2014.10.008).
- ▶ 155. del Toro D, Carrasquero-Ordaz MA, Chu A, Ruff T, Shahin M, Jackson VA, Chavent M, Berbeira-Santana M, Seyit-Bremer G, Brignani S, Kaufmann R, Lowe E, Klein R, Seiradake E. Structural basis of tenascin-R interaction in repulsive guidance of migrating neurons. *Cell* 180: 323–339.e19, 2020. doi:[10.1016/j.cell.2019.12.014](https://doi.org/10.1016/j.cell.2019.12.014).
- ▶ 156. Llinas-Benadero C, Borrell V. Deconstructing cortical folding: genetic, cellular and mechanical determinants. *Nat Rev Neurosci* 20: 161–176, 2019. doi:[10.1038/s41583-018-0112-2](https://doi.org/10.1038/s41583-018-0112-2).
- ▶ 157. Klyachko VA, Stevens CF. Connectivity optimization and the positioning of cortical areas. *Proc Natl Acad Sci U S A* 100: 7937–7941, 2003. doi:[10.1073/pnas.0932745100](https://doi.org/10.1073/pnas.0932745100).
- ▶ 158. Hilgetag CC, Barbas H. Role of mechanical factors in the morphology of the primate cerebral cortex. *PLoS Comput Biol* 2: e22, 2006. doi:[10.1371/journal.pcbi.0020022](https://doi.org/10.1371/journal.pcbi.0020022).
- ▶ 159. Welker W. In: *Cerebral Cortex*, edited by Peters A, Jones EG. New York: Plenum Press 1990, vol 8B, p. 3–136.
- ▶ 160. Barkovich AJ, Guerrini R, Kuzniecky RI, Jackson GD, Dobyns WB. A developmental and genetic classification for malformations of cortical development: update 2012. *Brain* 135: 1348–1369, 2012. doi:[10.1093/brain/aws019](https://doi.org/10.1093/brain/aws019).
- ▶ 161. van Essen DC. A 2020 view of tension-based cortical morphogenesis. *Proc Natl Acad Sci U S A* 117: 32868–32879, 2020. doi:[10.1073/pnas.2016830117](https://doi.org/10.1073/pnas.2016830117).
- ▶ 162. Van Essen DC. A tension-based theory of morphogenesis and compact wiring in the central nervous system. *Nature* 385: 313–318, 1997. doi:[10.1038/385313a0](https://doi.org/10.1038/385313a0).
- ▶ 163. Xu G, Knutsen AK, Dikranian K, Kroenke CD, Bayly PV, Taber LA. Axons pull on the brain, but tension does not drive cortical folding. *J Biomech Eng* 132: 71013, 2010. doi:[10.1115/1.4001683](https://doi.org/10.1115/1.4001683).
- ▶ 164. Richman DP, Stewart RM, Hutchinson JW, Caviness VS Jr. Mechanical model of brain convolitional development. *Science* 189: 18–21, 1975. doi:[10.1126/science.1135626](https://doi.org/10.1126/science.1135626).
- ▶ 165. Toro R, Burnod Y. A morphogenetic model for the development of cortical convolutions. *Cereb Cortex* 15: 1900–1913, 2005. doi:[10.1093/cercor/bhi068](https://doi.org/10.1093/cercor/bhi068).
- ▶ 166. Tallinen T, Chung JY, Biggins JS, Mahadevan L. Gyrfication from constrained cortical expansion. *Proc Natl Acad Sci U S A* 111: 12667–12672, 2014. doi:[10.1073/pnas.1406015111](https://doi.org/10.1073/pnas.1406015111).
- ▶ 167. Tallinen T, Chung JY, Rousseau F, Girard N, Lefèvre J, Mahadevan L. On the growth and form of cortical convolutions. *Nature Phys* 12: 588–593, 2016. doi:[10.1038/nphys3632](https://doi.org/10.1038/nphys3632).
- ▶ 168. Garcia KE, Kroenke CD, Bayly PV. Mechanics of cortical folding: stress, growth and stability. *Philos Trans R Soc L. B Biol Sci* 373: 20170321, 2018. doi:[10.1098/rstb.2017.0321](https://doi.org/10.1098/rstb.2017.0321).
- ▶ 169. Kroenke CD, Bayly PV. How forces fold the cerebral cortex. *J Neurosci* 38: 767–775, 2018. doi:[10.1523/JNEUROSCI.1105-17.2017](https://doi.org/10.1523/JNEUROSCI.1105-17.2017).
- ▶ 170. Long KR, Newland B, Florio M, Kalebic N, Langen B, Kolterer A, Wimberger P, Huttner WB. Extracellular matrix components HAPLN1, lumican, and collagen I cause hyaluronic acid-dependent folding of the developing human neocortex. *Neuron* 99: 702–719, 2018. doi:[10.1016/j.neuron.2018.07.013](https://doi.org/10.1016/j.neuron.2018.07.013).
- ▶ 171. Long KR, Huttner WB. How the extracellular matrix shapes neural development. *Open Biol* 9: 180216, 2019. doi:[10.1098/rsob.180216](https://doi.org/10.1098/rsob.180216).
- ▶ 172. Wang XX, Studholme C, Grigsby PL, Frias AE, Cuzon Carlson VC, Kroenke CD, Verginia X, Carlson CC, Christopher X, Kroenke CD. Folding, but not surface area expansion, is associated with cellular morphological maturation in the fetal cerebral cortex. *J Neurosci* 37: 1971–1983, 2017. doi:[10.1523/JNEUROSCI.3157-16.2017](https://doi.org/10.1523/JNEUROSCI.3157-16.2017).
- ▶ 173. Callaway EM, Borrell V. Developmental sculpting of dendritic morphology of layer 4 neurons in visual cortex: influence of retinal input. *J Neurosci* 31: 7456–7470, 2011. doi:[10.1523/JNEUROSCI.5222-10.2011](https://doi.org/10.1523/JNEUROSCI.5222-10.2011).
- ▶ 174. Borrell V, Callaway EM. Reorganization of exuberant axonal arbors contributes to the development of laminar specificity in ferret visual cortex. *J Neurosci* 22: 6682–6695, 2002. doi:[10.1523/JNEUROSCI.22-15-06682.2002](https://doi.org/10.1523/JNEUROSCI.22-15-06682.2002).

- ▶ 175. Striedter GF, Srinivasan S, Monuki ES. Cortical folding: when, where, how, and why? *Annu Rev Neurosci* 38: 291–307, 2015. doi:[10.1146/annurev-neuro-071714-034128](https://doi.org/10.1146/annurev-neuro-071714-034128).
- ▶ 176. Bayer SA, Altman J, The Human Brain during the Second Trimester. New York: CRC Press, 2005, vol 3.
- ▶ 177. Smart IH, McSherry GM. Gyrus formation in the cerebral cortex of the ferret. II. Description of the internal histological changes. *J Anat* 147: 27–43, 1986.
- ▶ 178. Kawasaki H, Toda T, Tanno K. In vivo genetic manipulation of cortical progenitors in gyrencephalic carnivores using in utero electroporation. *Biol Open* 2: 95–100, 2013. doi:[10.1242/bio.20123160](https://doi.org/10.1242/bio.20123160).
- ▶ 179. Zilles K, Armstrong E, Moser KH, Schleicher A, Stephan H. Gyrification in the cerebral cortex of primates. *Brain Behav Evol* 34: 143–150, 1989. doi:[10.1159/000116500](https://doi.org/10.1159/000116500).
- ▶ 180. Poluch S, Juliano SL. Fine-tuning of neurogenesis is essential for the evolutionary expansion of the cerebral cortex. *Cereb Cortex* 25: 346–364, 2015. doi:[10.1093/cercor/bht232](https://doi.org/10.1093/cercor/bht232).
- ▶ 181. Toda T, Shinmyo Y, Dinh Duong TA, Masuda K, Kawasaki H. An essential role of SVZ progenitors in cortical folding in gyrencephalic mammals. *Sci Rep* 6: 29578, 2016. doi:[10.1038/srep29578](https://doi.org/10.1038/srep29578).
- ▶ 182. Tang H, Hammack C, Ogden SC, Wen Z, Qian X, Li Y, Yao B, Shin J, Zhang F, Lee EM, Christian KM, Didier RA, Jin P, Song H, Ming GL. Zika virus infects human cortical neural progenitors and attenuates their growth. *Cell Stem Cell* 18: 587–590, 2016. doi:[10.1016/j.stem.2016.02.016](https://doi.org/10.1016/j.stem.2016.02.016).
- ▶ 183. Li C, Xu D, Ye Q, Hong S, Jiang Y, Liu X, Zhang N, Shi L, Qin CF, Xu Z. Zika virus disrupts neural progenitor development and leads to microcephaly in mice. *Cell Stem Cell* 19: 120–126, 2016. doi:[10.1016/j.stem.2016.04.017](https://doi.org/10.1016/j.stem.2016.04.017).
- ▶ 184. Kornack DR, Rakic P. Radial and horizontal deployment of clonally related cells in the primate neocortex: relationship to distinct mitotic lineages. *Neuron* 15: 311–321, 1995. doi:[10.1016/0896-6273\(95\)90036-5](https://doi.org/10.1016/0896-6273(95)90036-5).
- ▶ 185. Walsh CA, Cepko CL. Clonally related cortical cells show several migration patterns. *Science* 241: 1342–1345, 1988. doi:[10.1126/science.3137660](https://doi.org/10.1126/science.3137660).
- ▶ 186. Rakic P, Stensas LJ, Sayre E, Sidman RL. Computer-aided three-dimensional reconstruction and quantitative analysis of cells from serial electron microscopic montages of foetal monkey brain. *Nature* 250: 31–34, 1974. doi:[10.1038/250031a0](https://doi.org/10.1038/250031a0).
- ▶ 187. Martínez-Martínez MÁ, Cicero G, Espino, S A, Fernández V, Marín O, Borrell V. Extensive branching of radially-migrating neurons in the mammalian cerebral cortex. *J Comp Neurol* 527: 1558–1576, 2019. doi:[10.1002/cne.24597](https://doi.org/10.1002/cne.24597).
- ▶ 188. Cortay V, Delaunay D, Patti D, Gautier E, Doerflinger N, Giroud P, Knoblauch K, Huissoud C, Kennedy H, Dehay C. Radial migration dynamics is modulated in a laminar and area-specific manner during primate corticogenesis. *Front Cell Dev Biol* 8: 1108, 2020. doi:[10.3389/fcell.2020.588814](https://doi.org/10.3389/fcell.2020.588814).
- ▶ 189. Lohmann G, von Cramon DY, Colchester AC. Deep sulcal landmarks provide an organizing framework for human cortical folding. *Cereb Cortex* 18: 1415–1420, 2008. doi:[10.1093/cercor/bhm174](https://doi.org/10.1093/cercor/bhm174).
- ▶ 190. Dubois J, Benders M, Cachia A, Lazeyras F, Ha-Vinh Leuchter R, Sizonenko SV, Borradori-Tolsa C, Mangin JF, Huppi PS. Mapping the early cortical folding process in the preterm newborn brain. *Cereb Cortex* 18: 1444–1454, 2008. doi:[10.1093/cercor/bhm180](https://doi.org/10.1093/cercor/bhm180).
- ▶ 191. Yun HJ, Vasung L, Tarui T, Rollins CK, Ortinau CM, Grant PE, Im K. Temporal patterns of emergence and spatial distribution of sulcal pits during fetal life. *Cereb Cortex* 30: 4257–4268, 2020. doi:[10.1093/cercor/bhaa053](https://doi.org/10.1093/cercor/bhaa053).
- ▶ 192. Lohmann G, von Cramon DY, Steinmetz H. Sulcal variability of twins. *Cereb Cortex* 9: 754–763, 1999. doi:[10.1093/cercor/9.7.754](https://doi.org/10.1093/cercor/9.7.754).
- ▶ 193. de Juan Romero C, Borrell V. Genetic maps and patterns of cerebral cortex folding. *Curr Opin Cell Biol* 49: 31–37, 2017. doi:[10.1016/j.ceb.2017.11.009](https://doi.org/10.1016/j.ceb.2017.11.009).
- ▶ 194. Cadwell CR, Bhaduri A, Mostajo-Radji MA, Keefe MG, Nowakowski TJ. Development and arealization of the cerebral cortex. *Neuron* 103: 980–1004, 2019. doi:[10.1016/j.neuron.2019.07.009](https://doi.org/10.1016/j.neuron.2019.07.009).
- ▶ 195. Rubenstein JL, Anderson S, Shi L, Miyashita-Lin E, Bulfone A, Hevner R. Genetic control of cortical regionalization and connectivity. *Cereb Cortex* 9: 524–532, 1999. doi:[10.1093/cercor/9.6.524](https://doi.org/10.1093/cercor/9.6.524).
- ▶ 196. Geschwind DH, Rakic P. Cortical evolution: judge the brain by its cover. *Neuron* 80: 633–647, 2013. doi:[10.1016/j.neuron.2013.10.045](https://doi.org/10.1016/j.neuron.2013.10.045).
- ▶ 197. Larkum ME, Waters J, Sakmann B, Helmchen F. Dendritic spikes in apical dendrites of neocortical layer 2/3 pyramidal neurons. *J Neurosci* 27: 8999–9008, 2007. doi:[10.1523/JNEUROSCI.1717-07.2007](https://doi.org/10.1523/JNEUROSCI.1717-07.2007).
- ▶ 198. Romero CD, Borrell V. Coevolution of radial glial cells and the cerebral cortex. *Glia* 63: 1303–1319, 2015. doi:[10.1002/glia.22827](https://doi.org/10.1002/glia.22827).
- ▶ 199. Heuer K, Gulban OF, Bazin PL, Osoianu A, Valabregue R, Santin M, Herbin M, Toro R. Evolution of neocortical folding: a phylogenetic comparative analysis of MRI from 34 primate species. *Cortex* 118: 275–291, 2019. doi:[10.1016/j.cortex.2019.04.011](https://doi.org/10.1016/j.cortex.2019.04.011).
- ▶ 200. O’Leary MA, Bloch JI, Flynn JJ, Gaudin TJ, Giallombardo A, Giannini NP, Goldberg SL, Kraatz BP, Luo ZX, Meng J, Ni X, Novacek MJ, Perini FA, Randall ZS, Rougier GW, Sargis EJ, Silcox MT, Simmons NB, Spaulding M, Velasco PM, Weksler M, Wible JR, Cirranello AL. The placental mammal ancestor and the post-K-Pg radiation of placentals. *Science* 339: 662–667, 2013. doi:[10.1126/science.1229237](https://doi.org/10.1126/science.1229237).
- ▶ 201. Bininda-Emonds OR, Cardillo M, Jones KE, MacPhee RD, Beck RM, Grenyer R, Price SA, Vos RA, Gittleman JL, Purvis A. The delayed rise of present-day mammals. *Nature* 446: 507–512, 2007. doi:[10.1038/nature05634](https://doi.org/10.1038/nature05634).
- ▶ 202. Lewitus E, Kelava I, Kalinka AT, Tomancak P, Huttner WB. An adaptive threshold in mammalian neocortical evolution. *PLoS Biol* 12: e1002000, 2014. doi:[10.1371/journal.pbio.1002000](https://doi.org/10.1371/journal.pbio.1002000).
- ▶ 203. Zilles K, Armstrong E, Schleicher A, Kretschmann HJ. The human pattern of gyrification in the cerebral cortex. *Anat Embryol (Berl)* 179: 173–179, 1988. doi:[10.1007/BF00304699](https://doi.org/10.1007/BF00304699).
- ▶ 204. Zilles K, Palomero-Gallagher N, Amunts K. Development of cortical folding during evolution and ontogeny. *Trends Neurosci* 36: 275–284, 2013. doi:[10.1016/j.tins.2013.01.006](https://doi.org/10.1016/j.tins.2013.01.006).
- ▶ 205. Kazu RS, Maldonado J, Mota B, Manger PR, Herculano-Houzel S. Cellular scaling rules for the brain of Artiodactyla include a highly folded cortex with few neurons. *Front Neuroanat* 8: 128, 2014. doi:[10.3389/fnana.2014.00128](https://doi.org/10.3389/fnana.2014.00128).
- ▶ 206. Mota B, Herculano-Houzel S. Cortical folding scales universally with surface area and thickness, not number of neurons. *Science* 349: 74–77, 2015. doi:[10.1126/science.aaa9101](https://doi.org/10.1126/science.aaa9101).
- ▶ 207. Lewitus E, Kelava I, Huttner WB. Conical expansion of the outer subventricular zone and the role of neocortical folding in evolution and

- development. *Front Hum Neurosci* 7: 424, 2013. doi:[10.3389/fnhum.2013.00424](https://doi.org/10.3389/fnhum.2013.00424).
- ▶208. Florio M, Borrell V, Huttner WB. Human-specific genomic signatures of neocortical expansion. *Curr Opin Neurobiol* 42: 33–44, 2017. doi:[10.1016/j.conb.2016.11.004](https://doi.org/10.1016/j.conb.2016.11.004).
209. Klingler E, Francis F, Jabaudon D, Cappello S. Mapping the molecular and cellular complexity of cortical malformations. *Science* 371: eaba4517, 2021. doi:[10.1126/science.aba4517](https://doi.org/10.1126/science.aba4517).
- ▶210. True JR, Carroll SB. Gene co-option in physiological and morphological evolution. *Annu Rev Cell Dev Biol* 18: 53–80, 2002. doi:[10.1146/annurev.cellbio.18.020402.140619](https://doi.org/10.1146/annurev.cellbio.18.020402.140619).
- ▶211. Dorus S, Vallender EJ, Evans PD, Anderson JR, Gilbert SL, Mahowald M, Wyckoff GJ, Malcom CM, Lahn BT. Accelerated evolution of nervous system genes in the origin of *Homo sapiens*. *Cell* 119: 1027–1040, 2004. doi:[10.1016/j.cell.2004.11.040](https://doi.org/10.1016/j.cell.2004.11.040).
- ▶212. Evans PD, Anderson JR, Vallender EJ, Gilbert SL, Malcom CM, Dorus S, Lahn BT. Adaptive evolution of ASPM, a major determinant of cerebral cortical size in humans. *Hum Mol Genet* 13: 489–494, 2004. doi:[10.1093/hmg/ddh055](https://doi.org/10.1093/hmg/ddh055).
- ▶213. Pollard KS, Salama SR, Lambert N, Lambot MA, Coppens S, Pedersen JS, Katzman S, King B, Onodera C, Siepel A, Kern AD, Dehay C, Igel H, Ares M Jr, Vanderhaeghen P, Haussler D. An RNA gene expressed during cortical development evolved rapidly in humans. *Nature* 443: 167–172, 2006. doi:[10.1038/nature05113](https://doi.org/10.1038/nature05113).
- ▶214. Arcila ML, Betizeau M, Cambronne XA, Guzman E, Doerflinger N, Bouhallier F, Zhou H, Wu B, Rani N, Bassett DS, Borello U, Huissoud C, Goodman RH, Dehay C, Kosik KS. Novel primate miRNAs coevolved with ancient target genes in germinal zone-specific expression patterns. *Neuron* 81: 1255–1262, 2014. doi:[10.1016/j.neuron.2014.01.017](https://doi.org/10.1016/j.neuron.2014.01.017).
- ▶215. Evans PD, Gilbert SL, Mekel-Bobrov N, Vallender EJ, Anderson JR, Vaez-Azizi LM, Tishkoff SA, Hudson RR, Lahn BT. Microcephalin, a gene regulating brain size, continues to evolve adaptively in humans. *Science* 309: 1717–1720, 2005. doi:[10.1126/science.1113722](https://doi.org/10.1126/science.1113722).
- ▶216. Mekel-Bobrov N, Gilbert SL, Evans PD, Vallender EJ, Anderson JR, Hudson RR, Tishkoff SA, Lahn BT. Ongoing adaptive evolution of ASPM, a brain size determinant in *Homo sapiens*. *Science* 309: 1720–1722, 2005. doi:[10.1126/science.1116815](https://doi.org/10.1126/science.1116815).
- ▶217. Enard W, Khaitovich P, Klose J, Zollner S, Heissig F, Giavalisco P, Nieselt-Struwe K, Muchmore E, Varki A, Ravid R, Doxiadis GM, Bontrop RE, Paabo S. Intra- and interspecific variation in primate gene expression patterns. *Science* 296: 340–343, 2002. doi:[10.1126/science.1068996](https://doi.org/10.1126/science.1068996).
- ▶218. Enard W, Przeworski M, Fisher SE, Lai CS, Wiebe V, Kitano T, Monaco AP, Paabo S. Molecular evolution of FOXP2, a gene involved in speech and language. *Nature* 418: 869–872, 2002. doi:[10.1038/nature01025](https://doi.org/10.1038/nature01025).
- ▶219. Vallender EJ, Mekel-Bobrov N, Lahn BT. Genetic basis of human brain evolution. *Trends Neurosci* 31: 637–644, 2008. doi:[10.1016/j.tins.2008.08.010](https://doi.org/10.1016/j.tins.2008.08.010).
- ▶220. Eichler EE, Frazer KA. The nature, pattern and function of human sequence variation. *Genome Biol* 5: 318, 2004. doi:[10.1186/gb-2004-5-4-318](https://doi.org/10.1186/gb-2004-5-4-318).
- ▶221. Hurler M. Gene duplication: the genomic trade in spare parts. *PLoS Biol* 2: E206, 2004. doi:[10.1371/journal.pbio.0020206](https://doi.org/10.1371/journal.pbio.0020206).
- ▶222. Dougherty ML, Nuttle X, Penn O, Nelson BJ, Huddleston J, Baker C, Harshman L, Duyzend MH, Ventura M, Antonacci F, Sandstrom R, Dennis MY, Eichler EE. The birth of a human-specific neural gene by incomplete duplication and gene fusion. *Genome Biol* 18: 49, 2017. doi:[10.1186/s13059-017-1163-9](https://doi.org/10.1186/s13059-017-1163-9).
- ▶223. Nord AS, Pattabiraman K, Visel A, Rubenstein JL. Genomic perspectives of transcriptional regulation in forebrain development. *Neuron* 85: 27–47, 2015. doi:[10.1016/j.neuron.2014.11.011](https://doi.org/10.1016/j.neuron.2014.11.011).
- ▶224. Pollard KS, Salama SR, King B, Kern AD, Dreszer T, Katzman S, Siepel A, Pedersen JS, Bejerano G, Baertsch R, Rosenbloom KR, Kent J, Haussler D. Forces shaping the fastest evolving regions in the human genome. *PLoS Genet* 2: e168, 2006. doi:[10.1371/journal.pgen.0020168](https://doi.org/10.1371/journal.pgen.0020168).
- ▶225. Bejerano G, Lowe CB, Ahituv N, King B, Siepel A, Salama SR, Rubin EM, Kent WJ, Haussler D. A distal enhancer and an ultraconserved exon are derived from a novel retroposon. *Nature* 441: 87–90, 2006. doi:[10.1038/nature04696](https://doi.org/10.1038/nature04696).
- ▶226. Aprea J, Calegari F. Long non-coding RNAs in corticogenesis: deciphering the non-coding code of the brain. *EMBO J* 34: 2865–2884, 2015. doi:[10.15252/embj.201592655](https://doi.org/10.15252/embj.201592655).
- ▶227. Liu X, Sun T. microRNAs and molecular pathogenesis of microcephaly. *Curr Mol Pharmacol* 9: 300–304, 2016. doi:[10.2174/1874467208666150928153949](https://doi.org/10.2174/1874467208666150928153949).
- ▶228. Lewitus E, Huttner WB. Neurodevelopmental lincRNA microsynteny conservation and mammalian brain size evolution. *PLoS One* 10: e0131818, 2015. doi:[10.1371/journal.pone.0131818](https://doi.org/10.1371/journal.pone.0131818).
- ▶229. Dehay C, Kennedy H, Kosik KS. The outer subventricular zone and primate-specific cortical complexification. *Neuron* 85: 683–694, 2015. doi:[10.1016/j.neuron.2014.12.060](https://doi.org/10.1016/j.neuron.2014.12.060).
- ▶230. Dehay C, Kennedy H. Cell-cycle control and cortical development. *Nat Rev Neurosci* 8: 438–450, 2007. doi:[10.1038/nrn2097](https://doi.org/10.1038/nrn2097).
- ▶231. Walsh CA. Genetic malformations of the human cerebral cortex. *Neuron* 23: 19–29, 1999. doi:[10.1016/S0896-6273\(00\)80749-7](https://doi.org/10.1016/S0896-6273(00)80749-7).
- ▶232. Guerrini R, Dobyns WB, Barkovich AJ. Abnormal development of the human cerebral cortex: genetics, functional consequences and treatment options. *Trends Neurosci* 31: 154–162, 2008. doi:[10.1016/j.tins.2007.12.004](https://doi.org/10.1016/j.tins.2007.12.004).
- ▶233. Ross ME, Walsh CA. Human brain malformations and their lessons for neuronal migration. *Annu Rev Neurosci* 24: 1041–1070, 2001. doi:[10.1146/annurev.neuro.24.1.1041](https://doi.org/10.1146/annurev.neuro.24.1.1041).
- ▶234. Guerrini R, Marini C. Genetic malformations of cortical development. *Exp Brain Res* 173: 322–333, 2006. doi:[10.1007/s00221-006-0501-z](https://doi.org/10.1007/s00221-006-0501-z).
- ▶235. Francis F, Koulakoff A, Boucher D, Chafey P, Schaar B, Vinet M, McDonnell N, Reiner O, Kahn A, McConnell SK, Berwald-Netter Y, Denoulet P, Chelly J, Saint F. Doublecortin is a developmentally regulated, microtubule-associated protein expressed in migrating and differentiating neurons. *Neuron* 23: 247–256, 1999. doi:[10.1016/S0896-6273\(00\)80777-1](https://doi.org/10.1016/S0896-6273(00)80777-1).
- ▶236. Pilz DT, Matsumoto N, Minnerath S, Mills P, Gleeson JG, Allen KM, Walsh CA, Barkovich AJ, Dobyns WB, Ledbetter DH, Ross ME. LIS1 and XLIS (DCX) mutations cause most classical lissencephaly, but different patterns of malformation. *Hum Mol Genet* 7: 2029–2037, 1998. doi:[10.1093/hmg/7.13.2029](https://doi.org/10.1093/hmg/7.13.2029).
- ▶237. Gleeson JG, Allen KM, Fox JW, Lamperti ED, Berkovic S, Scheffer J, Cooper EC, Dobyns WB, Minnerath SR, Ross ME, Walsh CA. Doublecortin, a brain-specific gene mutated in human X-linked lissencephaly and double cortex syndrome, encodes a putative signaling protein. *Cell* 92: 63–72, 1998. doi:[10.1016/S0092-8674\(00\)80899-5](https://doi.org/10.1016/S0092-8674(00)80899-5).

- ▶ 238. Reiner O, Carrozzo R, Shen Y, Wehnert M, Faustinella F, Dobyns WB, Caskey CT, Ledbetter DH. Isolation of a Miller-Dieker lissencephaly gene containing G protein beta-subunit-like repeats. *Nature* 364: 717–721, 1993. doi:[10.1038/364717a0](https://doi.org/10.1038/364717a0).
- ▶ 239. Golden JA, Harding NB. In: *Developmental Neuropathology*, edited by Golden JA, Harding BN. Basel: Neuropath Press, 2004, p. 386.
- ▶ 240. Corbo JC, Deuel TA, Long JM, LaPorte P, Tsai E, Wynshaw-Boris A, Walsh CA. Doublecortin is required in mice for lamination of the hippocampus but not the neocortex. *J Neurosci* 22: 7548–7557, 2002. doi:[10.1523/JNEUROSCI.22-17-07548.2002](https://doi.org/10.1523/JNEUROSCI.22-17-07548.2002).
- ▶ 241. Bizzotto S, Francis F. Morphological and functional aspects of progenitors perturbed in cortical malformations. *Front Cell Neurosci* 9: 30, 2015. doi:[10.3389/fncel.2015.00030](https://doi.org/10.3389/fncel.2015.00030).
- ▶ 242. Sapir T, Elbaum M, Reiner O. Reduction of microtubule catastrophe events by LIS1, platelet-activating factor acetylhydrolase subunit. *EMBO J* 16: 6977–6984, 1997. doi:[10.1093/emboj/16.23.6977](https://doi.org/10.1093/emboj/16.23.6977).
- ▶ 243. Caspi M, Atlas R, Kantor A, Sapir T, Reiner O. Interaction between LIS1 and doublecortin, two lissencephaly gene products. *Hum Mol Genet* 9: 2205–2213, 2000. doi:[10.1093/oxfordjournals.hmg.a018911](https://doi.org/10.1093/oxfordjournals.hmg.a018911).
- ▶ 244. Morris-Rosendahl DJ, Najm J, Lachmeijer AM, Sztriha L, Martins M, Kuechler A, Haug V, Zeschneig C, Martin P, Santos M, Vasconcelos C, Omran H, Kraus U, Van der Knaap MS, Schuierer G, Kutsche K, Uyanik G. Refining the phenotype of alpha-1a Tubulin (TUBA1A) mutation in patients with classical lissencephaly. *Clin Genet* 74: 425–433, 2008. doi:[10.1111/j.1399-0004.2008.01093.x](https://doi.org/10.1111/j.1399-0004.2008.01093.x).
- ▶ 245. Kumar RA, Pilz DT, Babatz TD, Cushion TD, Harvey K, Topf M, Yates L, Robb S, Uyanik G, Mancini GM, Rees MI, Harvey RJ, Dobyns WB. TUBA1A mutations cause wide spectrum lissencephaly (smooth brain) and suggest that multiple neuronal migration pathways converge on alpha tubulins. *Hum Mol Genet* 19: 2817–2827, 2010. doi:[10.1093/hmg/ddq182](https://doi.org/10.1093/hmg/ddq182).
- ▶ 246. Hong SE, Shugart YY, Huang DT, Shahwan SA, Grant PE, Hourihane JO, Martin ND, Walsh CA. Autosomal recessive lissencephaly with cerebellar hypoplasia is associated with human RELN mutations. *Nat Genet* 26: 93–96, 2000. doi:[10.1038/79246](https://doi.org/10.1038/79246).
- ▶ 247. D'Arcangelo G, Miao GG, Chen SC, Soares HD, Morgan JL, Curran T. A protein related to extracellular matrix proteins deleted in the mouse mutant reeler. *Nature* 374: 719–723, 1995. doi:[10.1038/374719a0](https://doi.org/10.1038/374719a0).
- ▶ 248. Alcántara S, Ruiz M, D'Arcangelo G, Ezan F, de Lecea L, Curran T, Sotelo C, Soriano E. Regional and cellular patterns of reelin mRNA expression in the forebrain of the developing and adult mouse. *J Neurosci* 18: 7779–7799, 1998. doi:[10.1523/JNEUROSCI.18-19-07779.1998](https://doi.org/10.1523/JNEUROSCI.18-19-07779.1998).
- ▶ 249. Dulabon L, Olson EC, Taglienti MG, Eisenhuth S, McGrath B, Walsh CA, Kreidberg JA, Anton ES. Reelin binds alpha3beta1 integrin and inhibits neuronal migration. *Neuron* 27: 33–44, 2000. doi:[10.1016/S0896-6273\(00\)00007-6](https://doi.org/10.1016/S0896-6273(00)00007-6).
- ▶ 250. Rice DS, Curran T. Role of the reelin signaling pathway in central nervous system development. *Annu Rev Neurosci* 24: 1005–1039, 2001. doi:[10.1146/annurev.neuro.24.1.1005](https://doi.org/10.1146/annurev.neuro.24.1.1005).
- ▶ 251. D'Arcangelo G. Reelin mouse mutants as models of cortical development disorders. *Epilepsy Behav* 8: 81–90, 2006. doi:[10.1016/j.yebeh.2005.09.005](https://doi.org/10.1016/j.yebeh.2005.09.005).
- ▶ 252. Yamamoto T, Kato Y, Karita M, Kawaguchi M, Shibata N, Kobayashi M. Expression of genes related to muscular dystrophy with lissencephaly. *Pediatr Neurol* 31: 183–190, 2004. doi:[10.1016/j.pediatrneurol.2004.03.020](https://doi.org/10.1016/j.pediatrneurol.2004.03.020).
- ▶ 253. Luo R, Jeong SJ, Jin Z, Strokes N, Li S, Piao X. G protein-coupled receptor 56 and collagen III, a receptor-ligand pair, regulates cortical development and lamination. *Proc Natl Acad Sci U S A* 108: 12925–12930, 2011. doi:[10.1073/pnas.1104821108](https://doi.org/10.1073/pnas.1104821108).
- ▶ 254. van Reeuwijk J, Brunner HG, van Bokhoven H. Glyc-O-genetics of Walker-Warburg syndrome. *Clin Genet* 67: 281–289, 2005. doi:[10.1111/j.1399-0004.2004.00368.x](https://doi.org/10.1111/j.1399-0004.2004.00368.x).
- ▶ 255. Barkovich AJ, Hevner R, Guerrini R. Syndromes of bilateral symmetrical polymicrogyria. *AJNR Am J Neuroradiol* 20: 1814–1821, 1999.
- ▶ 256. Walsh CA. Neuroscience in the post-genome era: an overview. *Trends Neurosci* 24: 363–364, 2001. doi:[10.1016/S0166-2236\(00\)01866-X](https://doi.org/10.1016/S0166-2236(00)01866-X).
- ▶ 257. Bilguvar K, Ozturk AK, Louvi A, Kwan KY, Choi M, Tatli B, et al. Whole-exome sequencing identifies recessive WDR62 mutations in severe brain malformations. *Nature* 467: 207–210, 2010. doi:[10.1038/nature09327](https://doi.org/10.1038/nature09327).
- ▶ 258. Yu TW, Mochida GH, Tischfield DJ, Sgaier SK, Flores-Sarnat L, Sergi CM, Topcu M, McDonald MT, Barry BJ, Felie JM, Sunu C, Dobyns WB, Folkerth RD, Barkovich AJ, Walsh CA. Mutations in WDR62, encoding a centrosome-associated protein, cause microcephaly with simplified gyri and abnormal cortical architecture. *Nat Genet* 42: 1015–1020, 2010. doi:[10.1038/ng.683](https://doi.org/10.1038/ng.683).
- ▶ 259. Piao X, Chang BS, Bodell A, Woods K, Benzeev B, Topcu M, Guerrini R, Goldberg-Stern H, Sztriha L, Dobyns WB, Barkovich AJ, Walsh CA. Genotype-phenotype analysis of human frontoparietal polymicrogyria syndromes. *Ann Neurol* 58: 680–687, 2005. doi:[10.1002/ana.20616](https://doi.org/10.1002/ana.20616).
- ▶ 260. Mirzaa GM, Conti V, Timms AE, Smyser CD, Ahmed S, Carter M, Barnett S, Hufnagel RB, Goldstein A, Narumi-Kishimoto Y, Olds C, Collins S, Johnston K, Deleuze JF, Nitschke, P, Friend K, Harris C, Goetsch A, Martin B, Boyle EA, Parrini E, Mei D, Tattini L, Slavotinek A, Blair E, Barnett C, Shendure J, Chelly J, Dobyns WB, Guerrini R. Characterisation of mutations of the phosphoinositide-3-kinase regulatory subunit, PIK3R2, in perisylvian polymicrogyria: A next-generation sequencing study. *Lancet Neurol* 14: 1182–1195, 2015. doi:[10.1016/S1474-4422\(15\)00278-1](https://doi.org/10.1016/S1474-4422(15)00278-1).
- ▶ 261. Jacobs KM, Hwang BJ, Prince DA. Focal epileptogenesis in a rat model of polymicrogyria. *J Neurophysiol* 81: 159–173, 1999. doi:[10.1152/jn.1999.81.1.159](https://doi.org/10.1152/jn.1999.81.1.159).
- ▶ 262. Squier W, Jansen A. Polymicrogyria: pathology, fetal origins and mechanisms. *Acta Neuropathol Commun* 2: 80, 2014. doi:[10.1186/s40478-014-0080-3](https://doi.org/10.1186/s40478-014-0080-3).
- ▶ 263. Hartfuss E, Forster E, Bock HH, Hack MA, Leprince P, Luque JM, Herz J, Frotscher M, Götz M. Reelin signaling directly affects radial glia morphology and biochemical maturation. *Development* 130: 4597–4609, 2003. doi:[10.1242/dev.00654](https://doi.org/10.1242/dev.00654).
- ▶ 264. Cappello S, Bohringer CR, Bergami M, Conzelmann KK, Ghanem A, Tomassy GS, Arlotta P, Mainardi M, Allegra M, Caleo M, van Hengel J, Brakebusch C, Götz M. A radial glia-specific role of RhoA in double cortex formation. *Neuron* 73: 911–924, 2012. doi:[10.1016/j.neuron.2011.12.030](https://doi.org/10.1016/j.neuron.2011.12.030).
- ▶ 265. Schmid RS, Anton ES. Role of integrins in the development of the cerebral cortex. *Cereb Cortex* 13: 219–224, 2003. doi:[10.1093/cercor/13.3.219](https://doi.org/10.1093/cercor/13.3.219).
- ▶ 266. Depaape V, Suarez-Gonzalez N, Dufour A, Passante L, Gorski JA, Jones KR, Ledent C, Vanderhaeghen P. Ephrin signalling controls brain size by regulating apoptosis of neural progenitors. *Nature* 435: 1244–1250, 2005. doi:[10.1038/nature03651](https://doi.org/10.1038/nature03651).

- ▶ 267. Haydar TF, Kuan CY, Flavell RA, Rakic P. The role of cell death in regulating the size and shape of the mammalian forebrain. *Cereb Cortex* 9: 621–626, 1999. doi:[10.1093/cercor/9.6.621](https://doi.org/10.1093/cercor/9.6.621).
- ▶ 268. Sarkisian MR, Bartley CM, Chi H, Nakamura F, Hashimoto-Torii K, Torii M, Flavell RA, Rakic P. MEKK4 signaling regulates filamin expression and neuronal migration. *Neuron* 52: 789–801, 2006. doi:[10.1016/j.neuron.2006.10.024](https://doi.org/10.1016/j.neuron.2006.10.024).
- ▶ 269. Kielar M, Tuy FP, Bizzotto S, Lebrand C, de Juan Romero C, Poirier K, Oegema R, Mancini GM, Bahi-Buisson N, Olaso R, Le Moing AG, Boutourlinsky K, Boucher D, Carpentier W, Berquin P, Deleuze JF, Belvindrah R, Borrell V, Welker E, Chelly J, Croquelois A, Francis F. Mutations in *Eml1* lead to ectopic progenitors and neuronal heterotopia in mouse and human. *Nat Neurosci* 17: 923–933, 2014. doi:[10.1038/nn.3729](https://doi.org/10.1038/nn.3729).
- ▶ 270. Feng Y, Walsh CA. Mitotic spindle regulation by *Nde1* controls cerebral cortical size. *Neuron* 44: 279–293, 2004. doi:[10.1016/j.neuron.2004.09.023](https://doi.org/10.1016/j.neuron.2004.09.023).
- ▶ 271. Pulvers JN, Bryk J, Fish JL, Wilsch-Brauninger M, Arai Y, Schreier D, Naumann R, Helppi J, Habermann B, Vogt J, Nitsch R, Toth A, Enard W, Paabo S, Huttner WB. Mutations in mouse *Aspm* (abnormal spindle-like microcephaly associated) cause not only microcephaly but also major defects in the germline. *Proc Natl Acad Sci U S A* 107: 16595–16600, 2010. doi:[10.1073/pnas.1010494107](https://doi.org/10.1073/pnas.1010494107).
- ▶ 272. Shen J, Eyaid W, Mochida GH, Al-Moayyad F, Bodell A, Woods CG, Walsh CA. ASPM mutations identified in patients with primary microcephaly and seizures. *J Med Genet* 42: 725–729, 2005. doi:[10.1136/jmg.2004.027706](https://doi.org/10.1136/jmg.2004.027706).
- ▶ 273. Hirotsune S, Fleck MW, Gambello MJ, Bix GJ, Chen A, Clark GD, Ledbetter DH, McBain CJ, Wynshaw-Boris A. Graded reduction of *Pafah1b1* (*Lis1*) activity results in neuronal migration defects and early embryonic lethality. *Nat Genet* 19: 333–339, 1998. doi:[10.1038/1221](https://doi.org/10.1038/1221).
- ▶ 274. Sur M, Rubenstein JL. Patterning and plasticity of the cerebral cortex. *Science* 310: 805–810, 2005. doi:[10.1126/science.1112070](https://doi.org/10.1126/science.1112070).
- ▶ 275. White LE, Fitzpatrick D. Vision and cortical map development. *Neuron* 56: 327–338, 2007. doi:[10.1016/j.neuron.2007.10.011](https://doi.org/10.1016/j.neuron.2007.10.011).
- ▶ 276. Borrell V. In vivo gene delivery to the postnatal ferret cerebral cortex by DNA electroporation. *J Neurosci Methods* 186: 186–195, 2010. doi:[10.1016/j.jneumeth.2009.11.016](https://doi.org/10.1016/j.jneumeth.2009.11.016).
- ▶ 277. Borrell V, Kaspar BK, Gage FH, Callaway EM. In vivo evidence for radial migration of neurons by long-distance somal translocation in the developing ferret visual cortex. *Cereb Cortex* 16: 1571–1583, 2006. doi:[10.1093/cercor/bhj094](https://doi.org/10.1093/cercor/bhj094).
- ▶ 278. Kawasaki H, Iwai L, Tanno K. Rapid and efficient genetic manipulation of gyrencephalic carnivores using in utero electroporation. *Mol Brain* 5: 24, 2012. doi:[10.1186/1756-6606-5-24](https://doi.org/10.1186/1756-6606-5-24).
- ▶ 279. Saito K, Mizuguchi K, Horiike T, Dinh Duong TA, Shinmyo Y, Kawasaki H. Characterization of the inner and outer fiber layers in the developing cerebral cortex of gyrencephalic ferrets. *Cereb Cortex* 29: 4303–4311, 2019. doi:[10.1093/cercor/bhy312](https://doi.org/10.1093/cercor/bhy312).
- ▶ 280. Shinmyo Y, Tanaka S, Tsunoda S, Hosomichi K, Tajima A, Kawasaki H. CRISPR/Cas9-mediated gene knockout in the mouse brain using in utero electroporation. *Sci Rep* 6: 1–13, 2016. doi:[10.1038/s41598-016-0001-8](https://doi.org/10.1038/s41598-016-0001-8).
- ▶ 281. Matsumoto N, Kobayashi N, Uda N, Hirota M, Kawasaki H. Pathophysiological analyses of leptomeningeal heterotopia using gyrencephalic mammals. *Hum Mol Genet* 27: 985–991, 2018. doi:[10.1093/hmg/ddy014](https://doi.org/10.1093/hmg/ddy014).
- ▶ 282. Kou Z, Wu Q, Kou X, Yin C, Wang H, Zuo Z, Zhuo Y, Chen A, Gao S, Wang X. CRISPR/Cas9-mediated genome engineering of the ferret. *Cell Res* 25: 1372–1375, 2015. doi:[10.1038/cr.2015.130](https://doi.org/10.1038/cr.2015.130).
- ▶ 283. Matsumoto N, Hoshiba Y, Morita K, Uda N, Hirota M, Minamikawa M, Ebisu H, Shinmyo Y, Kawasaki H. Pathophysiological analyses of periventricular nodular heterotopia using gyrencephalic mammals. *Hum Mol Genet* 26: 1173–1181, 2017. doi:[10.1093/hmg/ddx038](https://doi.org/10.1093/hmg/ddx038).
- ▶ 284. Feng G, Jensen FE, Greely HT, Okano H, Treue S, Roberts AC, Fox JG, Caddick S, Poo MM, Newsome WT, Morrison JH. Opportunities and limitations of genetically modified nonhuman primate models for neuroscience research. *Proc Natl Acad Sci U S A* 117: 24022–24031, 2020. doi:[10.1073/pnas.2006515117](https://doi.org/10.1073/pnas.2006515117).
- ▶ 285. Murayama AY, Ichiro Kuwako K, Okahara J, Il Bae B, Okuno M, Mashiko H, Shimogori T, Walsh CA, Sasaki E, Okano H. The polymicrogyria-associated GPR56 promoter preferentially drives gene expression in developing GABAergic neurons in common marmosets. *Sci Rep* 10: 21516, 2020.
- ▶ 286. Donoghue MJ, Rakic P. Molecular gradients and compartments in the embryonic primate cerebral cortex. *Cereb Cortex* 9: 586–600, 1999. doi:[10.1093/cercor/9.6.586](https://doi.org/10.1093/cercor/9.6.586).
- ▶ 287. Schmechel DE, Rakic P. A Golgi study of radial glial cells in developing monkey telencephalon: morphogenesis and transformation into astrocytes. *Anat Embryol (Berl)* 156: 115–152, 1979. doi:[10.1007/BF00300010](https://doi.org/10.1007/BF00300010).
- ▶ 288. Rakic P. Radial versus tangential migration of neuronal clones in the developing cerebral cortex. *Proc Natl Acad Sci U S A* 92: 11323–11327, 1995. doi:[10.1073/pnas.92.25.11323](https://doi.org/10.1073/pnas.92.25.11323).
- ▶ 289. Komuro H, Rakic P. Distinct modes of neuronal migration in different domains of developing cerebellar cortex. *J Neurosci* 18: 1478–1490, 1998. doi:[10.1523/JNEUROSCI.18-04-01478.1998](https://doi.org/10.1523/JNEUROSCI.18-04-01478.1998).
- ▶ 290. Dehay C, Giroud P, Berland M, Killackey HP, Kennedy H. Phenotypic characterisation of respecified visual cortex subsequence to prenatal enucleation in the monkey: development of acetylcholinesterase and cytochrome oxidase patterns. *J Comp Neurol* 376: 386–402, 1996. doi:[10.1002/\(SICI\)1096-9861\(19961216\)376:3<386::AID-CNE3>3.0.CO;2-Z](https://doi.org/10.1002/(SICI)1096-9861(19961216)376:3<386::AID-CNE3>3.0.CO;2-Z).
- ▶ 291. Chan AW, Chong KY, Martinovich C, Simerly C, Schatten G. Transgenic monkeys produced by retroviral gene transfer into mature oocytes. *Science* 291: 309–312, 2001. doi:[10.1126/science.291.5502.309](https://doi.org/10.1126/science.291.5502.309).
- ▶ 292. Niu Y, Guo X, Chen Y, Wang CE, Gao J, Yang W, Kang Y, Si W, Wang H, Yang SH, Li S, Ji W, Li XJ. Early Parkinson's disease symptoms in a-synuclein transgenic monkeys. *Hum Mol Genet* 24: 2308–2317, 2015. doi:[10.1093/hmg/ddu748](https://doi.org/10.1093/hmg/ddu748).
- ▶ 293. Moran S, Chi T, Prucha MS, Ahn KS, Connor-Stroud F, Jean S, Gould K, Chan AW. Germline transmission in transgenic Huntington's disease monkeys. *Theriogenology* 84: 277–285, 2015. doi:[10.1016/j.theriogenology.2015.03.016](https://doi.org/10.1016/j.theriogenology.2015.03.016).
- ▶ 294. Mora-Bermudez F, Badsha F, Kanton S, Camp JG, Vernot B, Kohler K, Voigt B, Okita K, Maricic T, He Z, Lachmann R, Paabo S, Treutlein B, Huttner WB. Differences and similarities between human and chimpanzee neural progenitors during cerebral cortex development. *Elife* 5: e18683, 2016. doi:[10.7554/elife.18683](https://doi.org/10.7554/elife.18683).
- ▶ 295. Benito-Kwiecinski S, Giandomenico SL, Sutcliffe M, Riis ES, Freire-Pritchett P, Kelava I, Wunderlich S, Martin U, Wray GA, McDole K, Lancaster MA. An early cell shape transition drives evolutionary expansion of the human forebrain. *Cell* 184: 2084–2102.e19, 2021. doi:[10.1016/j.cell.2021.02.050](https://doi.org/10.1016/j.cell.2021.02.050).

- ▶ 296. Luo C, Lancaster MA, Castanon R, Nery JR, Knoblich JA, Ecker JR. Cerebral organoids recapitulate epigenomic signatures of the human fetal brain. *Cell Rep* 17: 3369–3384, 2016. doi:[10.1016/j.celrep.2016.12.001](https://doi.org/10.1016/j.celrep.2016.12.001).
- ▶ 297. Lancaster MA, Renner M, Martin CA, Wenzel D, Bicknell LS, Hurles ME, Homfray T, Penninger JM, Jackson AP, Knoblich JA. Cerebral organoids model human brain development and microcephaly. *Nature* 501: 373–379, 2013. doi:[10.1038/nature12517](https://doi.org/10.1038/nature12517).
- ▶ 298. Heide M, Huttner WB, Mora-Bermúdez F. Brain organoids as models to study human neocortex development and evolution. *Curr Opin Cell Biol* 55: 8–16, 2018. doi:[10.1016/j.jceb.2018.06.006](https://doi.org/10.1016/j.jceb.2018.06.006).
- ▶ 299. Quadrato G, Brown J, Arlotta P. The promises and challenges of human brain organoids as models of neuropsychiatric disease. *Nat Med* 22: 1220–1228, 2016. doi:[10.1038/nm.4214](https://doi.org/10.1038/nm.4214).
- ▶ 300. Arlotta P, Pa, sca SP. Cell diversity in the human cerebral cortex: from the embryo to brain organoids. *Curr Opin Neurobiol* 56: 194–198, 2019. doi:[10.1016/j.conb.2019.03.001](https://doi.org/10.1016/j.conb.2019.03.001).
- ▶ 301. Velasco S, Kedaigle AJ, Simmons SK, Nash A, Rocha M, Quadrato G, Paulsen B, Nguyen L, Adiconis X, Regev A, Levin JZ, Arlotta P. Individual brain organoids reproducibly form cell diversity of the human cerebral cortex. *Nature* 570: 523–527, 2019. doi:[10.1038/s41586-019-1289-x](https://doi.org/10.1038/s41586-019-1289-x).
- ▶ 302. Lancaster MA, Knoblich JA. Organogenesis in a dish: modeling development and disease using organoid technologies. *Science* 345: 1247125, 2014. doi:[10.1126/science.1247125](https://doi.org/10.1126/science.1247125).
- ▶ 303. Bian S, Repic M, Guo Z, Kavirayani A, Burkard T, Bagley JA, Krauditsch C, Knoblich JA. Genetically engineered cerebral organoids model brain tumor formation. *Nat Methods* 15: 631–639, 2018. doi:[10.1038/s41592-018-0070-7](https://doi.org/10.1038/s41592-018-0070-7).
304. Klaus J, Kanton S, Kyrrousi C, Ayo-Martin AC, Giaimo RD, Riesenberg S, O’Neill AC, Camp JG, Tocco C, Santel M, Rusha E, Drukker M, Schroeder M, Goetz M, Robertson SP, Treutlein B, Cappello S. Altered neuronal migratory trajectories in human cerebral organoids derived from individuals with neuronal heterotopia. *Nat Med* 25: 561–568, 2019. doi:[10.1038/s41591-019-0371-0](https://doi.org/10.1038/s41591-019-0371-0). ▶
305. Bershteyn M, Nowakowski TJ, Pollen AA, Lullo ED, Nene A, Wynshaw-Boris A, Kriegstein AR. Human iPSC-derived cerebral organoids model cellular features of lissencephaly and reveal prolonged mitosis of outer radial glia. *Cell Stem Cell* 20: 435–449 e4, 2017. doi:[10.1016/j.stem.2016.12.007](https://doi.org/10.1016/j.stem.2016.12.007). ▶
306. Karzbrun E, Kshirsagar A, Cohen SR, Hanna JH, Reiner O. Human brain organoids on a chip reveal the physics of folding. *Nat Phys* 14: 515–522, 2018. doi:[10.1038/s41567-018-0046-7](https://doi.org/10.1038/s41567-018-0046-7). ▶
307. Bertacchi M, Romano AL, Loubat A, Mau-Them FT, Willems M, Faivre L, Khau van Kien P, Perrin L, Devillard F, Sorlin A, Kuentz P, Philippe C, Garde A, Neri F, Giaimo RD, Oliviero S, Cappello S, D’Incerti L, Frassonni C, Studer M. NR2F1 regulates regional progenitor dynamics in the mouse neocortex and cortical gyrification in BBSOAS patients. *EMBO J* 39: e104163, 2020. ▶
308. Li Y, Muffat J, Omer A, Bosch I, Lancaster MA, Sur M, Gehrke L, Knoblich JA, Jaenisch R. Induction of expansion and folding in human cerebral organoids. *Cell Stem Cell* 20: 385–396.e3, 2017. doi:[10.1016/j.stem.2016.11.017](https://doi.org/10.1016/j.stem.2016.11.017). ▶



